MODULATION OF CANCER CELL INVASION BY EXTRACELLULAR VESICLES

Maria Laura Tognoli

Pembroke College



Thesis submitted to the University of Oxford in partial fulfilment of the requirements for the Degree of Doctor of Philosophy.

Trinity Term 2018
University of Oxford

Supervisors

Prof. Eric O'Neill (University of Oxford)

Prof. Adrian Harris (University of Oxford)



The work presented in this thesis was performed at the Cancer Research UK and Medical Research Council Oxford Institute for Radiation Oncology, Department of Oncology, University of Oxford. This study was funded by Cancer Research UK Oxford Centre Prize DPhil Studentship.

Abstract

Modulation of Cancer Cell Invasion by Extracellular Vesicles

Submitted for Degree of Doctor of Philosophy

Maria Laura Tognoli, Pembroke College, Trinity Term 2018

The cancer microenvironment is a receptacle of stimuli necessary to promote tumour growth. The role of extracellular vesicles (EVs) in orchestrating a crosstalk between cancer cells and other cell types in the surroundings is integral part of the tumour network. Extracellular vesicles are subcellular structures that emanate virtually from any cell type and carry information both within the primary tumour site and to distant sites. Here I show that two oncogenic stimuli control the release of EVs to render cancer and untransformed cells more aggressive. Firstly, I show that loss of the tumour suppressor RASSF1A in breast cancer cells allows the alternative transcript and oncogene RASSF1C to exploit its tumourigenic activity through enhanced secretion of EVs. I characterise RASSF1C EVs as able to drive migration and invasion in recipient breast cancer cells and I show that RASSF1C elicits exocytosis through activation of the small GTPase RhoA. Secondly, I explore the role of the TGF-β cytokine in altering extracellular vesicle secretion. Here, I report the selective enrichment of the tetraspanin CD9 on TGF-β driven EVs. I show that CD9 is a positive mediator of TGF-β pathway and conclude that TGF-β employs exocytosis as a route to secrete CD9 from pathway activated cells, as a negative feedback on the signalling cascade. Finally, I describe a novel role of CD9 positive EVs in propagating TGF-β signalling in recipient breast cancer cells and in mediating TGF-β driven invasion in untransformed breast epithelium. This work highlights the importance of tumourigenic stimuli, both intracellular (RASSF1C) and environmental (TGF-β), in fostering a pro-invasive cancer environment and the pivotal role that extracellular vesicles play in mediating oncogenic signalling.

Acknowledgements

Questa tesi é il frutto di quattro anni di impegno, passione, lacrime (molte) sorrisi (pochi ma guadagnati con tutte le lacrime).
First of all, I would like to thank my supervisor, Prof. Eric O'Neill. Your guidance and your encouragement helped me in becoming the scientist I am today. Thank you for the low-pressure environment, for the stimulating (and daunting, but just at the beginning!) one-to-one sessions, where I could take ideas for the next experiments and thank you for giving me many opportunities to present my work, challenging my stage fear!
A big thank you goes to my lab ladies, Dafni, Leanne and Delia, who cheered me up when I needed it and helped me troubleshooting science all the time. Dafni, thank you for being a mentor and a friend, for explaining me things over and over again (this applies to Nikola too..) and for giving me my first publication! LB and Deli… why did you two leave I don't know! Like you thought I would survive, with no windows!!! You evil pair. You made my life joyful and my results less painful to accept. A big thank you to Nikola, you were and still are my mentor, you taught me all I know about molecular biology and extracellular vesicles and you even took the time to read my thesis, I appreciate all your help throughout the years! Another thank you to Aswin, for having always a wise word in front of my despair, science-related or not. I would also like to thank the other lab members: Asmita, for all the patience and the help with experiments, Daniela for teaching me new techniques and the others, old and new, Luana, Michael, Simone, Maria, Frances. And non lab members: GG thank you for being such an enthusiastic example in science, life and a concert companion!
I want to thank my Oxford family as well, Daniela and Cristiana, I started this together, thanks for being wonderful housemates, for being so supportive in this madness of doing a PhD and for cheering my mornings with Girls´ breakfast.
And now I want to thank my Babraham family (oh yes, I was in Cambridge before being in Oxford…): Arianna, Katherine, Federico & Valentina. I still believe I have done this together. Do you remember four years ago, applying? Going to interviews together? I really think that having gone through that stage with you guys made me stronger. ONLY THE BRAVE!
Credo sia riduttivo circoscrivere alla parola Grazie tutte le schegge del mio cuore che ho lasciato quattro anni fa quando sono partita dall' Italia.
Daiana, Diletta e Chiara, mi avete sorretto quando pensavo di non farcela e motivato quando temevo fosse un passo troppo grande per me, quando non riuscivo ad immaginare questa vita come opzione, quando mi sminuivo (adesso ho smesso...!). Grazie per essere state persistenti, cocciute e testarde e avermi detto: Mary basta, parti!
Il Ringraziamento più sentito va alla mia famiglia. Grazie Tino per essere stato il fratello migliore che io potessi avere, per condividere le mie scelte, per supportarmi e spronarmi davanti ad ostacoli che mi sembravano insormontabili, grazie per averli razionalizzati e ridimensionati insieme a me. Grazie per essere stato la roccia a cui mi potevo appoggiare ogni volta che scivolavo, salendo la montagna. Grazie per essere stato un Fratello-Guerriero che ha condiviso le mie battaglie e mi ha sempre spalleggiato. Grazie per essere uno dei miei riferimenti più importanti, intellettualmente e moralmente, per stimolarmi sempre con nuovi concetti e prospettive differenti dalla mia.
Grazie alla mia Mina, da piccola grande donna mi hai insegnato a difendermi, a chinarmi senza spezzarmi. Grazie per aver contribuito all'evoluzione della mia sfera creativa, d'altronde per fare gli scienziati bisogna essere anche un po' artisti! Grazie per avermi lasciato andare, seppur con grande sofferenza, e per non avermi mai fatto pesare le mie scelte, nonostante il danno che ti hanno arrecato. Grazie per essere stata una madre avanguardista pur essendo chioccia e per volermi tanto tanto bene anche da lontano.
Infine tu, caro Papà. Ti ringrazio per essere stato il mio modello. Un modello di cultura, eclettismo, pensiero scientifico e amore per il proprio lavoro. Grazie per avermi instillato

fin da piccola il germe della curiosità e la necessità di trovare risposte al perchè delle cose. Ti ringrazio per avermi insegnato il piacere di imparare (dici che l´ho presa un po' troppo alla lettera, con tutta questa ricerca?) e per avermi fatto dono del metodo di studio (le parole-chiave!) e della programmazione. Questa Tesi si porta dentro un po' di me e anche un po' di te.
Greg, third, albeit only chronologically, man of my life. I have to thank all the past events in my life that, interlinked like in a domino, brought me to you. And I have to thank all the past events in your life that, interlinked like in a domino, brought you to me. You have been my most enthusiastic supporter since you met me. You unreservedly believed in my abilities in molecular biology, biochemistry, scientific thinking, lab managing, public speaking. You, most of all, listened to my despair and disbelief when things were difficult. Thank you for always showing me the bright side and for always reminding me, it is JUST a PhD (ah, wait, doesn't my whole life depend on tomorrow's western blot?!). Thank you for this and a thousand more things.

Grazie!

Table of Contents

Acknowledgements III

Table of Contents V

List of Figures XII

Abbreviations XVII

Chapter 1 Introduction 1

1.1 Cancer 1

1.2 The Tumour Microenvironment 2

1.3 Extracellular Vesicles 3

1.3.1 Classification of secreted membranous vesicles 3

1.3.2 Biogenesis and secretion of extracellular vesicles 4

1.3.3 Cargo characteristics 10

1.3.4 Extracellular vesicle uptake 13

1.3.5 Extracellular vesicle functions in cancer 13

1.4 Growth Factors 16

1.4.1 Transforming Growth Factor β superfamily 17

1.4.2 TGF-β signalling cascade 18

1.4.3 TGF-β in cancer 23

1.4.4 TGF-β crosstalk with the Hippo pathway 25

1.4.5 TGF-β and tetraspanins 34

1.5 Aims of the Project 37

Chapter 2 Materials and Methods 38
2.1 Materials 38
2.2 Methods 38
2.2.1 Cell culture 38
2.2.2 Transfection 39
2.2.3 Growth Factors and Inhibitors Treatment 40
2.2.4 Cell Lysate Quantification 40
2.2.5 SDS-Page and Western Blotting 41
2.2.6 Immunoprecipitation 43
2.2.7 Rho-GTP Pull-Down Assay 44
2.2.8 Immunofluorescence 45
2.2.9 Reverse Transcriptase PCR 45
2.2.10 Quantitative Real-Time PCR 46
2.2.11 Extracellular Vesicle Production and Isolation 47
2.2.12 Extracellular Vesicle Protein Quantification and Western Blotting 48
2.2.13 Nanoparticle Tracking Analysis of Extracellular Vesicles 49
2.2.14 Extracellular Vesicle Membrane Staining 50
2.2.15 Extracellular Vesicle Immunofluorescent Staining 51
2.2.16 Extracellular Vesicle Treatment of Cells 51
2.2.17 Migration Assay 52
2.2.18 xCELLigence 52

2.2.19 Boyden Chamber Invasion Assay 53
2.2.20 Cre-LoxP System for Study of EV Transfer 54
2.2.21 Transformation of Bacteria 55
2.2.22 Site-Directed Mutagenesis 55
2.2.23 ELISA Assay 56
2.2.24 Statistical analysis 56
2.3 Tables 57
Chapter 3 Optimisation of Extracellular Vesicle Isolation 61
3.1 Introduction 61
3.2 Aims 63
3.3 Extracellular Vesicles Isolation and Detection Methods 63
3.3.1 Comparison of differential centrifugation and polymer-based isolation protocols 63
3.3.2 Comparison of extracellular vesicle populations among breast cancer cell lines 65
3.3.3 Visualisation of extracellular vesicles via Total Internal Reflection Fluorescence 69
3.4 Discussion 71
Chapter 4 An Alternative *RASSF1* Isoform Contributes to Pro-Invasive Extracellular Vesicle Release via Rho/ROCK Pathway 73
4.1 Introduction 73
4.1.1 The role of RhoA signalling in cell migration and invasion 74

4.2 Aims 77

4.3 RASSF1C Promotes Extracellular Vesicles Release 77

4.3.1 *RASSF1* gene knockdown impairs extracellular vesicle release 77

4.3.2 Exogenous expression of RASSF1C leads to increase in extracellular vesicle secretion in breast cancer cells 80

4.4 RASSF1C Extracellular Vesicles Transfer the Invasive Phenotype to Recipient Cells 83

4.4.1 RASSF1C extracellular vesicles are internalised by recipient cells .. 83

4.4.2 RASSF1C extracellular vesicles promote migration in recipient cells 85

4.4.3 RASSF1C extracellular vesicles promote invasion in recipient cells. 87

4.4.4 The Cre-LoxP model confirms RASSF1C role in promoting EV release *in vitro* 90

4.5 RASSF1C Driven Aggressive Phenotype Requires Rho/ROCK Pathway Activation 94

4.5.1 RASSF1C cells display rounded morphology due to RhoA activation 94

4.5.2 RASSF1C interacts with and activates RhoA 98

4.5.3 RhoA is responsible for RASSF1C induced extracellular vesicle release 101

4.6 Discussion 106

Chapter 5 Modulation of TGF-β Signalling by Extracellular Vesicles in Breast Cancer Cells 111

5.1 Introduction 111

5.1.1 Crosstalk between Hippo and TGF-β pathways 111

5.1.2 Tetraspanins as regulators of extracellular vesicle trafficking 113

5.2 Aims 114

5.3 TGF-β Superfamily of Growth Factors Alters Extracellular Vesicle Shedding 114

5.3.1 TGF-β effect on extracellular vesicles is not dependent on RASSF1C 114

5.3.2 TGF-β and BMP4 affect extracellular vesicle release in breast cancer cells ……...118

5.3.3 The Cre-LoxP model confirms TGF-β role in promoting extracellular vesicle uptake *in vitro* 119

5.3.4 TGF-β derived extracellular vesicles do not affect migration in recipient cells 121

5.3.5 TGF-β derived extracellular vesicles mediate invasion in recipient cells…..……123

5.4 TGF-β Modulates Exocytosis of the Tetraspanin CD9 126

5.4.1 CD9 intracellular and extracellular pools depend on TGF-β 127

5.4.2 CD9 localises at the plasma membrane upon TGF-β stimulus..... 131

5.5 Discussion 135

Chapter 6 CD9 is a Positive Mediator of TGF-β Signalling 140

6.1 Introduction 140

6.1.1 CD9 regulates cell adhesion and migration 140

6.1.2 CD9 in cancer 141
6.2 Aims 142
6.3 Loss of CD9 Affects TGF-β Downstream Activation 143
6.3.1 CD9 knockdown reduces SMAD2 phosphorylation and nuclear translocation 143
6.3.2 CD9 depletion affects SMAD2 and SMAD4 coupling 148
6.3.3 CD9 knockdown results in delayed TGF-β target transcription 150
6.4 Inhibition of Extracellular Vesicle Synthesis Sustains TGF-β Signalling 154
6.4.1 Treatment with a nSMase inhibitor leads to maintained pSMAD2 over time 154
6.5 CD9 positive Extracellular Vesicles Elicit a Biological Response on Recipient Cells 156
6.5.1 Treatment of recipient cells with CD9 positive EVs results in SMAD2 activation 156
6.5.2 Treatment of recipient cells with CD9 positive EVs results in TGF-β mediated invasion 159
6.6 Discussion 162
Chapter 7 Discussion 167
Chapter 8 Appendix 184
8.1 RASSF1C and EV secretion in H1299 and MFC7 cells 184
8.2 RASSF1A levels in MDA-231 cells are negligible 185

8.3 RASSF1C exogenous expression leads to a 3-fold increase in RASSF1C mRNA levels 185

8.4 RASSF1C mutants that fail to activate RhoA are unable to induce the amoeboid phenotype 186

8.5 TGF-β may re-route CD9 to both degradative and exocytic pathways .. 187

8.6 SUM159PT cells express undetectable levels of CD9 protein 187

8.7 SMAD2/3 nuclear translocation is impaired upon CD9 depletion 188

8.8 CD9 exogenous expression elicits TGF-β cascade 190

8.9 Rab27a/b knockdown in correlation to TGF-β signalling 191

8.10 SRC protein is enriched in RASSF1C driven EVs 191

8.11 CD9 mRNA levels are elevated in breast cancer patients 192

8.12 Original copyright notices 192

Chapter 9 References 195

List of Figures

Table 1.1 Classification of the main types of extracellular vesicles. 4

Figure 1.1 The ESCRT machinery. 8

Figure 1.2 EV biogenesis and secretion. 10

Figure 1.3 Cargo of extracellular vesicles. 12

Figure 1.4 EVs are mediators of intercellular communication within the tumour microenvironment. 16

Figure 1.5 Canonical TGF-β signalling. 21

Figure 1.6 TGF-β dichotomous roles in cancer. 25

Figure 1.7 The Hippo pathway and TGF-β. 29

Figure 1.8 The two RASSF1 major isoforms RASSF1A and RASSF1C have opposing functions in cancer. 33

Figure 1.9 Tetraspanin family structure and functions. 36

Table 2.1 List of the cell lines used in this study. 57

Table 2.2 List of chemical reagents. 57

Table 2.3 siRNAs used for the study. 57

Table 2.4 Plasmid vectors. 58

Table 2.5 Antibodies. 58

Table 2.6 RT-qPCR primers. 59

Table 2.7 Site directed mutagenesis primers. 59

Table 2.8 Buffers. 60

Figure 3.1 Optimisation of extracellular vesicle isolation protocol. 64

Table 3.1 Cell lines tested for extracellular vesicle release. 66

Figure 3.2 Breast cancer cells release different amounts of extracellular vesicles. 67

Figure 3.3 Breast cancer cells differentially express extracellular vesicle markers. 68

Figure 3.4 TIRF microscopy as an alternative method for validation of protein markers on EVs. 70

Figure 4.1 RASSF1 knockdown reduces the amount of secreted EVs. 79

Figure 4.2 RASSF1C over-expression promotes extracellular vesicle secretion. 81

Figure 4.3 RASSF1C over-expression alters extracellular vesicle protein cargo. 82

Figure 4.4 Extracellular vesicles from control and RASSF1C cells are efficiently taken up by recipient cells. 84

Figure 4.5 RASSF1C EVs promote migration in recipient cells. 86

Figure 4.6 RASSF1C EVs promote 3D Matrigel invasion in recipient cells. 89

Figure 4.7 Graphical representation of the Cre-LoxP system to study EV transfer. 91

Figure 4.8 RASSF1C EVs are internalised at higher rates than control EVs by reporter^{+} cells in a co-culture setup. 92

Figure 4.9 RASSF1C EVs are internalised at higher rates than control EVs by reporter^{+} cells in a transwell assay. 93

Figure 4.10 RASSF1C promotes a rounded phenotype in breast cancer cells. 95

Figure 4.11 In RASSF1C cells MLCII and F-actin adopt cortical structures. 97

Figure 4.12 RASSF1C expression increases active Rho levels. 98

Figure 4.13 RASSF1C co-precipitates with the small GTPase RhoA. 99

Figure 4.14 Two RASSF1C mutants that fail to interact with RhoA impair RASSF1C mediated Rho activation. 100

Figure 4.15 RhoA over-expression alone promotes extracellular vesicle secretion. 102

Figure 4.16 RhoA EVs promote migration in recipient MDA-231 cells. 104

Figure 4.17 RhoA EVs promote Matrigel invasion in recipient MCF7 cells. 105

Figure 4.18 RASSF1C oncogene induces cell morphological changes and promotes release of pro-invasive EVs in RhoA mediated manner. 110

Figure 5.1 RASSF1C transcription is unaffected by TGF-β treatment. 115

Figure 5.2 RASSF1C knockdown does not alter TGF-β1 induced extracellular vesicle release. 117

Figure 5.3 TGF-β superfamily of growth factors alters extracellular vesicle secretion. 119

Figure 5.4 TGF-β1 derived EVs are internalised at higher rates than control EVs by reporter^{+} cells. 120

Figure 5.5 TGF-β1 driven EVs do not affect migratory ability of recipient cells. 122

Figure 5.6 The amount of TGF-β1 carried over on extracellular vesicles is in the order of pg/mL. 123

Figure 5.7 TGF-β1 driven EVs promote 3D Matrigel invasion in recipient cells, compared to control EVs. 125

Figure 5.8 TGF-β1 treatment alters tetraspanin CD9 intracellular and extracellular levels in MDA-MB-231 cells. 128

Figure 5.9 CD9 EV levels are not altered in MCF7 cells upon TGF-β1 treatment. 130

Figure 5.10 CD9 localises at the plasma membrane upon short term TGF-β1 treatment and ALK5 inhibitor II treatment impairs CD9 localisation. 132

Figure 5.11 SB431542 treatment reverts CD9 localisation at the plasma membrane following TGF-β1 stimulation. 134

Figure 5.12 TGF-β mediates the release of pro-invasive extracellular vesicles. 139

Figure 6.1 CD9 depletion leads to a decrease in SMAD2 phosphorylation in the presence of TGF-β. 144

Figure 6.2 CD9 depletion leads to decreased nuclear SMAD2 signal in the presence of TGF-β. 146

Figure 6.3 CD9 depletion results in delayed SMAD2 phosphorylation kinetics. 147

Figure 6.4 CD9 depletion affects SMAD2/SMAD4 binding. 149

Figure 6.5 CD9 depletion does not alter SMAD2/YAP binding. 150

Figure 6.6 TGF-β1 target genes induction is not altered in CD9 depleted cells. 151

Figure 6.7 TGF-β1 target genes induction is delayed is CD9 depleted cells. 153

Figure 6.8 Extracellular vesicle biogenesis is efficiently inhibited with the neutral sphingomyelinase inhibitor GW4869. 155

Figure 6.9 GW4869 treatment sustains TGF-β1 signalling. 156

Figure 6.10 CD9 enriched EVs elicit TGF-β signalling in recipient cells. 158

Figure 6.11 TGF-β transcriptional programme is not altered by $CD9^+$ EVs. 159

Figure 6.12 CD9 EVs stimulate TGF-β mediated invasion in MCF10A cells. 161

Figure 6.13 CD9 is a positive mediator of TGF-β signalling. 166

Figure 7.1 Graphical representation of the model generated from the data presented in this thesis. 183

Figure 8.1 RASSF1C over-expression does not alter EV release in H1299 and MCF7 cells. 184

Figure 8.2 RASSF1A expression is lost in MDA-231 cells. 185

Figure 8.3 RASSF1C exogenous expression increases mRNA levels within a physiological range. 185

Figure 8.4 RASSF1C driven amoeboid phenotype is mediated by RhoA. 186

Figure 8.5 Proteasomal inhibition leads to intracellular accumulation of CD9. 187

Figure 8.6 Comparison of protein levels of CD9 in different breast cancer cell lines. 187

Figure 8.7 SMAD2 and SMAD3 nuclear translocation is reduced in CD9 depleted cells. 189

Figure 8.8 CD9 over-expression promotes TGF-β signalling. 190

Figure 8.9 Rab27b depletion results in greater SMAD2 phosphorylation. 191

Figure 8.10 RASSF1C drives SRC accumulation on EVs. 191

Figure 8.11 CD9 expression in TCGA reveals higher levels in invasive breast carcinoma patients. 192

Abbreviations

18S	18 S Ribosomal RNA
aa	Amino Acid
AC	Adenocarcinoma
ADAM	A Disintegrin And Metalloproteinase
AKT	RAC-alpha serine/threonine-protein Kinase
Alix	ALG-2 Interacting protein X
ALK	(e.g. ALK5, ALK1) Activin Receptor-like Kinase Subunit
AMH	Anti-Mullerian Hormone
ARF	(e.g. Arf6) ADP-Ribosylation factor 6
ATCC	American Type Culture Collection
ATM	Ataxia Telangiectasia Mutated
ATP	Adenosine Triphosphate
BCA	Bicinchoninic Acid
BMP	Bone Morphogenetic Protein
BM	Bone Marrow
BSA	Bovine Serum Albumin
C1	Protein kinase C conserved region
CA	Constitutively Active mutant
CAS/CSE1L	Crk-Associated Substrate/ Cellular apoptosis susceptibility protein
CD	(e.g. CD63, CD9) Cluster of Differentiation
Cdc42	Cell Division Cycle 42
CDK	Cyclin-Dependent Kinase
cDNA	Complementary DNA
ChIP-Seq	Chromatin Immunoprecipitation Sequencing
CHMP	(e.g. CHMP1) Charged Multivesicular Body Protein
cm	Centimetre
c-Myc	MYC Proto-Oncogene, BHLH Transcription Factor
CNK1	Connector Enhancer of Kinase Suppressor of Ras (KRS) 1
co-SMAD	Co-mediator SMAD
CpG	Dinucleotide consisting of cytosine followed by guanine
CRUK	Cancer Research UK
CTGF	Connective Tissue Growth Factor
CTRL	Control
CXCR4	C-X-C Chemokine Receptor type 4
CYR61	Cysteine Rich Angiogenic Inducer 61
DAG	Diacylglycerol
DAPI	4′,6-diamidino-2-phenylindole

DMEM	Dulbecco's-Modified Eagles Medium
DMSO	Dimethylsulfoxide
DN	Dominant Negative mutant
DNA	Deoxyribonucleic Acid
DNMT	DNA Methyltransferase
DOA4	Ubiquitin Carboxyl-terminal Hydrolase 4
DsRed	*Discosoma* sp. red fluorescent protein
DTT	Dithiothreitol
EAP	(e.g. EAP45) ELL-Associated Protein Of 45 KDa
ECL	Enhanced Chemiluminescence
ECM	Extracellular Matrix
EEA1	Early Endosome Antigen 1
EGF	Epidermal Growth Factor
eGFP	Enhanced Green Fluorescent Protein
EGFR	Epidermal Growth Factor Receptor
EMT	Epithelial to Mesenchymal Transition
EpCAM	Epithelial Cell Adhesion Molecule
ER	Endoplasmic Reticulum
ERK	Extracellular Signal-regulated Kinases
ESCRT	Endosomal Sorting Complex Required for Transport
EtOH	Ethanol
EV	Extracellular Vesicle
FBS	Foetal Bovine Serum
Flag	An epitope tag of the sequence DYKDDDDK
F-actin	Filamentous actin
FOXH1	Forkhead box protein H1
g	Gram
GAP	GTPase-Activating Proteins
GAPDH	Glyceraldehyde-3-Phosphate Dehydrogenase
GDF	Growth and Differentiation Factor
GDP	Guanosine Diphosphate
GEF	Guanine Nucleotide Exchange Factors
GEF-H1	Rho/Rac Guanine Nucleotide Exchange Factor 1
Gln	Glutamine
Gly	Glycine, also G
GM130	Golgi Matrix Protein
GPRC	G-protein coupled Receptor 5
GS	Glycine-Serine rich
GSK3	Glycogen Synthase Kinase-3
GTP	Guanosine Triphosphate

h	Hour
H_2O	Water
HA	An epitope tag of the sequence YPYDVPDYA
HCl	Hydrogen Chloride
HER	Human Epidermal growth factor Receptor 2
hES	Human Embryonic Stem cells
HGF	Hepatocyte Growth Factor
HIF	Hypoxia Inducible Factor
HRS	HGF-regulated Tyrosine Kinase Substrate
hStCs	Hepatic stellate cells
HSP	(e.g. HSP70, HSP90) Heat Shock Protein
IDC	Intraductal Carcinoma
IgG	Immunoglobulin G
IgSF8	Immunoglobulin Superfamily Member 8
IKKα	Inhibitor Of Nuclear Factor Kappa-B Kinase Subunit Alpha
ILV	Intraluminal Vesicle
IP	Immunoprecipitation
I-SMAD	Inhibitory SMAD
ITCH	Itchy E3 Ubiquitin Protein Ligase
JNK	c-Jun N-terminal Kinase
KC	Kupffer cells
KDa	Kilo Dalton
L	Litre
LAMP	Lysosome Associated Membrane Protein
LAP	Latency Associated Peptide
LATS1/2	Large Tumour Suppressor 1/2, Warts in *Drosophila*
LB	Luria Broth
LE	Late Endosome
LEL	Large Extracellular Loop
LIMK	Lim Kinase
LLC	Large Latent Complex
LTBP	Latent TGF-β Binding Protein
M	Molar
MAPK	Mitogen-Activated Protein Kinase
MDSC	Myeloid-Derived Suppressor Cells
MeOH	Methanol
Met	Hepatocyte Growth Factor Receptor
mg	Milligram
MH	(e.g. MH1, MH2) MAD Homology domain
MHC	(e.g. MHC I, MHC II) Major Histocompatibility Complex

microBCA	Micro Bicinchoninic Acid assay
MIF	Macrophage migration Inhibitory Factor
min	Minute
miRNA	Micro RNA
Miro	Mitochondrial Rho (MIRO) GTPase
mL	Millilitre
MLC	Myosin Light Chain
mm	Millimetre
MMP	Matrix Metalloproteinase
mRNA	Messenger RNA
MSS	Methyl Methansulfonate
MST1/2	Mammalian Sterile 20-like Protein (also called KRS), Hpo in *Drosophila*
MTMR4	Myotubularin Related Protein 4
mTORC	Mammalian Target of Rapamycin Complex
MUT	Mutant
MV	Microvesicle
MVB/MVE	Multivesicular Body/Multivesicular Endosome
MVB12	Multivesicular Body Subunit
NaCl	Sodium Chloride
ng	Nanogram
NGF	Nerve Growth Factor
NK	Natural Killer lymphocytes
nm	Nanometre
NP40	Nonidet P40
nSMase2	Neutral Sphingomyelinase 2
NT	Non-Targeting sequence
NTA	Nanoparticle Tracking Analysis
Oct-4	Octamer-binding transcription factor 4
p38	Mitogen-Activated Protein Kinase
p68	DEAD/H (Asp-Glu-Ala-Asp/His) Box Polypeptide 5 (RNA Helicase, 68kD)
PAGE	Polyacrylamide Gel Electrophoresis
PAI-1	Plasminogen Activator Inhibitor Type 1
PBS	Phosphate Buffered Saline
PBST	PBS with the addition of 0.1% Tween 20
PCP	Planar Cell Polarity
PCR	Polymerase Chain Reaction
PDAC	Pancreatic Ductal Adenocarcinoma
PDCD6	Programmed Cell Death 6
PDI	Protein Disulfide Isomerase
PE	Pleural Effusion

PEG	Polyethylene Glycol
Pen/Strep	Penicillin/Streptomycin
PET	Polyethylene Terephthalate
pg	Picogram
PI3K	Phosphatidylinositol-4,5-Bisphosphate 3-Kinase
PI3P	Phosphatidylinositol-3-phosphate
PP2A	Protein Phosphatase 2A
PPM1A	Protein Phosphatase, Mg^{2}+/Mn^{2}+ Dependent 1A
PKC	Protein Kinase C
PTM	Post-Translational Modification
PVDF	Polyvinylidene Fluoride
RA	Ras Association domain or RalGDS/AF-6
Rab	Ras-related proteins in Brain
Rac	Ras-related C3 botulinum toxin substrate
Raf	Raf-1 Proto-Oncogene, Serine/Threonine Kinase
RalGDS/AF-6	Ral Guanine Nucleotide Dissociation Stimulator/ALL-1 fusion partner from chromosome 6
Ran	Ras-Related Nuclear Protein
Ras	Ras Proto-Oncogene
RASSF	Ras-Association Domain Family member
Rho	Ras Homolog Family Member
RhoBTB	Rho Related BTB Domain Containing Protein
RIPA	Radioimmunoprecipitation Assay buffer
RNA	Ribonucleic Acid
RNA-Seq	RNA Sequencing
Rnd	Rho-Related GTP-Binding Protein
ROCK	Rho Kinase
R-SMAD	Receptor SMAD
RT	Room Temperature
RT-qPCR	Real-Time Quantitative Polymerase Chain Reaction
SARA	Smad Anchor for Receptor Activation
SARAH	**Sa**v/**RA**SSF/**H**ippo
Sav	Salvador
$SCF^{\beta\text{-}TRCP}$	SKP1-CUL1-F-box
SDS	Sodium Dodecyl Sulphate
sec	Second
SEL	Short Extracellular Loop
SEM	Standard Error of the Mean
Ser	Serine, also S
SFK	SRC Family Kinases

siRNA	Small interfering RNA molecule
SMAD	Mothers Against Decapentaplegic Homolog
SMURF	(e.g. SMURF1, SMURF2) Smad Ubiquitin Regulatory Factor
SNARE	Soluble NSF (N-ethylmaleimide-sensitive factor) Attachment Protein) Receptor
SPC	Surfactant Protein C
SRC	Proto-oncogene Tyrosine-protein Kinase SRC
STAM	Signal Transducing Adaptor Molecule
SUMO	Small Ubiquitin-like Modifier
TAE	Tris-acetate-EDTA
TAK1	Mitogen-activated protein kinase kinase kinase 7
TAZ	Transcriptional co-activator with PDZ-binding motif
TBS	Tris Buffered Saline
TCGA	The Cancer Genome Atlas
TEAD	TEA Domain family, Scalloped in *Drosophila*
TEM	Tetraspanin-enriched Microdomain
TEM	Transmission Electron Microscopy
TfR	Transferrin Receptor
TGF-α	Transforming Growth Factor α
TGF-β	Transforming Growth Factor β
TGFβRI	Transforming Growth Factor β Receptor I
TGFβRII	Transforming Growth Factor β Receptor II
TGFβRIII	Transforming Growth Factor β Receptor III or beta-glycan
TGN	Trans-Golgi Network
Thr	Threonine, also T
TIRF	Total Internal Reflection Fluorescence Microscopy
TNBC	Triple Negative Breast Cancer
T_{regs}	Regulatory T cells
TRIM33	Tripartite Motif Containing 33
TSG101	Tumour Susceptibility Gene 101
Tyr	Tyrosine, also Y
UBAP1	Ubiquitin-associated Protein 1
UEV	Ubiquitin E2 Variant
UIM	Ubiquitin-Interacting Motif
UV	Ultra-Violet
v/v	Volume per Volume
VAMP	(e.g. VAMP3) Vesicle-associated Membrane Protein 3
VPS	Vacuolar Protein Sorting
VTA1	Vacuolar protein sorting-associated protein VTA1 homolog
w/v	Weight per Volume

WB	Western Blot
WCL	Whole Cell Lysate
Wnt	Wingless Related Integration Site
WT	Wild Type
YAP	Yes Associated Protein, Yorkie in *Drosophila*
ZO-1	Zonula Occludens 1
ZsGreen	*Zoanthus* Green Fluorescent Protein
µg	Microgram
µL	Microlitre
µm	Micrometre

Chapter 1 Introduction

1.1 Cancer

The steps that lead to carcinogenesis are slow and sequential. Cancer is a multifaceted disease that starts with normal cells undergoing genetic and phenotypic changes, dictated by tissue architecture, microenvironment and external stimuli. The modifications that normal cells encounter ultimately lead to uncontrolled growth and invasion of the surroundings as well as of distant sites. Moreover, the interplay between different cell types in the emerging neoplastic lesion extends the levels of complexity of this pathology.

Despite the specificity of each tumour type - according to the tissue of origin, the external stimuli the patient is exposed to and the genetic background - common essential alterations in cell physiology that collectively lead to malignant growth have been identified. Acquired capabilities of malignant cells have been initially enumerated as: growth signals autonomy, insensitivity to antiproliferative signals, apoptosis evasion, unlimited replicative potential, angiogenesis and tissue invasion (Hanahan et al., 2000). Other distinct attributes of cancer cells have been more recently elucidated, such as reprogramming energy metabolism and evading immune surveillance. All these attributes orchestrate the progression of a malignant lesion towards a metastatic tumour. However, acquisition of these multiple hallmarks highly relies on the succession of alterations in the genetic landscape of the cell. Genomic instability has thus been identified as turning point for the cell in acquiring malignant traits. Here, genetic mutations as well as

epigenetic remodelling confer selective advantage to a subclone of cells for tumour progression (Hanahan et al., 2011).

1.2 The Tumour Microenvironment

It is now apparent how cancer cells alone would not be able to sustain their own growth and expansion if there was not a compliant environment around them. The tumour microenvironment has been gaining interest in the last decades for playing a pivotal role in interacting with the cancer core and modulating its growth (Hanahan et al., 2011). The contribution of immune cells, endothelial cells, pericytes, cancer associated fibroblasts and tumour stroma is fundamental in fostering the tumour and setting up a permissive framework for cancer dissemination (Balkwill et al., 2012; Hanahan et al., 2011).

The crosstalk between different cell types present in the tumour microenvironment is orchestrated by cell-cell contact, soluble secreted factors and the exchange of subcellular structures such as extracellular vesicles. Moreover, the same factors that allow crosstalk in the tumour microenvironment in the primary site, are also involved in cell-cell communication in the pre-metastatic niche (Peinado et al., 2011). The release of growth factors from either cancer cells or other cell types initiates signalling pathways that confer survival and growth advantages to cancer cells (Witsch et al., 2010). Similarly, extracellular vesicles can also actively influence cell behaviour in the tumour surroundings and, perhaps more importantly, can reach out into the blood stream and perpetuate dissemination of the disease in a non-cell-autonomous manner (Kalluri, 2016; Kanada et al., 2016; Peinado et al., 2011).

1.3 Extracellular Vesicles

Extracellular vesicles (EVs) have been gaining interest in the study of multiple diseases since the discovery that these entities are actively secreted by virtually any cell type and that they are enriched in intracellular components (Johnstone et al., 1987). First evidence for the cells to secrete vesicles was obtained in maturing reticulocytes, where the transferrin receptor was found to associate with secreted 50 nm vesicles (Harding et al., 1983; Pan et al., 1983). It was apparent at the time how the maturing cells were using the exocytosis pathway to excrete redundant cargo and catabolites (Harding et al., 1984; Pan et al., 1985). However, later it was shown that these vesicles, referred to as exosomes, can horizontally transfer material from a donor to a recipient cell. Specifically, first evidence of this function was described in the immune system, where small nanosized EVs, referred to as exosomes, played the role of antigen presenting vesicles shed by either B lymphocytes (Raposo et al., 1996) or dendritic cells (Zitvogel et al., 1998).

It is now widely accepted that extracellular vesicles are means of cell-cell communication and are of extreme relevance in both physiological and pathological processes.

1.3.1 Classification of secreted membranous vesicles

The term extracellular vesicles includes a variety of micro and nanosized vesicles secreted by prokaryotic and eukaryotic cells, with a vesicle being a subcellular structure that encloses part of the cytosol within a limiting bilayer lipidic membrane (Colombo et al., 2014). EVs have been classified according to their size and subcellular origin and they are broadly divided into three main categories: apoptotic bodies, microvesicles and exosomes (see Table 1). Apoptotic bodies are

membranous vesicles of large size (50-500 nm, up to 1 µm) released by apoptotic cells. Microvesicles (MVs) are thought to bud directly from the plasma membrane and fall in a similar size range to apoptotic bodies (100-500 nm, up to 1 µm). Exosomes are synthesised in the endosomal compartments (multivesicular bodies, MVBs) and have the smallest size (50-150 nm) (Colombo et al., 2014; Théry et al., 2009; Van Niel et al., 2018). A growing body of literature, however, has been refining this classification, adding subcategories to both exosomes and microvesicles, often depending on the cell type of origin (Théry et al., 2009).

Feature	Exosomes	Microvesicles	Apoptotic bodies
Size	50-150 nm	100-1000 nm	50-1000 nm
Density in sucrose	1.13-1.19 g/mL	ND	1.16-1.28 g/mL
Appearance by electron microscopy	Cup shape	Irregular shape and electron dense	Heterogeneous
Sedimentation	100,000 g	10,000 g	1200 g , 10,000 g or 100,000 g
Intracellular origin	Endosomes	Plasma membrane	ND

ND, not determined.

Table 1.1 Classification of the main types of extracellular vesicles. The table summarises the features commonly used for classification of EVs. Reported are the three most studied categories of EVs. Adapted from (Théry et al., 2009).

1.3.2 Biogenesis and secretion of extracellular vesicles

The two main categories of extracellular vesicles are microvesicles and exosomes, since apoptotic bodies belong to a different shedding process, induced by programmed cell death. Biogenesis of these two types of vesicles happens in topologically different sites within the cell, despite there being an overlap in sorting machineries (Van Niel et al., 2018). As previously mentioned, microvesicles generate from outward budding of the plasma membrane, whereas exosomes are

first synthesised in intraluminal structures within the MVBs and then the MVBs fuse with the plasma membrane to release exosomes in the extracellular milieu (Colombo et al., 2014). In some cases the nomenclature may be misleading according to the cell type analysed. For example, T cells primarily generate EVs with the characteristics of exosomes, directly budded from the cell surface (Booth et al., 2006).

1.3.2.1 Biogenesis and secretion of exosomes

Biogenesis of exosomes happens in the multivesicular bodies (MVBs, also called late endosomes, LE). MVBs are integral part of the endocytic pathway, which consists of highly dynamic membrane structures involved in the internalisation of extracellular ligands or cellular components, their degradation and/or recycling to the plasma membrane (Klumperman et al., 2014). Early endosomes mature into MVB/LE and during this process they generate intraluminal vesicles (ILVs) (Stoorvogel et al., 1991). ILVs are formed by inward budding of the limiting membrane of endosomes with subsequent sequestering of cytosol, enriched with specifically sorted cellular components. Interestingly, at this stage MVBs can either fuse with lysosomes, to degrade the ILV cargo, or with the plasma membrane and thus release the ILVs, at this point called exosomes, in the extracellular milieu. It is thus apparent that different subpopulations of MVBs will exist in the cell, which redirect their cargo either for degradation or secretion (Van Niel et al., 2018).

The molecular mechanisms involved in exosome biogenesis have been classified as ESCRT dependent or independent. The ESCRT machinery (Endosomal Sorting Complex Required for Transport) is a key regulator of membrane shaping and scission, thus it is also a major player in the biogenesis of MVBs and ILVs

(Schmidt et al., 2012). The ESCRT is composed of four complexes (ESCRT-0, -I, -II and –III, see Fig. 1.1) with associated proteins (Alix, VPS4, VTA1), conserved from yeast to mammals (Hanson et al., 2012). The complexes act in an orchestrated manner. ESCRT-0, a 1:1 heterodimer of HRS:STAM proteins in mammals, binds to enriched PI3P moieties on the MVBs membrane where it recognises and sequesters ubiquitinated cargo. ESCRT-I is a hetero-tetramer consisting of TSG101, VPS37A-D, VPS28 and MVB12A/B or UBAP1, with the last two partners being selectively involved in viral budding or MVB sorting (Stefani et al., 2011). ESCRT-I, recruited by ESCRT-0, forms a rod-shaped complex that interacts with ESCRT-0 and ubiquitinated cargo on one end, and ESCRT-II on the other end. ESCRT-II is formed by a hetero-tetramer of EAP45 (VPS36), EAP30 (VPS22) and two molecules of EAP20 (VPS25). Via EAP45, ESCRT-II can interact with ESCRT-I, cargo and PI3P. Whereas the first three complexes normally exist in an assembled state in the cytosol, recruitment of ESCRT-III happens transiently after ESCRT-II and it drives inward budding of the endosomal membrane, with formation of a vesicle. ESCRT-III is made of four core subunits, CHMP6, CHMP4A-C, CHMP3 and CHMP2A-B.

Finally, the AAA-ATPase VPS4 disassembles ESCRT-III, terminating each round of MVB cargo sorting and vesicle formation (Hanson et al., 2012; Schmidt et al., 2012). Several accessory proteins are involved in this process, such as Alix, an interacting partner of ESCRT-I, often found in exosome preparations (Colombo et al., 2014; Théry et al., 2009).

Given the prominent role that the ESCRT machinery plays in ILV biogenesis, depletion of ESCRT components revealed a robust method to impair exosomes biogenesis (Colombo et al., 2013; Théry et al., 2001).

However, other players have now been uncovered in this pathway (see Fig. 1.2). For instance, Alix has been shown to cooperate with syntenin and syndecan in modulating exosome synthesis (Baietti et al., 2012). The tetraspanin CD63 has also been shown to regulate ESCRT-independent endosomal sorting in melanocytes (van Niel et al., 2011). Other tetraspanins, such as CD81, CD82, CD9 are directly involved in cargo sorting to exosomes (Buschow et al., 2009; Chairoungdua et al., 2010). Interestingly, a protein-free biogenesis mechanism has been discovered in oligodendroglial cells which requires the presence of the lipid ceramide (Trajkovic et al., 2008). Chemical inhibition of ceramide synthesis has thus become a standardised method for inhibiting exosome synthesis (D. Hoshino et al., 2013; Trajkovic et al., 2008; Willms et al., 2016).

Once ILVs are synthesised, MVBs are routed either to the lysosome or towards the plasma membrane. A balance between degrading and secreting events is required, at this stage, and potentially sorting partners and cargo modifications play a pivotal role in deciding the fate of each MVB.

In regard to the trafficking of MVBs and fusion with the plasma membrane, the Rab family of GTPases plays a prominent role. Rabs are proteins involved in endosomal sorting, with each family member having a specific function in different endosomal structures (Wandinger-Ness et al., 2014). Among Rabs, Rab7 has been involved in exosome release, with its depletion severely impairing this process (Baietti et al., 2012). Rab27a and Rab27b are also essential for exosome secretion (Bobrie et al., 2012; Ostrowski et al., 2010). Specifically, Rab27b modulates the motility of MVBs towards the plasma membrane and both Rab27 isoforms regulate MVB docking and fusion to the cell membrane.

Other Rabs, such as Rab35 and Rab11, have been described as modulators of exosome release, Rab35 possibly with a function in membrane tethering (Hsu et al., 2010; Savina et al., 2002).

The final steps that lead to MVB fusion to the plasma membrane are still largely unknown, with SNARE and synaptotagmin proteins as likely candidates for fusion events (Jahn et al., 2006).

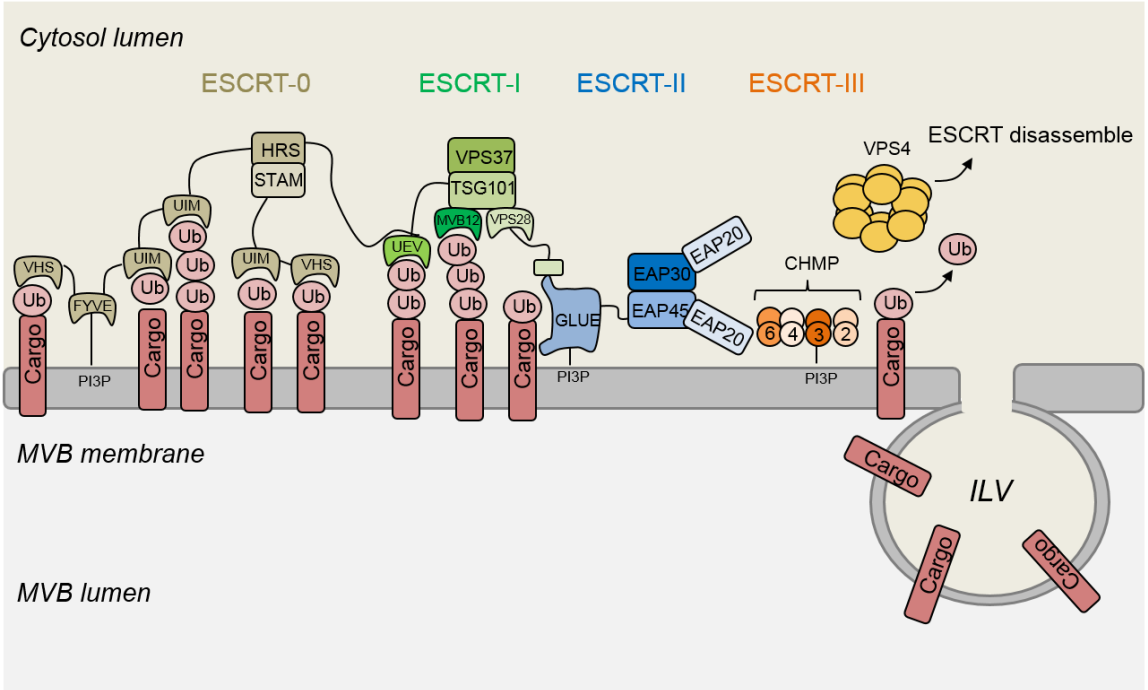


Figure 1.1 The ESCRT machinery. Schematic representation of the ESCRT components in mammalian cells. The four complexes are recruited to endosomes by interaction with membranes, ubiquitinated cargo and with each other. All of the ESCRTs except ESCRT-III recognise and bind the ubiquitinated cargo, either through a ubiquitin-interacting motif (UIM) (ESCRT-0), a ubiquitin E2 variant (UEV) domain (ESCRT-I) or the GLUE domain of VPS36/EAP45 (ESCRT-II). ESCRT-III orchestrates the last steps of the pathway in which ubiquitin is removed by a de-ubiquitinase (Doa4, not shown), and the complexes are disassembled by the AAA-ATPase VPS4. Budding away from the cytosol is facilitated by a curvature-inducing factor that could flex the membrane by being localised to the neck of the budding vesicle (not shown). Ub, ubiquitin; MVB, multivesicular body; ILV, intraluminal vesicle.

1.3.2.2 Biogenesis and secretion of microvesicles

Given the localisation of microvesicles (MVs) on the cell plasma membrane, biogenesis and secretion are in this case overlapping processes (see Fig. 1.2).

Moreover, an interplay between the formation of MVs and other plasma membrane derived structures (such as invadopodia) appears to take place. The family of Rho GTPases are key players in regulation of membrane dynamics (Anne J. Ridley, 2006). Two family members, RhoA and Rac1, have been linked to MV regulation. RhoA is thought to promote MV formation and shedding, in association with amoeboid mode of invasion, whereas Rac1 appears to antagonise this event, promoting invadopodia formation instead (Sedgwick et al., 2015). Another small GTPase, Arf6, has been also shown to be involved in MV shedding from tumour cells, in an ERK dependent manner (Muralidharan-Chari et al., 2009). In both cases, downstream activation of myosin light chain triggers membrane remodelling and MV budding. In another study on cancer cells, the v-SNARE VAMP3 has been found to regulate, in association with CD9, the delivery of cargo to nascent MVs (Clancy et al., 2015).

Notably, as for exosomes, lipids also contribute to formation of these structures, with cholesterol-rich domains on the membrane playing an important role in MV shedding (Al-Nedawi et al., 2008; del Conde et al., 2005). Moreover, studies in blood cells have defined an orchestrated activity of several enzymatic machineries (scramblase, flippase, floppase, calpain, aminophopsholipid translocase) for the regulation of cell membrane phospholipid asymmetry and thus for MV budding (Piccin et al., 2007).

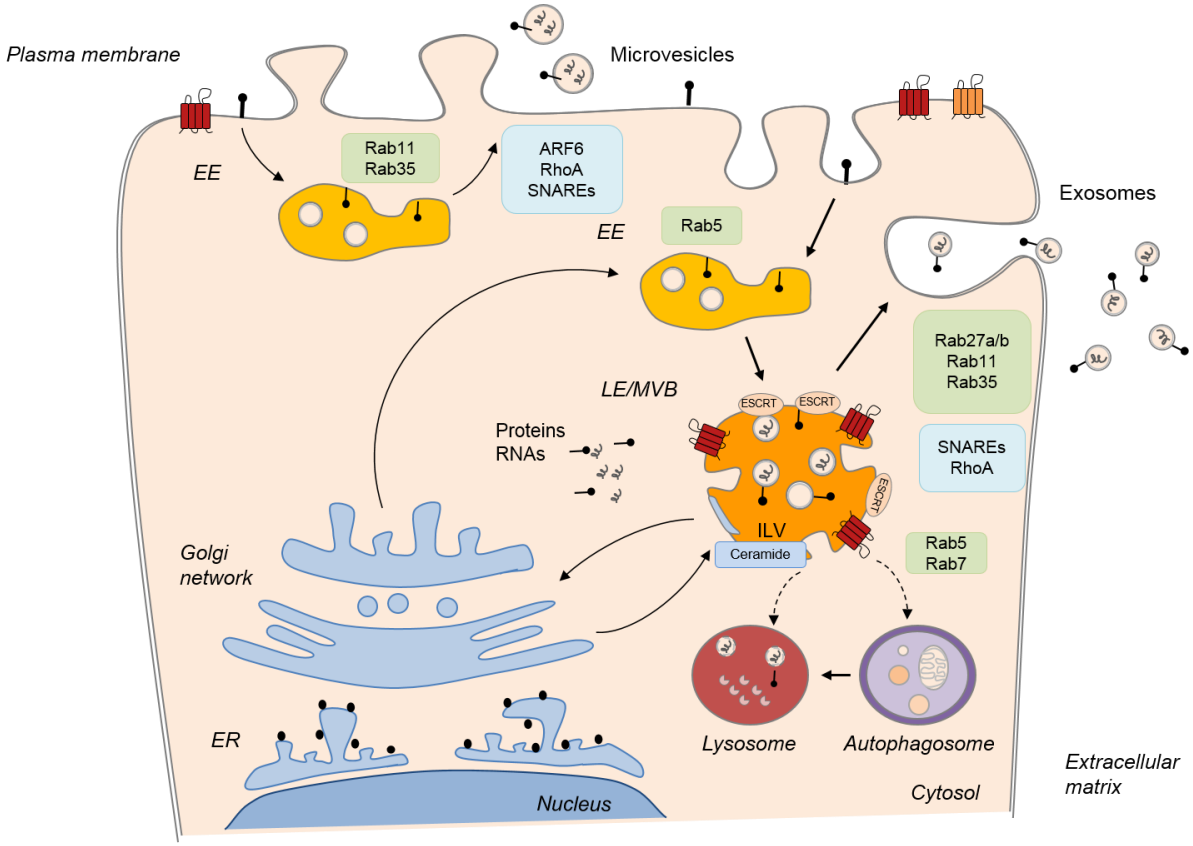


Figure 1.2 EV biogenesis and secretion. Cartoon representing a simplified model of cellular compartments and main protein players involved in biogenesis and secretion of both exosomes and microvesicles. Cargo targeted to MVBs originates from endocytosis at the plasma membrane or is directly targeted to MVBs or to early sorting endosomes via the biosynthetic pathway (from the trans-Golgi network, TGN). Retrograde transport from the MVBs to the TGN will divert cargo from its targeting to the MVBs (black arrows). These sorting processes are mostly regulated by Rab GTPases. Once matured, MVBs that are not targeted to the lysosomes or the autophagosomes for degradation (dashed arrows), will be routed towards the plasma membrane. Here, docking and fusion are the two final processes required for exosome release. Rabs, actin and SNARE proteins are involved in these steps. In regard to microvesicle biogenesis, the events are considered faster than for exosomes, given the localisation of MVs at the plasma membrane, with involvement mostly of early endosomal Rabs and other GTPases. Rabs involved in the illustrated processes are pictured in green, ESCRT in pink, other proteins in blue panels, tetraspanins are represented as red and orange transmembrane proteins. Ceramide is also pictured on MVBs, given its involvement in membrane curvature processes during ILV formation.

1.3.3 Cargo characteristics

The cargo of extracellular vesicles appears to be extremely heterogeneous, including proteins, DNA, mRNA, miRNA and lipids, as shown in Fig. 1.3 (Colombo et al., 2014; Van Niel et al., 2018).

Because of the limitations in isolation methods (see Introduction to Chapter 3), often the isolation of EVs leads to co-purification of different subtypes. For this

reason and for the shared processes in exosome and microvesicle sorting and trafficking, it is difficult to establish which proteins are mostly associated to one class or the other, making it hard to define markers of exosomes and microvesicles (Witwer et al., 2017).

The literature so far has been mainly exploring the protein cargo present on EVs. The nature and abundance of EV protein cargo is strictly dependent on the cell of origin, an observation that reiterates the difficulty in finding reproducible markers. Importantly, post-translational modifications, such as ubiquitination, phosphorylation, glycosylation and SUMOylation on the cargo are strong drivers of cargo sorting into different MVBs, including the ones en route for exocytosis (Moreno-Gonzalo et al., 2014).

Major representatives in protein cargo are biogenesis and secretion factors. Proteins that have been found to regulate EVs are often found in vesicle preparations. Among them, there are Alix, TSG101, syntenin, Rabs and Rho GTPases. As membrane organisers and to some extent EV modulators, also tetraspanins are highly enriched in EVs, with CD63, CD81 and CD9 being the most widely used as markers. In addition to these proteins, signal transduction factors (β-catenin, protein kinases), chaperones (HSP70, HSP90), enzymes, adhesion molecules (integrins, fibronectin), other transmembrane proteins (flotillin-1 and -2, LAMPs), cytoskeleton components (actin, tubulin) have been purified in EVs.

The first evidence of genetic material found in EVs was miRNA and mRNA in exosomes released by mast cells (Valadi et al., 2007) and in microvesicles derived from stem cells (Ratajczak et al., 2006). More recently DNA has also been found in EVs, both single and double stranded (Balaj et al., 2011; Kahlert et al., 2014;

Thakur et al., 2014). These observations raised the possibility that genetic information in EVs could be used as a potential circulating biomarker.

Fewer studies have been carried out on the lipidic composition of EVs. However, enrichment of glycosphingolipids, sphingomyelin, cholesterol and phosphatidylserine has been reported (Laulagnier et al., 2004; Llorente et al., 2013; Skotland et al., 2017; Wubbolts et al., 2003).

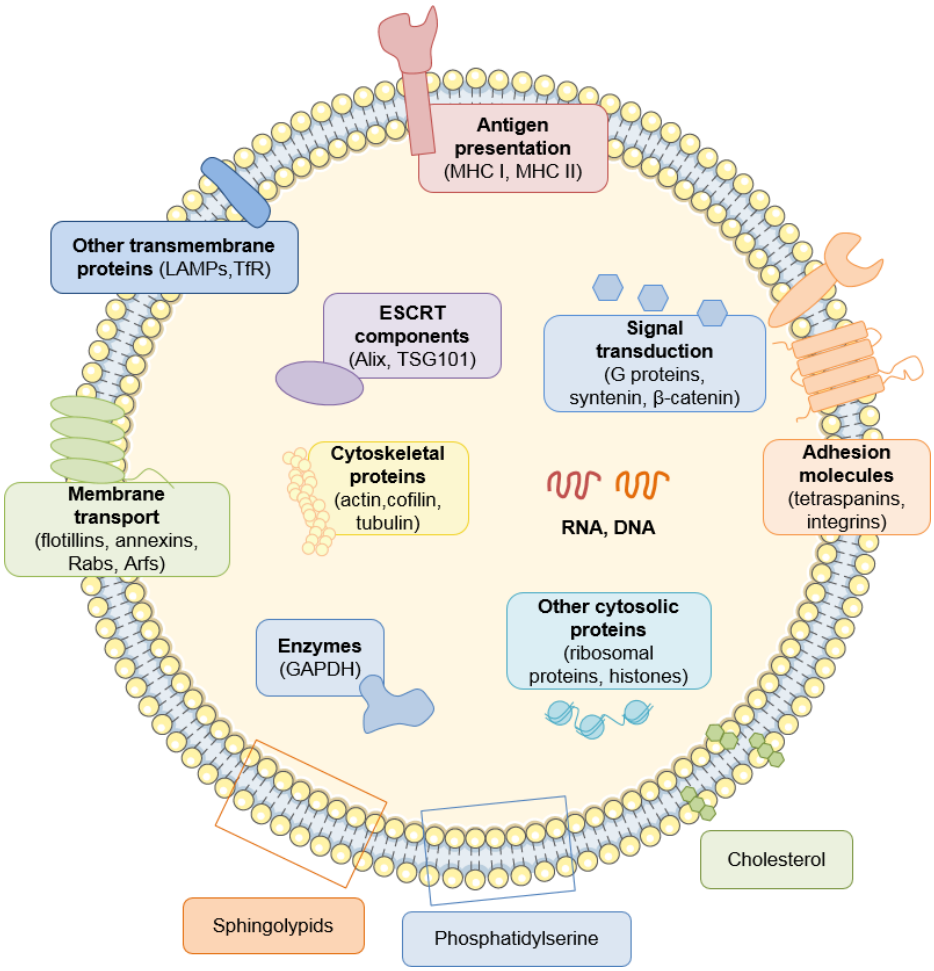


Figure 1.3 Cargo of extracellular vesicles. Graphical representation of the EV cargo (mostly referred to exosomes): proteins, lipids and nucleic acids. Adapted from (Colombo et al., 2014).

1.3.4 Extracellular vesicle uptake

Once released in the extracellular space, EVs are thought to target recipient cells to deliver their cargo and thus elicit functional responses. EV mediated intercellular communication requires docking to the plasma membrane of a recipient cell, followed by either vesicle internalisation (endocytosis) or fusion (Mulcahy et al., 2014). However, the modes of EV interaction with a recipient cell have not yet been fully explored.

Binding to the external leaflet of the plasma membrane may happen via surface interactions. In this process, adhesion molecules, integrins and tetraspanins have been shown to play a role (Morelli et al., 2004). Notably, integrins *in vivo* may direct exosomes to a certain tissue (A. Hoshino et al., 2015). Heparan sulphate proteoglycans and ECM components have also been described as modulators of EV uptake (Christianson et al., 2013; Purushothaman et al., 2016). In association with integrins or organised in micro-domains, tetraspanins mediate EV-cell interactions (Nazarenko et al., 2010; Rana et al., 2011). Furthermore, endocytosis processes have been described as most relevant for internalisation of EVs in recipient cells, with both clathrin dependent and independent processes taking place (Costa Verdera et al., 2017; Heusermann et al., 2016; Tian et al., 2014). Another route that has not been yet thoroughly explored is the lipid raft mediated uptake (Svensson et al., 2013).

1.3.5 Extracellular vesicle functions in cancer

The interest in studying EVs derives from their potential in transferring information from a donor to a recipient cell. For this reason, EVs have gained relevance in the study of both physiological and pathological processes. In cancer, tumour-secreted EVs have recently been included as an important feature of the

microenvironment surrounding solid tumours (Becker et al., 2016). Many studies have now reported how tumour EVs can influence neighbouring cells, by promoting invasive processes such as angiogenesis and fibroblast differentiation (Chowdhury et al., 2015a; Mineo et al., 2012; Sheldon et al., 2010; Webber et al., 2015); changing the fate of untransformed cells (Skog et al., 2008), or transferring oncogenic factors to less aggressive tumour cells (Al-Nedawi et al., 2008); and modulating immune surveillance (Chalmin et al., 2010; Plebanek et al., 2017; Zitvogel et al., 1998). All these processes happen in the primary tumour site, however, they pave the way for a more extensive response: the stage of tumour dissemination (see Fig. 1.4).

Furthermore, EVs have been strongly associated with metastatic niche formation. Peinado et al. in a pioneering study showed that melanoma growth and metastatic burden were enhanced in mice that were transplanted with bone marrow (BM) progenitors that had previously been exposed to metastatic melanoma exosomes, in a process termed “education”. Moreover, the proto-oncogene Met was identified as up-regulated in metastatic melanoma cell lines and horizontal transfer of Met from melanoma exosomes to BM cells was the key factor in promoting BM cell mobilisation and, ultimately, metastasis formation. (Peinado et al., 2012). A subsequent study in pancreatic cancer revealed that the same process of pre-education of mice with murine PDAC-derived exosomes rendered the mice more susceptible to liver metastasis, when injected with murine PDAC cells. Moreover, the study unravelled the steps required for metastatic niche formation in the liver. In brief, PDAC-derived exosomes were taken up by Kupffer cells (KC) in the liver, where they horizontally transferred MIF. Exosomal MIF induced the release of TGF-β by Kupffer cells, which subsequently promoted fibronectin (FN)

deposition by hepatic stellate cells (hStCs), thus initiating a fibrotic process. Furthermore, FN deposition promoted the migration of bone marrow-derived macrophages and neutrophils to the liver, completing the formation of the pre-metastatic niche (Costa-Silva et al., 2015).

In another seminal study, EVs from malignant breast cancer cells have been shown to be internalised by less malignant tumour cells, both in close and in distant sites *in vivo*. Moreover, analysis of the EV mRNA cargo revealed enrichment in mRNAs involved in migratory pathways. The transfer of EVs derived from metastatic breast cancer cells to non-metastatic recipient cells *in vivo* suggested that EVs elicit migratory behaviour and enhance metastatic capacity in recipient cells (Zomer et al., 2015). Notably, EV communication is bilateral, with cancer associated fibroblasts being able to promote breast cancer cell migration and metastatic spread *in vivo* via release of EVs (Luga et al., 2012; Richards et al., 2017). A compelling study has also proposed an organotropic role for exosomes, where tumour-derived exosomes internalised by organ-specific cells initiate pre-metastatic niche formation. Specifically, a defined integrin pattern within the exosomal cargo directs the vesicles to a certain cell type within the designated organ. The study uncovered $\alpha_6\beta_4$ and $\alpha_6\beta_1$ integrins on breast cancer exosomes as responsible for creating metastatic sites in the lung, particularly mediating the uptake of exosomes by $S100A4^+$ fibroblasts and surfactant protein C $(SPC)^+$ epithelial cells in the lung parenchyma. Similarly, expression of $\alpha_v\beta_5$ on pancreatic cancer exosomes promoted liver metastasis via fusion of the exosomes with Kupffer cells (A. Hoshino et al., 2015).

Taken together, this evidence from the literature extensively describes the great potential of extracellular vesicles in leading the main stages of tumour spread.

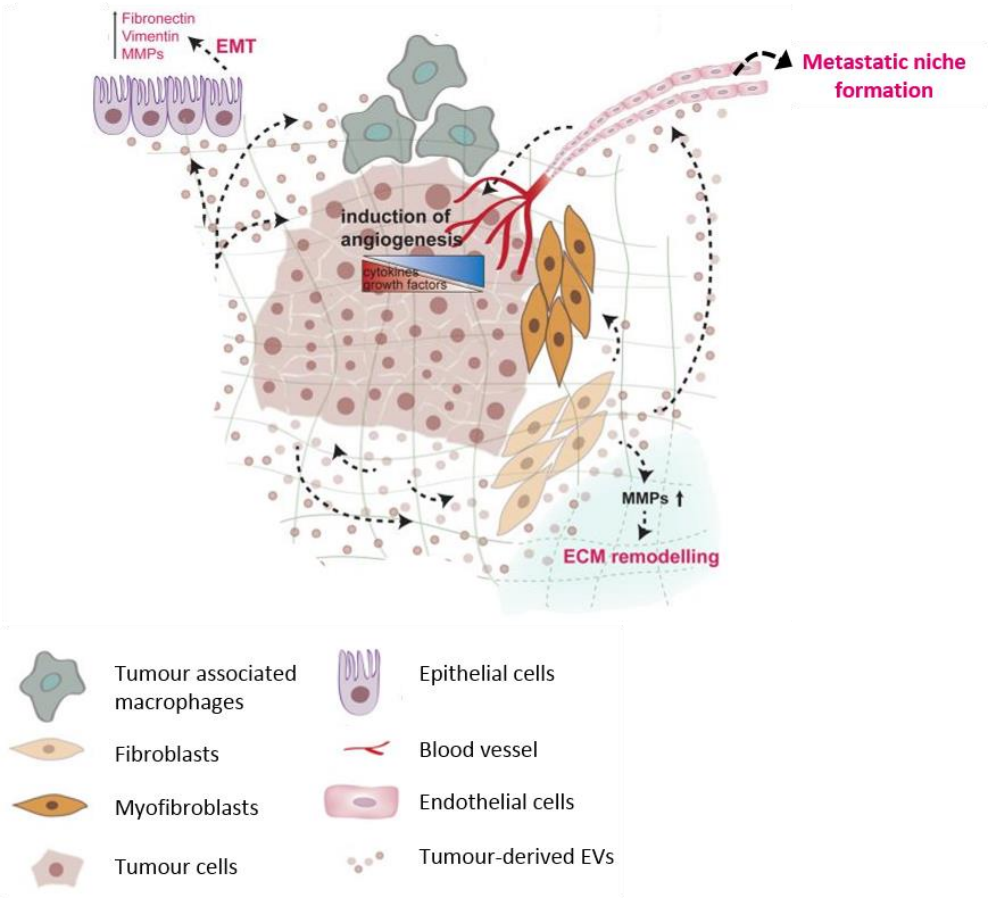


Figure 1.4 EVs are mediators of intercellular communication within the tumour microenvironment. Mostly regarded as a tumour promoting feature, EVs have an increasing importance in the crosstalk between the tumour and the neighbouring cells as well as the infiltrated immune cells. The cartoon depicts a simplified view on the role of tumour EVs in fibroblast to myofibroblast differentiation, with the consequent release of MMPs and ECM breakdown. Tumour EVs also activate tumour-associated macrophages to secrete growth factors which together promote angiogenesis and create an inflammatory niche. Furthermore, tumour EVs affect immune system homeostasis mostly by triggering immunosuppressive changes that protect the tumour (EV crosstalk with the immune system not shown). As the tumour grows, it develops metabolic demands that outgrow its blood supply and thus becomes increasingly hypoxic. In response to low oxygen concentrations, the tumour secrets angiogenic factors and EVs that promote blood vessel sprouting. EVs derived from the primary tumour can stimulate epithelial cells to release factors involved in EMT that trigger the loss of tumour cell adhesion, ECM remodelling and angiogenesis, which together eventually promote the release of tumour cells into distant sites. Adapted from (Becker et al., 2016).

1.4 Growth Factors

Under physiological conditions, cells receive fate-determining signals from their surroundings, mostly in the form of polypeptide growth factors. The capacity of cells to integrate these extracellular signals, through activation of intracellular signalling cascades, governs homeostasis. Growth factors are thus potent

modulators of the microenvironment in development, homeostasis, wound-healing, infection and disease (Aaronson, 1991).

First evidence of a link between soluble growth factors and cancer emerged from *in vivo* studies of mouse sarcomas transplanted onto chick embryos, where they prompted an exceptional outgrowth of nerve fibres (Cohen et al., 1954). This phenomenon was later explained with the isolation of the first two growth factors: nerve growth factor (NGF) and epidermal growth factor (EGF) (Cohen, 1960, 1962). Interestingly, in cancer, growth factor signalling is often altered and oncogenes may function as growth factor substitutes to elicit autocrine signalling within the tumour (Aaronson, 1991). Despite genetic mutations being at the basis of malignant transformation, the presence of altered growth factor signalling facilitates clonal expansion, accelerates intraepithelial proliferation and promotes invasive growth (Witsch et al., 2010).

1.4.1 Transforming Growth Factor β superfamily

Transforming growth factor β (TGF-β) was first isolated from murine sarcomas along with TGF-α and its ability to stimulate colony formation appeared to be enhanced by the presence of EGF (Roberts et al., 1982). Since then, the discovery of key steps in the TGF-β signalling cascade, from the Serine/Threonine kinase membrane receptors to SMAD (Mothers Against Decapentaplegic Homolog) transcription factors, has allowed the identification of a complex process of conversion of signals to gene activation and repression programmes. The pathway is evolutionarily conserved in metazoans and regulates cell fate and development, wound healing and tissue homeostasis, among other processes (Massagué et al., 2006). The TGF-β superfamily of growth factors includes several subfamilies of ubiquitous factors, largely classified in two subgroups: the

TGFβ-like, namely TGF-βs, activins, nodals and some growth and differentiation factors (GDFs); and the Bone Morphogenetic Proteins BMP-like group, composed of BMPs, anti-Mullerian hormone (AMH) and most GDFs. At the cellular level, the members of the family regulate cell proliferation and differentiation, death, cytoskeleton dynamics, epithelial to mesenchymal transition (EMT), migration and invasion (Weiss et al., 2013). Given its ubiquitous activity, aberrant TGF-β superfamily signalling is associated with a broad range of human pathologies including autoimmune, cardiovascular and fibrotic diseases as well as cancer.

1.4.2 TGF-β signalling cascade

Ligands and precursors

The subfamily of TGF-β ligands is comprised of three isoforms, TGF-β1, 2 and 3. The three isoforms share high similarity (71%-76% identity) and signal through the same downstream cascade, however, they present different affinity for the TGF-β receptors (Wrana et al., 1992) and they diverge in physiological roles (Laverty et al., 2009; Massagué et al., 1990). Among all three, TGF-β1 is the most abundant in tissues and well characterised isoform (hereafter referred to as TGF-β).

TGF-β is synthesised as a homodimeric pro-protein, with a dimeric pro-peptide of 65-75 KDa on the N-terminal, called latency associated peptide (LAP), and the mature TGF-β 24 KDa dimer, on the C-terminal. The LAP is also covalently bound to a latent TGF-β binding protein (LTBP), and the complex in this state is called large latent complex (LLC). Mature TGF-β is cleaved from the LAP by furin-like enzymes in the trans-Golgi, but the complex remains strongly associated via non-covalent interactions. The LLC is then secreted from the cell to the extracellular milieu, where the LTBP binds to extracellular matrix fibres. In this form, large reservoirs of latent TGF-β are secreted in the extracellular space and

stored prior to activation (Annes et al., 2003; Hayashi et al., 2012; Robertson et al., 2015).

TGF-β receptors

When the mature TGF-β dimer is activated, due to degradation of the latency complex by proteases, other factors or due to mechanical force, the soluble ligand is able to bind to its receptor and initiate an intracellular cascade (Robertson et al., 2015). Vertebrates have five type II and seven type I receptors and of them many pair up in different combinations to mediate signals from all TGF-β superfamily members (Weiss et al., 2013). In the case of TGF-β1 the receptors are TGFβRI and II, two transmembrane Serine/Threonine kinases. To initiate the cascade, the soluble ligand dimer binds to a homodimer of TGFβRII, a constitutively active kinase (Fig. 1.5). Binding of the growth factor to TGFβRII allows the recruitment of a homodimer of TGFβRI, which gets subsequently phosphorylated by TGFβRII at a Glycine-Serine (GS) rich domain upstream of the TGFβRI kinase domain. The phosphorylated residues in TGFβRI then promote its kinase activity (Y. Shi et al., 2003). Activated TGFβRI further propagates the signal through phosphorylation of the downstream effectors, SMAD proteins. The transmembrane proteoglycan betaglycan, also called TGFβRIII, has been identified as a co-receptor, required for ligand presentation to TGFβRII (López-Casillas et al., 1993).

Modulation of signalling at the receptor level is achieved via receptor association to ancillary proteins and further internalisation in endocytic structures. Receptor internalisation, via clathrin-mediated endocytosis, in early endosomes and interaction with the SMAD anchor protein, SARA, propagates TGF-β signalling. Conversely, internalisation mediated by caveolae and lipid rafts supports receptor interaction with the inhibitory SMAD, SMAD7, and subsequent targeting for

degradation via recruitment of the E3 ubiquitin ligases SMURF1 and SMURF2 (Di Guglielmo et al., 2003; Inoue et al., 2008).

SMADs

SMADs are well conserved intracellular mediators that can be divided into three classes: receptor SMADs (R-SMADs), in TGF-β signalling SMAD2 and SMAD3; co-SMAD, SMAD4, a common mediator to both TGFβ-like and BMP-like families; and inhibitory SMADs (I-SMADs), SMAD7 for TGF-β.

R-SMADs and SMAD4 share two Mad-homology domains, MH1 and MH2, coupled by a linker. The MH1 domain contains a β hairpin structure with DNA-binding ability. Interestingly, the most abundant variant of SMAD2 in vertebrates contains an insert in the vicinity of the β hairpin that prevents its binding to DNA. The MH2 domain mediates versatile interactions with cytoplasmic adaptor proteins, activated TGF-β receptors and various DNA-binding partners.

I-SMADs have a divergent MH1 domain and a conserved MH2 domain, important for receptor interaction (Y. Shi et al., 2003).

Once active, TGFβRI phosphorylates two Ser residues within a (S)SXS motif at the C-terminal end of R-SMADs. This allows the formation of a heterotrimeric complex of R-SMADs and SMAD4 (see Fig. 1.5). Activated SMAD complexes then translocate to the nucleus and, in conjunction with other nuclear co-factors, regulate the transcription of target genes (Weiss et al., 2013).

Several signals contribute to cessation of SMAD signalling. Phosphatases, such as PPM1A, PP2A or MTMR4, can dephosphorylate R-SMADs, either in the cytoplasm or in the nucleus, and terminate their activity (Heikkinen et al., 2010; Lin et al., 2006; Wrighton et al., 2008; J. Yu et al., 2010). Similarly to the receptors, R-SMADs can also be ubiquitinated and targeted for degradation. Ultimately,

nuclear shuttling as well as nuclear and cytoplasmic retention factors are a major force in controlling SMAD subcellular localisation, hence activity (L. Xu, 2006).

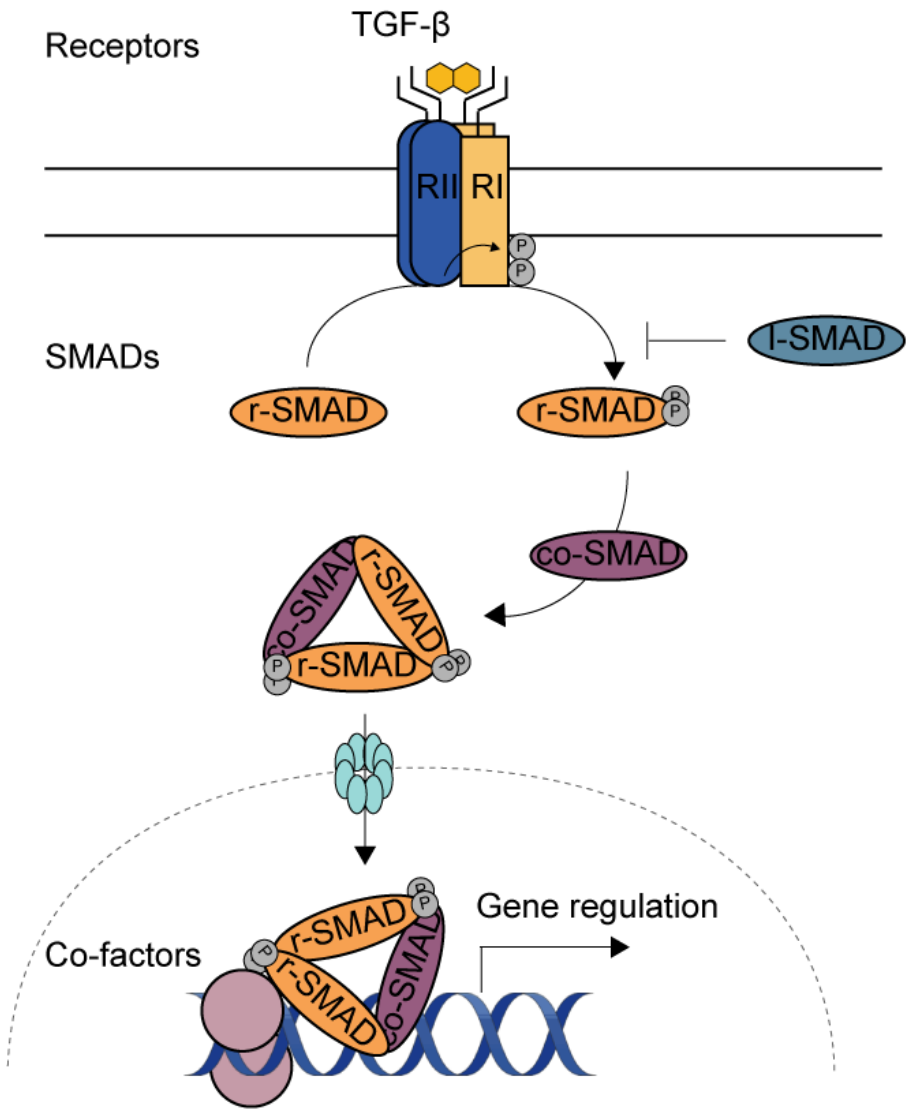


Figure 1.5 Canonical TGF-β signalling. Schematic representation of the fundamental steps involved in the TGF-β cascade. The active ligand dimer binds the TGFβRII homodimer. Active TGFβRII then phosphorylates TGFβRI with subsequent activation of its kinase domain. Active TGFβRI phosphorylates R-SMADs (SMAD2 and SMAD3) at two conserved Ser residues (Ser 465/467 for SMAD2 and Ser 423/425 for SMAD3). Active R-SMADs associate with co-SMAD in trimeric complexes and translocate to the nucleus to activate or repress target gene transcription. The I-SMAD, SMAD7, is one of the transcribed genes upon TGF-β signalling initiation and it starts a negative feedback loop by targeting R-SMADs for degradation.

Transcriptional programme

Once in the nucleus, SMADs can recognise the DNA sequence CAGAC and certain G+C-rich sequences, but have a low affinity for DNA. High affinity is only achieved by association with partner DNA-binding co-factors. The versatility of SMAD complexes binding to co-factors, as well as co-activators and co-repressors, is at the basis of specific TGF-β gene responses. Tissue specificity and environmental cues add layers of complexity to the gene response. (Massagué, 2000).

Non-canonical TGF-β signalling

SMAD signalling is ubiquitous and controls TGF-β transcriptional responses, however, non-SMAD signalling events elicited by TGF-β have also been reported. Among the SMAD-independent pathways are MAPK, PI3K and small GTPases pathways. One of the most relevant non-canonical TGF-β pathways is the activation of various branches of the MAPK pathway (namely ERK, JNK, p38). TGF-β receptors have a dual specificity in phosphorylating not only Ser/Thr but also Tyr residues. This specificity is important for the recruitment of SH2-domain proteins or the MAPK kinase TAK1 and ultimately for activation of MAPK cascades (Mu et al., 2012).

TGF-β activation of PI3K elicits the AKT-mTORC axis, which controls cell metabolism and growth. Moreover, TGF-β mediated EMT is at least partially controlled by this axis, through the regulation of protein translation and cell invasion (Lamouille et al., 2011).

TGF-β control on cytoskeleton remodelling is possible via a non-canonical interaction with the Rho family of small GTPases. TGF-β requires both Cdc42 and RhoA to mobilise the actin cytoskeleton and contribute to regulation of cell

adhesion (Bhowmick et al., 2001; Edlund et al., 2002). These steps may be critical in promoting one of the most studied processes driven by TGF-β, EMT (Ozdamar et al., 2005).

1.4.3 TGF-β in cancer

TGF-β pathway is a known tumour suppressor pathway in the early stages of cancer. However, some cancer cells commonly accumulate inactivating mutations at the level of the TGF-β receptors and SMAD proteins, to circumvent tumour-suppressive effects. Biallelic inactivation of *TGFBRII* by mutations that truncate the receptor protein or inactivate its kinase domain are reported for ovarian, oesophageal, colon, gastric, biliary, pulmonary and head and neck carcinomas. Other mutations, such as frameshift and missense mutations, in the *TGFBRI* coding region are present in subsets of ovarian, oesophageal, head and neck cancers. Alterations in receptor expression can also occur at the epigenetic level, with decreased expression of *TGFBRI* or *TGFBRII* frequently reported in lung, gastric, prostate and bladder cancers (Levy et al., 2006).

R-SMADs mutations are infrequent in cancer. In contrast, *SMAD4* is a notable target of inactivation, with *SMAD4* mutations present in more than 50% of pancreatic carcinomas and to a lower extent in other cancers (Hahn et al., 1996; Levy et al., 2006). The most frequent mutations generate a truncated SMAD4 variant that is unstable or unable to bind other SMADs.

The frequent disruption of TGF-β receptors and of SMAD4 in cancer reflects the relevance of the tumour suppressive function of these pathway components. However, these roles are highly contextual, depending on tissue specificity and stage of the tumour. The important role of TGFβRs and SMAD4 in constraining

cellular growth becomes apparent in the acceleration of neoplastic lesions initiated by oncogenic stimuli, in TGFβR o SMAD4 deficient systems.

As a tumour suppressor pathway TGF-β is involved in maintaining cytostasis, via activation of CDKs inhibitors and suppression of the oncogene c-Myc (see TGF-β functions in cancer in Fig. 1.6). According to cell type, different CDK inhibitors are induced by the TGF-β cytostatic response, all leading to a G1 phase arrest of cell cycle (Massagué, 2008). Another tumour suppressive feature of TGF-β is the induction of apoptosis, via SMAD-dependent and independent mechanisms (David et al., 2016; Pardali et al., 2007). Additionally, TGF-β controls stimuli from the microenvironment. Mitogens derived from stromal fibroblasts are readily inhibited by the pathway, and *TGFBRII* deletion in fibroblasts results in hyperplasia and neoplasia (Bhowmick et al., 2004). Finally, TGF-β is a key suppressor of cancer destructive immune and inflammatory reactions (Massagué, 2008).

Interestingly, while TGF-β acts as a tumour suppressor in normal cells and early carcinomas, its cytostatic effects are often lost during the progression of the disease. Indeed, many advanced cancers become resistant to TGF-β tumour suppressive functions, due to genetic and epigenetic alterations to components of the pathway or due to activation of pro-oncogenic signalling pathways.

Probably the most important tumourigenic function of TGF-β is the initiation of epithelial to mesenchymal transition (EMT). This process is a well-orchestrated event during embryonic development and a pathological feature of neoplasia (Thiery et al., 2009). Cells undergoing EMT lose expression of epithelial markers (E-cadherin, ZO-1, occludin, claudin, cytokeratins 8, 18, and 19, desmoplakin), gain mesenchymal ones (N-cadherin, vimentin, fibronectin, tenascin-C and vitronectin) and adopt morphological features that allow enhanced motility and

invasive capacity. TGF-β driven EMT is well documented in cancer and results in loss of polarity and adhesion, associated with increased migration and invasion (Massagué, 2008). Moreover, TGF-β acts on the tumour environment, for instance by converting fibroblasts to myofibroblasts, highly motile cells which retain features of smooth muscle cells and facilitate tumour progression via cell proliferation and neoangiogenesis. TGF-β also exerts immune evasion via repression of $CD8^+$ T-cells, deregulation of NK cells and promoting T-cell exclusion from the tumour site (Friese et al., 2004; Mehal et al., 2005; Thomas et al., 2005).

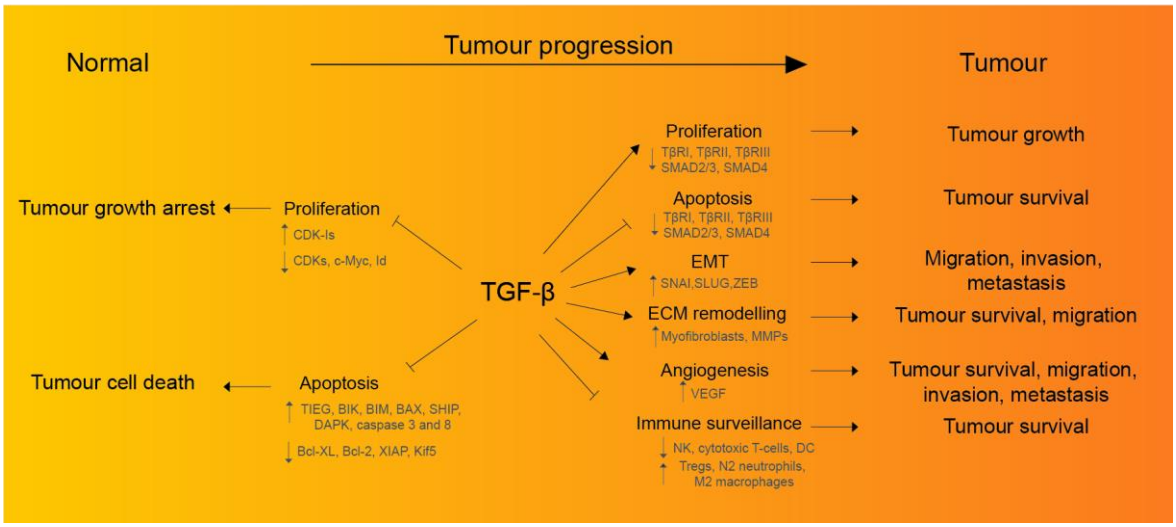


Figure 1.6 TGF-β dichotomous roles in cancer. TGF-β exerts both tumour suppressive functions via promoting cytostasis and apoptosis (represented on the left side of the schematics) as well as tumour promoting functions, such as, mediating epithelial to mesenchymal transition, proliferation, ECM remodelling, among others (summarised on the right side of the schematics). In dark grey the molecular players and cell types involved in both the tumour suppressive and the tumour promoting functions are listed. Adapted from (Huang et al., 2016).

1.4.4 TGF-β crosstalk with the Hippo pathway

Added complexity to the TGF-β pathway is given by the crosstalk with a plethora of other signalling cascades. Among other pathways, signal integration with the Hippo signalling cascade has been gaining interest, given the importance of both

pathways in tissue development and growth and given their deregulation in cancer.

The Hippo pathway was initially identified in *Drosophila*, but is well conserved in mammals and it controls tissue growth and organ size. Activation of the pathway, via cell-cell contact or epithelial cell polarisation, initiates a cascade comprising the core kinases MST1/2 (Hippo, Hpo in *Drosophila*), which phosphorylate the kinases LATS1/2 (Warts in *Drosophila*). Active LATS1/2 phosphorylate the Hippo effectors YAP/TAZ (Yorkie in *Drosophila*) on five different consensus HXRXXS motifs (Zhao et al., 2007). Phosphorylation at Ser 127 of YAP (Ser 89 for TAZ) creates a binding consensus for the adaptor protein 14-3-3, resulting in YAP/TAZ cytoplasmic retention and further proteasomal degradation (Zhao et al., 2010). In the absence of Hippo signalling, YAP/TAZ translocate to the nucleus and in complex with various DNA-binding factors, including TEADs (Scalloped in *Drosophila*) amongst others, promote transcription of numerous target genes involved in cell proliferation (see Fig. 1.7 for a simplified illustration of the Hippo pathway).

Of note, evidence of YAP nuclear translocation as a result of Hippo pathway activation has also been proposed. For instance, Hippo activation by proapoptotic signals results in LATS1 phosphorylation of YAP, subsequent YAP nuclear translocation and association to p73 to initiate transcription of proapoptotic genes (Matallanas et al., 2007).

Mutation of core components of the pathway in *Drosophila* such as Hpo, Warts and the adaptor proteins Salvador and Mats (respectively, Sav1 and Mob1 in mammals) lead to a strong overgrowth phenotype, characterised by increased proliferation and diminished cell death (F.-X. Yu et al., 2015).

Promiscuity in regulation of the effectors of the pathway, YAP/TAZ, has been shown for the Wnt and the TGF-β pathway (Attisano et al., 2013). Evidence for an interplay between the TGF-β and Hippo effectors has been reported both in development and in cancer. A complex of YAP/TAZ, SMADs and OCT4 has been found to regulate stem cell maintenance and loss of YAP/TAZ from this complex with further gain of the SMAD binding partner FOXH1 leads to mesendoderm specification (Beyer et al., 2013). It was also previously described how in human embryonic stem cells TAZ is required for pluripotency maintenance via interaction with SMAD complexes and control of their nuclear localisation (Varelas et al., 2008).

An important role for YAP/TAZ has been established as relays of mechano-transduction signals within the cell, in Hippo-dependent and -independent contexts. Numerous mechanical stimuli such as substrate stiffness, cell area, cell density and shear stress dictate YAP/TAZ nuclear/cytoplasmic localisation, thus enabling transcriptional responses that govern cell fate (Panciera et al., 2017). In human embryonic stem cells (hES), for instance, YAP/TAZ mechanic activation leads to self-renewal (Beyer et al., 2013). In mesenchymal stem cells (MSCs) cultured onto stiff ECM, expression of YAP/TAZ is promoted and it mediates MSC differentiation into osteoblasts; on soft ECM instead, YAP/TAZ activity is inhibited and this event re-programs MSCs into adipocytes (Dupont et al., 2011). In epithelial monolayers, mechanical forces regulate the cell proliferative ability through limiting YAP/TAZ activity. In high mechanical forces areas, YAP/TAZ signalling is active and cell proliferation is permitted; in low mechanical forces areas, such as high density clusters, YAP/TAZ activity, hence cell proliferation, is inhibited by cytoskeletal checkpoints (Aragona et al., 2013).

A key feature of the Hippo pathway is sensing of cell density information to regulate organ growth by sequestering in the cytoplasm its transcriptional co-factors YAP/TAZ. A higher regulation of TGF-β also occurs in this context, where YAP/TAZ are able to sequester effector SMADs, thus impairing TGF-β signalling (Varelas et al., 2010). Supporting the TGF-β/Hippo link, YAP interaction with SMAD proteins has also been shown to affect nuclear BMP signalling, inducing mouse stem cell self-renewal (Alarcón et al., 2009; Aragon et al., 2011).

Further evidence for a Hippo and TGF-β crosstalk has been reported in fibroblasts, in the mammary epithelium and in mesothelioma growth (Fujii et al., 2012; F. Liu et al., 2015; Y. Liu et al., 2017).

Similarly to development, YAP/TAZ interact with SMADs in breast cancer. Both effectors converge in regulating a TGF-β driven transcriptional programme and collaborate in driving a pro-tumourigenic phenotype (Hiemer et al., 2014).

So far, links between the two pathways have been made at the effectors (SMADs and YAP/TAZ) level. However, it has been recently reported that the Hippo scaffold and tumour suppressor RASSF1A is directly regulated by TGF-β. Namely, upon ligand stimulus, RASSF1A is recruited to the TGF-β receptor I, where is targeted for degradation by the co-recruited E3 ligase ITCH. Degradation of the RASSF1A allows YAP/SMAD2 nuclear localisation and the initiation of a TGF-β invasive programme (Pefani et al., 2016).

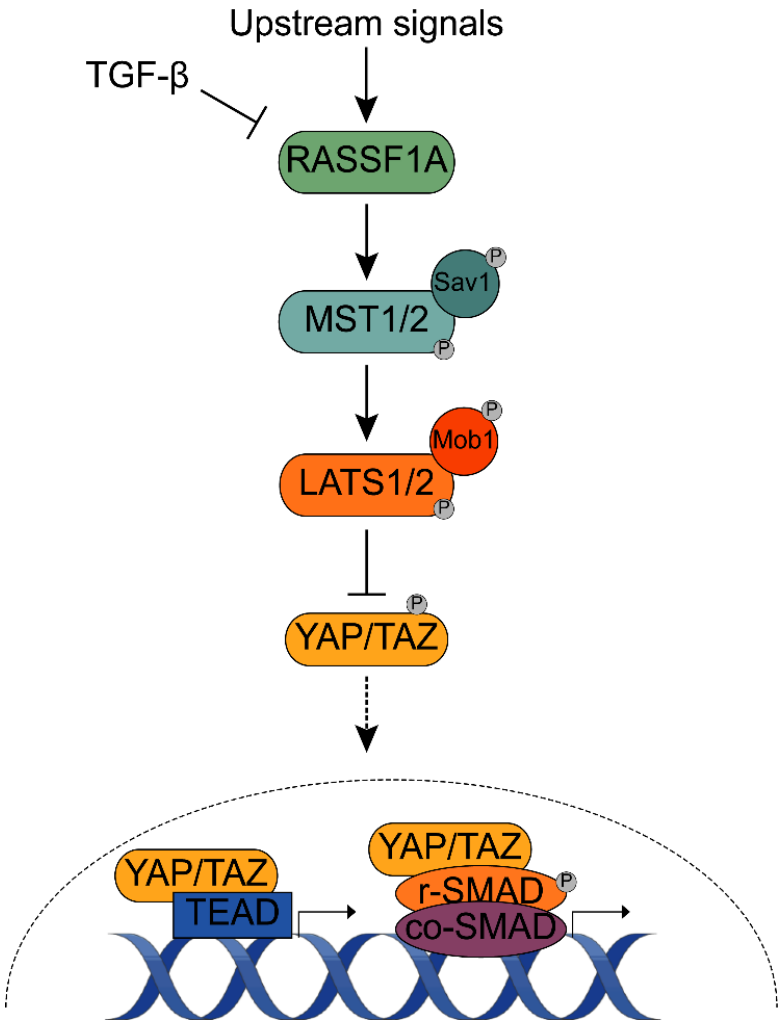


Figure 1.7 The Hippo pathway and TGF-β. Simplified representation of the core mammalian components of the Hippo pathway and one of the upstream regulators of the pathway, the scaffold RASSF1A. Upon external stimuli (such as cell density, stress) the Hippo cascade is activated and, in mammals, RASSF1A binds to and activate the MST1/2 kinases. Active MST1/2 phosphorylate LATS1/2 which in turn phosphorylate the effectors YAP/TAZ, creating a consensus sequence for 14-3-3 protein binding and thus driving YAP/TAZ cytoplasmic retention or further proteasomal degradation. When the Hippo pathway is inactive, YAP/TAZ are able to translocate to the nucleus, where they bind to several transcription factors (a main partner is the TEAD family). TGF-β is one of many upstream signals that converge on the Hippo cascade. As a consequence, YAP/TAZ can also associate to SMAD complexes to promote gene transcription.

1.4.4.1 The Hippo pathway tumour suppressor RASSF1A

The core Hippo signalling cascade is subject to several upstream regulators and adaptors, necessary to modulate the signal upon different stimuli, such as cell density, cell polarity, soluble factors and stress signals. One of the Hippo scaffolds is the tumour suppressor RASSF1A. In mammals, RASSF1A (Ras Association domain Family member 1) can bind to both MST1/2 and Sav1 and is a key

activator of the pathway (Donninger et al., 2011). RASSF1A is one of the 8 different isoforms that arise from the *RASSF1* gene at the 3p21.3 locus, a segment of the genome highly populated by tumour suppressor genes (Dammann et al., 2000; Hesson et al., 2007). RASSF1 belongs to a bigger family of 10 members (RASSF1-10) differentially implicated in physiological roles, of which many have been characterised as tumour suppressors (Volodko et al., 2014).

One of the first functions associated with RASSF1A was to bind and stabilise microtubules (Dallol et al., 2004; Rong et al., 2004; van der Weyden et al., 2005; Vos et al., 2004). This interaction was found to be crucial during mitosis, revealing an important tumour suppressive role of RASSF1A, which is limiting cell cycle progression (Donninger et al., 2014; Song et al., 2004).

RASSF1A exploits its tumour suppressor role with various other mechanisms: it regulates the Hippo pathway proapoptotic activity (Matallanas et al., 2011, 2007; Vos et al., 2006), it maintains genomic stability (Hamilton et al., 2009; Pefani et al., 2014, 2018) and restricts the cell cycle (Shivakumar et al., 2002; Thaler et al., 2009; Whang et al., 2005).

Interestingly, epigenetic inactivation, via methylation of the *RASSF1* promoter region, is infrequent in normal tissue, whereas it is one of the highest reported in the tumour tissue. Loss of expression of RASSF1A has been reported in breast, gastrointestinal and lung cancer, among others. High frequency of RASSF1A promoter methylation has also been associated with cancer pathogenesis and a more aggressive clinical phenotype (Grawenda et al., 2015; van der Weyden et al., 2007).

1.4.4.2 The *RASSF1* alternative transcript RASSF1C

RASSF1A is the most ubiquitously expressed and well characterised isoform of the *RASSF1* gene. Other isoforms are splicing variants of RASSF1A and tissue specific isoforms (RASSF1B-H). The second ubiquitously expressed transcript is RASSF1C. RASSF1C differs from RASSF1A for the absence of exon 1 (see Fig. 1.8 for isoform domains and functions). Transcription starts at exon 2γ and then continues with four terminal exons (from 3 to 6), shared with RASSF1A. This results in a smaller protein (270 amino acids for RASSF1C, comparing to 340 for RASSF1A), that lacks the N-terminal C1 domain, otherwise present in the tumour suppressor RASSF1A. An ATM phosphorylation site is conserved in both isoforms, as well as a Ras association (RA or RalGDS/AF-6) and a SARAH (Sav/RASSF/Hpo) domain. The RA domain mediates interactions with Ras and Ras-like small GTPases and the SARAH domain enables homodimerisation or binding to other components of the Hippo pathway (Bradley et al., 2018).

Conversely to RASSF1A, RASSF1C is expressed in many tumour types and does not show promoter hypermethylation (Burbee et al., 2001; Dammann et al., 2000).

Similarly to RASSF1A, RASSF1C has also been found to co-localise with and bind microtubules through the RA domain (Rong et al., 2004; Song et al., 2004; Vos et al., 2004). However, in the same studies, opposing results have been described for its role in stabilising these structures.

A function for RASSF1C in DNA damage has also been proposed. RASSF1C exerts a protective role against the destabilising effects of Ras mutant G12V (Vos et al., 2004); it has a proapoptotic effect in cells exposed to UV radiation or methyl methansulfonate (MSS)-induced DNA damage (Kitagawa et al., 2006); another proapoptotic role involves RASSF1C mediated sensitisation to cisplatin in ovarian

cancer cells that lack the expression of the oncogene CAS/CSE1L (Lorenzato et al., 2012).

An opposing study has showed that RASSF1C is degraded under stress conditions, after GSK3β phosphorylation and subsequent recognition of the phosphodegron by the E3 ligases Mule and $SCF^{\beta\text{-}TRCP}$. Inhibition of GSK3β phosphorylation by PI3K/AKT signalling upregulates RASSF1C (Zhou et al., 2012). Upregulation by AKT would suggest that RASSF1C could function as an oncogene. This hypothesis has been corroborated by many studies, with RASSF1C expression increasing proliferation in lung cancer cells, as well as migration in breast cancer cells (Amaar et al., 2006; Reeves et al., 2010, 2014). Genes that are activated downstream of RASSF1C also suggest an oncogenic profile for this protein. RASSF1C mediated upregulation of CXCR4 enhances breast cancer cell proliferation and metastasis (Reeves et al., 2010).

Notably, interplay between the two major isoforms RASSF1A and RASSF1C has been reported in breast cancer cells. In RASSF1A unmethylated cells, both isoforms compete for interaction with SRC, with RASSF1A binding inactive SRC and RASSF1C binding active SRC. In RASSF1A methylated cells, only RASSF1C remains expressed and it starts an invasive programme by targeting SRC to the cell plasma membrane to destabilise E-cadherin junctions. Moreover, RASSF1C promotes nuclear translocation of β-catenin and the Hippo effector YAP, resulting in YAP/β-catenin induced transcription of target genes and cell migration (Vlahov et al., 2015). RASSF1C mediated β-catenin nuclear accumulation and transactivation has also been shown in previous reports (Estrabaud et al., 2007).

Remarkably, a number of clinical studies supports the evidence of an oncogenic function for RASSF1C. RASSF1C expression is in fact upregulated in multiple

cancers, such as breast, pancreatic, endocrine and lung cancer (da Costa Prando et al., 2011; Malpeli et al., 2011; Pelosi et al., 2010; Volodko et al., 2016).

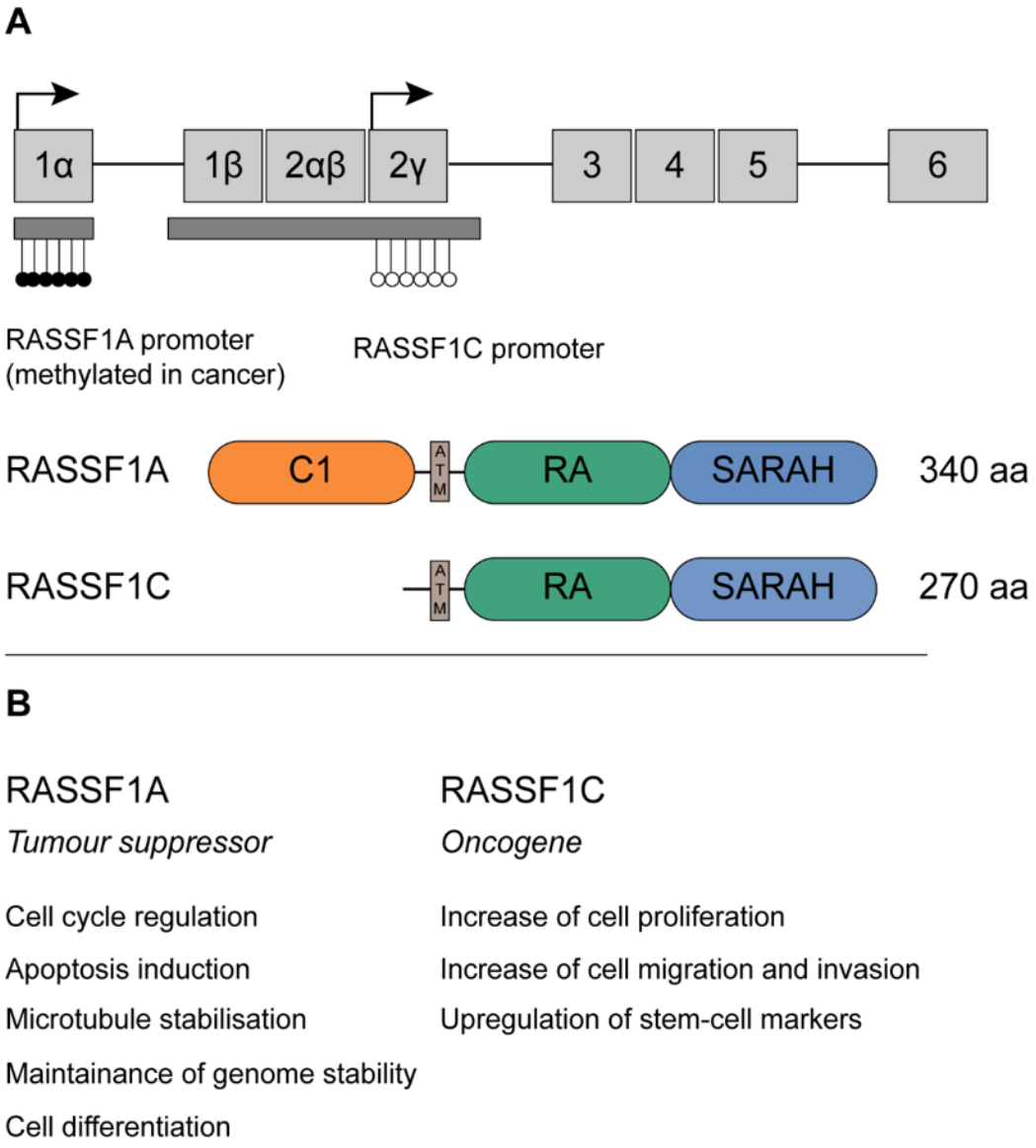


Figure 1.8 The two *RASSF1* major isoforms RASSF1A and RASSF1C have opposing functions in cancer. A. Schematic representation of the two ubiquitous isoforms of the *RASSF1* gene. The tumour suppressor RASSF1A is transcribed from exon 1α and encodes for a 340 amino acid long protein containing a diacylglycerol binding domain, also called protein kinase C conserved region (C1), an ATM phosphorylation consensus site (ATM), a Ras association domain (RA) and a SARAH (Sav/RASSF/Hpo) domain. The RASSF1C isoform is transcribed from exon 2γ and encodes for a 270 amino acid long protein that lacks the N-terminal C1 domain. In several malignancies RASSF1A expression is lost due to promoter hypermethylation (methylated CpG islands are represented in black). RASSF1C expression however is often unaltered (unmethylated CpG islands are represented in white). **B.** Summary of the tumour suppressive and tumour promoting functions of RASSF1A and RASSF1C. aa, amino acids.

1.4.5 TGF-β and tetraspanins

A less explored crosstalk of the TGF-β pathway is its interplay with tetraspanins. Tetraspanins are a family of four transmembrane domain proteins, evolutionarily conserved from invertebrates to vertebrates. Mammals express 33 tetraspanin members variably distributed on the plasma membrane as well as in subcellular organelles, in virtually any cell type. Structural features of the family include: a short extracellular loop (SEL) of 13-30 amino acids; a large extracellular loop of 70-130 amino acids (LEL), divided in into a constant region, containing three α-helices (A, B and E), and a hypervariable region, composed of helices C and D, where nearly all of the known tetraspanin protein-protein interaction sites are located (illustrated in Fig. 1.9A). Two to four disulfide bonds are made by conserved cysteine residues within the LEL (one of them occurring in an absolutely conserved CCG motif). Tetraspanins also typically have short amino- and carboxy-terminal cytoplasmic tails (6-19 amino acids) as well as a small inner loop (~ 4 amino acids). Almost all tetraspanins also contain membrane-proximal Cysteines that undergo palmitoylation (Hemler, 2014). As typical membrane proteins, they are known to cluster laterally in homo or heteromers and to associate with binding partners (integrins, immunoglobulins, lipids) to form tetraspanin-enriched microdomains (TEM) (Yáñez-Mó et al., 2009).

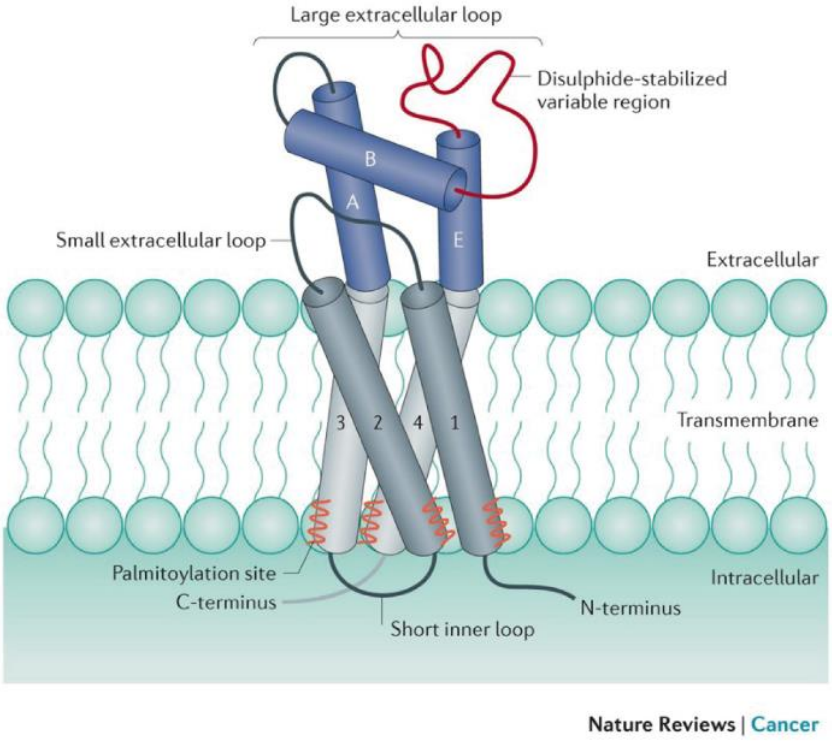
The tetraspanin family can strongly influence various physiological processes, such as cell adhesion, migration, invasion, signalling, cell-cell fusion (summarised in Fig. 1.9B). Deregulation of several members of the family, in cancer, has been correlated with metastasis onset. Insights in the mechanisms by which tetraspanins influence tumour behaviour can be linked to their role in cell-matrix and cell-cell interactions, which influence migration and invasion of

surrounding tissues and angiogenesis (Ashman et al., 2013; Hemler, 2014). Furthermore, tetraspanins are integral components of extracellular vesicles, which, as mentioned in section 1.3.5, are key modulators of the tumour microenvironment and are one of the triggers of metastatic dissemination.

Recent studies have proposed an emerging crosstalk between TGF-β and specific tetraspanins. Tetraspanin CD151 is upregulated in various cancers, often in association with increased metastasis and/or poor prognosis (Hemler, 2014). In breast cancer cells CD151 has been found to control compartmentalisation of TGFβRI and to regulate TGF-β activation of p38, a specific branch of non-canonical TGF-β signalling. In addition, CD151 depletion reduced the metastatic burden in the lungs *in vivo* (Sadej et al., 2010). In a similar manner, CD9 and CD81 have been shown to facilitate TGFβRI and TGFβRII coupling in late stage melanoma, facilitating TGF-β driven EMT and invasion (H. Wang et al., 2015).

Evidence for a link between tetraspanins and TGF-β superfamily of ligands has also been documented in *Caenorhabditis elegans*, where the two paralogues TSP-12 and TSP-14 function redundantly in promoting BMP signalling (Z. Liu et al., 2015; L. Wang et al., 2017).

A



B

Tetraspanins functions

Binding partners of integrins, immunoglobulins, metalloproteases, ADAMs, PKCs

Formation of plasma membrane microdomains involved in signalling

Cell-cell and cell-substratum adhesion

Cytoskeleton dynamics

Cell motility and migration

Endocytic trafficking / Cargo sorting

Tumour suppressor	*Tumour promoting*
Inhibition of cell migration and invasion	Promotion of cell migration and invasion
Promotion of cell-matrix adhesion	Promotion of angiogenesis

Figure 1.9 Tetraspanin family structure and functions. A. The intact protein presents a rod-like structure with 4 transmembrane helices (light and dark grey, labelled 1 to 4). The large extracellular loop (LEL, 70-130 aa) includes a conserved helical region (helices A, B and E, in indigo) and a variable region (depicted in dark red), typically involved in protein-protein interactions. The two to four conserved disulphide bonds that typically stabilise the variable region are not shown. The small extracellular loop (SEL, 13-30 aa) joins domains 1 and 2. Illustrated are also the typical amino- and carboxy-terminal tails as well as the short inner loop. Palmitoylation of juxta-membrane Cysteines (orange lines) facilitates association with other proteins within TEMs. Reprinted from (Hemler, 2014) with permission of Springer Nature, licence number 4401341343661. **B.** Summary of tetraspanin functions in the cell and their involvement in cancer (Detchokul et al., 2014).

1.5 Aims of the Project

Aim of this thesis is to investigate the pro-tumourigenic role of extracellular vesicles (EVs) released from breast cancer cells. In order to stimulate cancer cells to secrete EVs different oncogenic stimuli will be used: namely, expression of the oncogene RASSF1C and treatment with the TGF-β cytokine. Using these two different approaches I will, first, characterise RASSF1C-driven EVs and test them on recipient cells to assess their oncogenic potential. Subsequently, I will explore possible effectors downstream of RASSF1C that contribute to the observed release of EVs.

Secondly, I will assess whether the growth factor TGF-β plays a role in exocytosis and if the population of TGF-β driven vesicles has an oncogenic effect on recipient cells *in vitro*. Additionally, the selective enrichment of the tetraspanin CD9 in TGF-β driven EVs will be investigated and a novel role for CD9 in TGF-β signalling will be explored.

The data generated in this thesis will provide new mechanisms used by two different oncogenic signals to mediate an aggressive phenotype in breast cancer cells.

Chapter 2 Materials and Methods

2.1 Materials

All chemicals were purchased from either Sigma-Aldrich or Thermo Fisher Scientific and used according to manufacturer's guidelines, unless stated otherwise. Tissue culture plastic was purchased from Corning and Sarstedt. Glassware was purchased from VWR and Fisher.

2.2 Methods

2.2.1 Cell culture

Unless stated, all cell lines (Table 2.3.1) were maintained in Dulbecco's Modified Eagle Medium (DMEM) supplemented with 10% (v/v) Foetal Bovine Serum (FBS), 2 mM Glutamine and 100 U/mL Penicillin/Streptomycin (Pen/Strep). All media and supplements were purchased for Gibco® (Life Technologies). Cells were maintained at 37°C, with 5% CO_2 in a humidified incubator.

MCF10A cells were cultured in DMEM:F12 (1:1) medium supplemented with 5% (v/v) Horse Serum (Invitrogen), EGF 20 ng/mL, Hydrocortisone (0.5 mg/mL), Cholera toxin (100 ng/mL), Insulin (10 µg/mL), Pen/Strep as above.

T47D reporter$^+$ cells were cultured in DMEM:F12 (1:1) medium in the presence of selection (as reported in (Zomer et al., 2015)).

From frozen, cells were defrosted in a water bath at 37°C for 2 min. Once thawed, cells were diluted in complete medium and centrifuged at 350 x g for 5 min. Cell pellets were resuspended in 10 mL of complete medium and seeded into a T75 flask.

Once confluent, cells were washed in Phosphate Buffered Saline (PBS) and trypsinised using 0.25% Trypsin-EDTA solution (Life Technologies). Medium was then added to the trypsinised cells and an aliquot of the cells was reseeded into a new flask containing fresh complete medium.

Cells were routinely frozen down in freezing medium containing 90% (v/v) FBS, 10% (v/v) Dimethyl sulfoxide (DMSO). Cells were trypsinised, resuspended in complete medium, centrifuged at 350 x g for 5 min and the pellets resuspended in freezing medium and aliquoted into 2 mL cryovials (Thermo Scientific). Cryovials were placed into a Nalgene® Mr Frosty containing 200 mL isopropanol at room temperature (RT), and placed at -80°C for 24 h prior to long term storage in liquid nitrogen.

2.2.2 Transfection

All cells undergoing transfection were plated in complete DMEM, without antibiotics. All transfections, either with plasmid DNA or siRNA, were done using the Lipofectamine 2000 or 3000 transfection reagent (Life Technologies) and following the manufacturer's guidelines. This was done at a ratio of 1 µg siRNA to 1 µL of Lipofectamine or 1 µg plasmid DNA to 1 µL of Lipofectamine. All cells were transfected with 100 nM siRNA.

Appropriate volumes of siRNA or plasmid DNA and Lipofectamine were diluted in separate tubes in OptiMEM (Life Technologies) and incubated at room temperature for 5 min. Then the contents of the two tubes were mixed together carefully and left at room temperature for 20 min. After the incubation the mixture was gently added to the cells. After 6 h the medium containing the mixture of siRNA or plasmid DNA and Lipofectamine was aspirated and was changed to

fresh complete medium, in which, unless stated otherwise, the cells were kept until harvesting.

2.2.3 Growth Factors and Inhibitors Treatment

For growth factor treatment cells were seeded in complete DMEM and fresh 0.1% FBS DMEM was added the night prior to treatment. Fresh 0.1% FBS DMEM, supplemented or not with BMP4 (Peprotech) at 25 ng/mL concentration or TGF-β1 (Peprotech) at 10 ng/mL concentration, was added the next day for the indicated amount of time (Pefani et al., 2016).

To achieve TGF-β1 pathway inhibition two TGFβRI inhibitors were used. SB431542 (Selleckchem) at 10 μM or ALK5 inhibitor II (Calbiochem) at 1 μM, were added to cells for 30 min in fresh 0.1% FBS medium, prior to growth factor treatment. After 30 min fresh medium supplemented with both TGF-β1 and the indicated inhibitor was added to the cells. Cells were incubated for the indicated times prior to harvest. To achieve proteasomal inhibition MG132 (Sigma-Aldrich) was added to cells at 10 μM for the indicated time-points in fresh 0.1% FBS medium, prior to other treatments.

2.2.4 Cell Lysate Quantification

Cells were washed once with PBS and lysed directly in the plate by the addition of appropriate amounts of Laemmli lysis buffer (Table 2.3.8), supplemented with 1X protease inhibitor cocktail (Roche). Cells were scraped off the plate using a rubber cell scraper (Sarstedt) and the lysates transferred to a 1.5 mL universal tube. The lysates were then boiled at 100°C for 10 min, sonicated for 2 cycles of 30 sec each on a sonicator (Model 300 V/T, Ultrasonic homogenizer, Biologics Inc.) and stored at -20°C until needed.

The protein concentration for most experiments was determined using NanoDrop 1000 (Thermo Fisher) by measuring the absorbance of the samples at a wavelength of 260 nm, with an optical density (OD) OD = 1 equals 50 µg/mL.

In case of immunoprecipitation assay, the protein concentration of cell lysates was determined using Bradford assay. First, a standard curve was generated using Bovine Serum Albumin (BSA) (Thermo Scientific) at concentrations ranging 0-2000 µg/mL. Each standard concentration was run in duplicates and 5 µL were added to the wells of a 96-well plate. Lysates were diluted 1/10 with water and of this solution, 5 µL were added to the wells of a 96-well plate. To each well 245 µL of Bradford reagent (Thermo Scientific) was added. The absorbance of each well was measured at a wavelength of 595 nm using a plate reader (BMG POLARstar Omega). The standard curve was used to calculate the actual concentration of each sample in µg/µL and to normalise each sample with Laemmli lysis buffer, so that equal loading per experiment was achieved.

According to calculations, an appropriate volume of 4X SDS-PAGE sample buffer (Table 2.3.8) was added to each sample. Samples were boiled for 15 min, 100°C before loading onto an SDS-PAGE gel for electrophoresis or stored until needed at -20°C.

2.2.5 SDS-Page and Western Blotting

Protein samples were loaded onto a gel and separated by SDS-PAGE. NuPAGE® pre-cast gels (4-12% gradient or 10%) (Life Technologies) were loaded into a Novex® mini gel tank, filled with 1X NuPAGE® MOPS SDS running buffer (Life Technologies). Samples were loaded using gel loading tips (Starlabs), along with See Blue® plus 2 Pre-stained protein standard (Life Technologies) or Precision Plus Protein™ Dual Color Standards (Bio-Rad) as protein markers. Gels were run

at a constant voltage of 130 V using PowerPacTM HC High-current power supply (Bio-Rad). The protein samples were separated by gel electrophoresis and were transferred from the gel onto a PVDF (Immobilon-P, Millipore) membrane. The membrane was activated using methanol before the transfer was performed using the Bio-Rad mini gel blotting system, in which the gel and membrane were sandwiched between two sheets of Whatman paper and compacted using sponges. The transfer was performed in transfer buffer (Table 2.3.8) at a voltage of 100 V for 80 min using PowerPacTM HC High-current power supply (Bio-Rad).

Following transfer, PVDF membranes were blocked for 30 min on a SSL4 See-saw rocker (Stuart) at room temperature in 5% skimmed milk (w/v) (Marvel) in PBS-Tween (PBS-T, Table 2.3.8). After blocking, the primary antibody was added to the membrane at a concentration of 1:1000 (v/v) in 5% skimmed milk (w/v) in PBS-T. All primary antibodies were incubated with the membrane overnight at 4°C.

Following primary antibody incubation, membranes were washed (3 x 5 min) in PBS-T on a See-saw rocker before being incubated with secondary HRP-conjugated antibody (Table 2.3.5). Membranes were incubated at room temperature for 45 min prior to being washed (3 x 5 min) in PBS-T. The PVDF membranes were then exposed to either Enhanced chemiluminescence (ECL) solution (Thermo Scientific) for normal exposure or ECL advance (GE Healthcare) for low abundance proteins, according to manufacturer's protocol. Membranes were exposed to X-ray film (Scientific Laboratories Supplies) and developed using a XoGraph processor (XoGraph Imaging Systems) before being scanned onto a computer.

In order to allow membranes to be probed with multiple primary antibodies, membranes were de-activated/re-blocked in 5% milk supplemented with 1:500 sodium azide 10% (w/v) for 30 min on a See-saw rocker. Further to that, new primary antibody incubation was carried out.

2.2.6 Immunoprecipitation

Cells were washed two times with PBS before lysis with immunoprecipitation lysis buffer (Table 2.3.8) supplemented with protease inhibitor cocktail (Roche) and 50 mM sodium fluoride, 10 mM β-glycerophosphate and 0.5 mM sodium orthovanadate. Cells were scraped from the dish and collected into a 1.5 mL microfuge tube and incubated end over end for 20 min at 4°C. Lysates were then cleared by centrifugation (20,817 x g, 10 min, 4°C). The protein concentration of the lysates was then determined by Bradford assay, so that an equal amount of protein was loaded into each immunoprecipitation reaction.

Protein A and protein G metallic (A Millipore, G Invitrogen) or protein A/G agarose (St. Cruz Biotechnology) beads were used during this project. All beads were washed three times in immunoprecipitation lysis buffer before being aliquoted into 1.5 mL microfuge tubes. An aliquot of washed beads, namely 10 µL per reaction, was added to the normalised samples as a pre-clearing step. The pre-clearing samples were left on an end to end rotor for 30 min at 4°C. 1-2 µg of antibody or corresponding amounts of IgG (Mouse or Rabbit, Cell Signaling Technology) were added per 20 µL of the metallic beads or per 50 µL of agarose beads per each reaction and let rotate on an end to end rotor for 30 min at 4°C. Subsequently, equal protein amounts of pre-cleared lysate (1-2 mg of total protein) were added to the tubes and incubated end over end for 3 h at 4°C. In parallel, 1/10 of each sample was saved as input and mixed to 2X SDS-PAGE sample buffer (Life

Technologies) and stored at -20°C prior to western blot analysis. Samples containing protein A/G agarose beads were then washed three times by collecting the beads by centrifugation (2150 x g, 2 min, 4°C) before aspirating the supernatant and resuspending the beads. Protein A or G metallic beads were washed three times by immobilising the beads using a magnet, aspirating the supernatant and resuspending the beads. Protein was eluted from the antibody by boiling at 100°C for 15 min in 1X SDS-PAGE sample buffer (Life Technologies), along with the previously stored inputs. An equal volume of each immunoprecipitation and input sample was then loaded onto a gel for electrophoresis and western blot analysis (Section 2.2.5).

2.2.7 Rho-GTP Pull-Down Assay

Confluent cell cultures were washed with cold 1X PBS and lysed in modified RIPA buffer (50 mM Tris-HCl (pH 7.4), 150 mM NaCl, 5 mM EDTA, 1% NP40, 1% sodium deoxycholate, 50 mM NaF, 1% aprotinin and 0.1 mM Na_3VO_4). Rho pull-down assay was performed using GST-rhotekin and Rho-pull down detection kit according to manufacturer's instructions (Thermo Scientific). The levels of total and active Rho were determined by using a Rho-specific antibody. For immunoblotting, samples were separated on 12% SDS-PAGE gels and transferred onto nitrocellulose membrane. Non-specific activity was blocked in 1X TBS containing 0.05% Tween-20 and 4% Bovine Serum Albumin (BSA). Membranes were incubated overnight in Rho primary antibody, washed and then incubated in HRP-conjugated secondary antibody for 1 hour at RT. After extensive washing in TBS-T, the blots were developed as previously described (Section 2.2.5).

2.2.8 Immunofluorescence

Cells, plated onto glass coverslips (Fisher), were washed twice with PBS and fixed in 4% (v/v) paraformaldehyde solution (16% (v/v) paraformaldehyde diluted in PBS) for 15 min at RT or in 100% methanol for 10 min at -20°C, protected from light. Coverslips were washed twice with PBS before the cells were permeabilised with 0.2% (v/v) Triton-X solution (in PBS) for 10 min at RT. Cells were washed with PBS and blocked with 3% (w/v) Bovine Serum Albumin (BSA) (Sigma-Aldrich) in PBS for 30 min at RT. Cells were then incubated for 3 h at RT or overnight at 4°C with primary antibody (Table 2.3.5). Coverslips were washed three times with PBS for 5 min before the secondary antibody was added (Table 2.3.5) and the cells incubated for 1 h at RT. Coverslips were washed with PBS (3 x 5 min) and mounted onto microscope slides (Fisher) using Prolong® Gold antifade reagent with DAPI (Life Technologies). Slides were sealed with clear nail varnish and analysed by microscopy. Light microscopy was done using a Nikon 90i or a Nikon 2000TE microscope using the NIS elements software, versions 4.2 and 3.8, respectively. Confocal microscopy was done using a Zeiss LSM710 or Zeiss LSM780 with Zeiss Zen programme, version 2010 and 2011, respectively.

2.2.9 Reverse Transcriptase PCR

Reverse-Transcriptase PCR (RT-PCR) was prepared using the Power SYBR Green Cells-to-Ct Kit (Life Technologies) protocol. Cells (2 x 10^5/well) were plated onto 6 well plates or 6 cm dishes. Cells were washed, counted and 5 x 10^4 cells were used for cell lysis and cDNA preparation. Cells were centrifuged at 500 x g for 5 min, washed with ice-cold PBS and the pellet was lysed in 25 µL lysis buffer, in the presence of DNase I, for 5 min. The reaction was stopped by the addition of 2.5 µL Stop Solution from the kit. For the RT-PCR, each tube of the reaction mix

consisted of 5 µL RNA, 2.5 µL of 20X RT Enzyme Mix, 25 µL of 2X SYBR RT Buffer, and 17.5 µL of nuclease-free water. The tubes were then transferred to a thermal cycler (My Cycler, Bio-Rad) following the suggested protocol of 37°C for 60 min and 95°C for 5 min, for the inactivation of the RT enzyme. The samples were then stored at -20°C prior to RT-qPCR.

2.2.10 Quantitative Real-Time PCR

Quantitative Real-Time PCR (RT-qPCR) was performed according to the Power SYBR Green Cells-to-Ct Kit (Life Technologies) protocol. The generated cDNA was diluted 4 times in nuclease-free water. The PCR mix for each sample included 5 µL of Power SYBR Green PCR Master Mix, 0.2 µL of Forward and Reverse primer mix (10 µM stock concentrations) and 0.8 µL of nuclease-free water. 6 µL of the PCR mix and 4 µL of the cDNA/water mixture were added to a well of 96-well plate (Life Technologies) for a total volume of 10 µL per reaction. The plate was sealed with a plastic film (VWR) and spun down at 140 x g for 1 min at 4°C in a 5804R centrifuge (Eppendorf). The reaction was then run in StepOnePlus™ Real-Time PCR machine (Thermo Fisher Scientific). The protocol used was Holding Step (1X cycle: 95°C 10 min), Cycling Step (50X cycles: 95°C 15 sec, 60°C 1 min) and Melt Curve Step (1X cycle: 95°C 15 sec, 60°C 1 min, 95°C 30 sec, 60°C 15 sec), Hold (4°C). Each combination of target gene/condition was repeated in three technical replicates. GAPDH or 18S were used as internal controls for all the experiments. The calculation of the ΔΔCt was performed on Microsoft Excel.

For RASSF1A and RASSF1C mRNA RT-qPCR was performed with TaqMan reagents. In this case, cDNA was prepared from cells according to the Power

SYBR Green Cells-to-Ct Kit (Life Technologies) protocol. The cDNA used was diluted 4 times in nuclease-free water. The PCR mix for each sample included 4 µL diluted cDNA, 5 µL TaqMan Gene Expression Master Mix (Thermo Fisher Scientific), 0.5 µL TaqMan™ probe for the specific gene and 0.5 µL for the reference gene, for a total of 10 µL per reaction. Quantitative RT-PCR was carried out in a StepOnePlus Real-Time PCR machine (Thermo Fisher Scientific) with the following steps: Holding Step (1X cycle: 50°C 2 min, 95°C 10 min), Cycling Step (40X cycles: 95°C 15 s, 60°C 1 min), Hold (4°C). The differential mRNA expression of genes was calculated with the comparative Ct method. TaqMan assays were performed in multiplex format.

2.2.11 Extracellular Vesicle Production and Isolation

Cells were plated as 5 x 10^6 cells/plate on two 15 cm dishes per condition. Where indicated, cells were transfected or treated following the previously discussed method. For the RASSF1C project, cells were washed twice with PBS and incubated for three days with DMEM supplemented with 0.1 % (v/v) FBS (depleted of bovine extracellular vesicles by overnight centrifugation at 100,000 x g), 2 mM Glutamine and 100 U/mL Pen/Strep (EVs free DMEM), for the production of the conditioned medium. For the TGF-β1 project, the same medium as above was used, but on the third day of culture fresh 0.1% FBS medium was added with or without TGF-β1 for the indicated times (Section 2.2.3). In both cases the conditioned medium (40 mL/condition) was then collected and extracellular vesicles were isolated as previously described (Théry et al., 2006) by sequential centrifugations: 300 x g for 15 min, 2000 x g for 30 min, 10,000 x g for 40 min, 100,000 x g for 1.5-3 h in a Optima XPN-80 ultracentrifuge using a 70 Ti rotor and polycarbonate bottles (all Beckman & Coulter). The pellet was then resuspended

in 1 ml of PBS and aliquoted in 1.5 mL universal tubes according to further analysis. If samples needed normalisation (for western blotting or functional assays), 1/5 of the resuspended pellet in 1 mL of PBS (Gibco) was aliquoted in a separate tube for protein quantification. If Nanoparticle Tracking Analysis (NTA) of the samples was required, another 1/5 aliquot of the pellet was taken in a separate tube. All aliquots were then brought to a final volume of 1 mL in PBS and washed by centrifugation at 100,000 x g for 75 min in an Optima MAX-XP Ultracentrifuge (Beckman & Coulter). All centrifugations were performed at 4°C. After the last centrifugation, PBS was removed and the extracellular vesicles used for analysis or further treatment of cells.

The aliquot used for normalisation of protein content (1/5 of the total) was resuspended in 10 µL RIPA buffer (Cell Signaling Technology) and stored at -20°C prior to use.

The aliquot used for western blotting was resuspended in an arbitrary volume of 30 µL RIPA buffer (Cell Signaling Technology) and stored at -20°C prior to use.

If used for NTA, EV pellets (1/5 of the total) were resuspended in an arbitrary amount of 10 µL PBS and stored at 4°C for short-term storage (up to 7 days) or at -80°C for long-term storage (4 weeks).

If used for functional assays pellets were resuspended in an arbitrary volume of 50 µL PBS and stored at 4°C until used (usually not kept more than 7 days).

2.2.12 Extracellular Vesicle Protein Quantification and Western Blotting

Extracellular vesicle (EV) protein content was measured and normalised prior to western blot analysis or functional assays.

After the centrifugation steps, 1/5 of the original sample was resuspended in 10 µL of RIPA buffer (Cell Signaling Technology) and boiled for 10 min at 100°C. Protein content was measured with microBCA assay (Thermo Fisher) according to manufacturer's instructions with slight amendments due to limitations in EV yield. Briefly, a BSA standard curve was made with BSA concentrations ranging 5-400 µg/mL. The microBCA reagent was made fresh by mixing Reagent A 1:25, Reagent B 1:24 and Reagent C 1:50 for a final volume of 150 µL per well.

10 µL of BSA standards and samples were added per well and 140 µL of distilled water were added to maintain a 1:1 ratio with the microBCA reagent. The mix BSA or sample and microBCA reagent was left to incubate in a humidified incubator at 37°C for 2 h prior to absorbance reading at 562 nm on a plate reader (BMG POLARstar Omega).

The standard curve was used to calculate the actual concentration of each sample in µg/mL and to normalise samples either with Laemmli lysis buffer, if the final analysis was western blotting, or with PBS if EVs were further used for functional assays. In the case of western blotting an appropriate volume of 4X SDS-PAGE sample buffer (Table 2.3.8) was added to each sample. Samples were boiled at 100°C for 15 min, before loading onto an SDS-PAGE gel for electrophoresis or stored at -20°C until needed.

2.2.13 Nanoparticle Tracking Analysis of Extracellular Vesicles

One of the standard methods for EVs characterisation is Nanoparticle Tracking Analysis (NTA). NTA is a light scattering technique which uses the Brownian motion of particles in solution to measure average particle concentration and size. For this analysis 1/5 of the total EV pellet per sample was washed as described in section 2.2.11, resuspended in 10 µL PBS (Gibco) and stored at 4°C. Additional

990 µL PBS were added on the day of analysis and the EV pellet was vigorously resuspended by pipetting and kept on ice, before starting the analysis.

Before starting any measurement, the NTA instrument, NanoSight NS300 (Malvern Panalytical) was washed three times by loading distilled water onto a syringe pump using a 1 mL syringe (Terumo) and pressing the liquid into the flow-cell top plate of the NanoSight, avoiding the introduction of air in the plate.

PBS was used to prime the instrument and to control the purity of the diluent (i.e. absence of particulate in the solution or presence of particulate in a concentration lower than detectable level). After priming, 1 mL of sample was carefully loaded on the syringe pump, avoiding the introduction of air in the plate.

Every measurement was done automatically, with the aid of the syringe pump and a script for data acquisition was generated on the NTA 3.2 software. As from the script, 3 recordings of 60 min each were automatically taken once each sample was loaded in the chamber and the focus on the particles in solution was adjusted manually. Additionally, every sample was loaded onto the chamber twice and an average of 6 recordings was then used as a final value. NTA 3.2 software was used to generate data output.

2.2.14 Extracellular Vesicle Membrane Staining

Lipophilic dyes intercalating membranous structures were used for EV staining. Namely, the PKH67 Green Fluorescent Cell Linker Mini Kit (Sigma-Aldrich) was used following manufacturer's protocol. In brief, EVs were collected and washed as previously stated. Each EV pellet was resuspended in 250 µL of Diluent C in a universal tube. At the same time 1 µL of the 2X fluorescent dye solution was added to 250 µL of Diluent C in another universal tube. The EV solution was then rapidly added to the dye solution and mixed immediately by pipetting. The cell/dye

suspension was then incubated for 5 min with periodic inversion of the tube. After the incubation, 500 mL of complete DMEM supplemented with 10% (v/v) FBS (depleted of bovine EVs) was added to stop the staining and incubated for 1 min. The universal tube was then centrifuged at 100,000 x g for 80 min. After centrifugation, the solution was aspirated, the pellet washed in 1 mL PBS, transferred to another 1.5 universal tube and centrifuged again at 100,000 x g for 80 min. The collected pellet was then resuspended in complete DMEM supplemented with 0.1% (v/v) FBS (depleted of bovine EVs) and the solution added to the cells.

2.2.15 Extracellular Vesicle Immunofluorescent Staining

Nunc Lab-Tek chamber slides (8 wells, Thermo Scientific) were coated for 3 h at room temperature with 1:10 poly-L-Lysine solution (Sigma-Aldrich). Previously isolated EVs were incubated in PBS (Gibco) overnight on the coated chamber slides.

The next day, PBS was washed out and bound EVs were fixed in 4% PFA and the same immunofluorescence protocol as for cells was followed. Secondary antibody staining only was performed to ensure specific staining. No mounting medium was required, samples were stored in PBS at 4°C for up to two weeks. Imaging was performed on an Olympus TIRF IX83 microscope (Kennedy Institute of Rheumatology, Oxford).

2.2.16 Extracellular Vesicle Treatment of Cells

EVs were harvested and normalised for protein content as previously stated prior to the following functional assays on recipient cells: xCELLigence, Boyden chamber invasion, migration assay. If not specified otherwise, all functional assays

were performed in 0.1% FBS or 10% FBS DMEM, with FBS depleted of bovine EVs.

2.2.17 Migration Assay

2×10^5 cells per well were seeded in duplicates in 6 well plates and in complete medium 24 h prior to the assay. On the day, cells were washed in PBS prior to apply a precise scratch with a 200 µL tip from top to bottom of each well, allowing the formation of a neat line, void of cells. Scratched cell debris was then rapidly removed by aspirating and washing with PBS once. Cells were cultured in fresh 0.1% FBS supplemented with EVs, according to the experiment, or with PBS only. A first set of images of the scratches was taken on a Nikon 90i light microscope using the NIS elements software, version 4.2. Cells were then left incubating for 21 h and images of migrated cells were taken again the following day. Quantification of the ability of cells to migrate was assessed measuring the distance of the wound edges in 3 different areas of each wound (2 scratches were made per well) at t = 0 (t_0) after scratch and t = 21 h (t_{21}) after scratch. Distance was measured using NIS Elements 2.2 software, distance at t_{21} was subtracted to distance measured at t_0 and plotted as percentage of wound closure.

2.2.18 xCELLigence

The migratory capacity of cells was assessed also using the xCELLigence RTCA multiplate (ACEA Biosciences). xCELLigence employs a transwell setup where the passage of cells from the top to the bottom well occurs via a porous membrane surrounded of golden electrodes. In the absence of migrating cells a voltage is applied to the electrodes and current intensity travels unaffected. However, when cells are migrating, the current intensity decreases and impedance is increased,

due to the cell's sterical hindrance. The amount of impedance is proportional to the amount of migrating cells (measured by the instrument as Cell Index, CI).

Cells were seeded on the xCELLigence plate according to manufacturer's protocol. In brief, plates were first equilibrated with 160 µL/well of 10% FBS DMEM in the bottom wells of the transwell. 2 wells were left as controls and loaded with 160 µL/well 0.1% FBS DMEM. Top and bottom wells of the plate were then sealed together and 50 µL/well of 0.1% FBS DMEM were loaded on the top wells. Plates were left in the incubator for 30 min to equilibrate.

Meanwhile, cells were trypsinised and washed twice in 0.1% FBS DMEM. 50,000 cells/well were resuspended in 0.1% FBS DMEM supplemented with EVs or with PBS only as a control. Resuspended cells were added to the equilibrated top wells of the xCELLigence plate. Every condition was plated in 3 technical replicates.

xCELLigence plates were secured on the plate holder and placed in a humidified incubator for 36 h.

Cell migratory capacity, estimated as CI, could be followed real-time and later analysed with the RTCA 2.0 software on a PC directly connected to the instrument.

2.2.19 Boyden Chamber Invasion Assay

Cells were trypsinised, pelleted at 300 x g for 3 min and counted. Cells were then washed and 50,000 cells x 3 were pelleted again at 300 x g for 3 min and resuspended in 0.1% FBS DMEM supplemented with EV preparations in PBS or with PBS only. A volume equal to 50,000 cells per well was seeded in the upper wells (in triplicates) of Transwell Matrigel chambers (Corning) and allowed to invade toward bottom wells supplemented with 10% FBS. After 18-24 hours of incubation (according to cell type), invading cells were fixed and stained with

Richard-Allan Scientific™ Three-Step Stain (Thermo Fisher Scientific) and photographed on a Nikon 90i light microscope. ImageJ 1.51s software was used to count the invaded cells.

2.2.20 Cre-LoxP System for Study of EV Transfer

A Cre-LoxP model previously published (Zomer et al., 2015) to study extracellular vesicle transfer was employed in both projects. In the system a colour switch is specifically induced in reporter-expressing cells (reporter$^+$) that take up EVs released from cells expressing the Cre recombinase (Cre$^+$ donor cells). MDA-MB-231$^{CFP;Cre}$ were used as donor cells and T47D$^{dsRed\text{-}LoxP\text{-}eGFP}$ as reporter cells.

Co-culture or transwell assays were used to study EV transfer with the Cre-LoxP model. For the co-culture assay, different ratios of donor/reporter$^+$ cells were seeded in a 12-well plate and let grow in 0.1% FBS DMEM (depleted of bovine EVs) for 7 days with medium replacement every 48 h. For the transwell assay, donor cells were plated on the top well of a transwell, separated from the reporter$^+$ cells by a 0.4 µm filter to allow only EV transfer. Reporter$^+$ cells were plated in the bottom of the transwell. Both cell types were kept in 0.1% FBS DMEM for 7 days.

On day 7, cells were imaged on a Nikon TE2000 inverted microscope or on a Nikon 90i light microscope, at 20X magnification at 37°C and 5% CO_2, using the NIS elements software, version 4.0 or version 4.2, respectively.

Analysis of the amount of recombined reporter$^+$ cells that switched from DsRed to eGFP expression was performed on Imaris 7.71 software (Bitplane, ANDOR).

2.2.21 Transformation of Bacteria

Commercial plasmids were obtained from Addgene and a DNA yield 1-2 µg/mL was achieved by isolation using the QIAGEN Plasmid Maxi Kit, after transformation.

Briefly, to transform the plasmids into bacteria, One Shot TOP10 Chemically Competent *E. Coli* (Thermo Fisher Scientific) were thawed on ice. 50 µL of bacteria were incubated with 2 µL ligation mix (plasmid or control) on ice for 15 min. For transformation, the bacteria were placed in a heat block for 30 sec at 42°C following an incubation on ice for 5 min. 1 mL LB broth was added to the bacteria and incubation of bacteria at 37°C was allowed for 1 h while shaking at 750 rpm (Eppendorf heat block). Transformation reactions were spread onto LB agar plates supplemented with appropriated antibiotics and were incubated overnight at 37°C.

Single clones were picked and were incubated in 5 mL LB broth supplemented with selection for 6-10 h at 37°C while shaking at 300 rpm (Innova 44 Incubator). Overnight culture of 200 mL LB broth containing appropriate antibiotics were inoculated with 500 µL bacterial starter culture, shaking at 300 rpm. The next day, bacteria were harvested by centrifugation at 6000 g for 15 min at 4°C. Isolation of plasmid DNA was then achieved using the QIAGEN Plasmid Maxi Kit, according to manufacturer's instructions.

2.2.22 Site-Directed Mutagenesis

Site-directed mutagenesis was carried out using Agilent QuickChange II Site-directed Mutagenesis Kit following the manufacturer's protocol. The primers used were generated following the manufacturer's guidelines. Positive clones

were confirmed by Sanger sequencing for the presence of the introduced mutation.

2.2.23 ELISA Assay

In order to measure the concentration of soluble TGF-β in EVs, TGF-beta DuoSet ELISA kit (R&D) was used. EVs were harvested as stated in section 2.2.11 and an equal amount of conditioned medium was kept to compare the amount of detectable TGF-β. The ELISA was carried out according to manufacturer's instructions.

2.2.24 Statistical analysis

For all experiments, statistical analysis was carried out using two-tailed Student's t-test (unless stated otherwise), calculated on Microsoft Excel or Prism 6.0 (Graphpad). For quantification of immunofluorescent staining intensity and for xCELLigence measurements the nonparametric Mann-Whitney test was employed. The Standard Error Mean (SEM), used for error bars, was calculated by the division of the standard deviation by the square root of the number of measurements made.

2.3 Tables

Table 2.1 List of the cell lines used in this study. Table indicates the cell line, the tissue of origin and where they were acquired from.

Name	Type	Source
MCF-7	Breast adenocarcinoma	CRUK
MCF10A	Breast fibrocystic disease	ATCC
MDA-MB-231	Breast adenocarcinoma	CRUK
MDA-MB-436	Breast adenocarcinoma	Adrian Harris
CAL51	Breast adenocarcinoma	Adrian Harris
SUM159PT	Breast carcinoma	Adrian Harris
MDA-MB-231 $CFP^{+}Cre^{+}$	Breast adenocarcinoma cells stably expressing pcDNA3.1-CFP-Cre	Jacco van Rheenen
T47D	Breast ductal carcinoma stably expressing floxed-DsRed-floxed-eGFP, $reporter^{+}$ cells	Jacco van Rheenen

Table 2.2 List of chemical reagents.

Name	Provider
2-Propanol	Fisher Scientific
Agarose	Sigma-Aldrich UK
Bovine serum albumin (BSA)	Thermo Fisher Scientific
Dimethyl sulfoxide (DMSO)	Sigma-Aldrich UK
Dithiothreitol (DTT)	Sigma-Aldrich UK
Ethanol (EtOH)	Fisher Scientific
Formaldehyde (PFA)	Thermo Fisher Scientific
Glycine	Fisher Scientific
LB broth	Sigma-Aldrich UK
Lipofectamine 2000, Lipofectamine 3000	Thermo Fisher Scientific
β-Mercaptoethanol	Sigma-Aldrich UK
Methanol (MeOH)	Fisher Scientific
Milk powder	Marvel
NP40	Sigma-Aldrich UK
NuPAGE MOPS SDS Running Buffer (20X)	Thermo Fisher Scientific
Phosphatase inhibitors	Roche
Phosphate buffered saline (PBS) tablets	Oxoid
Protease inhibitors	Roche
RIPA buffer 1X	CST
Sodium chloride	Fisher Scientific
Sodium dodecyl sulphate (SDS)	Sigma-Aldrich UK
Tris Acetate 20x buffer	Thermo Fisher Scientific
Tris base	Fisher Scientific
Triton X 100	Sigma-Aldrich UK
Tween-20	Sigma-Aldrich UK

Table 2.3 siRNAs used for the study.

Target gene	siRNA target sequence	Provider
sihCD9 (siGenomeSMARTpool)	UGAAAUAGCUGCGGCCAUC (1) GAUAUUCCCACAAGGAUGA (2)	Thermo (Dharmacon)

	UUAAGGAAGUCCAGGAGUU CCAAGAAGGACGUACUCGA	
siRab27a	UCAGAAACUGGAUAAGCCAGCUACA (1) UGUAGCUGGCUUAUCCAGUUUCUGA (2)	Invitrogen
siRab27b	CCCUGAUACUGUCAAUGGUGGAAAU (1) AUUUCCACCAUUGACAGUAUCAGGG (2)	Invitrogen
siRASSF1 (siGenomeSMARTpool)	ACGCACAAGGGCACGUGAA CAAGGACGGUUCUUACACA GCAAGAAGCCACCCUCCUU CUACAUAACUUCCUACGUA	Thermo (Dharmacon)
siLuciferase	GCCAUUCUAUCCUCUAGAGGAUG	Eurofins MWG
siNT (Non-Targeting)	UAAGGCUAUGAAGAGAUAC	Eurofins MWG

Table 2.4 Plasmid vectors.

Plasmid	Backbone	Provider/Reference
mCherry-C1	mCherry	V. D'Angiolella
mCherry-CD9	mCherry	Addgene
Flag-RASSF1C	pcDNA3.1	N. Vlahov
HA-RASSF1C	pcDNA3.1	N. Vlahov
DsRed	pDsRed-Express2-C1	N. Vlahov
DsRed-RASSF1C	pDsRed-Express2-C1	N. Vlahov
ZsGreen	pZsGreen-C1	N. Vlahov
ZsGreen-RASSF1C	pZsGreen-C1	N. Vlahov
EGFP-RhoA-WT	pcDNA3-EFGP	Addgene
EGFP-RhoA-T19N (DN)	pcDNA3-EFGP	Addgene
EGFP-RhoA-Q63L (CA)	pcDNA3-EFGP	Addgene

Table 2.5 Antibodies.

Primary Antibody	Company	Catalogue No.	Use (Dilution)
Actin (I-19)	Santa Cruz Biot.	Sc-1616	1:1000 WB
Alix (3A9)	CST	2171s	1:500 WB
β-catenin	Santa Cruz Biot.	sc-7199	1:1000 WB, 1:100 IF
Caveolin-1	CST	3238	1:1000 WB, 1:100 IF
CD9 (D8O1A)	CST	13174	1:1000 WB, 1:100 IF
CD9	Sino Biological	11029-MM01	1:100 IF
CD63 (H-193)	Santa Cruz Biot.	sc-15363	1:500 WB
CD63 (MEM-259)	Thermo Scientific	MA1-19281	1:100 IF
CD63 (H5C6)	Novus Biological	NBP2-42225	1:500 WB, 1:100 IF
CD81 (B-11)	Santa Cruz Biot.	sc-166029	1:500 WB, 1:100 IF
Flag (M2)	Sigma-Aldrich	F1804-200ug	1:1000 WB
GAPDH	CST	97166S	1:1000 WB
GFP	CST	2956S	1:1000 WB
GM130	Abcam	ab52649	1:1000 WB
PCDC6 (EP3259)	Abcam	ab109181	1:1000 WB, 1:100 IF
PDI	CST	3501P	1:1000 WB
pMLCII	CST	3671S	1:1000 WB, 1:100 IF
pSRC (Y416)	CST	2101	1:1000 WB, 1:50 IF
RASSF1C	Abcam	ab24419	1:1000 WB
RhoA	CST	2117S	1:1000 WB
ROCK	CST	4035S	1:1000 WB
SMAD1	CST	9743S	1:1000 WB
pSMAD1/5/9	CST	13820S	1:1000 WB
SMAD2	CST	3103S	1:1000 WB, 1:100 IF
pSMAD2	CST	3108S	1:1000 WB

SMAD3	CST	9523P	1:1000 WB, 1:100 IF
SMAD4	CST	9515P	1:1000 WB, 1:100 IF
SRC	CST	2108S	1:1000 WB
TSG101	Santa Cruz Biot.	sc-7964	1:500 WB, 1:100 IF
YAP	CST	4912S	1:1000 WB, 1:100 IF
Secondary Antibody	Company	Catalogue No.	Use (Dilution)
Phalloidin	Life Technologies	A12380	
Alexa fluor® goat anti-mouse 488 nm	Invitrogen, Life Tech	A-11001	1:1000 IF
Alexa fluor® goat anti-mouse 568 nm	Invitrogen, Life Tech	A-21422	1:1000 IF
Alexa fluor® goat anti-mouse 594 nm	Invitrogen, Life Tech	A-11005	1:1000 IF
Alexa fluor® goat anti-rabbit 488 nm	Invitrogen, Life Tech	A-11008	1:1000 IF
Alexa fluor® goat anti-rabbit 594 nm	Invitrogen, Life Tech	A-11012	1:1000 IF
Alexa fluor® goat anti-rabbit 633 nm	Invitrogen, Life Tech	A-31576	1:1000 IF
HRP conjugated anti-mouse	Jackson ImmunoResearch	315-035-048	1:5000 WB
HRP conjugated anti-rabbit	CST	7074S	1:5000 WB
HRP conjugated anti-goat	Jackson ImmunoResearch	705-035-003	1:5000 WB

Table 2.6 RT-qPCR primers.

Sybr Green	Forward	Reverse
CD9	ATGATGCTGGTGGGCTTC	GCTCATCCTTGGTTTTCAGC
CTGF	CACCCGGGTTACCAATGACA	GGATGCACTTTTTGCCCTTCTTA
CYR61	AAACCCGGATTTGTGAGGT	GCTGCATTTCTTGCCCTTT
SMAD7	CCCCATCACCTTAGCCGACTCTGC	CCCAGGGGCCAGATAATTCGTTCC
PAI-1	ATTCAAGCAGCTATGGGATTCAA	CTGGACGAAGATCGCGTCTG
GAPDH	AATCCCATCACCATCTTCCA	TGGACTCCACGACGTACTCA

TaqMan Assay	Assay ID
RASSF1C	Hs0094679_m1
RASSF1A	Hs00945257_m1
18S	Hs99999901_s1
GAPDH	Hs99999905_m1

Table 2.7 Site directed mutagenesis primers.

Primer name	Forward	Reverse
R197W	GAGCCGCAGCCACAGGGGCTGCT	AGCAGCCCCTGTGGCTGCGGCTC
R199F	GCCCTGCCAGGAGGAACAGCCGCAGGGGC	GCCCCTGCGGCTGTTCCTCCTGGCAGGGC

Table 2.8 Buffers.

Buffer Name	Contents	For 1 L
4X SDS-PAGE Sample buffer	40% (v/v) Glycerol 250 mM Tris-HCl pH 6.8 8% SDS 11.56 mM Bromophenol Blue 8% (v/v) 2-mercaptoethanol	400 mL Glycerol 250 mL Tris-HCl pH 6.8 80 g SDS 2.5 g Bromophenol Blue 80 mL 2-mercaptoethanol
5% Skimmed milk blocking solution	5% (w/v) skimmed milk powder in 1X PBS-T	50 g skimmed milk powder 1 L PBS-T
Immunoprecipitation lysis buffer	150 mM NaCl 0.5% (v/v) NP40 20 mM Hepes pH 7.5	30 mL of 5 M NaCl 50 mL of 10 % (v/v) NP40 50 mL of 1 M Hepes pH 7.5
Laemmli Lysis Buffer	50 mM Tris-HCl pH 6.8 2% (w/v) SDS 1X Protease inhibitor cocktail	20 mL Tris-HCl pH 6.8 20 g SDS
PBS (Phosphate-buffered Saline)	137 mM NaCl 2.7 mM KCl 10 mM Na_2HPO_4 1.76 mM KH_2PO_4 pH 7.4	8.01 g NaCl 0.2 g KCl 1.78 g Na_2HPO_4 0.27 g KH_2PO_4
PBS-T (PBS Tween)	PBS as above 0.1% (v/v) Tween 20	1 mL Tween per L of PBS
SDS-PAGE Running Buffer	25 mM Tris 190 mM Glycine 0.1% (w/v) SDS	3.03 g Tris 14.4 g Glycine 1 g SDS
SDS-PAGE Sample Buffer	10% (v/v) Glycerol 62.5 mM Tris-HCl pH 6.8 2% (w/v) SDS 2.89 mM Bromophenol Blue 2% (v/v) 2-mercaptoethanol	100 mL Glycerol 62.5 mL Tris-HCl pH 6.8 20 g SDS 0.625 g Bromophenol blue 20 mL 2-mercaptoethanol
Western Blot Transfer Buffer	25 mM Tris 190 mM Glycine 20% (v/v) Methanol	3.03 g Tris 14.4 g Glycine 200 mL Methanol
TAE Buffer	40 mM Tris 18 mM Glacial acetic acid 1 mM EDTA pH 8.0	4.48 g Tris 1.14 mL Glacial acetic acid 2 mL 0.5 M EDTA pH 8.0
4X DNA Loading buffer	50% (v/v) Glycerol 1X TAE Orange G	500 mL Glycerol 500 mL 1X TAE Orange G to colour.
LB Broth	2% (w/v) LB broth	20 g LB broth

Chapter 3 Optimisation of Extracellular Vesicle Isolation

3.1 Introduction

Extracellular vesicles (EVs) have been gaining interest in the study of multiple diseases since the discovery that these entities are actively secreted by virtually any cell type and that they are enriched in intracellular components (Johnstone et al., 1987). Despite being first characterised as a mean for the cell to excrete redundant cargo and catabolites (Harding et al., 1984; Pan et al., 1985), it was later on shown that EVs can transfer material from a donor to a recipient cell. Specifically, first evidence of this function was described in the immune system, where small nanosized EVs, referred to as exosomes, played the role of antigen presenting vesicles shed by either B lymphocytes (Raposo et al., 1996) or dendritic cells (Zitvogel et al., 1998).

The term extracellular vesicles includes a variety of micro and nanosized vesicles secreted by prokaryotic and eukaryotic cells, with a vesicle defined as a subcellular structure that encloses part of the cytosol within a limiting bilayer lipidic membrane (Colombo et al., 2014). Generally, EVs are classified in three categories, according to their size range and subcellular origin: apoptotic bodies, which range between 1-10 μm of size and are released during apoptosis; microvesicles, which range between 200 nm-1 μm and are direct protrusions of the plasma membrane; and exosomes, which are defined as between 50-150 nm

and are produced within the late endosomal compartments (LE, or multivesicular bodies, MVB) (Colombo et al., 2014; Van Niel et al., 2018).

However, this classification still lacks in representing the complexity and heterogeneity of EVs released by a single cell type and the differences in populations secreted by different cell types (Tkach et al., 2016).

One of the challenges of working with EVs is the lack of a consensus in isolation methods. Since the first evidence of their presence in the extracellular milieu, various approaches have been taken in order to isolate populations of EVs from cultured cells, from mice or from human body fluids, such as blood, urine, breast milk, saliva, among others (Colombo et al., 2014; Raposo et al., 2013). More recently the International Society of Extracellular Vesicles has released guidelines that summarise the available techniques for isolation of EVs as well as the minimal requirements for EV characterisation (Lötvall et al., 2014; Witwer et al., 2017). Among various approaches, differential centrifugations protocols are the most widely used, especially if followed by a sucrose density gradient step (Kalra et al., 2013; Théry et al., 2006), to further separate different subpopulations of vesicles present in the collected specimen.

Other techniques have been proposed such as size exclusion chromatography, filtration, immunoaffinity capture and polymer-based precipitation (Kowal et al., 2016; Taylor et al., 2015). However, all of them harbour limitations due to heterogeneity, in terms of size and protein markers, of the populations of EVs released by different cell types and due to lack of sensitivity and reproducibility of different methods.

3.2 Aims

In this chapter I aim to compare extracellular vesicle isolation methods and choose a quick and reliable protocol to use in this study. Moreover, I sought to characterise EVs released by a panel of breast cancer cells with conventional methods as well as imaging techniques and eventually identify a suitable cell line for this project.

3.3 Extracellular Vesicles Isolation and Detection Methods

3.3.1 Comparison of differential centrifugation and polymer-based isolation protocols

In this study I compared a differential centrifugation and a polymer-based precipitation method. These two methods were chosen because they are two widely used and relatively quick protocols that would allow us first to characterise EVs, then to evaluate potential differences in EV cargo upon specific treatment and finally to further use the isolated EVs for functional assays on recipient cells, without altering their physical characteristics.

I first used the adenocarcinoma breast cancer cell line MDA-MB-231 (hereafter referred to as MDA-231) to evaluate the recovery of EVs via differential centrifugations or using a commercially available kit for the polymer-based method (Total Exosome Isolation Reagent, Invitrogen). To this end, evaluation of size distribution and particle concentration was acquired via Nanoparticle Tracking Analysis (NTA). NTA is a light scattering technique which uses the Brownian motion of particles in solution to measure average particle concentration and size.

NTA measurements, in Fig. 3.1A, revealed a lower EV concentration in the sample isolated with the commercial kit, compared to the ultracentrifugation protocol. Moreover, in Fig. 3.1B the original NTA averaged curve of three technical replicates per condition shows a broader size range of EVs for the sample purified with the isolation kit, compared to the centrifugation protocol, potentially reflecting the presence of polymer contaminants in the preparations (Taylor et al., 2015).

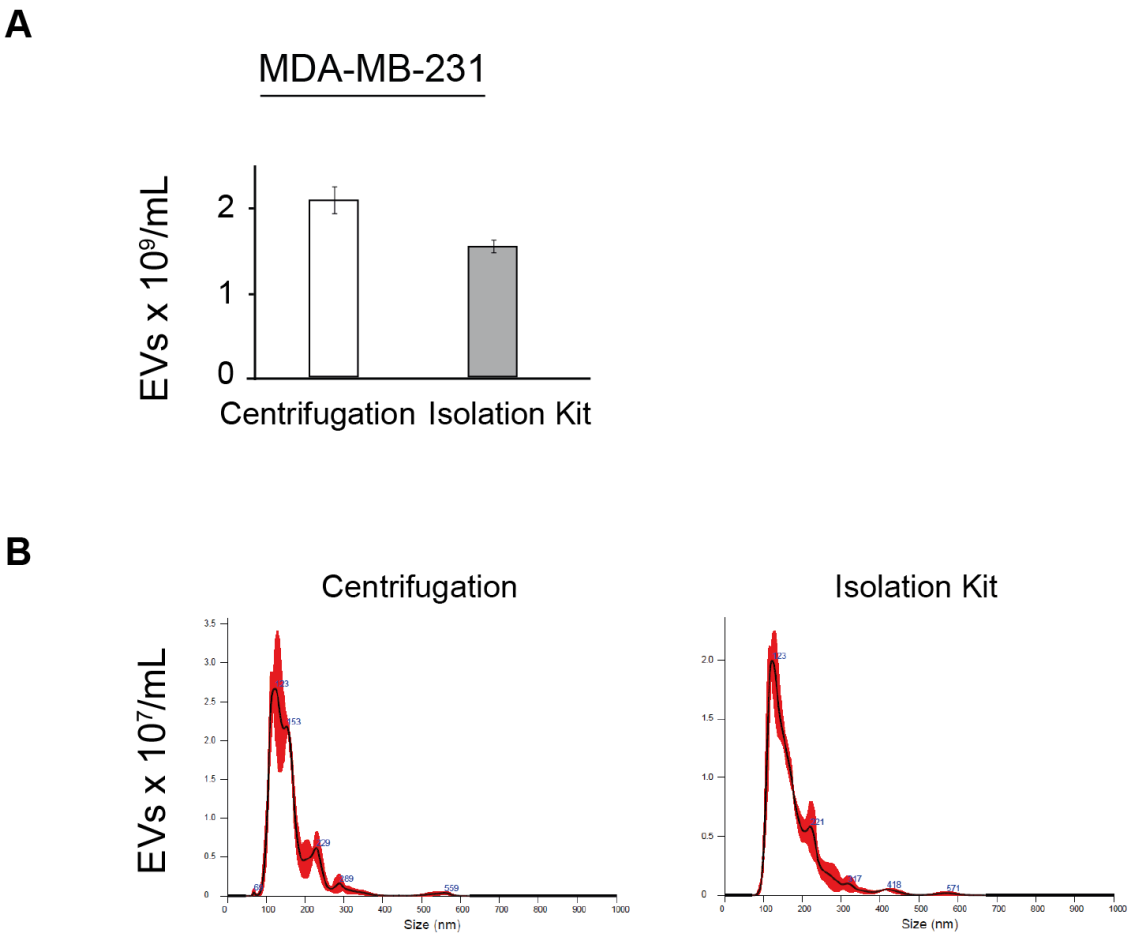


Figure 3.1 Optimisation of extracellular vesicle isolation protocol. MDA-MB-231 cells were seeded into 15 cm dishes (5 x 10^6 cells/plate) and cultured for 72 h in 0.1% FBS (depleted of bovine serum EVs) medium. Conditioned medium was then collected and EVs were isolated using a differential centrifugation protocol or an isolation kit (Invitrogen). Isolated EVs were resuspended in PBS (Gibco) and diluted 1:100 prior to NTA analysis. **A.** Particle concentration and **B.** size range were then assessed by Nanoparticle Tracking Analysis (NS300, Malvern Panalytical). The differential centrifugation protocol enriches for a higher number of particle per mL. In **A**, NTA measurements are represented as mean ± SEM from 3 technical replicates. In **B**, the average values are depicted by the black line on the NTA profiles, the SD boundaries are depicted by the underlying red area.

The data presented above prompted us to choose differential centrifugations as a protocol to employ throughout my study, as it gives better yield and likely attracts fewer contaminants than the polymer-based isolation.

3.3.2 Comparison of extracellular vesicle populations among breast cancer cell lines

Given previous knowledge on how different cell types release a variety of subpopulations of EVs, I decided to characterise a panel of breast cancer cell lines for the abundance of EV markers. A growing body of literature has been proposing a pro-metastatic role for EVs (Costa-Silva et al., 2015; Peinado et al., 2012; L. Zhang et al., 2015) and, among others, breast cancer has been previously implicated in metastasis formation via EV dissemination (A. Hoshino et al., 2015; Li et al., 2012; Zomer et al., 2015). I thus reasoned that aggressive breast cancer cells may be optimal candidates to study EV release and dynamics. I chose MDA-MB-231, MDA-MB-436 and CAL51 as triple negative breast cancer cells derived from basal carcinomas; and MCF7 cells, $HER2^-$ luminal adenocarcinoma cells, commonly considered less aggressive (Table 3.1). After isolation of EVs, specifically the pool of small EVs that are generally recovered after 100,000 x g ultracentrifugation and are generally termed exosomes, I analysed the size distribution and sample concentration via NTA as well as a panel of proteins commonly associated with EVs via western blotting. In order to investigate the EV physical properties and sample concentration I used NTA, as shown in Fig. 3.2. In panel 3.2A the number of particles/mL is represented per cell line. Interestingly MDA-231 seemed to secrete a higher number of particles than MCF7, which was not reflected by the western blot data (Fig. 3.3A). The NTA measurements could be interpreted as more comprehensive in term of

representing the whole population of EVs isolated with the current centrifugation method. The western blotting instead will give a partial representation of EVs enriched for the chosen protein markers, therefore highlighting a subpopulation of EVs. On the other hand, NTA data may include possible contaminants (i.e. particulate, EV aggregates), due to the limitations of the protocol used, and thus overestimate the amount of particles present in a sample. In Fig. 3.2B the mean size of EVs is represented. The graph shows that the average size was close to 100 nm for all cell lines tested, indicating again that the protocol used successfully enriched for a population of small nanosized vesicles, likely to be exosomes.

Cell line	Site of origin	Pathology	Molecular classification	P53	BRCA1	Receptor status
MDA-MB-231	PE	AC	TNB, Basal	MUT	WT	TN
MDA-MB-436	PE	AC	TNA, Basal	MUT	MUT	TN
CAL51	PE	AC	TNB	WT	WT	TN
MCF7	PE	IDC	Luminal	WT	WT	$HER2^-$

PE, Pleural Effusion, AC, Adenocarcinoma, IDC Intraductal Carcinoma, TN Triple Negative, WT wild type, MUT mutant.

Table 3.1 Cell lines tested for extracellular vesicle release. The table highlights the differences in molecular classification, common mutations and receptor status of the chosen cell lines.

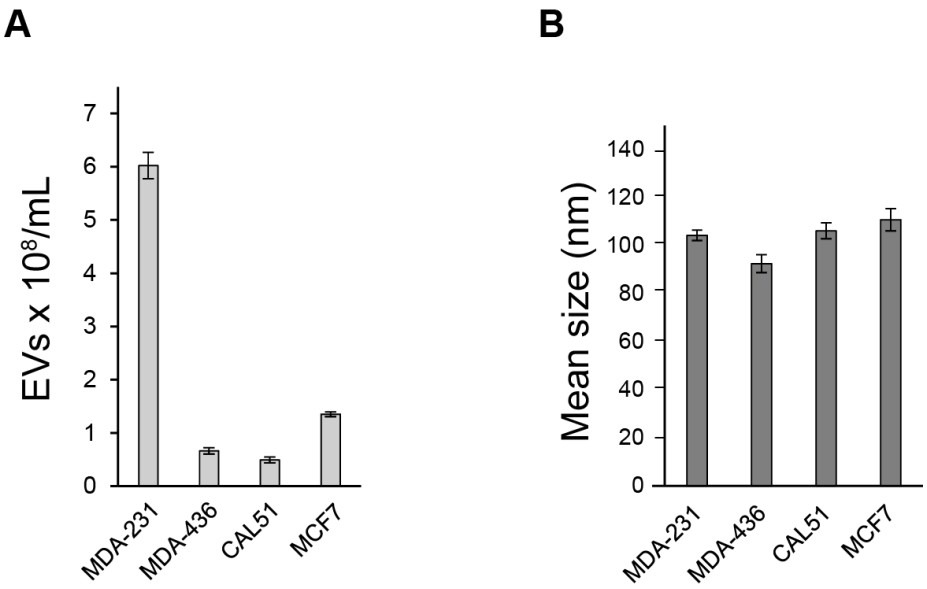


Figure 3.2 Breast cancer cells release different amounts of extracellular vesicles. MDA-MB-231, MDA-MB-436, CAL51 and MCF7 breast cancer cells were tested for EV production. Each cell line was seeded (5 x 10^6 cells/plate) and cultured as in Fig. 3.1. EVs were isolated from conditioned medium following the previously tested centrifugation protocol**. A.** An aliquot of EVs per each cell line was taken from the same experiment as in Fig. 3.2 and was diluted 1:100 in PBS (Gibco) and analysed via NTA for particle concentration (**A**) and size (**B**). MDA-MB-231 cells secrete the highest amount of EVs/mL among the cell lines tested. NTA measurements are represented as mean ± SEM from 3 technical replicates.

In Fig. 3.3A, western blotting analysis shows that EVs isolated from four cell lines were differentially enriched in positive EV markers: MCF7 EVs were, for instance, enriched with the endosomal machinery interactor Alix and the ESCRT-I component TSG101, whereas EVs derived from the other three cell lines seemed to have lower enrichment in Alix and undetectable levels of TSG101. On the other hand, one of the mediators of caveolae-dependent endocytosis, Caveolin-1, was strongly enriched in MDA-MB-231 EVs, less represented in MDA-MB-436 and CAL51 and undetectable in MCF7 EVs. Transmembrane proteins of the tetraspanin family are often used as positive markers for EVs (Lötvall et al., 2014). I could detect the tetraspanin CD63, a marker of late endosomes, in EV preparations, in variable amounts according to the cell line tested. Negative markers, such as the cis-Golgi marker GM130 and the ER marker PDI, were

undetectable in EVs from all cell lines used, suggesting the absence of cross-contamination during the isolation process.

In Fig. 3.3B measurement of the protein content of EVs isolated from each cell line showed that MDA-231 and MCF7 cells seem to have the highest levels of protein in the EVs (120-130 µg/mL), reflecting the pattern detected in western blot.

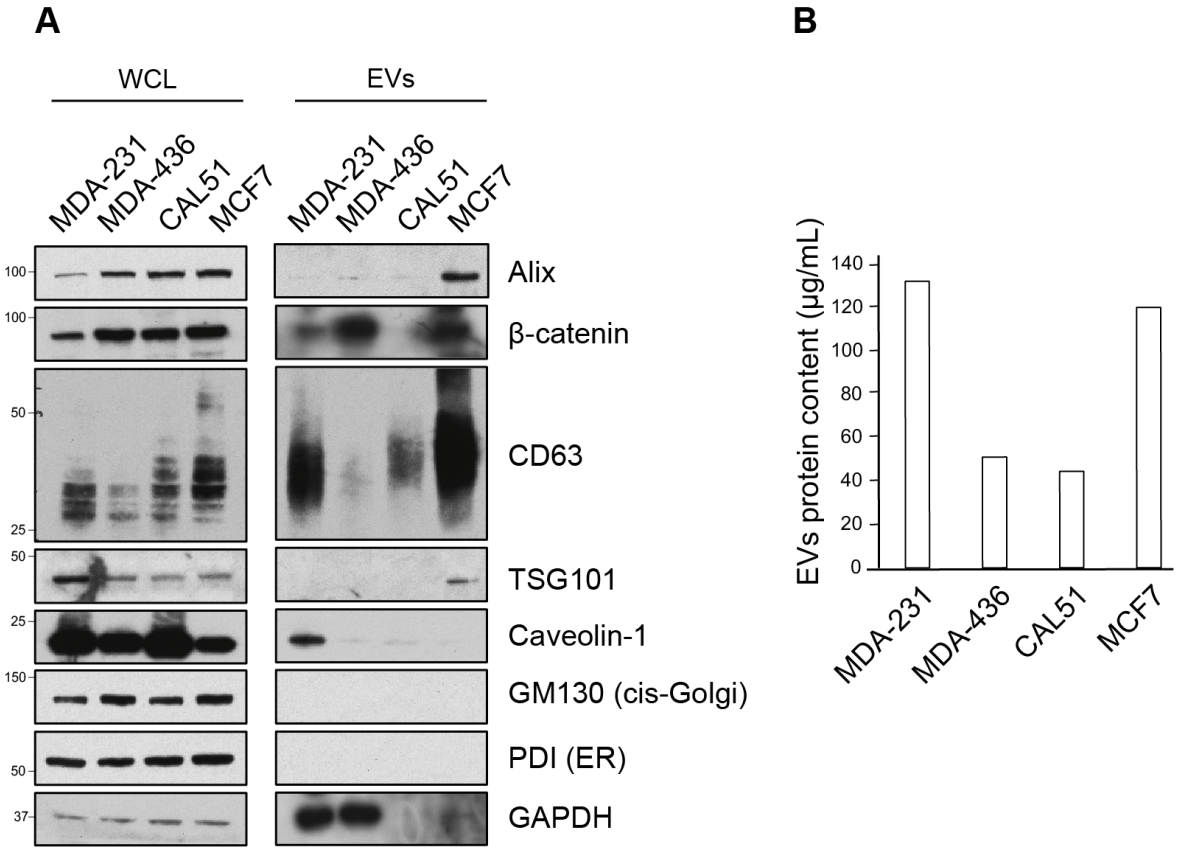


Figure 3.3 Breast cancer cells differentially express extracellular vesicle markers. MDA-MB-231, MDA-MB-436, CAL51 and MCF7 breast cancer cells were tested for EV production. Each cell line was seeded (5 x 10^6 cells/plate) and cultured as previously described. EVs were isolated from conditioned medium following the previously tested centrifugation protocol**. A.** An aliquot of EVs was resuspended in RIPA buffer and subsequent SDS-PAGE and western blot analysis for EV markers with the indicated antibodies was carried out. Equal protein loading was achieved by protein quantification using a microBCA assay kit (Thermo Scientific) and roughly 1:50 ratio of WCL:EV protein amount was loaded on a gel. Cells were lysed in Laemmli sample buffer and analysed in parallel to the EVs to ensure enrichment for EV markers in the vesicles. Negative markers such as ER or cis-Golgi markers were also used to verify the purity of the preparations. MDA-MB-231 and MCF7 cells reveal the highest amount of total protein associated to EVs (**B**) as well as the highest enrichment of protein markers analysed (**A**). Representative western blot is shown. On the left side, indicative molecular weights expressed as KDa are reported. WCL, whole cell lysate. EVs, extracellular vesicles.

Overall, from this analysis, the breast cancer cell line MDA-231 showed the highest release of EVs, in the absence of external stimuli. EVs isolated from this cell line carry several of the common proteins associated with EVs and this cell line has been used in previous studies aimed to assess the metastatic potential of EVs (Li et al., 2012; Zomer et al., 2015). I therefore decided to perform my studies focusing mainly on this cell line.

3.3.3 Visualisation of extracellular vesicles via Total Internal Reflection Fluorescence

In order to further confirm that the EV population isolated with the chosen protocol carries the common markers used to classify EVs, I employed Total Internal Reflection Fluorescence microscopy (TIRF, in collaboration with the Kennedy Institute, Oxford) to visualise EVs.

I were able to detect a variety of proteins, associated with EVs (Fig. 3.4). Interestingly, using TIRF microscopy, I observed EV markers that were undetectable via western blot analysis. For instance, high levels of the tetraspanin CD81 were detectable with immunofluorescent staining, whereas the protein was not detectable in western blotting (data not shown). The variability in detection techniques could be explained by a limitation in the range of antibodies used for western blotting in the detection of this particular tetraspanin.

The tetraspanin CD63, a marker of MVBs (Colombo et al., 2014), seemed to be highly enriched in EV preparations, suggesting that the isolated EVs have endosomal origin.

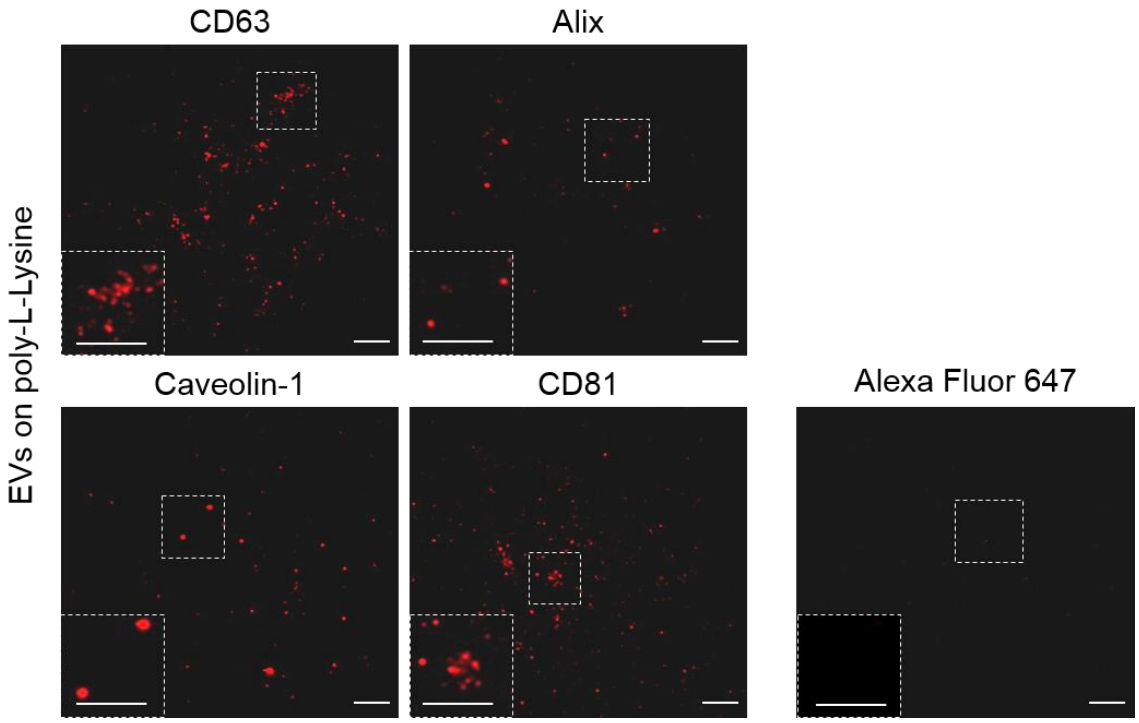


Figure 3.4 TIRF microscopy as an alternative method for validation of protein markers on EVs. MDA-MB-231 cells were seeded (5 x 10^6 cells/plate) and cultured for 72 h in 0.1% FBS (depleted of bovine serum EVs) medium. Conditioned medium was collected and EVs isolated as stated before. EVs were then incubated overnight at 4°C on a poly-L-Lysine coated chamber. The next day EVs were washed in PBS, fixed in 4% PFA and stained with the indicated antibodies. A secondary antibody only sample is shown on the right, as a negative control. Zoomed images of EVs are represented in the blow-ups. TIRF allows visualisation of markers commonly associated to EVs in MDA-MB-231 derived vesicles. Representative images are shown. Scale bar represents 5 µm.

Other markers previously shown via western blotting (Fig. 3.2A, MDA-231 lane), were also visualised via TIRF microscopy, such as Caveolin-1 and Alix (Fig. 3.4). Therefore, I can confirm successful isolation of small EVs, exosomes, released from a panel of breast cancer cells, with the current isolation method.

Using an advanced microscopy technique I were able to confirm the previously gathered data from the NTA and the western blot, suggesting that the isolation method used is reproducible and reliable to proceed with further experiments.

3.4 Discussion

One of the biggest limitations in the field of extracellular vesicles is the lack of a consensus on isolation methods. On one hand, there is an urgent need to standardise protocols in order to allow reproducibility of the studies and to exhaustively classify the type of vesicles secreted *in vitro* and *in vivo* (Witwer et al., 2017). On the other hand, the length of isolation protocols might affect the yield of the samples as well as their stability, therefore impairing further downstream analysis.

Firstly, in this chapter I aimed to compare the quality of two relatively quick isolation protocols: differential centrifugation and polymer-based precipitation, in order to choose one of them to further proceed with my study. Polymer-based precipitation is a time-saving protocol, however, NTA analysis revealed lower sample yield with this protocol, if compared to the commonly used centrifugation steps. Furthermore, a limiting factor of this technique is the presence of PEG as a precipitation reagent, a compound that might interfere with downstream analysis, e.g. mass spectrometry (Hodge et al., 2013; Taylor et al., 2015).

I therefore selected differential centrifugations as a routine isolation protocol to use in this study.

Secondly, I aimed to characterise the pool of EVs released by a panel of breast cancer cell lines. I focused on triple negative breast (TNB) cancer cells, known to be more aggressive (Dai et al., 2017), hypothesising that the chosen cell lines might secrete a consistent amount of EVs, a requirement for my study. MCF7 cells were also included in the panel, in order to have a less malignant cell line as a comparison. I successfully characterised EVs from this panel with two different approaches, NTA and western blotting of positive and negative EV markers

(Fig. 3.2 and 3.3). From my analysis MDA-231, amongst the three TNB cancer cell lines screened, were secreting the highest number of EVs. This observation led us to select this cell line for further experiments. I further substantiated the initial results on MDA-231 EVs by TIRF (Fig. 3.4).

Of note, western blot analysis showed that different cell lines secrete EVs enriched with different levels of protein markers (Fig. 3.3A). This observation reflects the difficulty in finding universal markers for EVs and is corroborated by other studies in the literature. Comparison of conventional EV proteins in various breast and prostate cancer cell lines highlighted a very diverse abundance of each marker, often correlated to the levels of the given protein in the cell type of origin (Harris et al., 2015; Yoshioka et al., 2013).

MDA-231 have been characterised as basal B carcinoma, poorly differentiated and highly metastatic (Dai et al., 2017). This cell line has been previously used in various seminal studies aimed to understand the role of EVs in metastasis and spread of the tumour (A. Hoshino et al., 2015; Melo et al., 2014; Zomer et al., 2015). For this reason and according to the characterisation carried out in this chapter I decided to focus on this cell line for my future work.

Chapter 4 An Alternative *RASSF1* Isoform Contributes to Pro-Invasive Extracellular Vesicle Release via Rho/ROCK Pathway

4.1 Introduction

The RASSF1C oncogenic isoform of the *RASSF1* gene has been detected in almost all lung, breast, paediatric and pancreatic endocrine tumours and cancer cell lines tested in various works (Burbee et al., 2001; Dammann et al., 2003; Harada et al., 2002; Malpeli et al., 2011; Reeves et al., 2013). Conversely to the major isoform encoded by the *RASSF1* gene, the *bona fide* tumour suppressor RASSF1A, a definitive role for RASSF1C in tumourigenesis has not been defined yet. However, a growing body of literature has proposed oncogenic functions for this isoform, as shown in lung, breast and oesophageal studies (Amaar et al., 2006; W. Guo et al., 2014; Reeves et al., 2010). Moreover, previously published work from our lab supported an oncogenic potential for RASSF1C in breast cancer cells. I showed that RASSF1A and RASSF1C have antagonistic roles. Both isoforms interact with the SRC kinase and respectively inhibit or promote its activity. Additionally, RASSF1C activation of SRC leads to a phenotypic switch with loss of epithelial phenotype, via E-cadherin internalisation, and promotion of cell motility and invasiveness (Vlahov et al., 2015). Interestingly, data previously generated in the lab linked RASSF1C tumourigenic activity to the release of extracellular vesicles.

4.1.1 The role of RhoA signalling in cell migration and invasion

Several proteins are known to orchestrate extracellular vesicle biogenesis, from the classical ESCRT (Endosomal Sorting Complex Required for Transport) machinery and Rab family of GTPases, to tetraspanins, SNARE complexes, syndecans as well as lipids such as ceramide. Interestingly, also the Rho family of small GTPases has been involved in this process (Li et al., 2012; Muralidharan-Chari et al., 2009).

Rho GTPases are a subgroup of the Ras family of GTPases, namely Ras, Rho, Rab, Arf and Ran. As other members of the family, Rho GTPases function as a molecular switch from the inactive (GDP-bound) state, to the active (GTP-bound) one. When active, they recognise effectors, thereby generating a response until GTP is hydrolysed and the GTPase is rendered once again inactive. Except for GTP hydrolysis, the regulation of these proteins can be achieved in other ways. In the human genome there are over 60 activators (guanine nucleotide exchange factors, GEFs) and over 70 inactivators (GTPase-activating proteins, GAPs) for these proteins. Within the Rho family more than 20 members can be identified, divided in 6 subfamilies: RhoA-related, Rac1-related, Cdc42-related, Rnd, RhoBTB, and the Miro subfamily (Bryan et al., 2005; Paduch et al., 2001). The best characterised members are RhoA, Rac1 and Cdc42 and each of them has a pivotal role in controlling cytoskeleton reorganisation, cell motility and mode of migration (Etienne-Manneville et al., 2002). Precisely, RhoA regulates actin stress fibres and the assembly of focal adhesions (A. J. Ridley & Hall, 1992), whereas Rac1 orchestrates actin-rich membrane ruffling (lamellipodia) formation (A. J. Ridley, Paterson, et al., 1992) and Cdc42 is involved in generation of two different

actin-rich, finger-like membrane extensions, named filopodia and invadopodia (Kozma et al., 1995; Nobes et al., 1995).

In regard to direction of movement, a tight interplay between RhoA, Rac1 and Cdc42 is necessary for the cell to relocate. High Rac1 activity is required for the cell leading edge, to establish movement (Kraynov et al., 2000). Cdc42 is required for directionality of the movement, controlling the input from external cues, such as chemotactic gradient formation (Allen et al. 1998). RhoA and its effector ROCK are instead needed for actomyosin contractility at the back of a migrating cell (A. J. Ridley et al., 2003; Worthylake et al., 2001). Remarkably, RhoA/ROCK can also drive the so called bleb-driven motility. In this case, RhoA activates ROCK that in turn phosphorylates myosin light chain II at Ser 19 (pMLCII). At this stage, cortical actomyosin contractility is enhanced and is particularly apparent at the front and rear, but not on the sides, of the cell. Phenotypically, the cell adopts a rounded amoeboid shape, associated with highly dynamic membrane blebbing processes (Sahai et al., 2003).

In virtue of its functions in relation to cell motility, the Rho family is also orchestrating modes of invasion, a phenomenon particularly relevant to cell development as well as tumour dissemination. There are two main types of invasion. An elongated mesenchymal type is mostly ascribed to Rac1 activity in concert with other complexes, where cells combine migration and extracellular matrix (ECM) degradation. The matrix breakdown process is mediated by metalloproteases (MMPs), released at the leading edge by the moving cells in order to create a path through the matrix. A rounded amoeboid type, where cells do not need to degrade the surrounding matrix, instead they remodel their cytoskeleton in order to squeeze through gaps in the ECM, is governed by RhoA

(Pandya et al., 2017; Sahai, 2005). *In vivo* these two modes are often interchangeable, as invading cells are able to switch from one mode to the other according to external stimuli or physical barriers.

Importantly, all the three main members of the Rho family, RhoA, Rac1 and Cdc42, have been implicated in regulating endocytosis and intracellular transport (Lamaze et al., 1996; Anne J. Ridley, 2001). Moreover, links to exocytosis have already been established in secretory cells (Pinxteren et al., 2000).

Interestingly, a recent number of studies has highlighted a novel role for the family member RhoA in promoting the secretion of extracellular vesicles. In one of these reports EVs have been classified as microvesicles (MVs, in the size range of 1-10 μm). However, the isolation approaches used in this study strongly resemble the protocols for isolation of smaller EVs (i.e. exosomes, 50-150 nm, isolated with ultracentrifugation). Regardless of the discrepancy in nomenclature used, the study showed that RhoA, and not Rac1, Cdc42 or Ras, activation, leading to distinct downstream events involving the ROCK-LIMK-Cofilin axis, culminated in the release of extracellular vesicles able to induce fibroblast transformation in vivo (Li et al., 2012). Another study remarkably linked modes of tumour invasion to extracellular vesicle shedding. Specifically, according to the compliance of the environment (i.e. stiffness of the matrix), cancer cells would either adopt a mesenchymal or amoeboid type of motility, the latter being associated to the release of EVs (Sedgwick et al., 2015). More appropriately in this case the vesicles were referred to as microvesicles and isolated with a different method (lower centrifugation speed), compared to the previous publication (Li et al., 2012). Interestingly another study proved that Rac1 activity is inhibitory to EVs shedding, whereas RhoA/ROCK/pMLCII signalling promotes it, in this case as downstream

effectors of the small GTPase, Arf6 (Muralidharan-Chari et al., 2009). Collectively, these reports suggested a novel function for RhoA GTPase in promoting EV secretion.

4.2 Aims

Previous work in the lab has demonstrated a tumour promoting role for RASSF1C associated to breast cancer invasiveness, *in vitro* and *in vivo*. Moreover, preliminary data supported the hypothesis that one of RASSF1C mechanisms in mediating tumour progression is the release of extracellular vesicles. My aim in this chapter is: (I) to understand the functionality of EVs released by RASSF1C cells, (II) to examine the ability of these EVs to transfer the oncogenic phenotype on to recipient cells and (III) to investigate the underlying mechanism that RASSF1C triggers to promote extracellular vesicle secretion.

4.3 RASSF1C Promotes Extracellular Vesicles Release

4.3.1 *RASSF1* gene knockdown impairs extracellular vesicle release

The two major isoforms encoded by the *RASSF1* gene are RASSF1A and RASSF1C. In MDA-231 cells the tumour suppressor *RASSF1A* promoter region is heavily methylated, leading to epigenetic inactivation and loss of expression. However, the alternative isoform RASSF1C is not methylated and often loss of RASSF1A correlates with higher expression of RASSF1C (Grawenda et al., 2015; Volodko et al., 2016). I validated mRNA levels of both isoforms in MDA-231 cells

as shown in Fig. 8.2 (Appendix) and observed that RASSF1A mRNA levels were significantly down-regulated, if compared to RASSF1C ones. I first decided to test whether RASSF1C depletion could alter EV secretion. In order to achieve that, I depleted RASSF1C in MDA-231 cells via siRNA-mediated knockdown, using a siRNA that targets exon 3 of the *RASSF1* gene, common to both RASSF1A and RASSF1C isoforms. However, given that RASSF1A mRNA levels in these cells were negligible (see Appendix Fig. 8.2), the knockdown targeted mostly the RASSF1C isoform. After RNAi treatment, cells were cultured in 0.1% FBS medium for 72 h prior to harvest of extracellular vesicles.

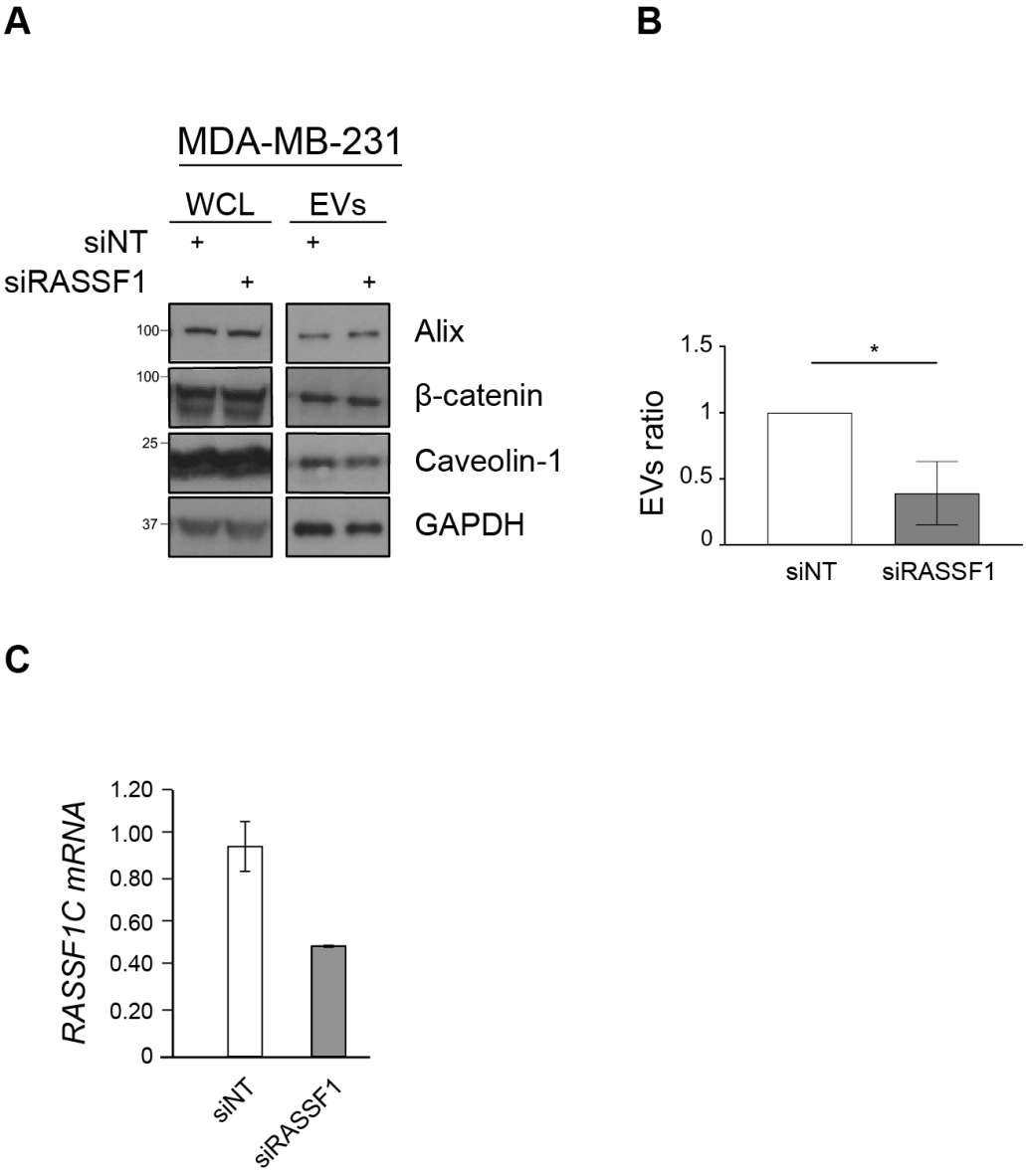


Figure 4.1 RASSF1 knockdown reduces the amount of secreted EVs. MDA-MB-231 cells were seeded (5 x 10^6 cells/plate) and transfected with siRNAs targeting the C-terminal sequence of RASSF1 (shared by both isoforms RASSF1A and RASSF1C) or Non-Targeting (NT) siRNA. Cells were incubated in 0.1% FBS medium for 72 h prior to harvest of both cell lysates and EVs. **A.** Cell and EV lysates were normalised for protein content, run on a SDS-PAGE gel and analysed with the indicated antibodies. Upon RASSF1 knockdown the levels of EV markers are reduced. **B.** An aliquot of EVs was diluted 1:100 in PBS and NTA analysis revealed a decrease in particle concentration upon RASSF1 depletion. EVs ratio was calculated per each replicate as particle concentration of treated condition (siRASSF1) divided by particle concentration of control condition (siNT). **C.** RNA was isolated from cell lysates and cDNA was prepared. RT-qPCR (TaqMan assay) was performed on a StepOnePlus™ Real-Time PCR machine, to ensure efficient RASSF1C depletion. Expression of 18S was used as an internal control. *RASSF1* depletion results in the decrease of overall particle count (**B**). Data are represented as mean ± SEM of N=3 experiments. * $p \leq 0.05$ with one-tailed Student's t-test.

Knockdown of RASSF1C caused a significant decrease in the overall amount of EVs, as shown by NTA data in Fig. 4.1B. However, most EV markers chosen to

characterise the protein cargo were not affected (Fig. 4.1A). In Fig. 4.1C qPCR of RASSF1C mRNA levels upon knockdown are shown, confirming a 50% depletion.

4.3.2 Exogenous expression of RASSF1C leads to increase in extracellular vesicle secretion in breast cancer cells

Data previously generated in the lab by Nikola Vlahov have shown that ectopic expression of RASSF1C in MDA-231 cells over a period of 72 h is sufficient to stimulate secretion of exosomes in the range of 10^9 particles/mL. In Fig. 4.2A a representative graph of the amount of EVs harvested after 72 h of culture in the presence or in the absence of a transfected Flag-RASSF1C construct is shown. RASSF1C ectopic expression did not alter EVs size range, however, as the quantification shows in Fig. 4.2B, the overall amount of secreted EVs was significantly higher in the RASSF1C condition, compared to control. These data support my previous observation that RASSF1C knock-down decreases the overall particle concentration, as measured by NTA (Fig. 4.1B).

Importantly, exogenous expression of a RASSF1C construct did not lead to supra-physiological levels of RASSF1C mRNA, generating only a 3-fold increase in RASSF1C, as shown in Appendix Fig. 8.3.

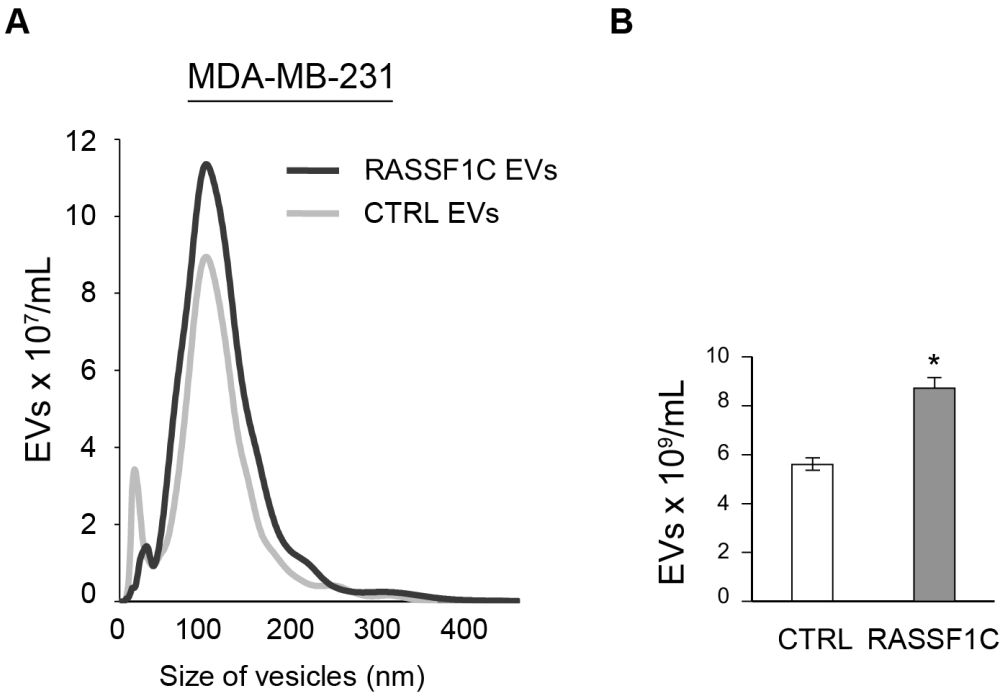


Figure 4.2 RASSF1C over-expression promotes extracellular vesicle secretion. MDA-MB-231 cells were seeded (5 x 10^6 cells/plate) and transiently transfected with pcDNA3.1 or Flag-RASSF1C constructs. Cells were grown in 0.1% FBS medium for 72 h and EVs were isolated from conditioned media as stated before. NTA was employed to quantify the amount of EVs released in each condition. Isolated EVs were resuspended in PBS and diluted 1:100 prior to NTA analysis. **A.** Representative graph of the NTA analysis for pcDNA3.1 and Flag-RASSF1C samples. RASSF1C over-expression does not alter the EV profile. **B.** Quantification of NTA data. RASSF1C promotes the release of a significantly higher amount of EVs compared to control. Data are represented as mean ± SEM of N>3 independent experiments. * $p \leq 0.05$ as with Student's t-test. These experiments were done in collaboration with Nikola Vlahov.

Next, I intended to evaluate if RASSF1C expression could cause any alteration in EV protein cargo. Knock-down experiments did not result in any significant change in EV protein cargo (Fig. 4.1A). I thus analysed via western blotting the enrichment for commonly used markers in EV preparations and added to the previously used markers also CD63, a tetraspanin commonly used to characterise EV preparations. Fig. 4.3 shows that, among the chosen markers, CD63 was enriched in the RASSF1C vesicles. Interestingly, other markers did not follow this pattern. Namely, levels of the ESCRT interacting partner Alix in EVs were not affected by RASSF1C over-expression. This observation well reflects the possibility that different subpopulations of EVs may be differentially affected by treatments or

environmental stimuli and could also provide a reasoning for not detecting cargo down-regulation in the knock-down experiments (Fig.4.1). Of note, when probed for RASSF1C (Flag) in the EV lysates, the protein was not detectable, indicating potentially that RASSF1C mechanism of action for EV release is upstream to the secretion event and the protein itself is not released in association with EVs.

Interestingly, other cell lines, such as MCF7 or the lung adenocarcinoma cells line H1299, did not show altered EV release upon RASSF1C ectopic expression (Appendix, Fig. 8.1).

Taken together, the data suggest that RASSF1C plays a role in modulating overall EV release, as shown by both knock-down and over-expression results. Furthermore, over-expression of RASSF1C in MDA-231 cells leads to enrichment in $CD63^+$ EVs.

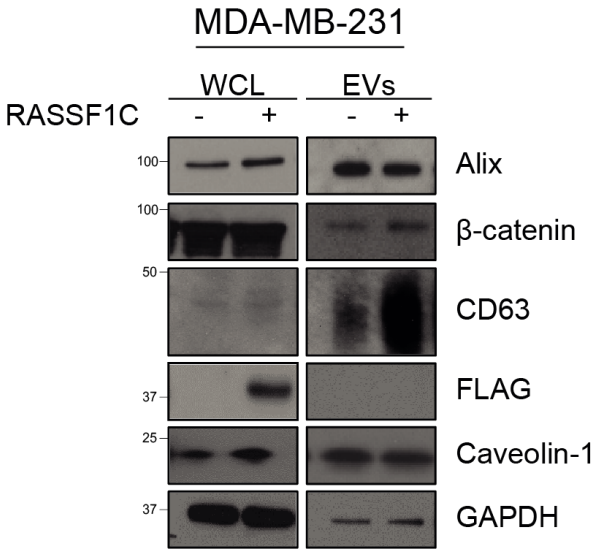


Figure 4.3 RASSF1C over-expression alters extracellular vesicle protein cargo. MDA-MB-231 cells were seeded (5 x 10^6 cells/plate) and transiently transfected with pcDNA3.1 or Flag-RASSF1C constructs. Cells were grown in 0.1% FBS medium for 72 h and EVs were isolated from conditioned media as stated before. An aliquot of EVs was lysed in 1X RIPA buffer and kept for protein markers evaluation. EV protein content was normalised against the number of cells present in the plate at the end of the experiment, prior to SDS-PAGE and western blot analysis with the indicated antibodies. RASSF1C expression promotes the secretion of a specific pool of EVs, decorated with CD63 and β-catenin. Data are representative of N>3 independent experiments. These experiments were done in collaboration with Nikola Vlahov.

4.4 RASSF1C Extracellular Vesicles Transfer the Invasive Phenotype to Recipient Cells

4.4.1 RASSF1C extracellular vesicles are internalised by recipient cells

It is well understood in the literature how extracellular vesicle transfer of material from a more aggressive cell type to a less malignant one drives phenotypic changes in the latter (Garnier et al., 2012; Schillaci et al., 2017). Having showed that the oncogene RASSF1C promotes EV secretion and conversely its depletion leads to partial impairment of EV release, I sought to understand whether the population of EVs driven by RASSF1C could transfer oncogenic behaviour to recipient cancer cells.

Firstly, I determined whether EVs isolated with the chosen protocol maintain biological activity and are internalised by recipient cells. I seeded and transfected MDA-231 cells with either a control or Flag-RASSF1C plasmid, as previously described, and collected EVs after 72 h of incubation in 0.1% FBS medium. In order to ensure the loading of equal amounts of EVs onto the recipient cells, one aliquot of EVs was measured with Bicinchoninic Acid Microprotein Assay kit (microBCA), a method used for detection of proteins in the range of 0.5-20 µg/mL. The remainder of isolated EVs were stained with PKH67, a lipophilic dye used for membrane labelling, following a previously published protocol (Sheldon et al., 2010). In order to visualise internalisation of EVs, I treated recipient MDA-231 cells for 18 h with either vehicle (PBS), control EVs or RASSF1C EVs. After 18 h cells were fixed and stained for CD63 to visualise both multivesicular bodies (MVBs, marked in red) in the cells and the internalised EVs (in green). Fig. 4.4 shows

representative cells per condition. In the vehicle treated cells (top panel) no PKH67 dye was visible and only MVBs, marked with CD63, were visible. Both control and RASSF1C EVs were visible after 18 h of treatment, as PKH67 staining is detectable in both middle and bottom panels of Fig. 4.4.

These data show that extracellular vesicles from donor cells can be internalised by recipient cells and subsequently visualised.

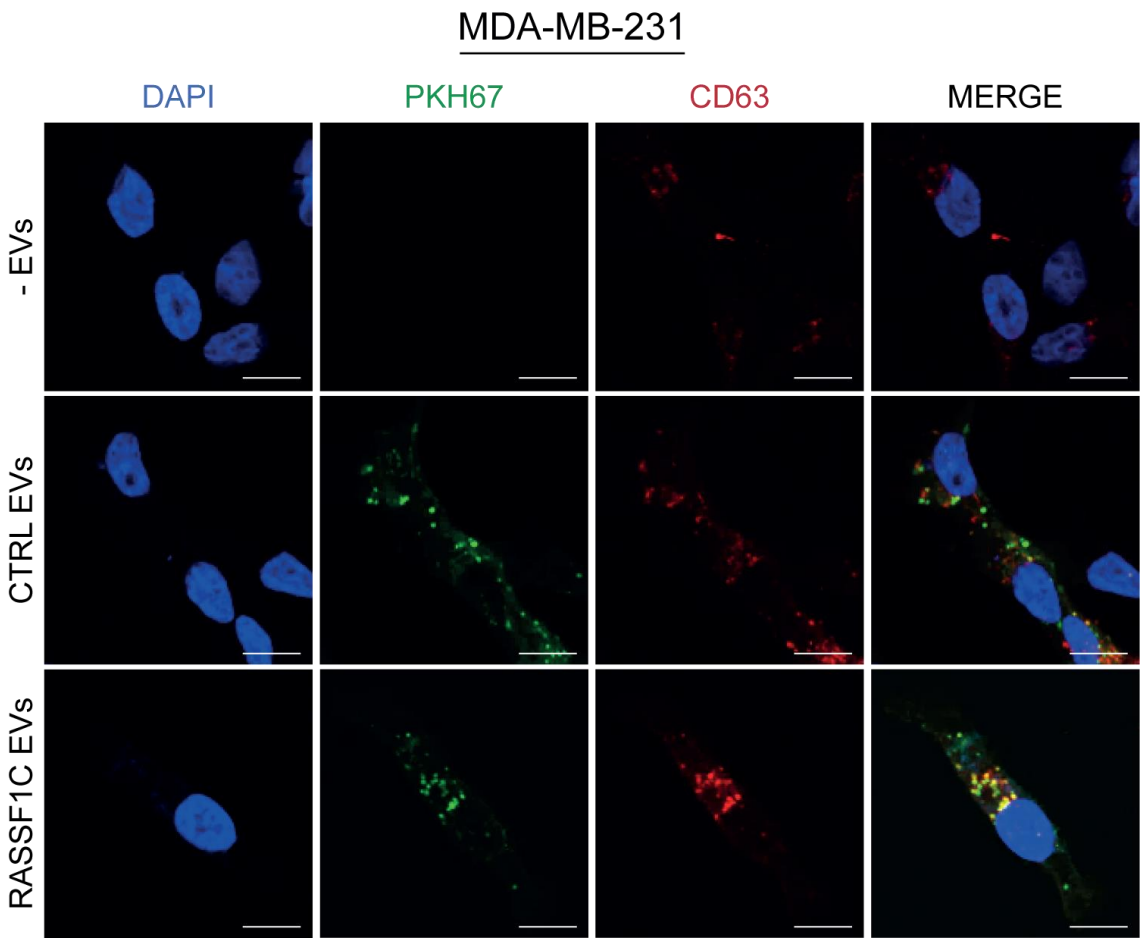


Figure 4.4 Extracellular vesicles from control and RASSF1C cells are efficiently taken up by recipient cells. MDA-MB-231 cells were seeded (5 x 10^6 cells/plate) and transfected or not with either control (pcDNA3.1) or Flag-RASSF1C constructs and cultured in 0.1% FBS medium for 72 h. EVs were harvested via differential centrifugations and an aliquot was resuspended in 1X RIPA buffer for protein quantification with microBCA assay, to ensure equal loading onto recipient cells. The remainder were resuspended in PBS prior to membrane labelling with PKH67 dye (Sigma-Aldrich) according to manufacturer's instructions. PKH67 labelled EVs were then incubated or not with recipient MDA-MB-231 cells, plated as 2 x 10^5 cells/well in 6-well plates, for 18 h. Recipient cells were fixed in 4% PFA and stained for the indicated antibodies. Both control and RASSF1C EVs were internalised by recipient cells. Scale bars represent 20 μm. This experiment was done in collaboration with Nikola Vlahov.

4.4.2 RASSF1C extracellular vesicles promote migration in recipient cells

Having confirmed that control and RASSF1C EVs are efficiently taken up by recipient cells I focussed on testing their biological activity on target cells. Firstly, I evaluated the ability of recipient MDA-231 cells to migrate towards a chemoattractant, in the presence or absence of EVs. The assay used is xCELLigence (ACEA Biosciences), an electronically integrated Boyden chamber where upper and lower wells are separated by a polyethylene terephthalate (PET) microporous membrane. The bottom side of the upper membrane is coated with gold microelectrode sensors that have a reduced ability to conduct electric current when cells adhere to their surface. This is the impedance signal which enables a quantitative measurement of cell movement towards a chemoattractant (10% FBS medium) placed in the lower chamber.

The same protocol as previously described was followed to harvest EVs from control or RASSF1C transfected cells. EVs were then normalised according to the protein content and equal amounts (arbitrarily chosen, 15 ng/mL and 30 ng/mL) were incubated with recipient MDA-231 cells in the upper well of an xCELLigence plate in 0.1% FBS medium. After 36 h of incubation, the cell migration index was extrapolated (see Fig. 4.5, Experimental setup).

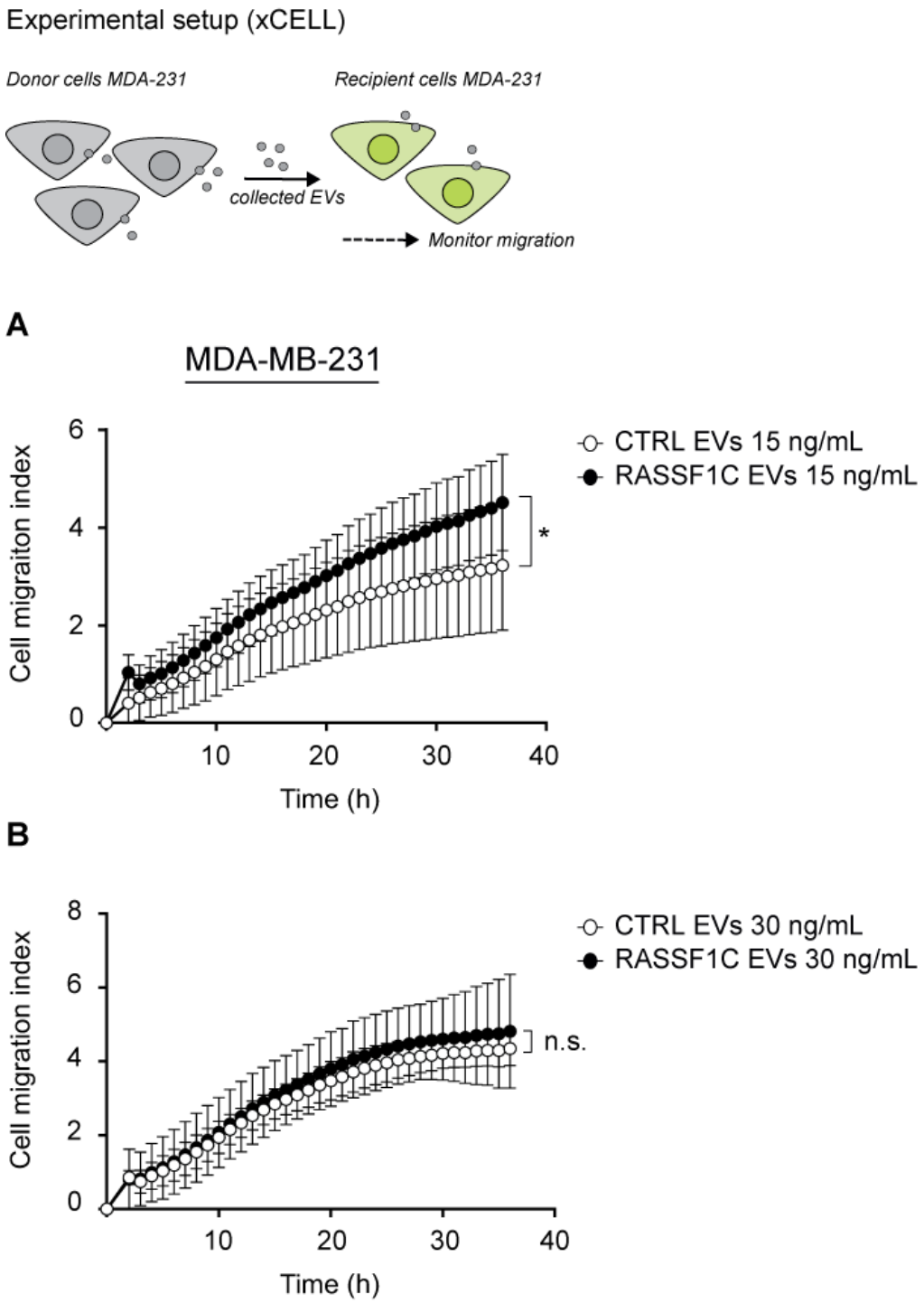


Figure 4.5 RASSF1C EVs promote migration in recipient cells. MDA-MB-231 cells were seeded (5 x 10^6 cells/plate) and transfected with either control (pcDNA3.1) or Flag-RASSF1C constructs and cultured in 0.1% FBS medium for 72 h. EVs were harvested via differential centrifugations and an aliquot was resuspended in 1X RIPA buffer for protein quantification (microBCA assay), to ensure equal loading onto recipient cells. The remainder was resuspended in PBS, normalised and the indicated amounts incubated or not with recipient MDA-MB-231 cells, plated as 5 x 10^4 cells/well onto xCELLigence Real-Time Cell Analyser CIM plate (Roche) for 36 h, according to manufacturer's protocol. Cell migration index in each condition was normalised against an untreated control and was quantified over 36 h of incubation by RTCA software 2.0. Top, experimental setup is shown. **A.** 15 ng/mL and **B.** 30 ng/mL of EVs were incubated with recipient cells in each condition. The lower concentration chosen (15 ng/mL) revealed a window of differential response of the recipient cells to the EVs. The signal was then saturated at the higher concentration (30 ng/mL). Data are represented as mean ± SEM of N=3 independent experiments. * $p \leq 0.05$ was calculated with the nonparametric Mann-Whitney test.

Notably, treatment with EVs resulted in faster migration of recipient cells, if compared to baseline untreated cells (data not shown but incorporated in the calculation). In Fig. 4.5A the graph spanning the 36 h of incubation period shows that 15 ng/mL RASSF1C EVs significantly increased recipient cells migratory index, compared to control EVs. However, when the amount of EVs was doubled (30 ng/mL), RASSF1C and control EVs efficacy on cells migratory ability became comparable.

These results suggest that any qualitative differences in cargo between control and RASSF1C EVs that may result in a biological effect on recipient cells might be neutralised by increasing EV quantity, revealing a very narrow window for functional assays *in vitro*.

4.4.3 RASSF1C extracellular vesicles promote invasion in recipient cells

Cell migratory capacity is fundamental to cancer progression, however, the ability to invade neighbouring tissues moving through the extracellular matrix (ECM) is an equally important feature of aggressive tumours (Friedl et al., 2012). To address whether RASSF1C driven EVs were also able to drive invasion in recipient cells I isolated control and RASSF1C EVs from MDA-231 cells as previously described and incubated recipient MCF7 cells for 18 h in the presence of vehicle (PBS) or EVs, in Matrigel coated Boyden chambers (Corning). MCF7 breast cancer cells were chosen because they are considered less invasive than MDA-231 (Dai et al., 2017). In the employed system upper and lower chambers are separated by a porous membrane coated with a thin layer of Matrigel matrix, which recapitulates the composition of the basement membrane. Invasive, or rendered invasive, cells detach from the top well and squeeze through the matrix

in order to reach the chemoattractant (10% FBS medium) placed in the bottom well of the system. In light of the results obtained in Fig. 4.5, we decided to treat MCF7 cells with a single concentration of EVs: 15 ng/mL. After 18 h, untreated MCF7 cells were able to invade through the matrix (Fig. 4.6A, left picture). Remarkably, MCF7 cells treated with RASSF1C EVs showed significantly higher invasive capacity than both untreated and control EV-treated cells (Fig. 4.6A and 4.6B).

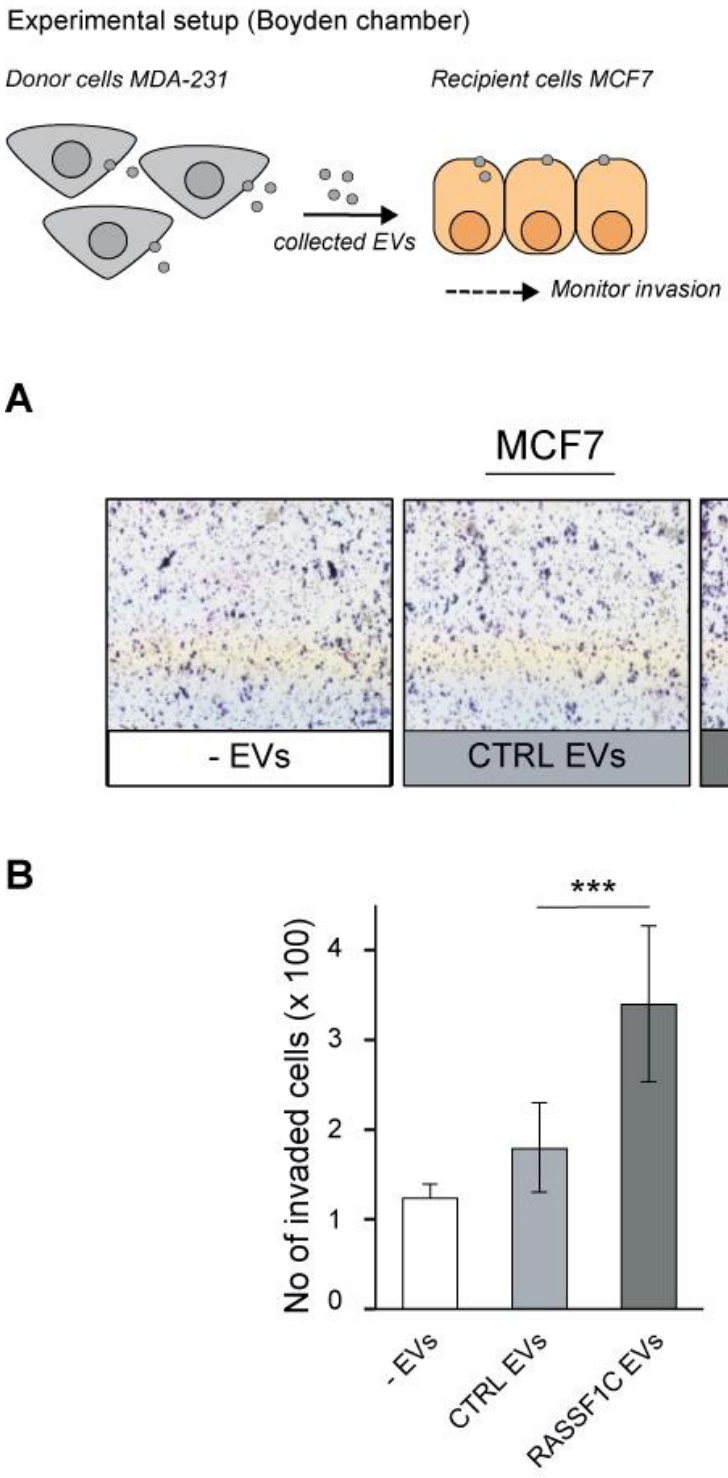


Figure 4.6 RASSF1C EVs promote 3D Matrigel invasion in recipient cells. MDA-MB-231 cells were seeded (5 x 10^6 cells/plate) and transfected with the same constructs as in Figure 4.5. EVs were collected via differential centrifugations and an aliquot was resuspended in 1X RIPA buffer for protein quantification (microBCA assay), to ensure equal loading onto recipient cells. The remainder was resuspended in PBS, normalised and incubated or not with recipient MCF7 cells, plated as 5 x 10^4 cells/well onto Transwell Matrigel chambers (Corning). After 18 h, invaded cells were fixed and stained and brightfield images were taken on a Nikon 90i light microscope. The number of cells that invaded the Matrigel was quantified with ImageJ software 1.51s. Top, experimental setup is shown. **A.** Representative brightfield images per condition. **B.** Quantification of the number of invaded cells. RASSF1C EVs drive significantly higher Matrigel invasion in recipient MCF7 cells, compared to control EVs. Data are represented as mean ± SEM of N=3 independent experiments. *** $p \leq 0.001$ as with Student's t-test. This experiment was done in collaboration with Daniela Pankova.

4.4.4 The Cre-LoxP model confirms RASSF1C role in promoting EV release *in vitro*

In vitro and *in vivo* treatment with extracellular vesicles often poses a challenge on using an arbitrary amount of vesicles, frequently not representative of physiological events. *In vitro* experiments for instance will ignore the biodistribution and bioavailability of EVs released by a certain cell type *in vivo* and will focus only on a selected recipient cell type, possibly exacerbating this cell type´s response by treating it directly with EVs. This scenario *in vivo* is much more complex, where EVs released from donor cells face physical barriers and layers of various cell types. Thus, *in vitro* treatment of recipient cells might be an unfaithful representation of *in vivo* events. In order to encompass some of the limitations of an *in vitro* setup I referred to a recently published EV transfer system which uses the Cre-LoxP recombination technique (Zomer et al., 2015). The system includes a donor cell line, stably expressing CFP and the Cre recombinase enzyme, and a reporter$^+$ cell line harbouring a Cre-LoxP locus, which normally expresses a DsRed reporter (i.e. fluoresces in red). When the two cell types are either co-cultured or incubated in a transwell assay, the donor cells will release Cre mRNA$^+$ EVs (Zomer et al., 2015). These EVs, if internalised by the reporter$^+$ cells, will induce a colour switch due to the Cre recombinase activity, and the reporter$^+$ cells will start expressing an eGFP reporter (i.e. fluoresce in green), normally silenced within the Cre-LoxP locus (schematics represented in Fig. 4.7). This system is applicable both *in vitro* and *in vivo* and it allows to quantify and follow reporter$^+$ cells that have internalised Cre$^+$ EVs (the recombined green cells) and distinguish them from reporter$^+$ cells that have not taken up EVs (the unrecombined red cells).

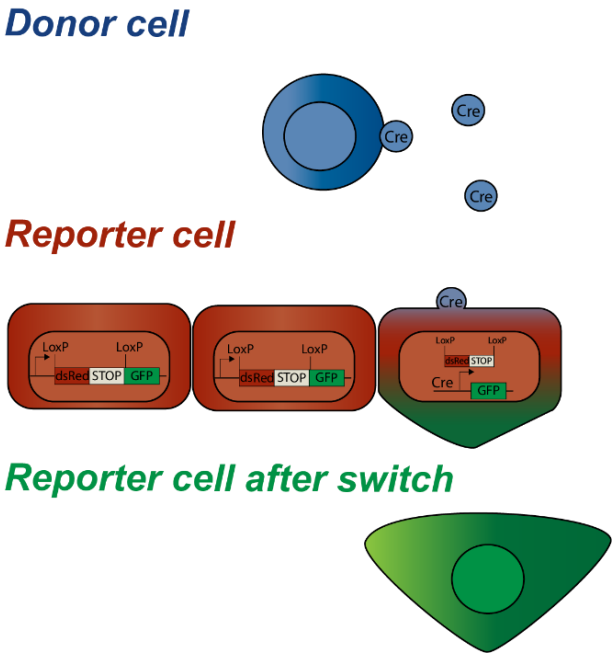


Figure 4.7 Graphical representation of the Cre-LoxP system to study EV transfer. The Cre-LoxP model employs a donor cell line, MDA-MB-231-Cre^{+} expressing a CFP reporter and the Cre recombinase, and a reporter cell line, T47D reporter^{+} cells expressing a DsRed^{+} reporter. The donor cells release EVs loaded with Cre recombinase mRNA. When cultured together, either in co-culture or in a transwell assay, the Cre^{+} EVs are internalised by reporter^{+} cells. The reporter^{+} cells undergo a colour switch due to the Cre-mediated excision of DsRed^{+} and they start expressing an eGFP^{+} reporter. Thus, recipient cells that do not take up EVs are marked in DsRed, whereas cells that have taken up EVs are marked in eGFP.

This system allowed us to assess the intrinsic ability of RASSF1C cells to release vesicles and of recipient cells to internalise them, without artificially establishing a precise amount of vesicles to treat cells. As a donor cell line I chose MDA-MB-231 cells stably expressing CFP-Cre (control) or also expressing a HA-RASSF1C construct (RASSF1C). As a reporter^{+} cell line I used T47D cells, HER2^{-} intraductal carcinoma, generally considered less aggressive than the donor cells (cell lines kindly given by J. Van Rheenen).

Donor, either control or RASSF1C expressing, and reporter^{+} cells were co-cultured at a ratio of 1:100 reporter^{+}/donor for 7 days in 0.1% FBS medium, prior to imaging (following a previously published protocol (Zomer et al., 2015)). In Fig. 4.8A representative images of co-cultures in both conditions are shown.

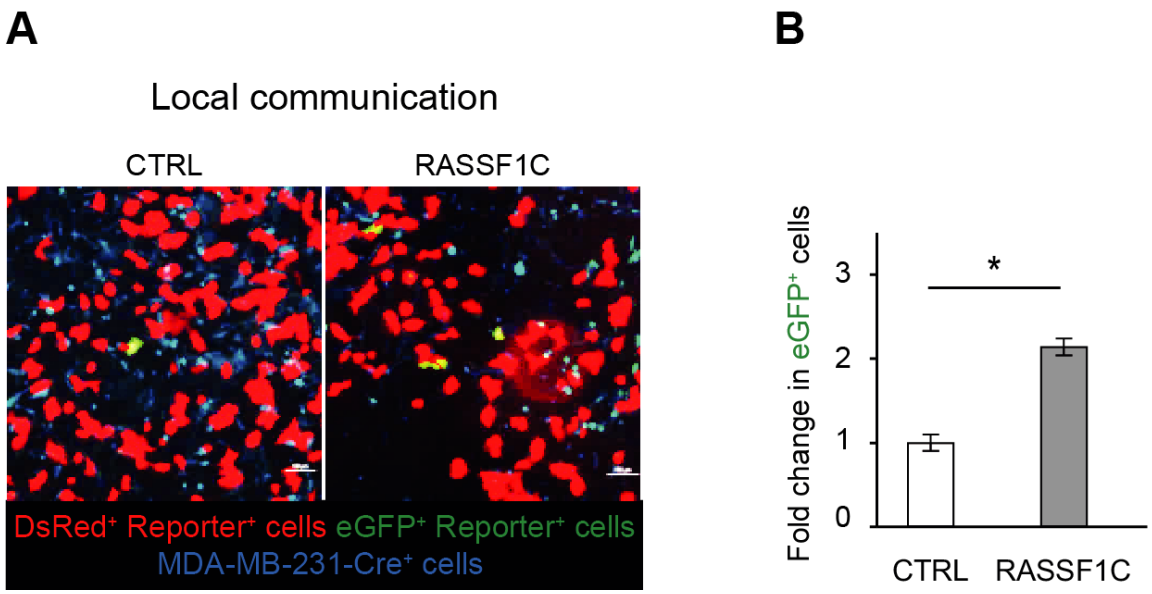


Figure 4.8 RASSF1C EVs are internalised at higher rates than control EVs by reporter$^+$ cells in a co-culture setup. Cre$^+$ donor cells were transfected with either a control (pcDNA3.1) or HA-RASSF1C construct. Cre$^+$ and DsRed reporter$^+$ cells were seeded in a 1:100 reporter$^+$/donor ratio and co-cultured for 7 days in 0.1% FBS medium. On day 7, cells were imaged on a Nikon TE2000 inverted microscope for green, red and CFP channels. **A.** Representative images of control and RASSF1C conditions were taken. **B.** Quantification expressed as fold change over control of the amount of eGFP$^+$ cells is shown. RASSF1C donor cells induce a significantly higher reporter$^+$ cells switch, compared to control donor cells. Scale bars represent 100 µm. Data are represented as mean ± SEM of N=3 independent experiments. * $p \leq 0.05$ as with Student's t-test.

In Fig. 4.8B the number of eGFP$^+$ reporter$^+$ cells was quantified for both conditions and expressed as fold change over control. RASSF1C donor cells induced a significantly higher amount of reporter$^+$ cells to switch from red to green, compared to control.

Since the co-culture assay would not exclude transfer of material via cell-cell contact, a transwell experiment was also set up in the same conditions. In the transwell chamber, donor cells are placed in the top wells and reporter$^+$ cells in the bottom wells of the chamber. The two wells are separated by a membrane with 0.4 µm pores, sufficient to allow EV transfer, but not cell-cell contact.

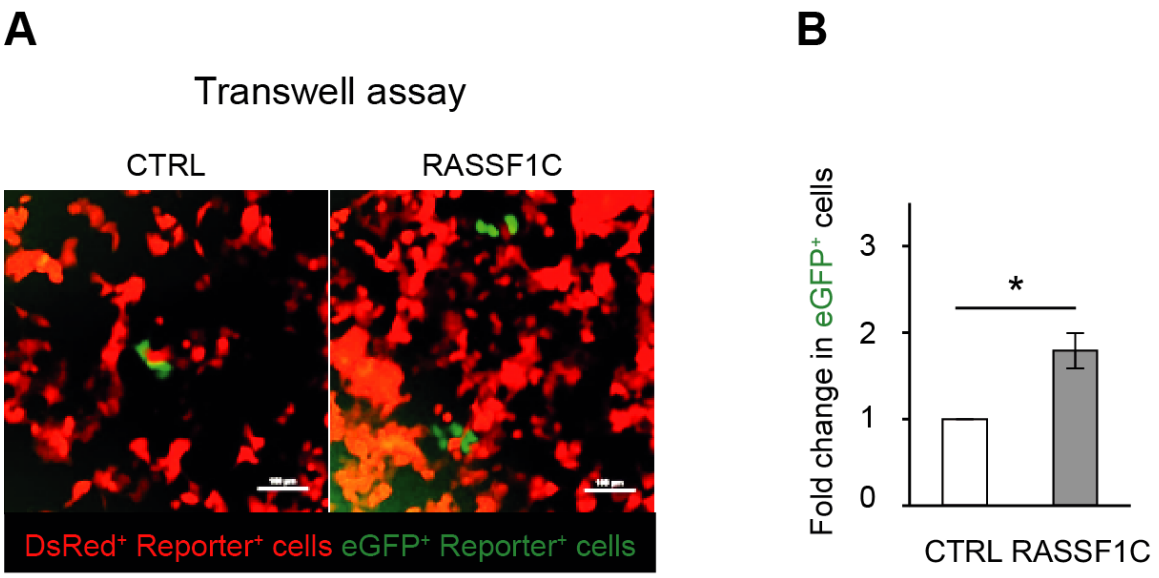


Figure 4.9 RASSF1C EVs are internalised at higher rates than control EVs by reporter$^+$ cells in a transwell assay. Cre$^+$ cells were transfected with either a control (pcDNA3.1) or HA-RASSF1C construct. Cre$^+$ donor and DsRed reporter$^+$ cells were seeded in a transwell in a 1:100 reporter$^+$/donor ratio and cultured for 7 days in 0.1% FBS medium. The 0.4 µm porous membrane allows only EV transfer between wells rather than cell-cell contact. On day 7, cells were imaged on a Nikon TE2000 inverted microscope for green, red and CFP channels. **A.** Representative images of control and RASSF1C conditions. **B.** Quantification expressed as fold change over control of the amount of eGFP+ cells. RASSF1C donor cells induce a significantly higher reporter$^+$ cells switch, compared to control donor cells, in a transwell setup. Scale bars represent 100 µm. Data are represented as mean ± SEM of N=3 independent experiments. * $p \leq 0.05$ as with Student's t-test.

In Fig. 4.9 similar results to Fig. 4.8 were obtained, reinforcing the hypothesis that RASSF1C leads to higher reporter$^+$ cells switch due to EV transfer. In both setups reporter$^+$ cells were also cultured separately from donor cells in order to monitor spontaneous recombination events (for the described incubation time no spontaneous events were observed, data not shown).

Taken together these results suggest that RASSF1C driven extracellular vesicles can be internalised by recipient cells and are able to transfer the malignant phenotype, as shown with different functional assays.

4.5 RASSF1C Driven Aggressive Phenotype Requires Rho/ROCK Pathway Activation

4.5.1 RASSF1C cells display rounded morphology due to RhoA activation

The ability of RASSF1C cells to release extracellular vesicles with a pro-migratory and pro-invasive potential led us to question the intracellular mechanisms involved.

Previous data from our lab prompted our attention to the morphology of RASSF1C positive cells. In fact, RASSF1C cells had typically a more rounded shape, despite MDA-231 cells being normally mesenchymal and elongated.

In Fig. 4.10 a ZsGreen and a ZsGreen-RASSF1C (hereafter Zs-RASSF1C) constructs were transfected in MDA-231 cells, seeded on fibronectin coated coverslips and cell morphology was assessed via immunofluorescence.

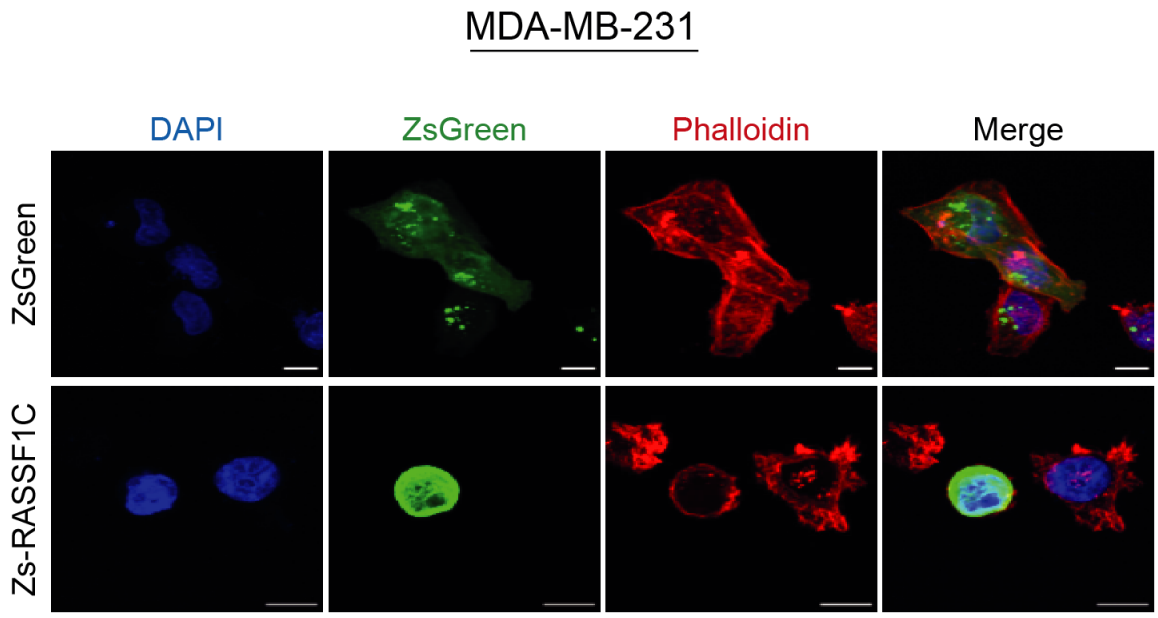


Figure 4.10 RASSF1C promotes a rounded phenotype in breast cancer cells. MDA-MB-231 cells were grown (1 x 10^5 cells/plate) on coverslips coated with fibronectin and a ZsGreen or ZsGreen-RASSF1C constructs were transfected for 48 h. Cells were then fixed in 4% PFA and immunofluorescent staining of Phalloidin-568 was carried out. Cover slips were mounted onto slides using mounting media containing DAPI. Zs-RASSF1C cells appear more rounded and contractile than control ZsGreen cells. Scale bars represent 10 µm. This experiment was done by Nikola Vlahov.

We observed that Zs-RASSF1C cells adopted a highly contractile, rounded shape, compared to ZsGreen control cells. Moreover, staining of F-actin with the Phalloidin dye revealed changes in the cytoskeleton, from actin stress fibres present in the control (Fig. 4.10, top panel), to more cortical actin in RASSF1C cells (Fig. 4.10, bottom panel). These results were confirmed in other cell lines, supporting the idea that RASSF1C promoted changes regardless of cell type (MCF7 and H1299 cells, data not shown). The changes in actin structures prompted us to hypothesise that cell contractility and motility pathways could be activated. The small family of Rho GTPases is one of the most important regulators of cell contractility and migration. Interestingly, previous links in the literature have been made between members of the Rho and RASSF1 families. The tumour suppressor RASSF1A has been found to interact with RhoA in HeLa cells and inhibit its activity facilitating SMURF1-mediated ubiquitination of RhoA

(M.-G. Lee et al., 2016). In lung cancer cells RASSF1A depletion has been linked to epithelial to mesenchymal transition (EMT) in a RhoB dependent fashion (Dubois et al., 2016). We thus reasoned that the morphological changes observed in RASSF1C cells could be due to Rho signalling activation. One of the major readouts for Rho activation is phosphorylation at Ser 19 of myosin light chain II (MLCII) by the Rho Kinase, ROCK. MLCII phosphorylation is considered a measure of actomyosin contractility and it leads to cytoskeletal reorganisation with myosin organised in stress fibres, in a more elongated-mesenchymal phenotype, or polarised at the cell edges, in a more rounded-amoeboid one (Chrzanowska-Wodnicka et al., 1996; Lämmermann et al., 2009). Since cell contractility is best studied in 3D platforms rather than 2D assays (Friedl et al., 2010), we assessed pMLCII and F-actin structures in MDA-231 cells grown in 3D collagen and transfected with ZsGreen control or Zs-RASSF1C constructs (Fig. 4.11). RASSF1C cells acquired a more rounded phenotype also in 3D and both F-actin and pMLCII reorganised in cortical structures rather than stress fibres, suggesting that RASSF1C cells adopt a more amoeboid-like shape (compare RASSF1C to control in Fig. 4.11A). Moreover, quantification of the amount of amoeboid (rounded) and mesenchymal (elongated) cells suggested a significant shift to amoeboid-like cells in the RASSF1C condition, compared to control (Fig. 4.11B). In parallel, the amount of mesenchymal cells in the RASSF1C condition was significantly decreased, compared to control (Fig. 4.11B).

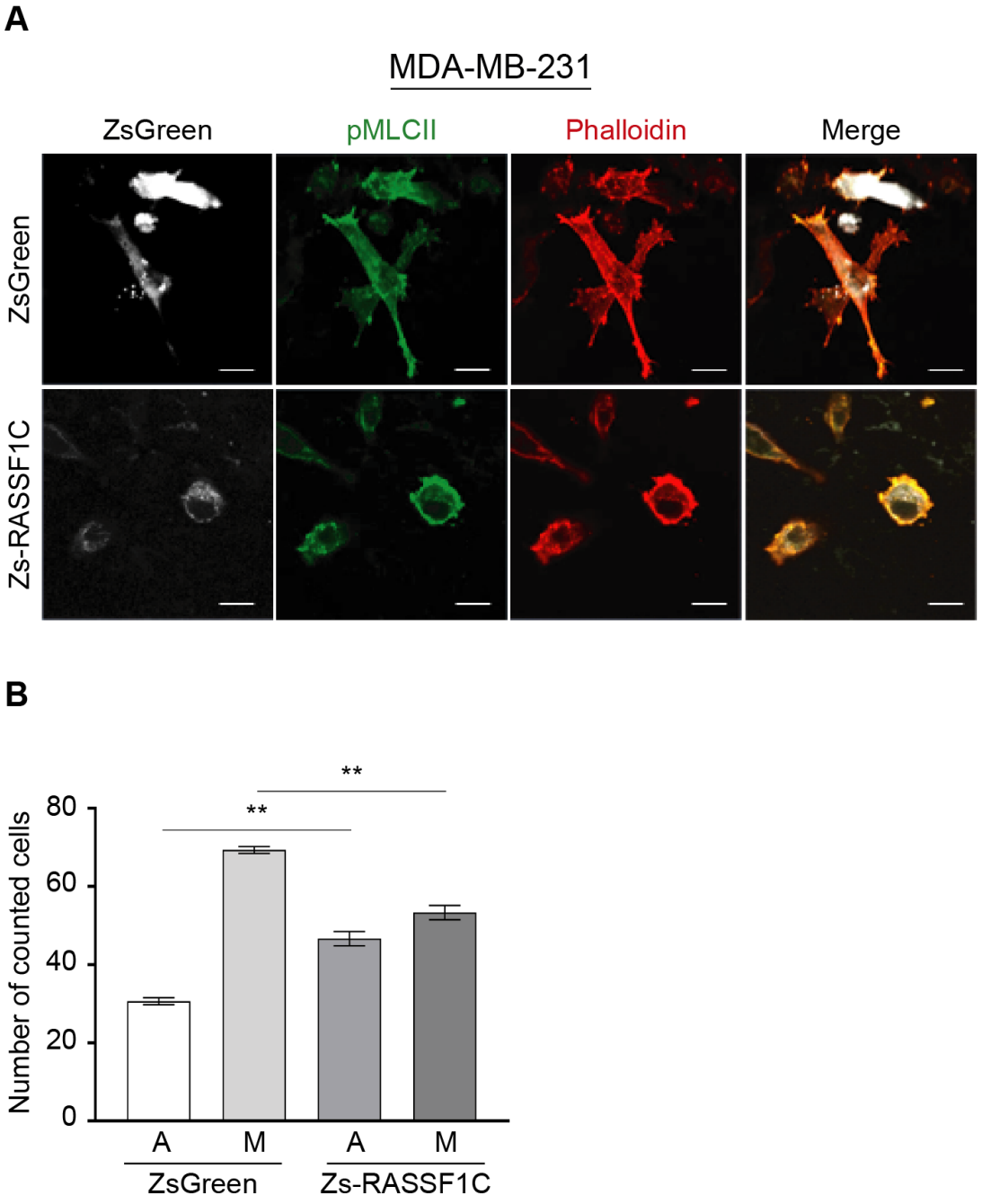


Figure 4.11 In RASSF1C cells MLCII and F-actin adopt cortical structures. MDA-MB-231 cells were grown (5 x 10^4 cells/well in 6-well plates) in 3D collagen and transfected with ZsGreen or Zs-RASSF1C for 48 h. Cells were fixed in 4% PFA, stained with Phalloidin-568 (red), pMLCII/Alexa 633 (false-coloured green) and imaged for ZsGreen (false-coloured white). **A.** Representative images per condition are shown. **B.** Quantification of the number of amoeboid (A) versus mesenchymal (M) cells per condition is shown. Zs-RASSF1C cells display cortical MLCII and switch to an amoeboid phenotype, compared to control ZsGreen cells, in 3D. Data are represented as mean ± SEM of N=3 independent experiments. * $p \leq 0.01$ as with Student's t-test. Scale bars represent 20 µm. These experiments were done by Daniela Pankova.

In order to confirm Rho activation in RASSF1C cells, we performed a Rho-GTP pull-down assay. In Fig. 4.12 MDA-231 and MCF7 cells were transfected with

control or Flag-RASSF1C plasmids for 48 h and activation of Rho was measured as the fraction of Rho bound to GTP. In both cell lines RASSF1C cells showed higher Rho-GTP compared to control, confirming Rho activation.

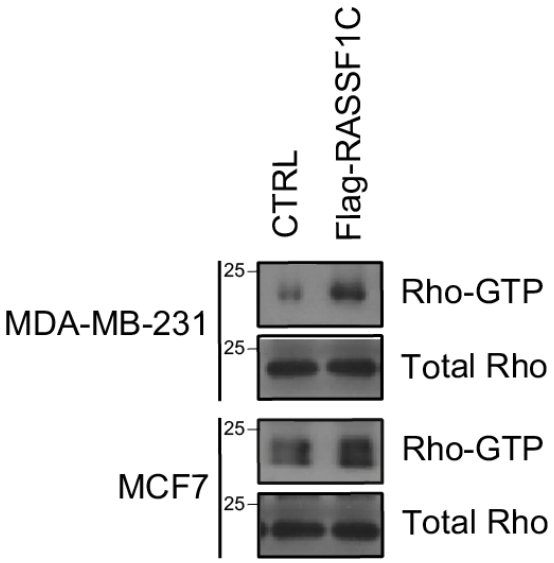


Figure 4.12 RASSF1C expression increases active Rho levels. MCF7 and MDA-MB-231 cells were seeded (1 x 10^6 cells/plate) and transiently transfected with either control (pcDNA3.1) or Flag-RASSF1C constructs. Rho-GTP pull-down assay (Active Rho pull-down kit, Thermo Scientific) was carried out 48 h after transfection and lysates were run and probed for the indicated antibodies. RASSF1C expression increases the amount of active Rho-GTP in both MDA-MB-231 and MCF7 cells. These experiments were done by Daniela Pankova. Representative western blot image is shown.

4.5.2 RASSF1C interacts with and activates RhoA

The two major isoforms of the *RASSF1* gene share homology in two domains, the Ras Association (RA) and the Sav/RASSF/Hpo (SARAH) domains, with RASSF1C being 70 amino acids shorter than RASSF1A and lacking the N-terminal C1 domain. Since it was previously shown that RASSF1A can interact with RhoA via its RA domain (M.-G. Lee et al., 2016), we questioned whether RASSF1C could share similar properties. Immunoprecipitation with a GFP antibody was carried out in MCF7 cells transiently transfected with EGFP-RhoA and control (pcDNA3.1, Flag) or Flag-RASSF1C constructs for 48 h. In Fig. 4.13 the concomitant

precipitation of RASSF1C and RhoA in the same pull-down confirmed the existence of these two proteins in a complex. However, a more stringent control, such as GFP immunoprecipitation in RASSF1C over-expressing cells with endogenous RhoA expression, is needed to further confirm the interaction.

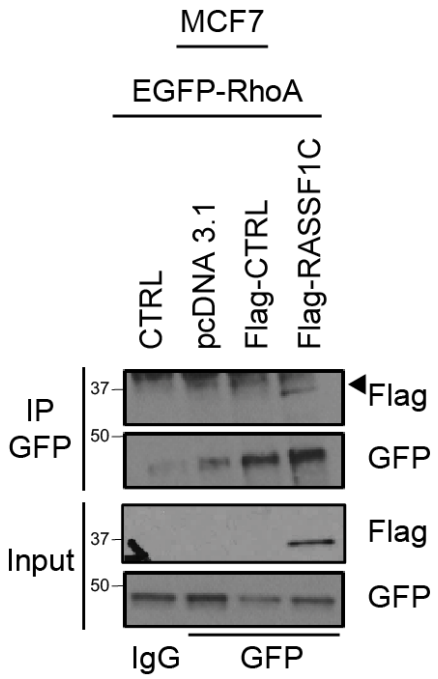


Figure 4.13 RASSF1C co-precipitates with the small GTPase RhoA. MCF7 cells were seeded (1 x 10^6 cells/plate) and transfected with EGFP-RhoA alone or in combination with control plasmids (pcDNA3.1 or Flag) or Flag-RASSF1C. Cells were lysed 48 h after transfection by scraping into 1% NP40, 150 mM NaCl lysis buffer supplemented with protease and phosphatase inhibitors. Cells were immunoprecipitated for 3 h with αGFP antibody (RhoA) or same species IgG bound to protein A magnetic beads. Protein was recovered from the beads by boiling in 1X loading buffer for 5 mins. Samples were analysed by SDS-PAGE and western blot for the indicated antibodies. IgG refers to the IgG lane. Exogenous RASSF1C and RhoA co-precipitate in a complex. Representative western blot image is shown.

The data so far suggest that changes in cell morphology are caused by RASSF1C mediated RhoA/ROCK/pMLCII axis activation and these changes lead to a rounded amoeboid-like phenotype. We next aimed to understand whether RASSF1C binding to RhoA was important in mediating these events. It has been shown previously that mutation of two residues in the RA domain of RASSF1A (arginine to phenylalanine at residues 267 and 269) prevents RhoA binding (M.-G.

Lee et al., 2016). We thus reasoned that mutation of the corresponding residues in the RASSF1C sequence would cause loss of RhoA axis activation. We performed site directed mutagenesis on residue 197 (arginine to tryptophan) and 199 (arginine to phenylalanine) of a DsRed-RASSF1C construct (a schematic representation of the RASSF1C domains and the mutated residues are showed in Fig. 4.14A). Prior to use of the plasmids, the mutations were confirmed by sequencing. In Fig. 4.14B DsRed, DsRed-RASSF1C and the two mutant derivatives were transfected in MDA-231 cells for 48 h. Rho activation was then assessed via GTP pull-down assay. Indeed, the GTP-bound fraction of Rho was consistently reduced when the two mutants, instead of the wild type RASSF1C protein, were expressed.

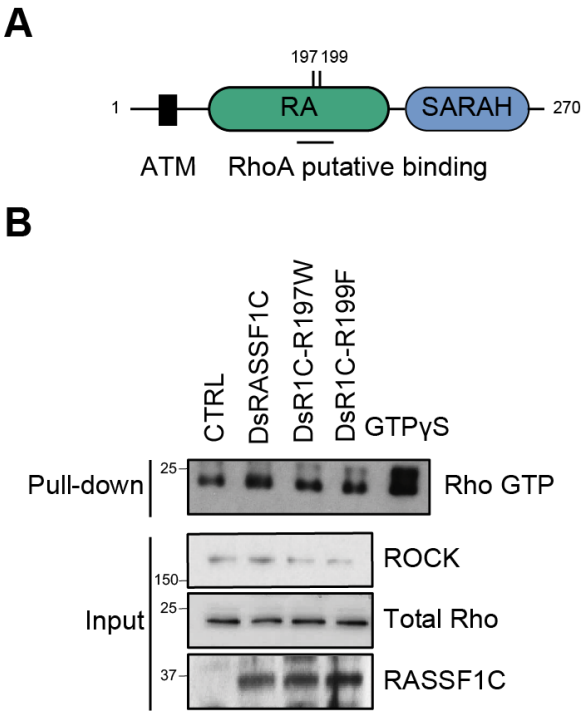


Figure 4.14 Two RASSF1C mutants that fail to interact with RhoA impair RASSF1C mediated Rho activation. A. Schematics of RASSF1C protein structural domains, highlighted is the putative Rho binding site and the two mutations within the site. **B.** MDA-MB-231 were seeded (1 x 10^6 cells/plate) and transfected with either control (DsRed), DsRed-RASSF1C (DsRASSF1C), DsRed-RASSF1C-R197W (DsR1C-R197W) or DsRed-RASSF1C-R199F (DsR1C-R199F). Rho-GTP pull-down assay was carried out 48 h after transfection and lysates were run and probed for the indicated antibodies. Site directed mutagenesis was carried out by Maria Laura Tognoli, Rho-GTP pull-down assays were carried out by Daniela Pankova. Expression of RASSF1C mutants that do not activate RhoA impair Rho activation (measured as Rho-GTP). Representative western blot image is shown.

Loss of the rounded-amoeboid phenotype upon expression of the generated RASSF1C mutants was further confirmed via immunofluorescent staining with pMLCII and Phalloidin (Appendix Fig. 8.4). The data so far suggest activation of the RhoA/ROCK/pMLCII axis downstream of RASSF1C, which causes morphological alterations in the cells that lead to high contractility.

4.5.3 RhoA is responsible for RASSF1C induced extracellular vesicle release

The establishment of a link between the phenotypic changes seen upon RASSF1C expression and RhoA activity prompted us to investigate whether the increase in extracellular vesicle (EV) secretion was also mediated by Rho signalling. RhoA has already been linked to EV release by cancer cells upon growth factor stimulation (Li et al., 2012). I used Nanoparticle Tracking Analysis to evaluate whether expression of a RhoA wild type (WT), a constitutively active mutant (CA, RhoA-Q63L) or a RhoA defective mutant (DN, RhoA-T19N, (Subauste et al., 2000)) could alter EV release in MDA-231 cells. Cells were transfected with the described RhoA constructs (see Fig. 4.15), in the presence or absence of a RASSF1C plasmid, for 48 h. One of the two previously generated RASSF1C mutants (RASSF1C-R199F, Fig. 4.14) was also transfected alone, to evaluate the mutant's ability to promote EV shedding. EVs were isolated 72 h post transfection and particle concentration was measured with NTA.

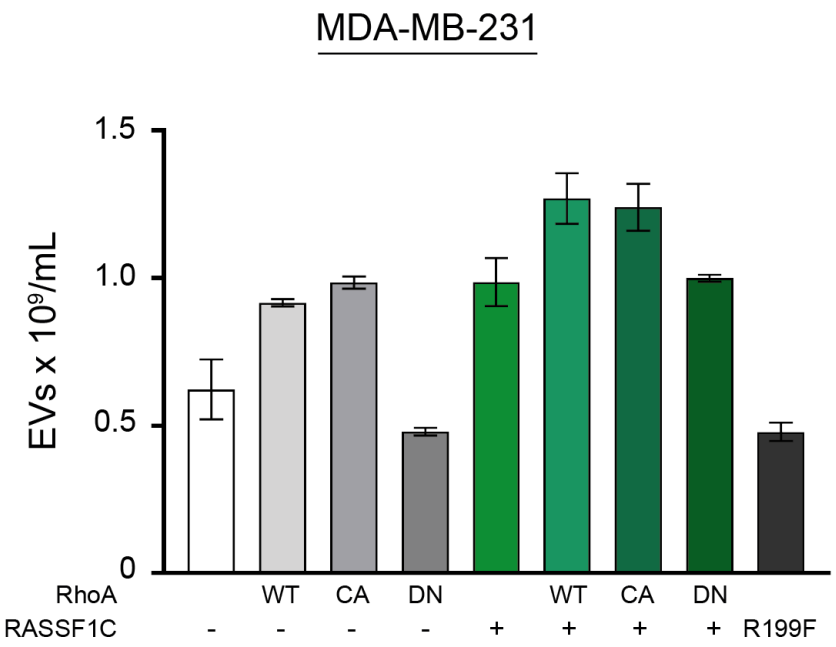


Figure 4.15 RhoA over-expression alone promotes extracellular vesicle secretion. MDA-MB-231 cells were seeded (5 x 10^6 cells/plate) and transiently transfected with the indicated plasmids (EGFP-RhoA for all RhoA constructs; pcDNA3.1 as a control plasmid (-); Flag-RASSF1C for RASSF1C constructs (+)). Cells were grown in 0.1% FBS medium for 72 h and EVs were isolated from conditioned media as stated before. NTA was employed to quantify the amount of EVs released in each condition. Isolated EVs were resuspended in PBS and diluted 1:100 prior to NTA analysis. Expression of RhoA alone promotes EV shedding. Both RhoA-WT and RhoA-CA promote EV release, whereas RhoA-DN impairs it. RASSF1C positive effect on EV secretion can be reverted by co-transfection of a RhoA-DN construct or by the use of a RASSF1C mutant (R1C-R199F) that fails to activate RhoA. Data are represented as mean ± SEM of N=3 technical replicates.

Compared to a control plasmid, introduction of a RhoA-WT or a RhoA-CA mutant enhanced EV release, as measured by NTA (white and light grey bars from the left in Fig. 4.15). Moreover, a defective RhoA-DN mutant could revert this pattern (dark grey bar). Over-expression of RASSF1C promoted EV secretion, as previously shown (see first green bar from the left and Fig. 4.2). Co-expression of RASSF1C and a RhoA construct (WT or CA) potentiated EV secretion, if compared to control condition, to RASSF1C alone and to the RhoA-WT and RhoA-CA mutants alone (green bars for RASSF1C and light grey bars for RhoA). However, expression of a RASSF1C R199F mutant failed to promote release (dark grey bar on the right). Finally, when the RhoA-DN mutant was co-transfected with RASSF1C, the release of EVs was also reduced (dark green bar).

The data thus suggest that RhoA can modulate EV shedding and its action on EVs is potentiated by RASSF1C.

I had previously shown that RASSF1C EVs promote migration and invasion in recipient cells (Fig. 4.5 and 4.6). Given the importance of RhoA in the process of EV release (Fig. 4.15), I hypothesised that treatment with RhoA driven EVs alone would be sufficient for recipient cells to acquire the invasive phenotype. In Fig. 4.16 a control or a RhoA wild type plasmid were transfected in MDA-231 cells for 48 h. EVs were isolated as previously described, 72 h post transfection. The collected EVs were then incubated for 36 h with MDA-231 recipient cells in an xCELLigence plate, as previously described. Interestingly, the migration index of MDA-231 cells exposed to RhoA EVs was significantly higher than the index of cells exposed to control EVs, as shown in Fig. 4.16A. As previously shown for RASSF1C (Fig. 4.5), treatment of target cells with a higher concentration (30 ng/mL) of control or RhoA EVs revealed a similar outcome on the migration index (Fig. 4.16B).

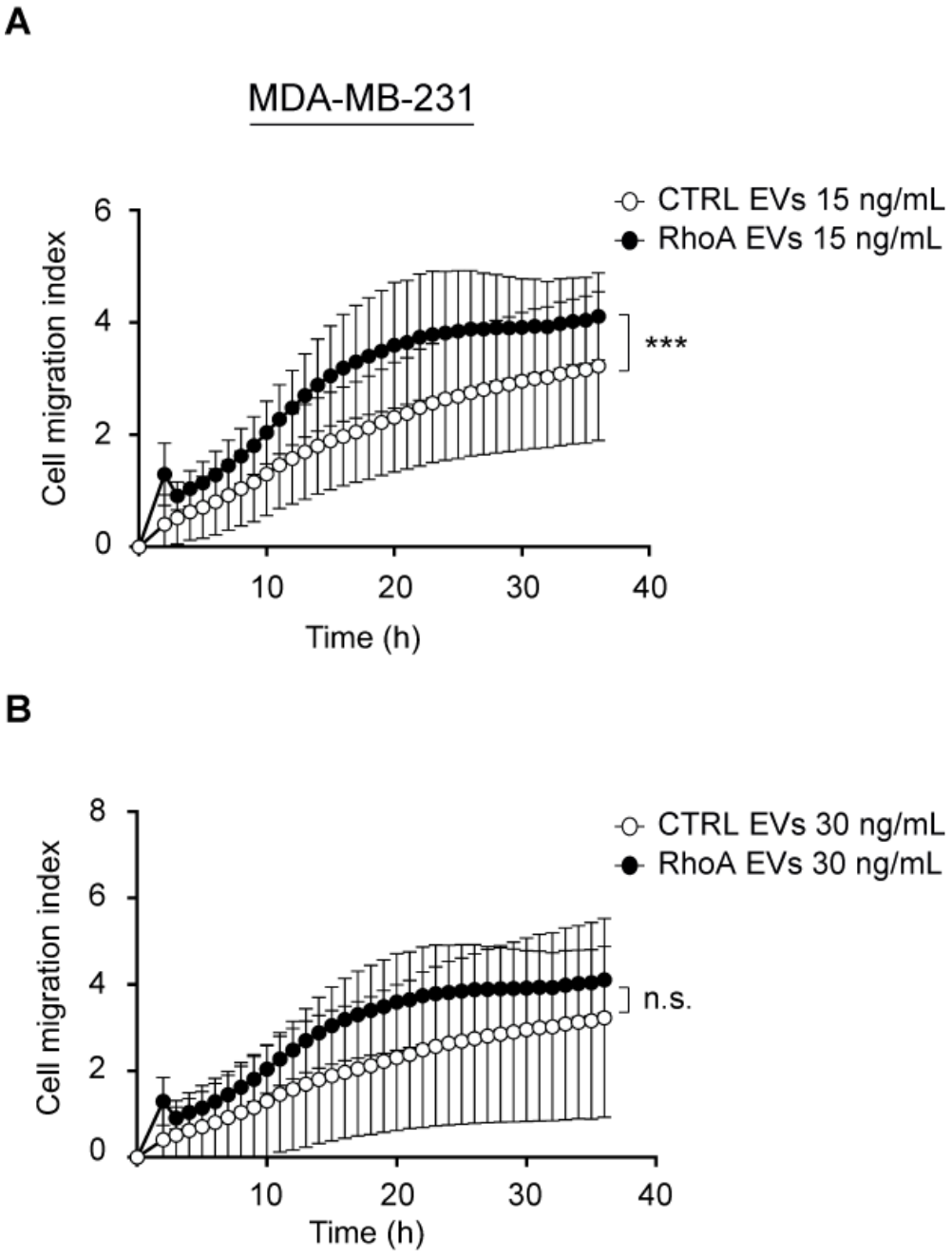


Figure 4.16 RhoA EVs promote migration in recipient MDA-231 cells. MDA-MB-231 cells were seeded (1 x 10^6 cells/plate), transfected with either control (pcDNA3.1) or EGFP-RhoA constructs and cultured in 0.1% FBS medium for 72 h. EVs were harvested via differential centrifugations and an aliquot was resuspended in 1X RIPA buffer for protein quantification (microBCA assay), to ensure equal loading onto recipient cells. The remainder was resuspended in PBS, normalised and the indicated amounts incubated or not with recipient MDA-MB-231 cells, plated as 5 x 10^4 cells/well onto xCELLigence Real-Time Cell Analyser CIM plate (Roche) for 36 h, according to manufacturer's protocol. Cell migration index in each condition was normalised against an untreated control and was quantified over 36 h of incubation by RTCA software 2.0. **A.** 15 ng/mL and **B.** 30 ng/mL of EVs were incubated with recipient cells in each condition. Note that EVs isolated from cells expressing a wild type RhoA construct promote significantly higher migration in recipient cells, compared to control EVs. The lower concentration chosen (15 ng/mL) revealed a window of differential response of the recipient cells to the EVs. The signal was then saturated at the higher concentration (30 ng/mL). Data are represented as mean ± SEM of N=3 independent experiments. *** $p \leq 0.001$ was calculated with the nonparametric Mann-Whitney test.

We also assessed the ability of RhoA EVs to promote Matrigel invasion in recipient MCF7 cells. The same protocol as for the xCELLigence assay was followed and similarly RhoA EVs induced significantly greater invasion of recipient cells than control EVs in a Boyden chamber assay.

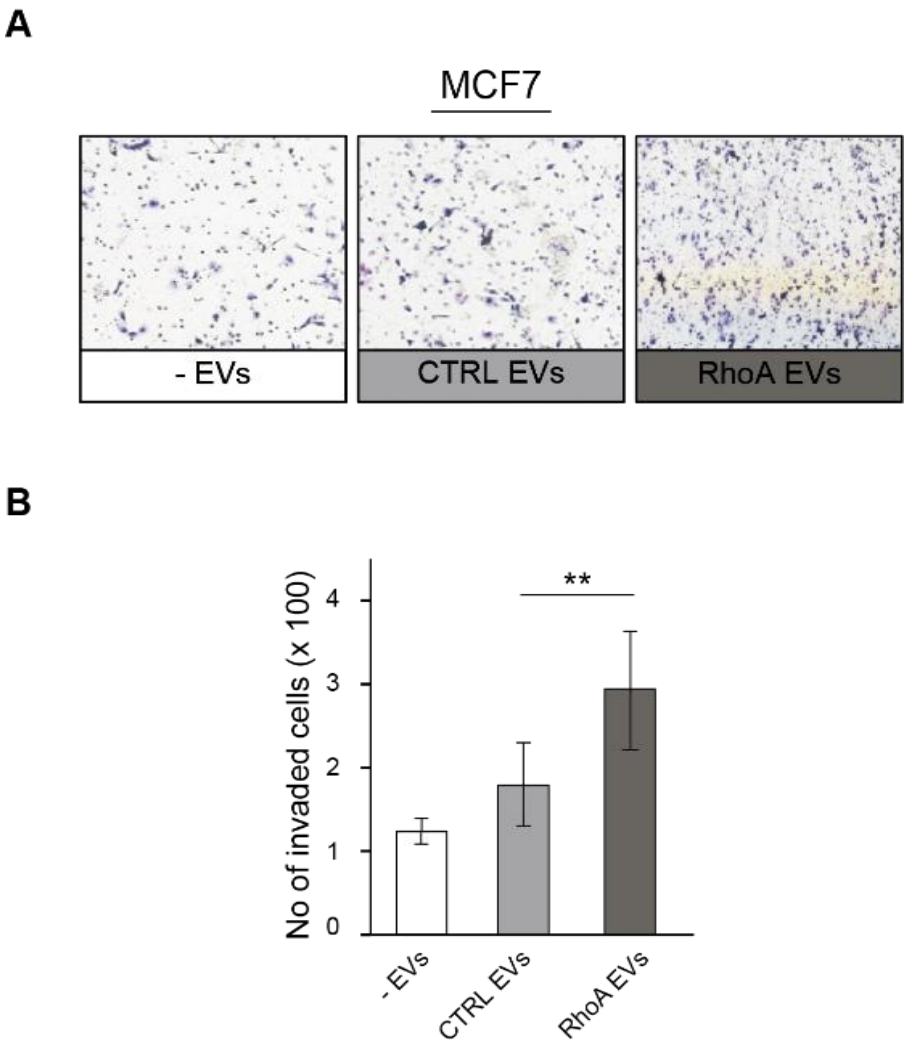


Figure 4.17 RhoA EVs promote Matrigel invasion in recipient MCF7 cells. MDA-MB-231 cells were seeded (5 x 10^6 cells/plate) and transfected with the same constructs as in Figure 4.16. EVs were collected via differential centrifugations and an aliquot was resuspended in 1X RIPA buffer for protein quantification (microBCA assay), to ensure equal loading onto recipient cells. The remainder was resuspended in PBS, normalised and incubated or not with recipient MCF7 cells, plated as 5 x 10^4 cells/well onto Transwell Matrigel chambers (Corning). After 18 h, invaded cells were fixed and stained and brightfield images were taken on a Nikon 90i light microscope. The number of cells that invaded the Matrigel was quantified with ImageJ software 1.51s and quantification of the number of invaded cells is shown. **A.** Representative brightfield images per condition are shown. **B.** Quantification of the number of invaded cells. EVs isolated from cells expressing a wild type RhoA construct promote significantly higher Matrigel invasion in recipient MCF7 cells, compared to control EVs. Data are represented as mean ± SEM of N=3 independent experiments. ** $p \leq 0.01$ as with Student's t-test. This experiment was done in collaboration with Daniela Pankova.

Altogether the data support the hypothesis that RASSF1C stimulation of EV secretion is mediated by RhoA, which is ultimately the trigger for the release of a pro-invasive pool of EVs.

4.6 Discussion

In this chapter I explored the role of the oncogene RASSF1C in eliciting extracellular vesicle (EV) secretion with both over-expression and knockdown experiments. Interestingly, most of the markers used for EV characterisation were not altered upon RASSF1C exogenous transfection or depletion, despite the overall amount of secreted vesicles being respectively increased or decreased (Fig. 4.1-4.3). This observation reflects the presence of different and differentially regulated subpopulations of EVs, probably not distinguishable with the currently used protocol (Kowal et al., 2016). The addition of a gradient ultracentrifugation step to the protocol will be of help in understanding which subpopulations of EVs are truly affected by RASSF1C expression. Moreover, western blotting would give only a partial picture of the changes in the EV protein cargo. A combined approach of differential ultracentrifugations, density gradient and mass spectrometry could potentially result in a more exhaustive analysis of the differences between RASSF1C and control EVs.

In regard to the mechanism RASSF1C employs to promote exocytosis, we observed an activation of the RhoA/ROCK pathway in RASSF1C cells, to which EV release could be ascribed (Fig. 4.12, 4.15-4.17). However, the major players in extracellular trafficking are the ESCRT machinery, Rab27a and 27b GTPases

(Ostrowski et al., 2010), tetraspanins such as CD63 (van Niel et al., 2011), Alix in concert with ESCRT or via other complexes, such as syndecan and syntenin (Baietti et al., 2012), as well as ceramide and cholesterol (Trajkovic et al., 2008). It would thus be important to systematically study these master regulators of exocytosis in the presence and absence of RASSF1C. To this end, knockdown or chemical inhibition experiments could provide insight on which secreting routes are taken by RASSF1C cells.

Furthermore, utilising various functional assays, I have provided evidence for RASSF1C EVs to be transferring an aggressive phenotype onto recipient cells (Fig. 4.5-4.9), demonstrating a novel mechanism of RASSF1C oncogenic potential. However, the presented *in vitro* studies have the already discussed dose-response limitation in EV treatment (Fig. 4.5 and 4.16). Instead, it would be interesting to apply the Cre-LoxP model (Zomer et al., 2016) to different cancer cells, endogenously expressing RASSF1C or not, and monitor reporter^{+} cell switch as well as follow the recombined reporter^{+} cells for alteration in migratory and invasive behaviour.

During the characterisation of RASSF1C cells, we demonstrated that these cells undergo cytoskeleton reorganisation upon RASSF1C expression, become more rounded and contractile, acquiring an amoeboid-like phenotype and this happened regardless of the matrix cells were seeded onto (2D, Fig. 4.10 or 3D, Fig. 4.11). Moreover, the presented data was reproduced in MCF7 cells (data not shown), reinforcing the hypothesis that RASSF1C is able to drive phenotypic changes in cells, regardless of their epithelial or mesenchymal origin.

Both *RASSF1* isoforms co-localise with microtubules and RASSF1A is known to interact and stabilise these structures (Dallol et al., 2004; Rong et al., 2004; Song

et al., 2004), whereas the role of RASSF1C in microtubule stabilisation is not yet fully understood (L. Liu et al., 2005; Vos et al., 2004).

Notably, RASSF1A depletion has been shown to activate the Rho-like GTPase Rac1 in cancer cells (Dallol et al., 2005), whereas RASSF1A expression has been reported to restrict EMT and cancer invasion via activation of the GEF-H1/RhoB pathway (Dubois et al., 2016) or suppression of the RhoA/ROCK pathway (M.-G. Lee et al., 2016).

Collectively, these mechanisms suggest that RASSF1A exerts its tumour suppressive function also by modulating cytoskeleton effectors. In RASSF1A inactivated cells, such as in MDA-231, it was likely that RASSF1C could exert an opposite function to RASSF1A in cytoskeleton dynamics.

In fact, these data suggest that the rounded-amoeboid morphology observed in the cells is caused by RASSF1C activation of the RhoA/ROCK pathway (Fig. 4.12-4.14). The acquisition of an amoeboid-like phenotype in RASSF1C cells adds evidence to the oncogenic potential of this protein.

It would be interesting to investigate this phenotype also *in vivo*. Based on our *in vitro* results, I could speculate that RASSF1C cells may adopt mostly rounded-amoeboid morphology to invade the surroundings *in vivo*.

In agreement with this, *in vivo* intravital imaging studies performed in melanoma and breast cancer have proved that these two tumour types adopt an amoeboid mode of invasion at the tumour front (Giampieri et al., 2009; Sanz-Moreno et al., 2008).

Previously published results from our group have described how both *RASSF1* isoforms interact and control SRC family kinase activity (Vlahov et al., 2015). Notably, SRC family is involved in cell proliferation, adhesion and migration

processes, and several reports have described a crosstalk between SRC and Rho pathways (Arthur et al., 2000; Huveneers et al., 2009). It would be thus of value to determine SRC involvement in RASSF1C activation of RhoA. Immunoprecipitation assays could reveal the presence of SRC in a RASSF1C/RhoA complex and the use of SRC mutants defective in RASSF1C binding could establish SRC role in this complex.

Together the work in this chapter (summarised in Fig. 4.18) provides a new insight for RASSF1C mediated aggressive phenotype, where the release of pro-invasive extracellular vesicles is a major event that dictates behavioural changes in recipient cells.

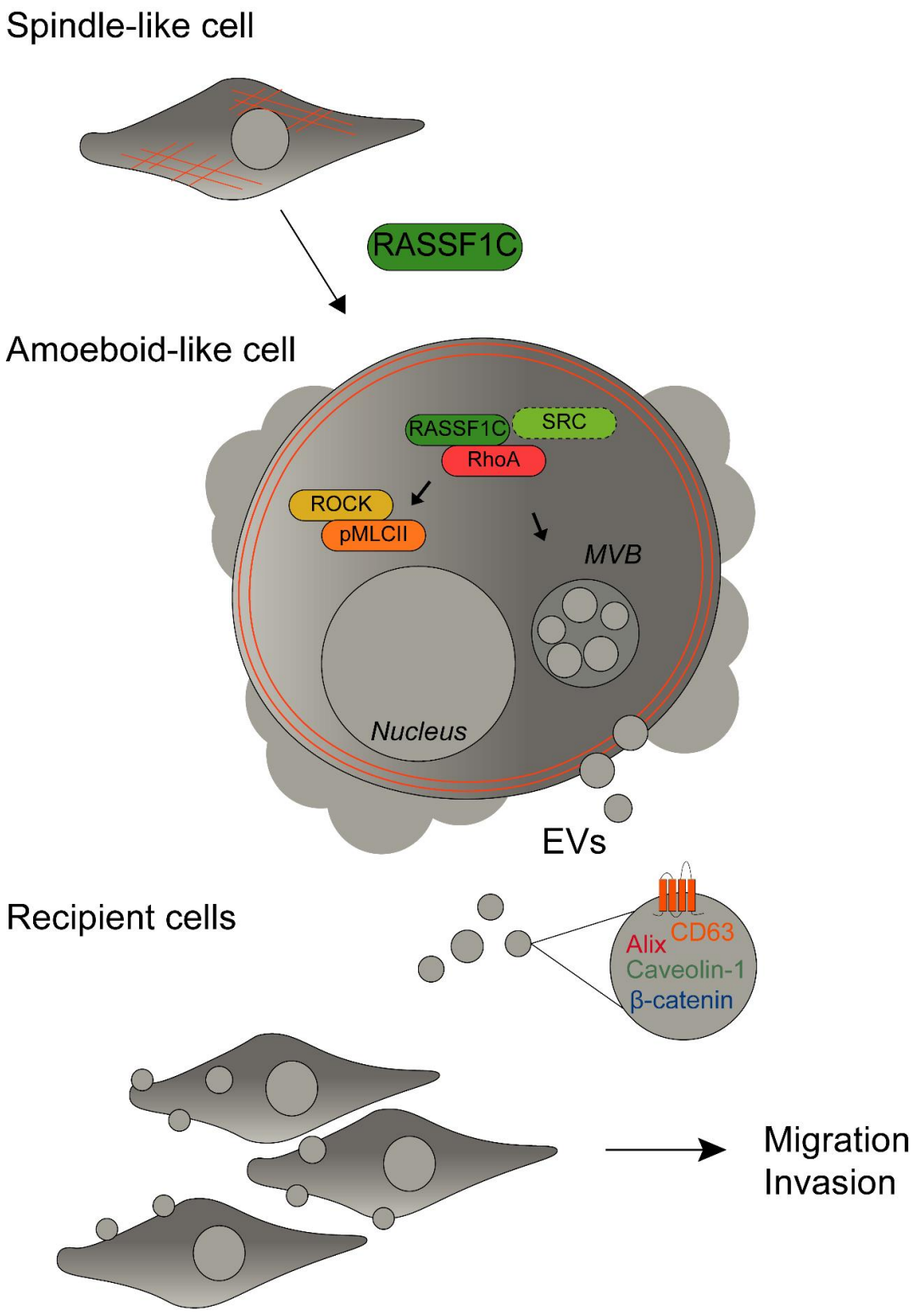


Figure 4.18 RASSF1C oncogene induces cell morphological changes and promotes release of pro-invasive EVs in RhoA mediated manner. Schematic cartoon depicting a cell expressing RASSF1C, switching from a spindle-like phenotype to a more rounded, amoeboid-like one, via activation of the RhoA signalling axis, possibly via direct interaction and SRC activation. Activation of RhoA also causes the release of extracellular vesicles that are able to transfer a pro-invasive phenotype to less aggressive cells. Different pMLCII structures (stress fibres in the spindle-like cell and cortical pMLCII in the amoeboid one) within the cell are highlighted in orange.

Chapter 5 Modulation of TGF-β Signalling by Extracellular Vesicles in Breast Cancer Cells

5.1 Introduction

In chapter 4 I studied the role of the oncogene RASSF1C in promoting the release of pro-invasive extracellular vesicles. In this chapter I aim to broaden my understanding on how factors in the tumour microenvironment may alter extracellular vesicle release.

5.1.1 Crosstalk between Hippo and TGF-β pathways

Having demonstrated that RASSF1C can promote exosome release, I next wanted to determine whether this pro-invasive signal is integrated to other oncogenic stimuli in the tumour microenvironment. Our group has previously reported a link between the Hippo pathway tumour suppressor RASSF1A and Transforming Growth Factor β (TGF-β), where the cytokine promotes RASSF1A degradation via the E3 ligase ITCH. RASSF1A degradation is necessary to permit association of the Hippo effector YAP with SMADs and subsequent nuclear oncogenic signalling. In turn, RASSF1A regulates YAP/SMAD interaction via cytoplasmic retention and it acts as a tumour suppressor inhibiting TGF-β mediated invasion (Pefani et al., 2016).

Given the opposing roles that were previously demonstrated for the Hippo scaffold RASSF1A and its alternative isoform RASSF1C in SRC activation and YAP/β-catenin mediated breast cancer invasion (Vlahov et al., 2015), I

hypothesised that similar antagonistic roles could occur for RASSF1A and RASSF1C in modulating the TGF-β cascade.

Previous research has uncovered numerous links between the Hippo and TGF-β signalling pathways. Namely, the effectors of both pathways, YAP/TAZ for Hippo and SMADs for TGF-β, co-regulate transcriptional programmes activated in different cellular scenarios, such as stem cell self-renewal in the embryo (Varelas et al., 2008) and tumourigenesis in breast cancer (Hiemer et al., 2014). The Hippo pathway has also been found to regulate TGF-β pathway in relation to cell density. Namely, in high density cell cultures, active Hippo pathway drives cytoplasmic localisation of YAP/TAZ, which sequesters SMAD complexes, thereby suppressing TGF-β signalling. Conversely, in low density cultures, Hippo signalling is off and YAP/TAZ nuclear localisation dictates nuclear translocation of SMAD complexes (Varelas et al., 2010).

Interestingly, both signalling pathways have been connected to extracellular vesicle release. Recently, a study proposed that deletion of the core hippo kinases LATS1/2 from melanoma cells acts as a boost for cancer immunity *in vivo* via release of immune-stimulatory EVs (Moroishi et al., 2016). TGF-β ligand, on the other hand, has been found bound to the surface of prostate cancer exosomes and, in this form, it exploited its functions in fibroblast to myofibroblast differentiation more efficiently than as a soluble ligand alone (Webber et al., 2010). Additionally, exosomal TGF-β from cancer cells is required for inducing angiogenesis *in vitro* and promoting stroma-assisted tumour growth *in vivo* (Chowdhury et al., 2015b; Webber et al., 2015).

I have shown in Chapter 4 that one of RASSF1C´s oncogenic functions is to mediate release of pro-invasive extracellular vesicles. In this chapter I intend to

investigate more endogenous signals coming from the cancer microenvironment that may impact vesicle secretion. To this end, and considering its previous links to the Hippo pathway, I decided to test the role of TGF-β in extracellular vesicle release.

5.1.2 Tetraspanins as regulators of extracellular vesicle trafficking

I previously introduced the master regulators of vesicle biogenesis and secretion (Chapter 1.3.2). Among others, tetraspanins have been gaining interest both as biogenesis modulators and as markers of extracellular vesicles (Colombo et al., 2013; Van Niel et al., 2018). The tetraspanin family includes proteins with four transmembrane domains that self-organise in membrane microdomains (referred to as tetraspanin-enriched microdomains, TEM), through several homotypic and heterotypic interactions. The most common tetraspanin interactors include integrins, immunoglobulins and metalloproteinases (Andreu et al., 2014). Tetraspanins are thought to regulate adhesion signalling, cell motility and fusion (Hemler, 2005) and some members of the family have been correlated to tumour progression, as mediators of metastasis, angiogenesis and lymphangiogenesis (Hemler, 2014).

In regard to extracellular vesicle biogenesis, CD63 is one of the most relevant tetraspanins. Being associated to both multivesicular bodies (MVBs) and lysosomes, CD63 has been reported to specifically modulate endosome biogenesis, exosome biogenesis and to sort exosomal cargo in melanocytes (Stuffers et al., 2009; van Niel et al., 2015; van Niel et al., 2011). Other tetraspanins, such as CD9 and CD82 have been implicated in inducing release of the Wnt effector β-catenin via exosomes (Chairoungdua et al., 2010). CD9 alone has been linked to sorting of the MHCII molecule on dendritic cell exosomes

(Buschow et al., 2009). In mouse models of breast cancer, exosomal CD81 derived from cancer-associated fibroblasts was found responsible of Wnt11 cargo sorting to EVs (Luga et al., 2012).

5.2 Aims

In this chapter I aim to understand whether the TGF-β family of growth factors is responsible for RASSF1C mediated extracellular vesicle trafficking in breast cancer cells. Furthermore, I ask whether EV production can be altered by TGF-β treatment and if the produced vesicles have a functional effect on recipient cells.

5.3 TGF-β Superfamily of Growth Factors Alters Extracellular Vesicle Shedding

5.3.1 TGF-β effect on extracellular vesicles is not dependent on RASSF1C

Our previous work has described how TGF-β regulates the tumour suppressor RASSF1A by initiating its degradation (Pefani et al., 2016). I first hypothesised that the cytokine may, in contrast, sustain RASSF1C expression.

MDA-231 cells were treated with recombinant TGF-β1 (10 ng/mL) at the indicated time-points, previously reported as sufficient to activate the cascade (Inman et al., 2002; Pefani et al., 2016), and subsequently mRNA was isolated from each condition. RASSF1C mRNA levels were assessed via qPCR and are reported in

Fig. 5.1. No significant differences in RASSF1C mRNA expression were detected upon TGF-β stimulation.

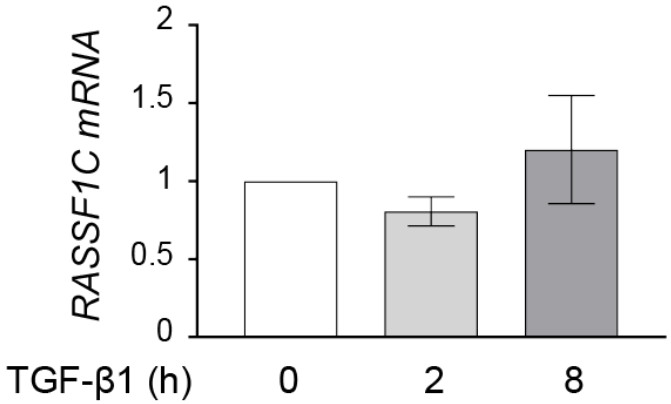


Figure 5.1 RASSF1C transcription is unaffected by TGF-β treatment. MDA-MB-231 cells were seeded (5×10^5 cells in 6-well plates). After 24 h fresh 0.1% FBS medium was added in the presence or not of TGF-β1 at the indicated time-points. mRNA was then isolated and cDNA was prepared. qPCR was performed on a StepOnePlus™ Real-Time PCR machine. Expression of GAPDH was used as internal control. RASSF1C mRNA levels are not altered upon TGF-β treatment. Data are represented as mean ± SEM of N=3 experiments.

In Chapter 4 I have addressed RASSF1C´s role in extracellular vesicle release, I next asked whether TGF-β may mediate the release of extracellular vesicles in the presence or absence of RASSF1C.

Knockdown of RASSF1C was performed as previously described (Fig. 4.1) on MDA-231 cells. 72 h after transfection cells were treated with recombinant TGF-β1 (10 ng/mL) at the same time-points as for Fig. 5.1 and EVs were subsequently harvested. After normalisation of protein content, enrichment of EV markers at different conditions was assessed via western blotting and NTA (Fig. 5.2). As expected, some EV markers are affected by RASSF1C depletion (compare β-catenin and caveolin-1 in lane 7 and 9 in the EV panel of Fig. 5.2A).

In control siRNA treated cells, TGF-β1 treatment led to increase of EV markers (compare lanes 7-8 in Fig. 5.2A, EV panel).

In addition, 8 h after TGF-β1 treatment in RASSF1C depleted cells, some of the EV markers seemed to be reduced, whereas others seemed to be enriched (see lane 10 in Fig. 5.2A).

This observation may imply that RASSF1C and TGF-β control different subpopulations of exosomes.

To determine whether protein cargo or total exosomes were being affected I performed NTA analysis (Fig. 5.2B). A significant decrease in EVs was observed upon RASSF1C depletion (light cyan bar compared to white bar in 5.2B), in agreement with previous findings in Chapter 4 (Fig. 4.1). Interestingly, NTA analysis confirmed that TGF-β stimulus on EVs is independent of RASSF1C, as shown in Fig. 5.2B (grey bars and dark cyan bars).

Collectively, western blot markers and NTA data thus suggest that TGF-β alters EV shedding, leading to an increase in EV markers 8 h after treatment, regardless of RASSF1C status.

Moreover, TGF-β downstream activation appeared unaffected by RASSF1C loss, as assessed via phosphorylation of the effector SMAD2 (Fig. 5.2A). RASSF1C knockdown efficiency was assessed via qPCR (Fig. 5.2C).

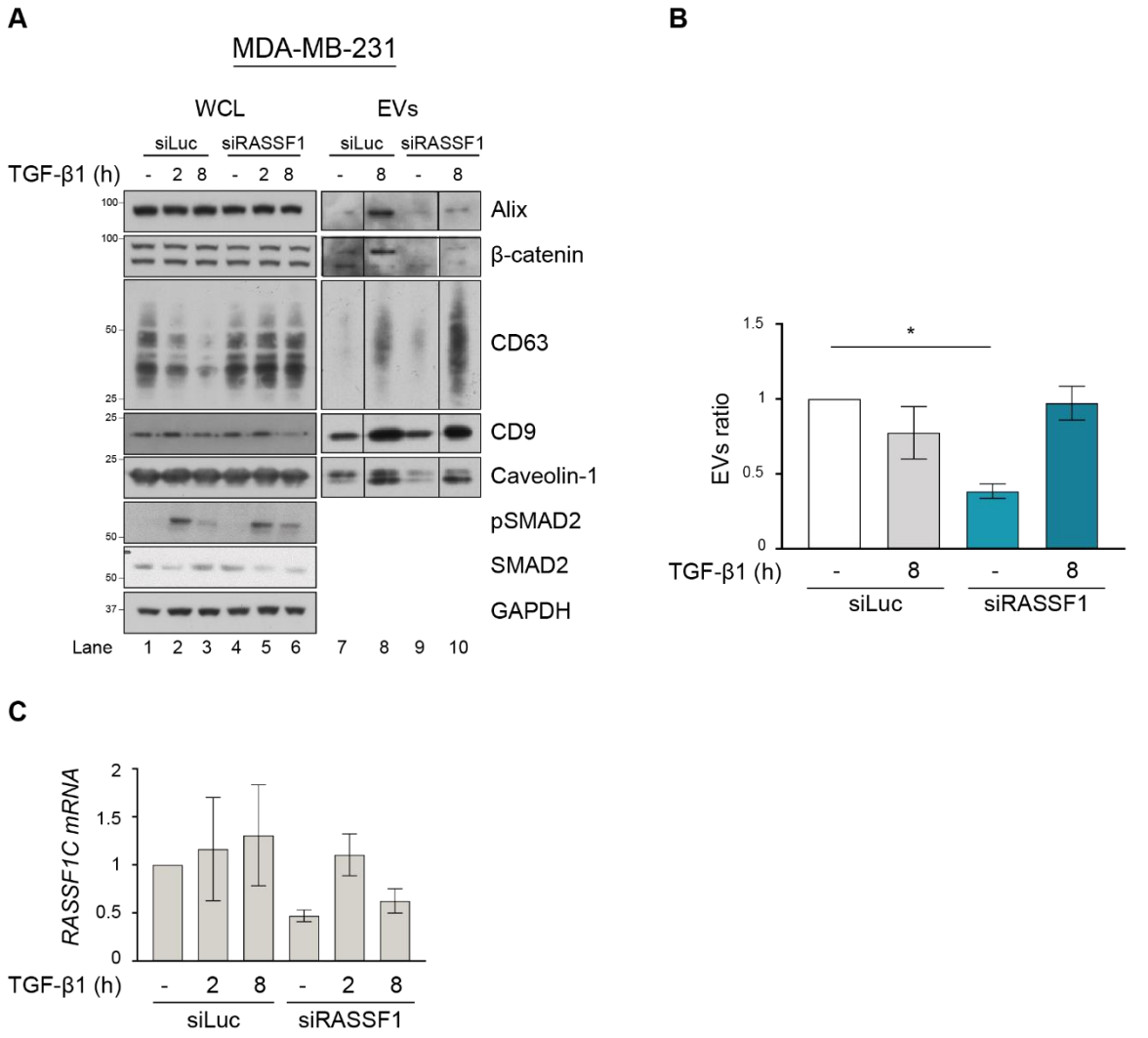


Figure 5.2 RASSF1C knockdown does not alter TGF-β1 induced extracellular vesicle release. MDA-MB-231 were seeded (5 x 10^6 cells/plate) and transiently transfected with siRNA against a non-targeting (Luciferase) sequence or a RASSF1 sequence, then cultured in 0.1% FBS medium for 72 h. On day 3, cells were treated or not with TGF-β1 for 2 or 8 h in 0.1% FBS medium. EVs were collected from the conditioned medium via differential centrifugations only for the control and the 8 h time-points and an aliquot was resuspended in 1X RIPA buffer for protein quantification. **A.** Western blot analysis of EVs and cell lysates with the indicated antibodies. **B.** An aliquot was resuspended in PBS and diluted 1:100 prior to NTA analysis. EVs ratio was calculated per each replicate as particle concentration of treated condition (i.e. siRASSF1) divided by particle concentration of control condition (siLuc). **C.** RNA from cells was isolated and cDNA prepared. qPCR was performed on a StepOnePlus™ Real-Time PCR machine in order to ensure efficient siRNA-mediated knockdown of RASSF1C. Expression of 18S was used as internal control. Representative western blot and qPCR are shown. *RASSF1* depletion results in a decrease of EV markers (**A**) and overall EV count (**B**). Treatment with TGF-β results in moderate enrichment of protein markers (8 h time-point) and does not appear to be altered by the absence of RASSF1C. Data are represented as mean ± SEM of N=3 experiments for NTA. * $p \leq 0.05$ as with Student's t-test.

5.3.2 TGF-β and BMP4 affect extracellular vesicle release in breast cancer cells

Despite previously established links between the Hippo and TGF-β pathways, I could not demonstrate a crosstalk between the growth factor pathway and RASSF1C in the release of EVs. However, TGF-β alone seemed to alter exosome secretion (Fig. 5.2). Given the interesting pattern observed in Fig. 5.2, I decided to treat MDA-231 breast cancer cells with 10 ng/mL of recombinant TGF-β1 at the described time-points. I also treated cells with the BMP4 signalling peptide because it was previously shown that BMP regulates exosome biogenesis in the accessory gland of male *Drosophila* (Corrigan et al., 2014).

In Fig. 5.3A extracellular vesicles were isolated as previously stated and EV markers were analysed via western blotting. Both TGF-β1 and BMP4 treatment generated an increase in the amount of EVs released by MDA-231 cells.

When I measured the harvested particles by NTA I discovered that the particle number did not correspond to the levels of EV proteins analysed with western blot. In Fig. 5.3B I observed a slight increase in EVs secreted from cells treated with TGF-β1 for 8 h (8 h EVs). Surprisingly, at this time-point I observed correlation between the levels of protein and numbers of vesicles secreted (Fig 5.3A and B).

For the BMP4 treatment, instead, the NTA data did not reflect the pattern observed for the protein markers, marking a minimal effect in EV secretion after 8 h (Fig. 5.3B). Activation of both TGF-β and BMP pathways was assessed in the cell lysates via phosphorylation of the respective effector SMAD, SMAD2 and SMAD1 (Fig. 5.3A, WCL).

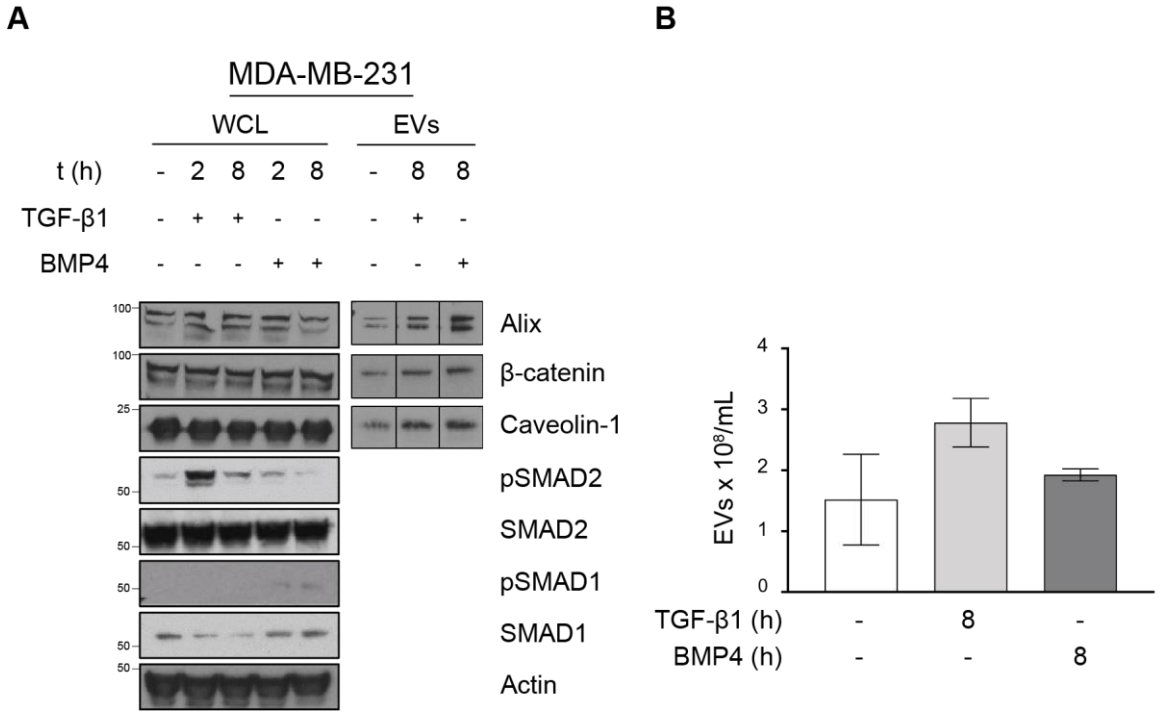


Figure 5.3 TGF-β superfamily of growth factors alters extracellular vesicle secretion. MDA-MB-231 cells were seeded (5 x 10^6 cells/plate) and cultured in 0.1% FBS medium for 72 h. On the last day medium was replaced and cells were treated or not for 2 or 8 h with growth factors, TGF-β1 (10 ng/mL) or BMP4 (25 ng/mL). EVs were subsequently harvested via differential centrifugations only for the control and 8 h time-points and an aliquot was resuspended in 1X RIPA buffer for protein quantification. The remainder was normalised and SDS-PAGE loading and western blot analysis with the indicated antibodies followed. A second aliquot was resuspended in PBS and diluted 1:100 prior to NTA analysis. **A.** Western blot analysis of EVs and cell lysates reveals an alteration in the release upon growth factor treatment. Activation of TGF-β1 and BMP4 pathways was assessed via effector SMADs phosphorylation. **B.** NTA analysis shows a trend of increase in EV secretion upon 8 h of TGF-β treatment. Both TGF-β1 and BMP4 appear to promote the release of a pool of EVs (**A**) after 8 h of treatment. Representative western blot is shown. NTA data are represented as mean ± SEM from 3 technical replicates.

The data so far suggest that TGF-β and BMP4 treatments differentially alter EV secretion. In case of TGF-β, in MDA-231 cells, this event is not dependent on RASSF1C.

5.3.3 The Cre-LoxP model confirms TGF-β role in promoting extracellular vesicle uptake *in vitro*

The data presented in Fig. 5.2 and 5.3 suggested a possible role of TGF-β in modulating EV release. I thus decided to take an alternative approach to study EV secretion, employing the previously described Cre-LoxP system, where isolation

artefacts are avoided (Fig. 4.7 and (Zomer et al., 2016)). For these experiments I used the co-culture assay and incubated cells at a ratio of 1:100 reporter$^+$/donor for 7 days in 0.1% FBS medium, treating with 10 ng/mL of TGF-β1 every 48 h, prior to imaging. In Fig. 5.4A representative pictures of both conditions are shown.

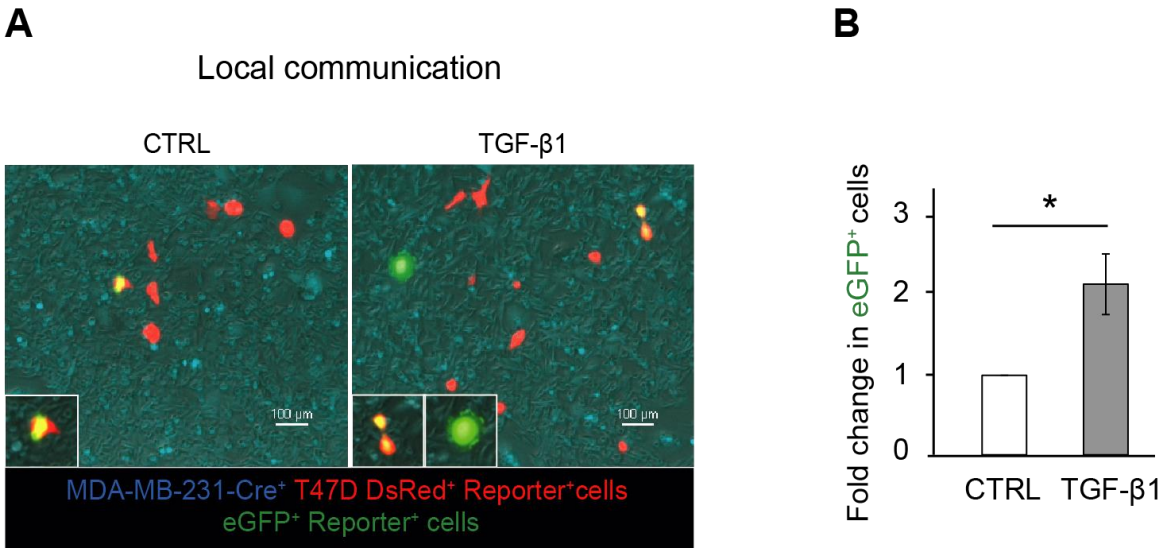


Figure 5.4 TGF-β1 derived EVs are internalised at higher rates than control EVs by reporter$^+$ cells. MDA-MB-231 Cre$^+$ and T47D DsRed reporter$^+$ cells were co-cultured for 7 days in the presence or absence of TGF-β1 treatment every 48 h, in 0.1% FBS medium. On day 7, cells were imaged on a Nikon TE2000 inverted microscope for green, red and CFP channels. **A.** Representative images for both conditions are shown. Picture insets show magnification on a single recombined reporter$^+$ cell. **B.** Quantification expressed as fold change over control of the amount of eGFP$^+$ cells. TGF-β1 treated donor cells induce a significantly higher amount a reporter$^+$ cells switch, compared to control donor cells. Scale bars represent 100 µm. Data are represented as mean ± SEM of N=3 independent experiments. * $p \leq 0.05$ as with Student's t-test.

In Fig. 5.4B quantification of the amount of recombined reporter$^+$ cells shows that TGF-β1 treatment promoted significantly higher recombination events in reporter$^+$ cells compared control condition, likely to correlate with a higher EV uptake. Reporter$^+$ cells were also cultured separately from donor cells in order to monitor spontaneous recombination events (for the described incubation time no spontaneous events were observed, data not shown).

The data shown so far suggest a novel role for TGF-β1 growth factor in altering extracellular vesicle release. Short-time (8 h) TGF-β1 treatment results in an increase of EV release, compared to untreated cells. Furthermore, long-term treatment with TGF-β1 promoted TGF-β driven EVs internalisation by a higher number of recipient cells, as shown with the Cre-LoxP system.

5.3.4 TGF-β derived extracellular vesicles do not affect migration in recipient cells

Having already shown the efficient internalisation of EVs in Chapter 4 (Fig. 4.4) and in this chapter (Fig. 5.4), I sought to understand whether the vesicles released by TGF-β1 treated cells could affect the behaviour of recipient cells. TGF-β plays a dual role in cancer. During early events of carcinogenesis, it maintains cytostasis and induces apoptosis, exploiting a tumour suppressor function (David et al., 2016). In later stages of the disease, it promotes cell proliferation and migration (Padua et al., 2008). In highly metastatic cancer cells, such as MDA-231, I hypothesised that the cytokine would have an oncogenic role and in order to evaluate that I performed a wound healing assay to assess cell migration. In Fig. 5.5, extracellular vesicles were harvested from MDA-231 cells treated or not with TGF-β1 for 8 h. EVs were then normalised according to protein content and an equal amount of EVs from each condition was incubated with recipient MDA-231 cells, after having performed a scratch on the culture dish. The ability of recipient cells to migrate towards the scratch (wound healing) was assessed 21 h after the addition on EVs. Fig. 5.5 shows that vesicles harvested from control MDA-231 cells drove a comparable percentage of wound closure to TGF-β derived EVs, suggesting that in this setup TGF-β does not impact the ability of EVs in promoting migration.

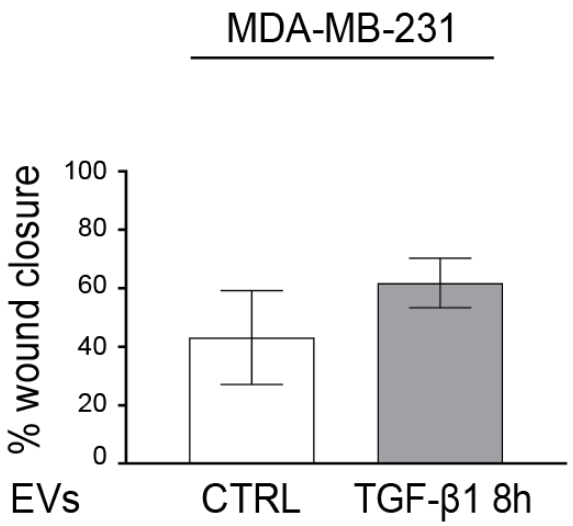


Figure 5.5 TGF-β1 driven EVs do not affect migratory ability of recipient cells. MDA-MB-231 cells were seeded (5 x 10^6 cells/plate) and cultured in 0.1% FBS medium for 72 h. On the last day medium was replaced and cells were treated or not with TGF-β1 for 8 h, in 0.1% FBS medium. EVs were collected from the conditioned medium via differential centrifugations. An aliquot was resuspended in 1X RIPA buffer for protein quantification, to ensure equal loading onto recipient cells. The remainder was resuspended in PBS, normalised and incubated with recipient MDA-MB-231 cells, plated as 2 x 10^5 cells/well in duplicates. After 21 h, brightfield images were taken on a Nikon Eclipse Ti-E inverted microscope. The ability of cells to migrate was measured as described in Methods section 2.2.17. TGF-β derived EVs do not appear to alter the ability of recipient recipient cells to migrate, compared to control EVs. Data are represented as mean ± SEM of N=3 experiments.

Next, I aimed to elucidate whether soluble TGF-β was carried over on EVs. If this was the case, any biological effect driven by EVs on recipient cells, could be attributed to the presence of soluble ligand on the vesicles, rather than to the activity of the vesicles. It has been previously demonstrated that TGF-β1 can be transported on exosomes released from cancer cells and that the cytokine exploits its functions on recipient cells using EVs as carriers (Webber et al., 2015). In order to quantify the amount of ligand carried over to recipient cells on EVs, I performed an ELISA assay on both conditioned medium of cells treated or not with TGF-β1 for 8 h and EVs isolated from cells treated in the same conditions (Fig. 5.6).

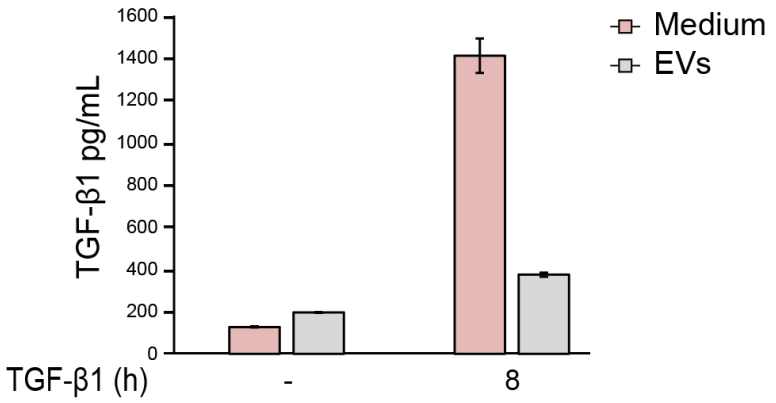


Figure 5.6 The amount of TGF-β1 carried over on extracellular vesicles is in the order of pg/mL. MDA-MB-231 cells were seeded (5 x 10^6 cells/plate) and cultured in 0.1% FBS medium for 72 h. On the last day medium was replaced and cells were treated or not with TGF-β1 for 8 h, in 0.1% FBS medium. EVs were harvested from the conditioned medium via differential centrifugations. An aliquot of conditioned medium from each condition was also collected as an internal control, since the ligand will concentrate mostly there. EVs and conditioned medium were tested for TGF-β1 enrichment using the TGF-β1 DuoSet ELISA kit (R&D). Most of TGF-β cytokine is found in the medium (pink bars) and not in the vesicles (grey bars). Data are represented as mean ± SEM of N=2 technical replicates.

Interestingly, in Fig. 5.6 I observed that, at a basal (untreated) level, MDA-231 vesicles already carried 200 pg/mL, however, after treatment, the increase in EV-bound TGF-β was less than 2-fold (Fig. 5.6, grey bars). In the conditioned medium, however, the cytokine had a 14-fold increase from before to after treatment (Fig. 5.6, pink bars). The data suggest that the EV-bound portion of TGF-β is lower than the amount carried over in the medium and thus any biological effect seen on recipient cells treated with the vesicles should not derive from direct ligand transfer, but most likely from the pool of TGF-β driven vesicles.

5.3.5 TGF-β derived extracellular vesicles mediate invasion in recipient cells

One of the most established functions of TGF-β is its role in promoting epithelial to mesenchymal transition and invasion (Massagué, 2008). My initial experiments showed that vesicles released following TGF-β treatment did not affect the motility of recipient cells (Fig. 5.5). Previous reports have shown that the response to

TGF-β affects both 2D and 3D invasion (Cantelli et al., 2015; Hachim et al., 2017; Wiercinska et al., 2011). I therefore performed a Boyden chamber invasion assay to assess the capacity of recipient cells, treated with TGF-β driven EVs, to invade through Matrigel. In Fig. 5.7, extracellular vesicles were harvested from MDA-231 cells treated or not with TGF-β1 for 8 h. EVs were then normalised according to protein content and an equal amount of EVs from each condition was incubated with MDA-231 cells, seeded on a thin layer of Matrigel, as previously described (Fig. 4.6). The ability of MDA-231 cells to invade in the presence of EVs was measured 18 h after incubation.

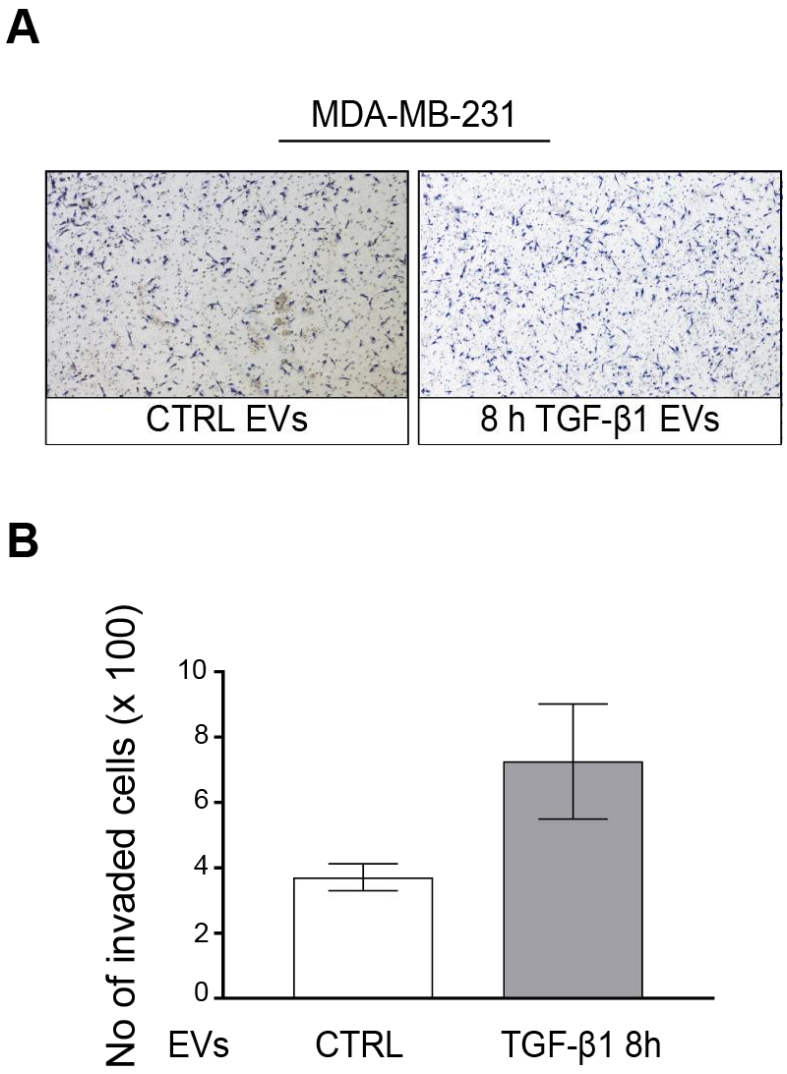


Figure 5.7 TGF-β1 driven EVs promote 3D Matrigel invasion in recipient cells, compared to control EVs. MDA-MB-231 cells were seeded (5 x 10^6 cells/plate) and cultured in 0.1% FBS medium for 72 h. On the last day medium was replaced and cells were treated or not with TGF-β1 for 8 h, in 0.1% FBS medium. EVs were collected from the conditioned medium via differential centrifugations. An aliquot was resuspended in 1X RIPA buffer for protein quantification, to ensure equal loading onto recipient cells. The remainder was resuspended in PBS, normalised and incubated with recipient MDA-MB-231 cells, plated as 5 x 10^4 cells/well onto Transwell Matrigel chambers (Corning). After 18 h, invaded cells were fixed and stained and brightfield images were taken on a Nikon 90i light microscope. The number of cells that invaded the Matrigel was quantified with ImageJ software 1.51s. **A.** Representative brightfield images per condition are shown. **B.** Bar graph showing the quantification of the amount of invaded cells. TGF-β derived EVs drive higher Matrigel invasion of recipient cells, compared to control EVs. Data are represented as mean ± SEM of N=2 experiments (of each, N=3 technical replicates).

Interestingly, incubation of recipient cells with TGF-β derived EVs appeared to promote the ability of cells to invade the Matrigel, compared to control EVs (Fig. 5.7). TGF-β derived EVs seemed to have an effect, despite not significant, on recipient cells.

In summary, the data showed thus far suggest that TGF-β EVs are not affecting recipient cell migration but may play a role in promoting invasion. Furthermore, the effect shown by EVs in the functional assays is not likely to be derived from a direct transfer of the growth factor onto the vesicles.

5.4 TGF-β Modulates Exocytosis of the Tetraspanin CD9

So far in this chapter I have studied a role for Transforming Growth Factor β in modulating EV trafficking. I have also demonstrated that TGF-β effect on EV release is not ascribable to RASSF1C presence in the cell (Fig. 5.2).

Interestingly, I observed that levels of EV markers such as Alix, β-catenin and Caveolin-1 did not change at the cellular level, upon TGF-β stimulus (see Fig. 5.2A, WCL panel). In an effort to extend the panel of EV markers I also included in the analysis the tetraspanins CD63 and CD9. Surprisingly, CD9 protein levels were markedly reduced in the cell lysates 8 h after TGF-β1 treatment (Fig. 5.2A, WCL panel). As other markers were not altered, I asked whether TGF-β may be redirecting tetraspanins specifically to secretion via extracellular vesicles in the observed time frame. I focused specifically on CD9, as a previous report in melanoma had highlighted a role for this tetraspanin in mediating TGF-β signalling. This study described that during early melanoma stages, the immunoglobulin IgSF8 was bound to both CD9 and CD81 at the plasma membrane and inhibited their interaction with TGF-β receptors I and II, thus impairing downstream signalling. In more advanced melanoma stages, IgSF8 was not expressed and both CD9 and CD81 were able to bind the receptors and positively mediate TGF-β downstream activation (H. Wang et al., 2015).

My preliminary data (described in Fig. 5.2A, CD9 lane) suggested that TGF-β signalling may be rerouting CD9 towards exocytosis. Given the link established between CD9 and TGF-β signalling in melanoma, I hypothesised that a similar recruitment of CD9, upon TGF-β treatment, could be taking place in breast cancer cells.

5.4.1 CD9 intracellular and extracellular pools depend on TGF-β

In order to investigate whether TGF-β could be regulating CD9 trafficking I first analysed CD9 intracellular localisation upon TGF-β treatment. MDA-231 cells were seeded on glass coverslips and treated or not with TGF-β1 at the indicated time-points. Cells were then fixed and stained with the indicated antibodies. I observed that, in untreated MDA-231 cells, CD9 localised both at the plasma membrane and in the cytosol (Fig. 5.8A, top panel). However, 8 h after TGF-β treatment, CD9 levels in the cells drastically decreased (Fig. 5.8A, bottom panel). Quantification of CD9 fluorescence intensity in each condition is presented in Fig. 5.8B, showing that CD9 intracellular levels significantly dropped 8 h after TGF-β treatment. TGF-β downstream activation was monitored via SMAD2 staining. At 2 h of treatment SMAD2 translocated from the cytosol (Fig. 5.8A, top panel) to the nucleus (Fig. 5.8A, middle panel). SMAD2 nuclear signal decreased after 8 h of treatment (Fig. 5.8A, bottom panel).

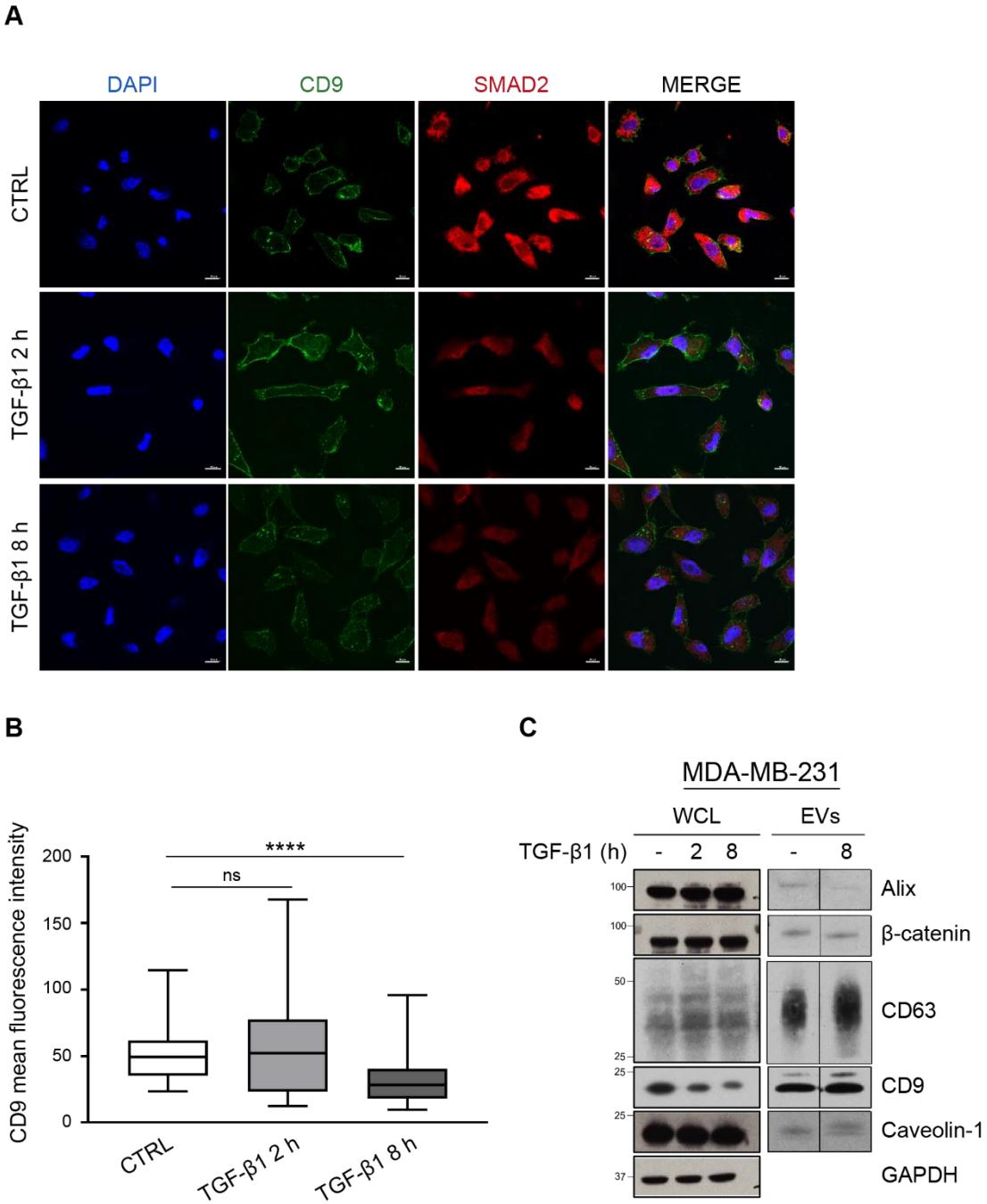


Figure 5.8 TGF-β1 treatment alters tetraspanin CD9 intracellular and extracellular levels in MDA-MB-231 cells. MDA-MB-231 cells were seeded (5 x 10^6 cells/plate) and treated or not with TGF-β1 for 2 or 8 h in 0.1% FBS medium, as previously described. **A.** Cells were fixed in 100% MeOH and stained for the indicated antibodies for immunofluorescence. Coverslips were mounted onto slides using mounting media containing DAPI. Representative pictures were taken at 40X magnification. Scale bars represent 10 µm. **B.** Quantification of CD9 intracellular fluorescence intensity was measured per each condition with the use of ImageJ software. Two fields of view were taken and at least 180 cells per condition were quantified. Data are represented as box-and-whiskers graph of N=2 experiments, with boxes delimiting the 25th and 75th percentiles and whiskers showing the min and the max values. The horizontal line defines the median. **** $p \leq 0.0001$ was calculated using the Mann-Whitney nonparametric test. Quantification reflects a decrease in the intracellular fluorescence of CD9, 8 h after TGF-β1 treatment. **C.** EVs were also collected from the conditioned medium via differential centrifugations and an aliquot was resuspended in 1X RIPA buffer for protein quantification. Representative western blot of EVs and cell lysates for EV markers showed loss of CD9 intracellular pool 8 h after treatment, in agreement with the quantification shown in **B**, with concomitant gain of CD9 in the EV preparations. Data are representative of N=2 biological replicates for immunofluorescence quantification and N=3 replicates for western blot.

In Fig. 5.8C extracellular vesicles were harvested from MDA-231 cells as previously described and EV markers were analysed. Whereas other markers did not vary intracellularly (see Fig. 5.8C, Alix, β-catenin, Caveolin-1), CD9 levels decreased upon TGF-β treatment.

In order to understand whether CD9 cellular pool was deprived upon TGF-β treatment only in MDA-231 cells, I employed an epithelial cell line, MCF7, to repeat the experiment. MCF7 showed a more defined CD9 pool present at the plasma membrane, compared to MDA-231 (Fig. 5.9A). However, upon treatment, I did not observe any change in the extracellular pools of CD9 (Fig. 5.9C, EV panel). Surprisingly, fluorescence intensity quantification, in Fig. 5.9B, showed a significant increase of CD9 intensity, upon 2 and 8 h of TGF-β1 treatment, in MCF7 cells.

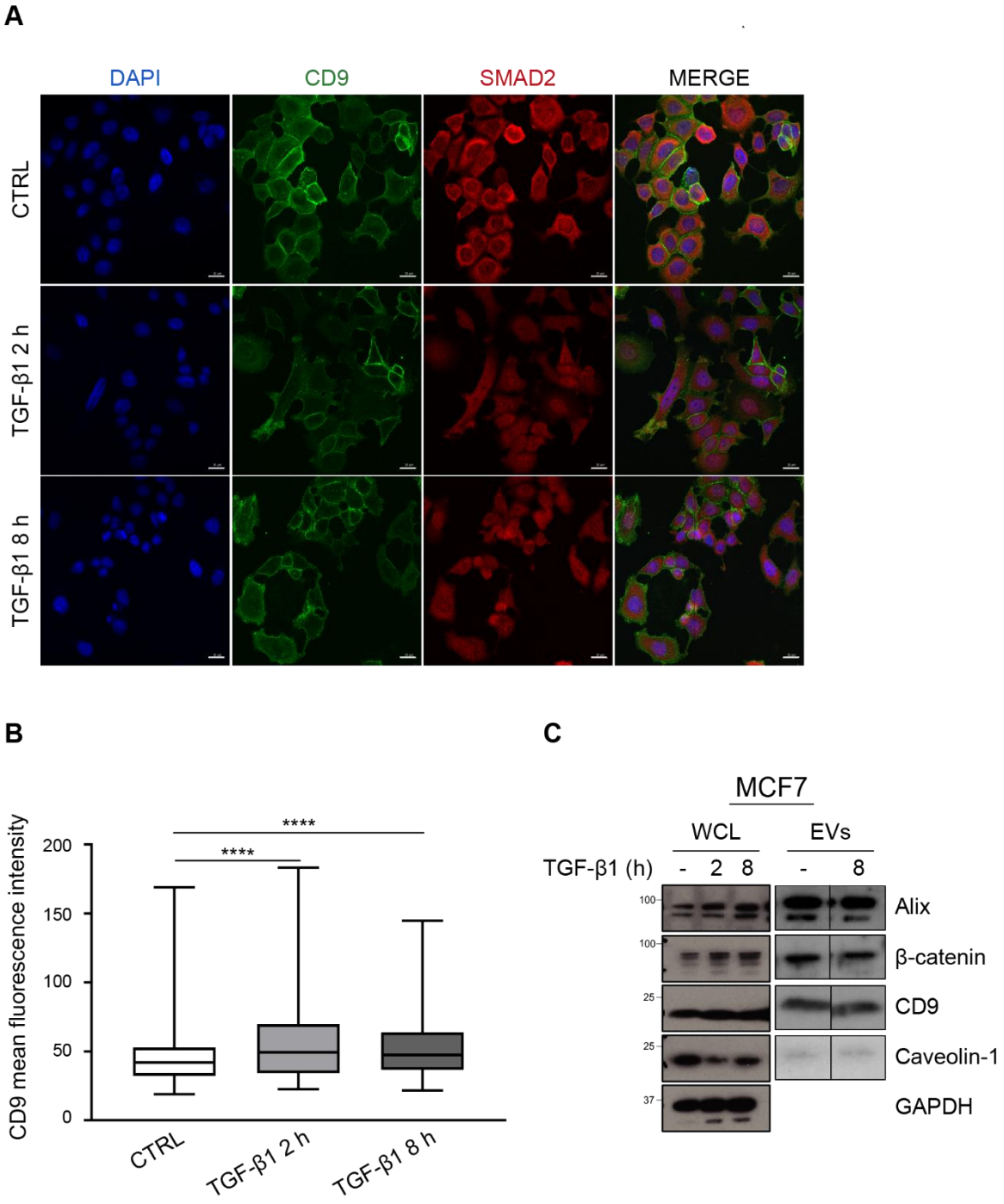


Figure 5.9 CD9 EV levels are not altered in MCF7 cells upon TGF-β1 treatment. MCF7 cells were seeded (5 x 10^6 cells/plate) and treated or not with TGF-β1 for 2 or 8 h in 0.1% FBS medium, as previously described. **A.** Cells were fixed in 100% MeOH and stained for the indicated antibodies for immunofluorescence. Coverslips were mounted onto slides using mounting media containing DAPI. Representative pictures were taken at 40X magnification. Scale bars represent 20 µm. **B.** Quantification of CD9 intracellular fluorescence intensity was measured per each condition with the use of ImageJ software. Two fields of view were taken and at least 180 cells per condition were quantified. Data are represented as box-and-whiskers graph of N=2 experiments, with boxes delimiting the 25th and 75th percentiles and whiskers showing the min and the max values. The horizontal line defines the median. **** $p \leq 0.0001$ was calculated using the Mann-Whitney nonparametric test. Quantification reflects a significant increase in the intracellular fluorescence of CD9 2 and 8 h after TGF-β1 treatment. **C.** EVs were also collected from the conditioned medium via differential centrifugations and an aliquot was resuspended in 1X RIPA buffer for protein quantification. Representative western blot showed no change in the extracellular levels (EVs) of CD9 after TGF-β1 treatment.

The results presented so far suggest that TGF-β employs the secretion of EVs to decrease CD9 intracellular levels, in MDA-231 cells. However, another possibility to reduce the amount of intracellular CD9 would be to promote proteasomal degradation. I next asked whether inhibition of the proteasome complex would result in intracellular accumulation of CD9. Incubation of MDA-231 cells with the proteasome inhibitor MG132, prior to TGF-β treatment, showed partial accumulation of CD9, suggesting that TGF-β may regulate CD9 levels using both routes, either promoting its secretion from the cell (in EVs, Fig. 5.8) or by promoting its degradation (Appendix Fig. 8.5).

Taken together the data so far suggest that TGF-β might differentially modulate CD9 intra- and extracellular levels. In mesenchymal cells, such as MDA-231, CD9 is less bound to the plasma membrane and seems to be enriched in EVs upon ligand treatment. In epithelial cells, such as MCF7, CD9 strongly localises at the plasma membrane and its extracellular levels do not appear to be affected by TGF-β.

5.4.2 CD9 localises at the plasma membrane upon TGF-β stimulus

According to previous findings in melanoma, CD9 crosstalk with the TGF-β cascade takes place at the plasma membrane, during TGF-β receptor I and II coupling (H. Wang et al., 2015). Hence, I hypothesised that CD9 recruitment at the plasma membrane should take place upon short term TGF-β treatment and that receptor blockage should impair CD9 localisation at the membrane, in MDA-231 cells. To test this hypothesis I used two commercially available TGFβRI inhibitors. In Fig. 5.10 MDA-231 cells were treated with the TGFβRI subunit ALK5 inhibitor II (Calbiochem), an ATP competitive inhibitor of the kinase domain of RI (Gellibert et al., 2004). Inhibitor treatment was carried out prior to addition of TGF-β1, as well

as with the cytokine. Cells were fixed and stained at the indicated time points. After 2 h of ligand treatment CD9 mostly localised at the plasma membrane and this localisation was lost 8 h after treatment (Fig. 5.10A, top panel). In the presence of the inhibitor CD9 was pan-cellular with no specific membrane staining (Fig. 5.10A, bottom panel).

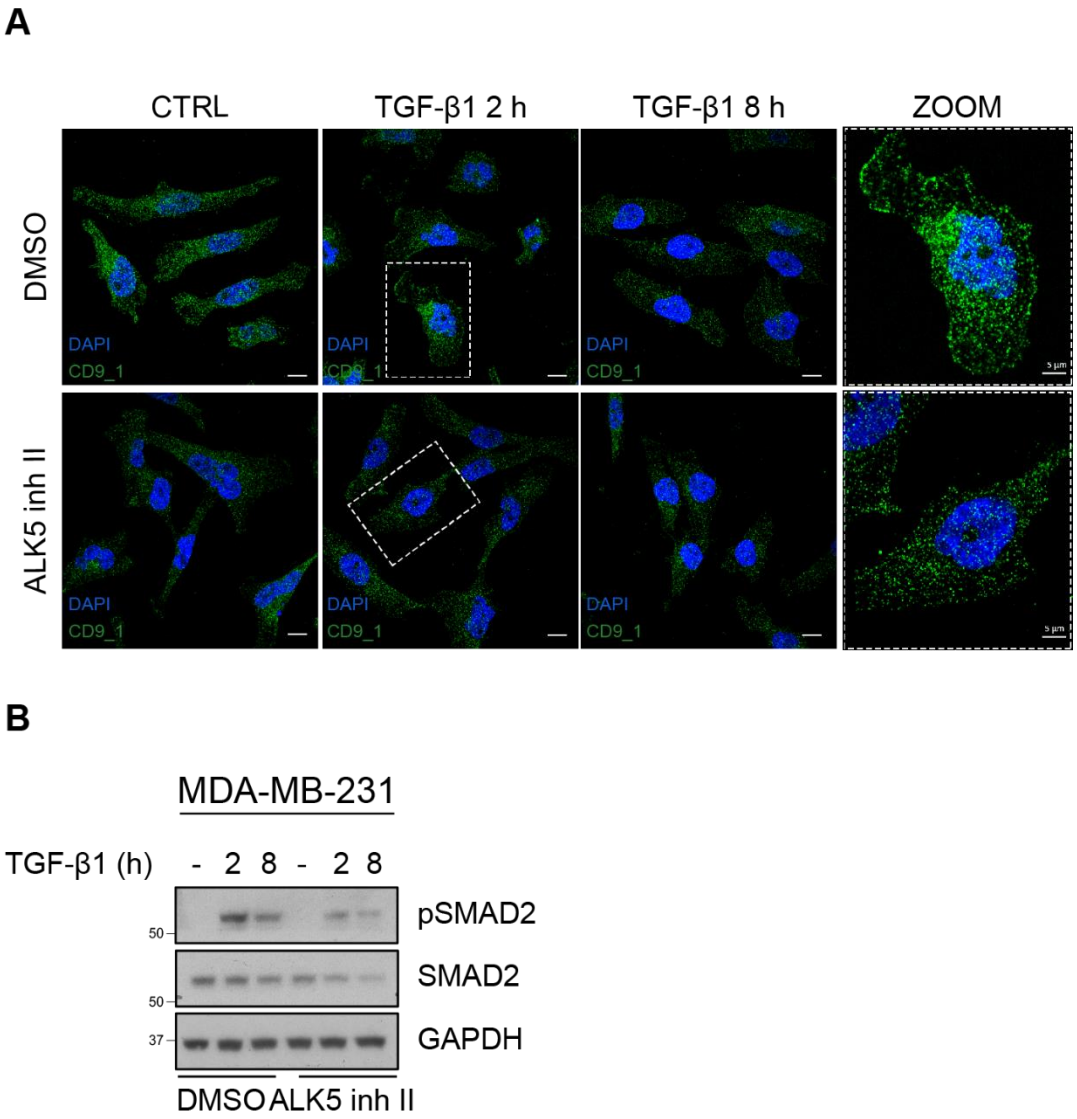


Figure 5.10 CD9 localises at the plasma membrane upon short term TGF-β1 treatment and ALK5 inhibitor II treatment impairs CD9 localisation. MDA-MB-231 were seeded (5 x 10^5 cells/well in 6-well plates) treated with 1 µM ALK5 inhibitor II (TGF-β receptor I subunit ALK5 inhibitor II, Calbiochem) or DMSO for 30 min prior to changing media and adding the inhibitor/DMSO and the growth factor for the indicated times. **A.** Cells were fixed in 4% PFA and stained with a CD9 antibody for immunofluorescence. Coverslips were mounted onto slides using mounting media containing DAPI. Scale bars represent 10 µm. **B.** Cell lysates were collected for western blot analysis to ensure pathway activation in the presence of the cytokine as well as inhibition in the presence of the inhibitor. At 2 h of treatment CD9 localises at the plasma membrane of cells and this localisation is impaired upon pathway inhibition with the ALK5 inhibitor II. Representative images and western blot are shown.

In Fig. 5.10B, I confirmed activation of the pathway upon cytokine treatment (phosphorylation levels of the TGF-β effector pSMAD2 are increased) and inhibition of the cascade (SMAD2 phosphorylation levels are decreased), after inhibitor treatment.

By using another ATP binding site competitive TGFβRI ALK5 inhibitor (Inman et al., 2002), SB431542 (Selleckem), I obtained similar results. MDA-231 cells were treated with the inhibitor first and then with a mixture of cytokine and inhibitor. Cells were then fixed and stained at the indicated time-points. Fig. 5.11A shows that accumulation of CD9 at the plasma membrane occurred 2 h after TGF-β treatment (5.11A, top panel). This accumulation was lost upon SB431542 treatment (Fig. 5.11A, bottom panel). In Fig. 5.11B I assessed inhibition of the pathway, as a measure of loss of SMAD2 phosphorylation in the presence of SB431542.

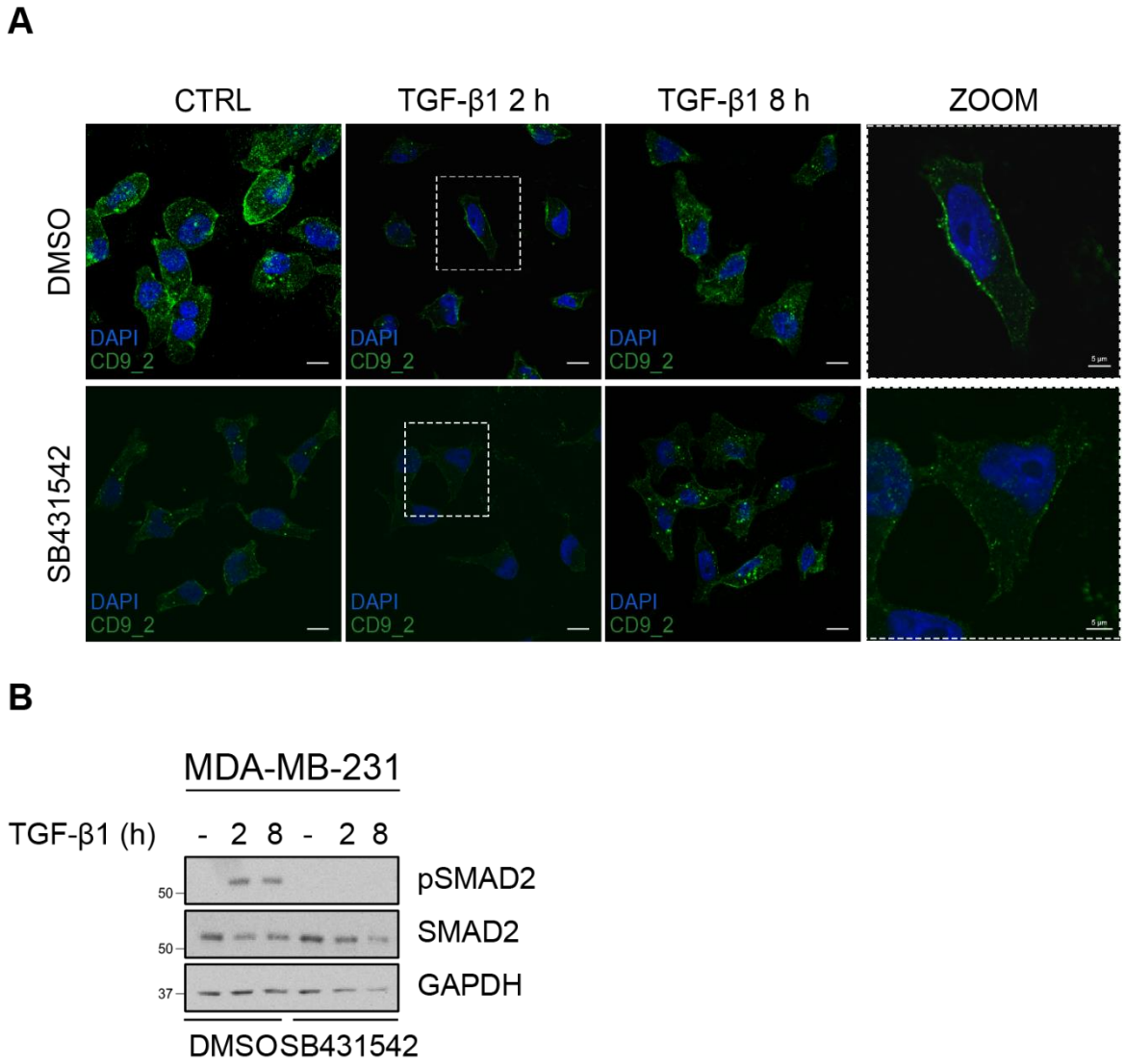


Figure 5.11 SB431542 treatment reverts CD9 localisation at the plasma membrane following TGF-β1 stimulation. MDA-MB-231 were seeded (5 x 10^5 cells/well in 6-well plates) and treated with 10 μM SB431542 (TGF-β receptor I subunit ALK5 selective inhibitor, Selleckchem) or DMSO for 30 min prior to changing media and adding the inhibitor/DMSO and the growth factor for the indicated times. **A.** Cells were fixed in 100% MeOH and stained for the indicated antibodies for immunofluorescence. Coverslips were mounted onto slides using mounting media containing DAPI. Scale bars represent 10 μm. **B.** Cell lysates were collected for western blot analysis to ensure pathway activation in the presence of the cytokine as well as inhibition in the presence of the inhibitor. Similarly to the results obtained in Fig. 5.10 with the ALK5 inhibitor II, the use of another potent receptor inhibitor (SB431542) affects CD9 localisation at the plasma membrane of cells upon TGF-β1 treatment, suggesting an involvement of tetraspanin CD9 in TGF-β1 pathway. Representative images and western blot are shown.

The data so far suggest that in MDA-231 cells CD9 is first recruited to the plasma membrane as an early event upon TGF-β pathway activation (at 2 h) and this recruitment is independently impaired by two TGFβRI inhibitors. Additionally, CD9 seems to be selectively secreted on EVs at later time-points (8 h). These

observations will be further corroborated in Chapter 6, where a novel role for the tetraspanin CD9 in TGF-β signalling will be described.

5.5 Discussion

In Chapter 5 I investigated the potential role of Transforming Growth Factor β in exocytosis. Time-course experiments suggested that TGF-β modulates exosome secretion in breast cancer cells and these results were further confirmed by employing the Cre-LoxP co-culture assay. BMP has been previously described as a regulator of exosome secretion in the secondary gland of male *Drosophila* (Corrigan et al., 2014). Preliminary evidence in MDA-231 cells suggested that BMP4 ligand may play a role in EV shedding (Fig. 5.3). However, the data on BMP4 would have to be repeated to confirm the discrepancy between NTA and protein levels. Nevertheless, it is important to consider that only three EV protein markers were analysed, which may represent a subpopulation of EVs, not affected by BMP4 treatment. Additionally, the previously followed protocol (in Chapter 3 and 4), where cells were left to accumulate EVs for 72 h, had to be adjusted for this new set of experiments, where the treatments were shorter, and thus might not allow enough time for the cells to accumulate a representative pool of EVs in the medium. Performing the BMP4 experiment with the Cre-LoxP system might allow us to better understand the involvement of this growth factor in EV trafficking, in this setup.

In this chapter, I have also shown that TGF-β effect on EV release is not correlated to RASSF1C levels in the cell. TGF-β controls a plethora of signals within the cell, it would be interesting to investigate the mechanisms employed by

the cytokine to modulate extracellular trafficking. A well-established connection has been made between TGF-β and Rho pathway: TGF-β is sufficient to sustain RhoA/ROCK signalling and this cascade is necessary to initiate ^{V12}HaRas, V-Raf and ^{V600E}BRAF malignant transformations in fibroblasts (Fleming et al., 2009). Moreover, Rho/ROCK pathway is one of the downstream effectors of TGF-β driven EMT programme (Bhowmick et al., 2001).

In Chapter 4 I have investigated the activation of Rho/ROCK pathway upon RASSF1C expression and how RhoA is one of the necessary steps for RASSF1C mediated EV release. Interestingly, a study in melanoma correlated TGF-β driven transcriptional programme to amoeboid phenotype, which is normally sustained by Rho/ROCK signalling (Cantelli et al., 2015). It would be thus interesting to explore Rho activation in the context of TGF-β signalling, in MDA-231 cells. Specifically, I could monitor extracellular vesicle release upon TGF-β1 treatment, in the presence of Rho/ROCK inhibitors or Rho mutants. This would clarify whether Rho acts downstream of TGF-β in the shedding of EVs in these cells.

In Chapter 5 I have also introduced the potential of TGF-β vesicles to induce invasion, but not migration, in recipient cells (Fig. 5.5, 5.7). EVs isolated after 8 h of treatment with TGF-β did not show any significant difference in promoting cell migration. However, treatment of cells with TGF-β derived EVs stimulated invasion. Given that the growth factor promotes phenotypic changes within the cell, such as EMT, in a longer time-frame than the one examined, it would be informative to isolate EVs after longer treatment and with multiple time-points, and test their ability to trigger a response on recipient cells.

The use of less invasive or untransformed recipient cells, for instance MCF7 or MCF10A, along with the use of different EV concentrations on the recipient cells

(as previously done in Chapter 4), may be important to better characterise this function of TGF-β EVs. In a recent study on the role of exosomes in fibroblast migration, exosomes were added to recipient cells in two formats: either added to the media at the time of migration (in a similar manner to the setup used in functional assays), or coated overnight onto tissue culture plates, prior to seeding of the recipient cells (Sung et al., 2015). Notably, with the second method a significant increase in cell migration was achieved. This method could be also adopted for the performed functional assays as a comparison to the more traditional addition of EVs to the culture medium. As an alternative technique, the Cre-LoxP system could also be used, either in co-culture or in transwell assay, to follow the migratory and invasive capacity of recombined reporter^{+} cells, as it was previously reported (Zomer et al., 2015).

Finally, in this chapter I have introduced the novel concept of the tetraspanin CD9 being selectively secreted on TGF-β EVs in MDA-231 cells. I have also shown that this cellular exclusion of CD9 is specific to MDA-231 and not to MCF7 cells. To define a correlation between CD9 and TGF-β, the screening of CD9 cellular levels upon TGF-β treatment in a panel of mesenchymal and epithelial breast cancer cells is required.

In order to confirm that CD9 secretion on vesicles is selectively enhanced by TGF-β, it would be important to treat cells with a TGFβRI inhibitor, in the presence of TGF-β, and subsequently isolate extracellular vesicles. I would speculate that, upon TGF-β pathway inhibition, CD9 is retained in the cell and conversely it is lost in the vesicles.

Our preliminary data on alternative routes employed by TGF-β signalling to regulate CD9 levels leave open the possibility that the cytokine may not only

promote CD9 exocytosis but also its degradation. However, further experiments are needed to strengthen this finding, by exploring both the proteasomal and lysosomal degradative routes.

As a transmembrane protein, CD9 has been previously shown to mediate TGF-β receptors coupling at the plasma membrane (H. Wang et al., 2015). It is a well-established integrin binding partner (Jones et al., 1996), an immunoglobulin partner (Yang et al., 2006) and an EGFR partner (W. Shi et al., 2000). Co-localisation studies of CD9 with the TGF-β receptors I and II would be of particular importance in understanding CD9 role in TGF-β signalling. Further insight on the importance of CD9 in Transforming Growth Factor β pathway will be reported in Chapter 6.

Together the work in this chapter (summarised in Fig. 5.12) provides evidence of a novel tumour promoting role for TGF-β. The growth factor elicits the release of EVs, in a RASSF1C independent manner, and these EVs are internalised and can trigger invasion of recipient cells. Moreover, the tetraspanin CD9 seems to be selectively enriched in TGF-β EVs in MDA-231 cells.

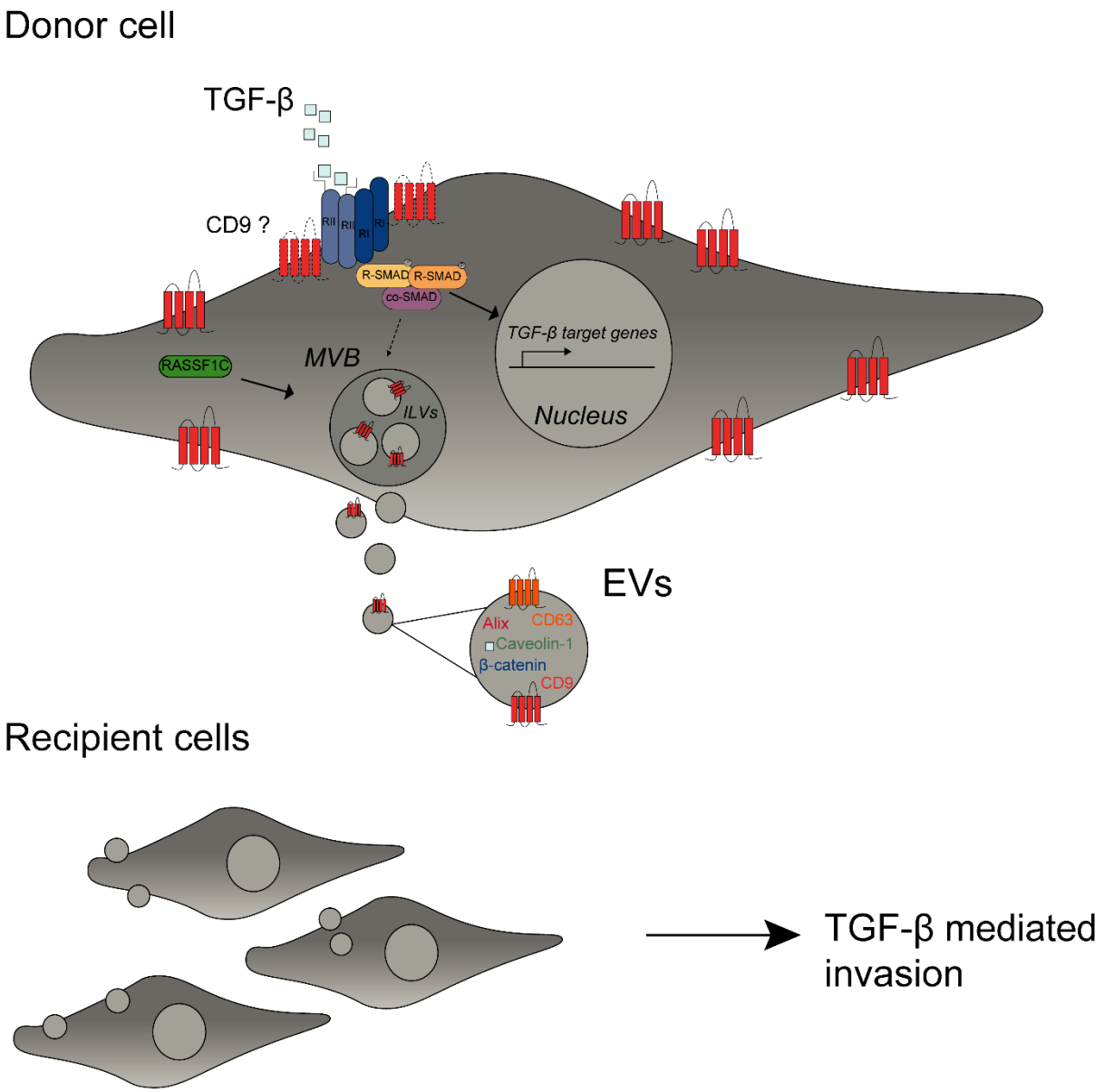


Figure 5.12 TGF-β mediates the release of pro-invasive extracellular vesicles. Schematic cartoon depicting a cell activated by TGF-β signalling, with the tetraspanin CD9 decorating the plasma membrane upon TGF-β signalling initiation and then enriched in EVs at a later stage. CD9 is proposed to be in close proximity to the TGFβRs on the membrane (dotted line CD9). The cartoon highlights the pro-invasive function of TGF-β driven EVs and the independence of RASSF1C and TGF-β signalling in mediating EV secretion.

Chapter 6 CD9 is a Positive Mediator of TGF-β Signalling

In Chapter 5 I have introduced evidence for a link between the tetraspanin CD9 and TGF-β pathway. So far, I have shown that TGF-β seems to control the cellular pools of CD9 and may promote its secretion from the cell, via EVs. In Chapter 6 I further expand these findings investigating CD9´s function in TGF-β signalling.

6.1 Introduction

6.1.1 CD9 regulates cell adhesion and migration

In humans, the tetraspanin family is comprised of 33 members, some of them are expressed ubiquitously and some others are tissue specific (de Winde et al., 2015). The members act as molecular scaffolds that distribute proteins into highly organised microdomains consisting of adhesion, signalling and adaptor proteins (Termini et al., 2017) (a more comprehensive introduction to tetraspanins is covered in Chapter 1.4.5). CD9 shows a wide tissue distribution and it was initially identified as a lymphohematopoietic marker, expressed in all major subsets of leukocytes and endothelial cells (Boucheix et al., 1988). Along with other members of the family, CD9 has also been validated in EV preparations deriving from leukocyte cell types in culture and plasma from healthy donors, being found particularly enriched in EVs from B cells and monocytes (Pugholm et al., 2016). Multiple functions in cell fusion, proliferation, adhesion and motility have been assigned to CD9. One of the most important roles of CD9 is mediating sperm-egg fusion, with CD9 null mice showing impaired oocyte fertilisation (Kaji et al., 2000;

Le Naour et al., 2000; Miyado et al., 2000). Cell adhesion is another important feature of CD9. The tetraspanin has been found to influence adhesion and spreading in Chinese hamster ovary cells (Cook et al., 2002, 1999); to regulate leukocyte adhesion during extravasation (Barreiro et al., 2005); to modulate the adhesive ability of lymphocyte progenitors and bone marrow fibroblasts (Masellis-Smith et al., 1994). More recently, a role for CD9 at the immune synapse has been shown, where it mediates integrin adhesion (Reyes et al., 2015). The extensively described interaction between tetraspanins and integrins explains the pivotal role of CD9 and other members of the family in cell adhesion and migration (Berditchevski et al., 1999). Additionally, CD9 has been also shown to promote cell proliferation and regulate apoptosis (Murayama et al., 2004; Tachibana et al., 1999).

6.1.2 CD9 in cancer

Notably, CD9 has been described as a metastasis suppressor (Hemler, 2014; Zöller, 2009). However, CD9´s role in cancer may be dependent on its binding partners and its post-translational modifications (Yang et al., 2006). CD9 can hamper metastasis formation by maintaining the architecture of integrins and adhesion molecules. In ovarian carcinoma cells CD9 down-regulation has been associated with an altered adhesion pattern (Furuya et al., 2005). In bladder carcinoma cells, association of CD9 with integrin α3β1 and ganglioside 3 was described as a metastasis-suppressing event (Mitsuzuka et al., 2005). Moreover, a study in breast cancer showed that CD9 expression inversely correlated with incidence of metastasis (Miyake et al., 1995). More recent results in an autochthonous prostate cancer mouse model showed that mice lacking CD9 had increased number of metastases in the liver (Copeland et al., 2013).

Despite being reported as a metastasis suppressor, contrasting evidence on the tumour promoting role of CD9 is also highlighted in the literature. Two reports independently proposed a correlation between CD9 expression and poor prognosis in gastric cancer (Hori et al., 2004; Soyuer et al., 2010). CD9 expression also leads to increased melanoma invasion *in vitro* (Fan et al., 2009). In a report on breast cancer cells, CD9 was described as a promoter of stroma invasion and CD9 depletion led to alterations in filopodia and lamellipodia structures (Rappa et al., 2015). In another melanoma study, CD9, CD81 and their binding partner IgSF8 were shown to differentially regulate TGF-β signalling, according to the stage of the disease. In early stage melanoma, IgSF8 was expressed and inhibited oncogenic TGF-β signalling by blocking CD9 and CD81 association to the TGF-β receptors. In late stage melanoma, IgSF8 expression was lost and CD9 and CD81 were thus able to facilitate TGF-β downstream activation, mediating receptor coupling (H. Wang et al., 2015).

The opposing roles CD9 plays in different tumour types may be due to association with different partner proteins, such as different tetraspanins, integrins, immunoglobulins, and this could result in opposite effects on tumour invasion and metastasis.

6.2 Aims

In Chapter 6 the aim is to investigate whether CD9 plays a role in mediating TGF-β signalling in breast cancer cells. Specifically, I hypothesise that CD9 may be a positive regulator of the pathway and its loss may impair downstream activation. Furthermore, I intend to study the biological activity of extracellular vesicles enriched with CD9 on recipient cells.

6.3 Loss of CD9 Affects TGF-β Downstream Activation

6.3.1 CD9 knockdown reduces SMAD2 phosphorylation and nuclear translocation

In Chapter 5 I have shown that the tetraspanin CD9 is selectively secreted from cells upon 8 h of TGF-β treatment and this coincides with enrichment of CD9 pools in the extracellular vesicle fraction of MDA-231 cells (Fig. 5.8). Since this phenomenon appeared to be cell type specific (see Fig. 5.9, not visible in MCF7 cells), I decided to further elucidate CD9´s role in MDA-231 cells. The results in Chapter 5 suggested that TGF-β may use EVs as a secreting route to decrease intracellular pools of the CD9 protein. Given the evidence in the literature that CD9 may mediate TGF-β signalling, I decided to test this possibility in MDA-231 cells. Cells were treated with siRNA targeting a control sequence (siLuc) or CD9 mRNA (siCD9). 48 h after transfection cells were cultured in 0.1% FBS medium and treated with TGF-β1 for the indicated time-points. Cells were then lysed for western blot analysis and cells grown on glass coverslips in the same conditions were fixed in 100% MeOH and stained for immunofluorescence. Interestingly, CD9 depletion led to a significant decrease in phosphorylation at Ser 465/467 of the TGF-β effector SMAD2 (pSMAD2), 2 h after TGF-β1 treatment, as quantified in Fig. 6.1B.

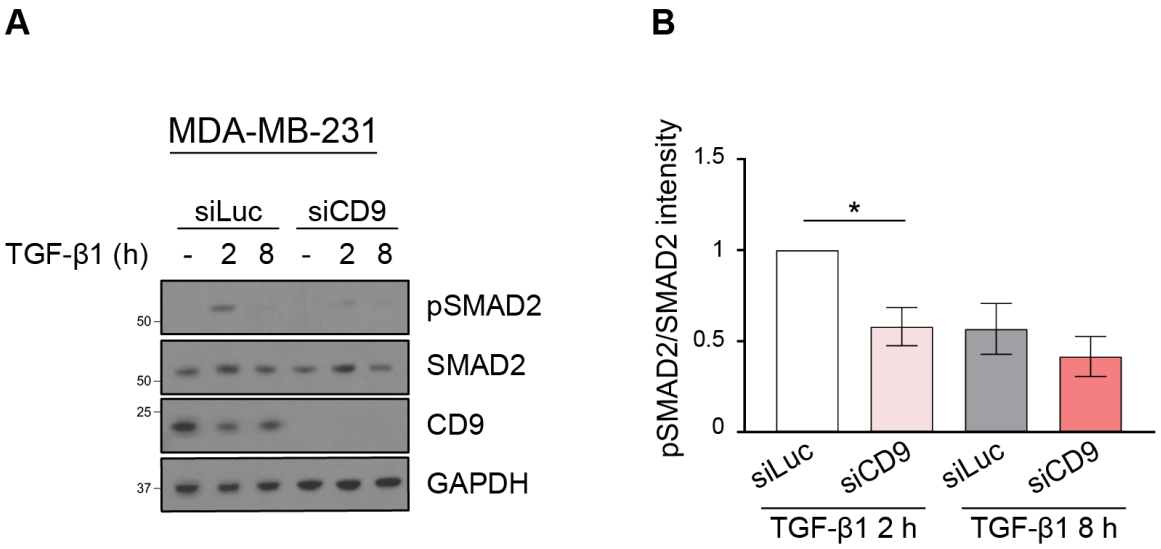


Figure 6.1 CD9 depletion leads to a decrease in SMAD2 phosphorylation in the presence of TGF-β. MDA-MB-231 were seeded (1 x 10^5 cells/plate) and transiently transfected with control siRNA (siLuc) or siRNA targeting CD9 mRNA. 48 h after transfection cells were treated or not with TGF-β1 for 2 or 8 h. **A.** Cells were lysed and western blot analysis of TGF-β1 downstream activation was performed using a pSMAD2 antibody raised against the two receptor phosphorylation sites of SMAD2 (S465/S467). CD9 knockdown efficiency was also assessed. **B.** Quantification of WB band intensity of pSMAD2 normalised against total SMAD2 in 3 biological replicates shows a significant decrease in SMAD2 phosphorylation upon CD9 knockdown. Data are represented as mean ± SEM.* $p \leq 0.05$ as with Student's t-test. Representative western blot is shown.

SMAD2 phosphorylation is mediated by the kinase domain of activated TGFβRI, which is phosphorylated in the first instance by TGFβRII, after binding of the soluble ligand to TGFβRII (Y. Shi et al., 2003). SMAD2 phosphorylation is then followed by association of pSMAD2 (and pSMAD3) in homo or heteroligomers with the co-SMAD, SMAD4. In these trimeric complexes R-SMADs (SMAD2 and 3) and co-SMAD (SMAD4) translocate to the nucleus where they start a complex transcriptional programme. I thus hypothesised that if levels of pSMAD2 are reduced, SMAD2 nuclear translocation may also be impaired.

In Fig. 6.2 immunofluorescence analysis revealed a significant decrease of SMAD2 nuclear signal upon CD9 depletion, as quantified in 6.2B. For the immunofluorescence quantification only the 2 h time-point was considered as

SMAD2 phosphorylation and subsequent nuclear translocation are early events in the cascade with a peak between 30 minutes and 5 h (Inman et al., 2002).

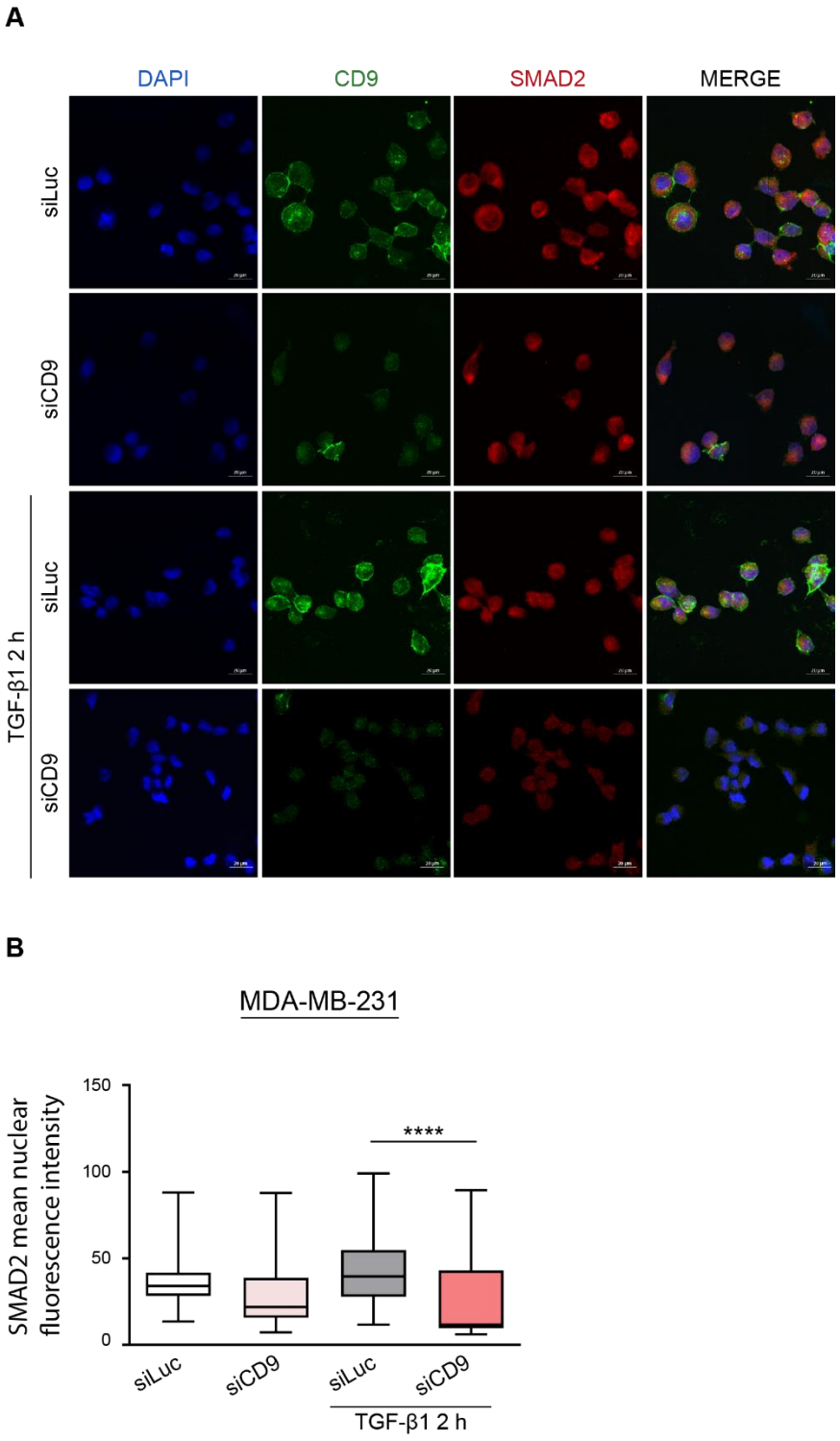


Figure 6.2 CD9 depletion leads to decreased nuclear SMAD2 signal in the presence of TGF-β. MDA-MB-231 were seeded on to glass coverslips (1 x 10^5 cells/plate) and transiently transfected with control siRNA (siLuc) or siRNA targeting CD9 mRNA. 48 h after transfection cells were treated or not with TGF-β1 for 2 h. **A.** Cells were fixed in MeOH 100% and stained for the indicated antibodies. Coverslips were mounted onto slides using mounting media containing DAPI. Scale bars represent 20 μm. **B.** SMAD2 nuclear intensity in the indicated conditions was quantified with NIS Elements using DAPI as a nuclear mask. Two fields of view were taken per condition and at least 180 cells per condition were quantified. Data are represented as box-and-whiskers graph of N=2 experiments, with boxes delimiting the 25th and 75th percentiles and whiskers showing the min and the max values. The horizontal line defines the median. Quantification shows a significant decrease in SMAD2 nuclear localisation upon TGF-β treatment, in CD9 depleted cells. **** $p \leq 0.0001$ was calculated using the Mann-Whitney nonparametric test.

To understand whether CD9 knockdown would cause a complete loss or generate a delay in SMAD2 phosphorylation I performed a time-point experiment where MDA-231 cells were treated with TGF-β1 for up to 4 h in the presence or absence of CD9. Interestingly, CD9 knockdown seemed to delay the phosphorylation establishment as well as generally decrease the intensity of the signal (Fig. 6.3).

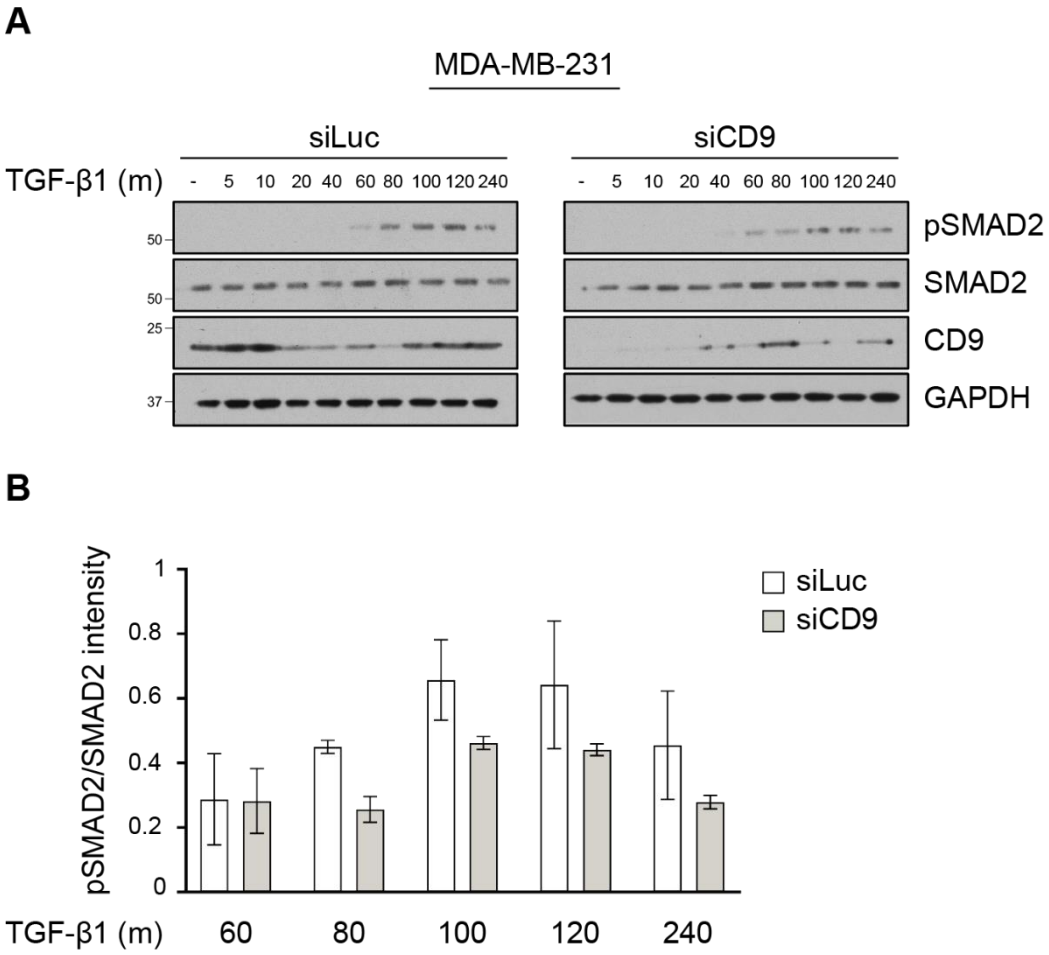


Figure 6.3 CD9 depletion results in delayed SMAD2 phosphorylation kinetics. MDA-MB-231 were seeded (1 x 10^5 cells/plate) and transiently transfected with control siRNA (siLuc) or siRNA targeting CD9 mRNA. 48 h after transfection, cells were treated or not with TGF-β1 for the indicated time-points. **A.** Cells were lysed and western blot analysis with the indicated antibodies was performed. **B.** Quantification of WB band intensity of pSMAD2 normalised against total SMAD2 in 2 biological replicates shows a trend in delayed establishment of SMAD2 S465/S467 phosphorylation and a decrease in the potency of the phospho-signal upon CD9 knockdown. Representative western blot is shown.

The data so far suggest that CD9 may mediate events downstream of TGF-β, with a decrease in the levels of active SMAD2 and an observed cytoplasmic retention of SMAD2 in the absence of CD9.

6.3.2 CD9 depletion affects SMAD2 and SMAD4 coupling

As previously mentioned, upon TGF-β stimulus, R-SMADs (SMAD2 and SMAD3 in TGF-β signalling) translocate to the nucleus in association with the co-SMAD, SMAD4. Therefore, I decided to investigate whether SMAD2 and SMAD4 binding was impaired in CD9 depleted cells. In agreement with the literature, I could see establishment of SMAD2 phosphorylation already after 1 h of ligand treatment (Fig. 6.3). I thus performed an immunoprecipitation assay in MDA-231 lysates transfected with siLuc or siCD9 and treated with TGF-β1 for 1 h. In the presence of ligand, SMAD2 and SMAD4 precipitated in a complex (see Fig. 6.4, lane 3 of IP, black arrow refers to the SMAD4 band). However, in CD9 depleted cells the amount of SMAD4 bound to SMAD2 was decreased (Fig. 6.4, lane 5).

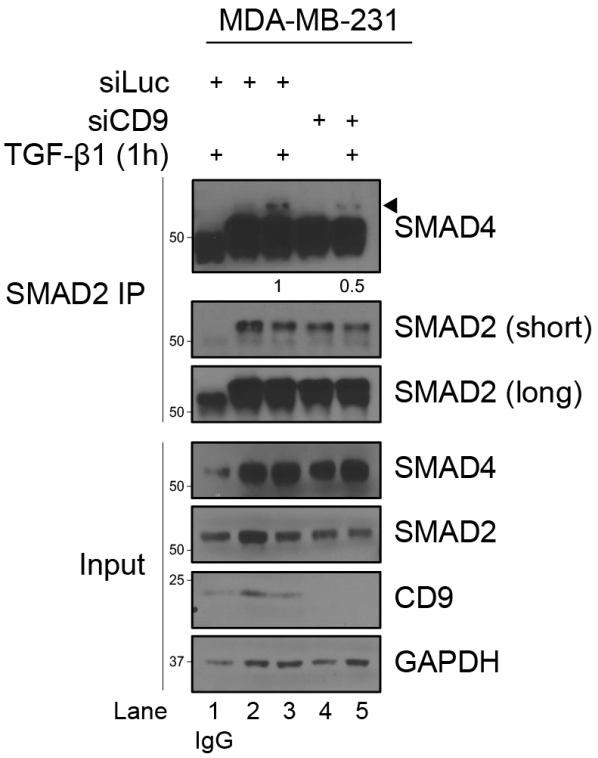


Figure 6.4 CD9 depletion affects SMAD2/SMAD4 binding. MDA-MB-231 cells were seeded (1 x 10^6 cells/plate) and transiently transfected with control siRNA (siLuc) or siRNA targeting CD9 mRNA. 48 h after transfection cells were treated or not with TGF-β1 for 1 h. Cells were lysed in 1% NP40, 150 mM NaCl lysis buffer supplemented with protease and phosphatase inhibitors. Lysates were immunoprecipitated for 3 h with a SMAD2 antibody or IgG control bound to protein G dynabeads (Millipore). Proteins were recovered from the beads by boiling for 10 min in 1X loading buffer and samples were analysed by SDS-PAGE and western blot for the indicated antibodies. SMAD4 WB band quantification is normalised against SMAD2 pull-down. SMAD2/SMAD4 interaction (top band of SMAD4, black arrow) is affected by loss of CD9. IgG refers to the IgG lane. Representative western blot is shown.

Previous reports in the literature have identified a crosstalk between the TGF-β and the Hippo pathway (Mauviel et al., 2012). Since SMAD complexes can interact with the Hippo effectors YAP/TAZ and they share common target genes (Hiemer et al., 2014; Pefani et al., 2016; Varelas et al., 2008), I performed YAP immunoprecipitation to assess SMAD2/YAP binding in CD9 depleted cells. In Fig. 6.5, MDA-231 cells were treated as in Fig. 6.4 and YAP protein was immunoprecipitated. Interestingly, SMAD2 levels in the complex were not strongly affected by CD9 depletion, with a slight increase in YAP binding.

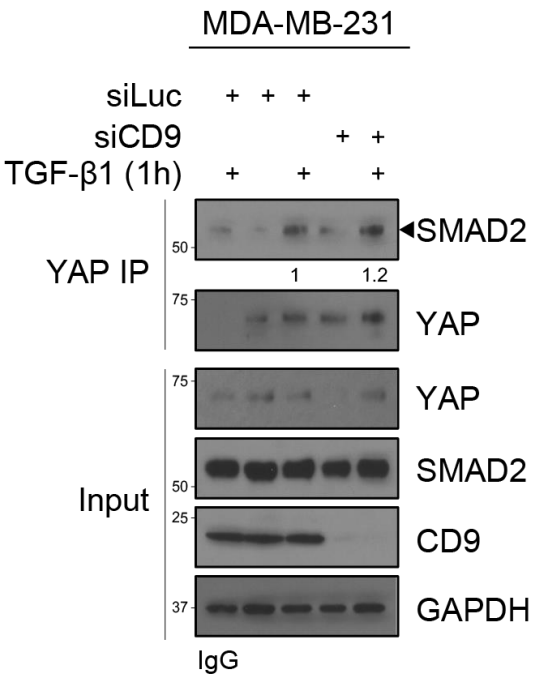


Figure 6.5 CD9 depletion does not alter SMAD2/YAP binding. MDA-MB-231 cells were seeded (1 x 10^6 cells/plate) and transiently transfected with control siRNA (siLuc) or siRNA targeting CD9 mRNA. 48 h after transfection cells were treated or not with TGF-β1 for 1 h. Cells were lysed in 1% NP40, 150 mM NaCl lysis buffer supplemented with protease and phosphatase inhibitors. Lysates were immunoprecipitated for 3 h with YAP antibody or IgG control bound to protein G dynabeads (Millipore). Proteins were recovered from the beads by boiling for 10 min in 1X loading buffer and samples were analysed by SDS-PAGE and western blot for the indicated antibodies. SMAD2 WB band quantification is normalised against YAP pull-down. SMAD2/YAP interaction does not appear to be altered upon CD9 depletion. IgG refers to the IgG lane. Representative western blot is shown.

Therefore, the data so far describe a role for CD9 in mediating canonical TGF-β downstream, but not the crosstalk with the Hippo pathway.

6.3.3 CD9 knockdown results in delayed TGF-β target transcription

Once in the nucleus, SMAD complexes and their interacting partners target specific promoters to regulate gene expression patterns. I next evaluated TGF-β1 canonical target gene expression in the presence or absence of CD9 in MDA-231 cells. Cells were treated as previously reported, mRNA isolated and cDNA prepared. qPCR of target genes is shown in Fig. 6.6. Interestingly, different target genes have different peaks of transcription. *SMAD7, CTGF* and *CYR61* for

instance were induced at 2 h of treatment and transcription decreased at 8 h, whereas *PAI-1* was induced later, with a peak at 8 h (Fig. 6.6A).

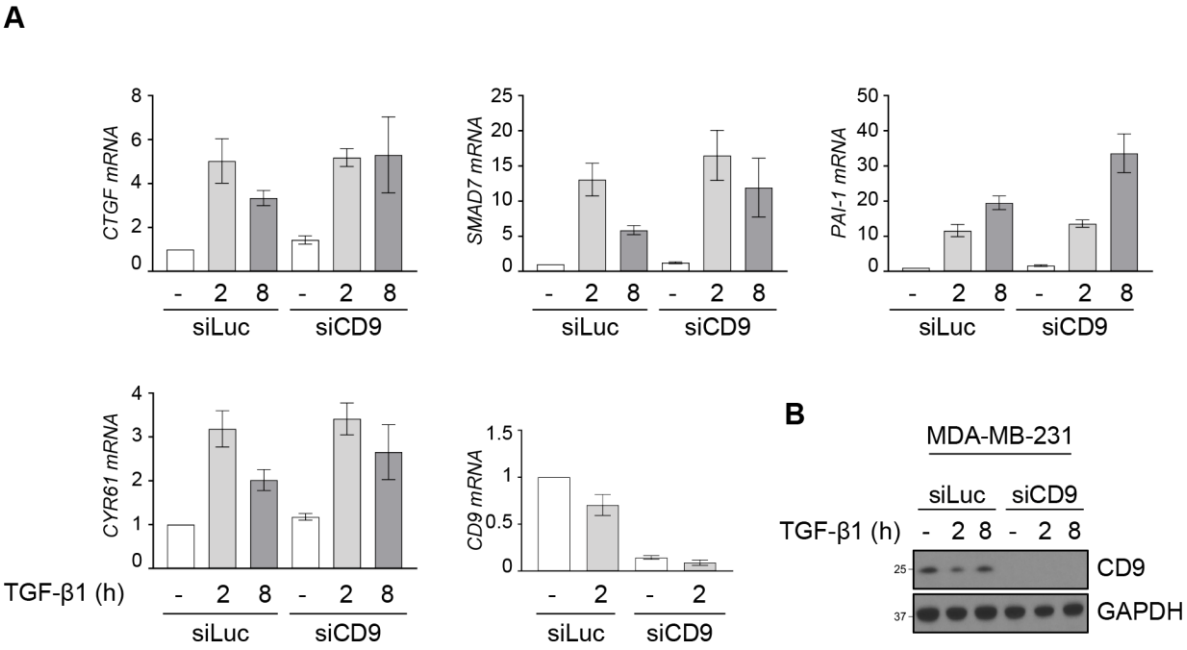


Figure 6.6 TGF-β1 target genes induction is not altered in CD9 depleted cells. MDA-MB-231 were seeded (5 x 10^5 cells/well in 6-well plates) and transiently transfected with control siRNA (siLuc) or siRNA targeting CD9 mRNA. 48 h after transfection cells were treated or not with TGF-β1 for the indicated time-points. **A.** 50,000 cells per condition were lysed, cDNA prepared and qPCR was performed on a StepOnePlus™ Real-Time PCR machine. Expression of GAPDH was used as an internal control. **B.** The remainder of cells were lysed and western blot analysis with the indicated antibodies was performed, to confirm CD9 depletion. Canonical TGF-β1 target gene expression was assessed after TGF-β1 treatment and no significant changes in gene expression upon CD9 knockdown were observed. Efficient CD9 mRNA knockdown was also assessed via qPCR for the indicated time-points. Data are represented as mean ± SEM of N=3. Representative western blot is shown.

Interestingly, TGF-β driven transcription of the selected target genes was not affected upon CD9 knockdown (Fig. 6.6A). CD9 efficient depletion was assessed both with qPCR (Fig. 6.6A) and western blot (Fig. 6.6B). Given that I previously showed that CD9 loss leads to a delay in pSMAD2 establishment (Fig. 6.3), I reasoned that earlier time-points could reveal a delay in transcription which is overcome at later time-points, such as 2 and 8 h.

To this end, I transfected MDA-231 cells, as previously reported, and then treated them with TGF-β1 for 40 and 60 min. Cells were then harvested for western blotting and mRNA was isolated and cDNA prepared for qPCR. In Fig. 6.7A the same target genes as before were analysed and notably some of them (*PAI-1, CYR61*) showed a significantly reduced transcription in CD9 depleted cells, 60 min after TGF-β1 treatment. In Fig. 6.7B, pSMAD2 levels and CD9 levels were also evaluated and decrease in pSMAD2 levels, in CD9 depleted cells, was confirmed.

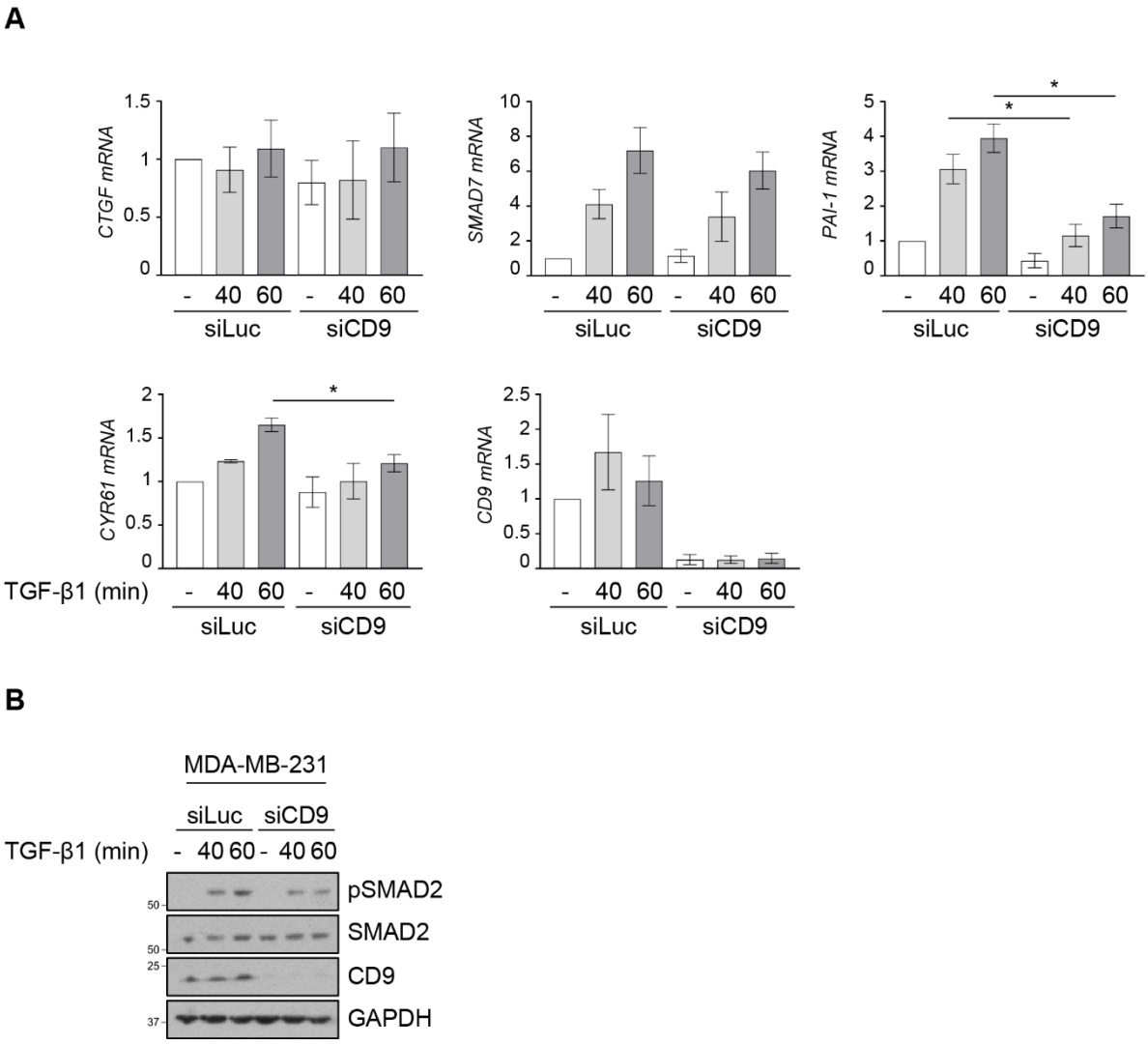


Figure 6.7 TGF-β1 target genes induction is delayed is CD9 depleted cells. MDA-MB-231 were seeded (5 x 10^5 cells/well in 6-well plates) and transiently transfected with control siRNA (siLuc) or siRNA targeting CD9 mRNA. 48 h after transfection cells were treated or not with TGF-β1 for the indicated time-points. Cells were either lysed for western blotting or 50,000 cells were lysed, cDNA prepared and qPCR was performed on a StepOnePlus™ Real-Time PCR machine. Expression of GAPDH was used as an internal control. **A.** Canonical TGF-β1 target gene expression was assessed after TGF-β1 treatment and a delay in induction was observed in two of the target genes (*PAI-1*, *CYR61*). Efficient CD9 mRNA knockdown was also analysed. **B.** TGF-β1 downstream activation was assessed via western blotting. Data are represented as mean ± SEM of N=2. * $p \leq 0.05$ was calculated using one-tailed Student's t-test. Representative western blot is shown.

The data so far indicate that CD9 depletion causes a delay in the onset of TGF-β induced gene transcription, visible only at early time-points and overcome at later ones.

6.4 Inhibition of Extracellular Vesicle Synthesis Sustains TGF-β Signalling

6.4.1 Treatment with a nSMase inhibitor leads to maintained pSMAD2 over time

In Chapter 5 I have proposed that CD9 is selectively loaded on EVs upon TGF-β stimulation. I hypothesised that the pathway utilises exocytosis as an alternative method to degradation, in order to diminish CD9 intracellular levels. Here I suggest that secretion of CD9 is a negative feedback loop of the pathway. CD9, as a positive modulator of the TGF-β cascade, is eliminated from the cell and the overall TGF-β signalling is dampened over time. The kinetics of CD9 secretion on vesicles/loss from the cell, upon TGF-β treatment, is similar to the kinetics of decrease in pSMAD2 signal, both happening around 8 h after ligand treatment (see Fig. 5.8 for CD9 in the EVs, Fig. 5.3 for pSMAD2 levels).

Given that my results suggested a secreting route for CD9 via EVs, I hypothesised that inhibition of EV biogenesis would thus retain CD9 in the cell, even during exposure to TGF-β. This should maintain TGF-β signalling, measured as pSMAD2 signal, for as long as 8 h.

Chemical inhibition of extracellular vesicle biogenesis has been reported with the use of a neutral sphingomyelinase 2 (nSMase2) inhibitor, GW4869, which inhibits the synthesis of ceramide, a lipidic component of EV membranes (Trajkovic et al., 2008). The inhibitor was first tested on MDA-231 cells at different concentrations to ensure cell viability (data not shown). Two of the tested concentrations were then chosen to test EV inhibition. MDA-231 cells were seeded and cultured for 48 h in 0.1% FBS. Cells were treated with GW4869 at either 0.1 or 0.5 μM

concentration for 2 h prior to EV isolation with differential centrifugations. In Fig. 6.8A both cell and EV lysates were analysed via western blotting and in 6.8B NTA was employed to measure the overall amount of EVs. Most of the protein markers were markedly decreased at 0.5 μM of GW4869 and the particle count was also 4.6-fold reduced, compared to DMSO treatment.

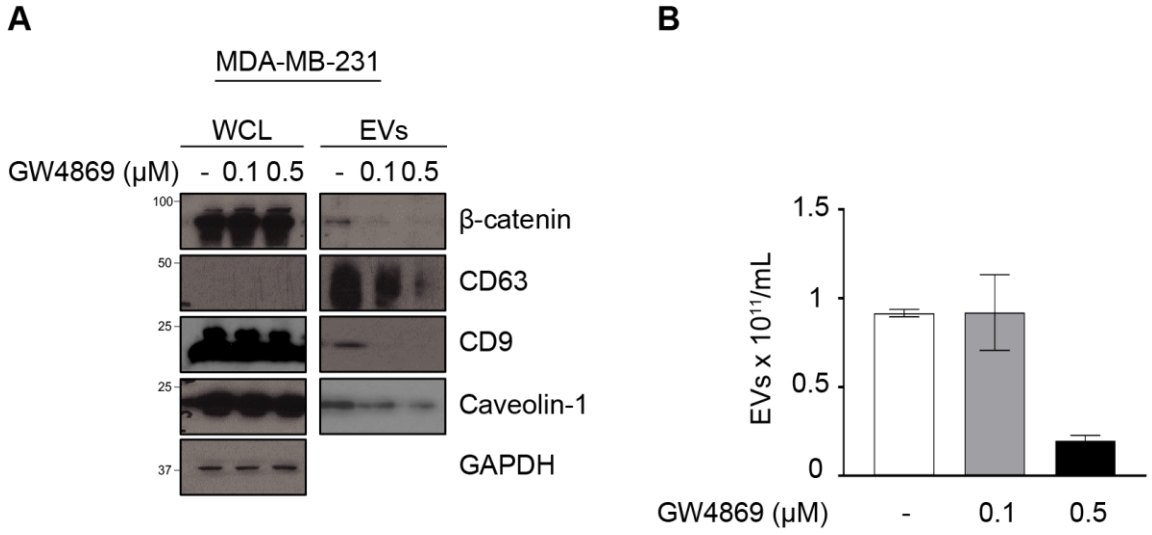


Figure 6.8 Extracellular vesicle biogenesis is efficiently inhibited with the neutral sphingomyelinase inhibitor GW4869. MDA-MB-231 were seeded (5 x 10^6 cells/plate), cultured in 0.1% FBS for 48 h and treated with 0.1 or 0.5 μM of GW4869 or DMSO for 2 h in 0.1% FBS medium. EVs were collected after treatment with a differential centrifugation protocol. **A.** After normalisation, total cell lysates and EV lysates were analysed for protein content with western blotting. **B.** An aliquot of EVs was also analysed for particle concentration with NTA. 0.5 μM GW4869 treatment resulted in better inhibition of EV biogenesis. NTA measurements are represented as mean ± SEM of N=3 technical replicates. Representative western blot is shown.

I thus decided to use the selected inhibitor concentrations on MDA-231 cells treated or not with TGF-β for 2 or 8 h.

In Fig. 6.9 cell lysates were analysed for SMAD2 phosphorylation. Interestingly, I could observe a trend of sustained phospho-signal in cells treated with both TGF-β1 and the EV inhibitor at 0.5 μM, as shown by the band intensity quantification in Fig. 6.9B.

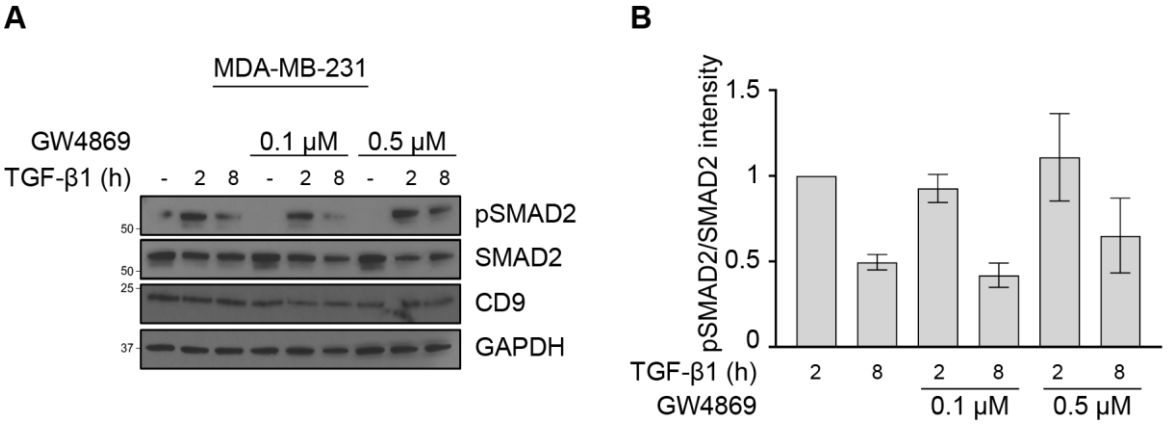


Figure 6.9 GW4869 treatment sustains TGF-β1 signalling. MDA-MB-231 were seeded (1 x 10^5 cells/plate) treated with increasing concentrations of GW4869 for 2 h prior to treatment with TGF-β1 for the indicated time-points. **A.** Cells were lysed and SMAD2 protein levels were analysed via western blotting. **B.** Quantification of WB band intensity of pSMAD2 normalised against total SMAD2 in 2 biological replicates shows a trend in maintained SMAD2 S465/S467 phosphorylation at 8 h after treatment with TGF-β1, in the samples treated with the highest concentration of GW4869. Data are represented as mean ± SEM of N=2. Representative western blot is shown.

The data suggest that treatment with an EV inhibitor, GW4869, may result in perpetuating TGF-β downstream for longer time-points, such as 8 h.

6.5 CD9 positive Extracellular Vesicles Elicit a Biological Response on Recipient Cells

6.5.1 Treatment of recipient cells with CD9 positive EVs results in SMAD2 activation

So far in this chapter I have investigated a novel role for CD9 in mediating TGF-β signalling. However, the function of EV-bound CD9 has not been explored. I hypothesised that CD9 carried on EVs to recipient cells may be able to mediate TGF-β response in cells that do not normally express CD9. To this end I transfected MDA-231 donor cells with a control siRNA or siCD9 and 48 h after transfection EVs were isolated. In this way I generated a CD9 positive ($CD9^+$) and

a CD9 negative ($CD9^-$) pool of EVs. As recipient cells, to treat with $CD9^+$ and $CD9^-$ EVs, I chose SUM159PT adenocarcinoma cells, because they express a negligible amount of CD9 protein (see Appendix Fig. 8.6). SUM159PT were incubated for 30 min with the EVs prior to TGF-β treatment for 1 h, to allow cascade initiation (see experimental setup in Fig. 6.10).

In Fig. 6.10, SUM159PT recipient cells were lysed and protein levels of pSMAD2 probed for western blotting. In the absence of EVs, SUM159PT cells initiated TGF-β signalling, when treated with the ligand (see Fig. 6.10A, lane 1 compared to lane 4). Interestingly, pre-treatment with $CD9^+$ EVs followed by TGF-β1 significantly increased pSMAD2 levels in recipient cells, whereas $CD9^-$ EVs did not elicit the signal to the same extent (Fig. 6.10A and B for phospho-signal quantification).

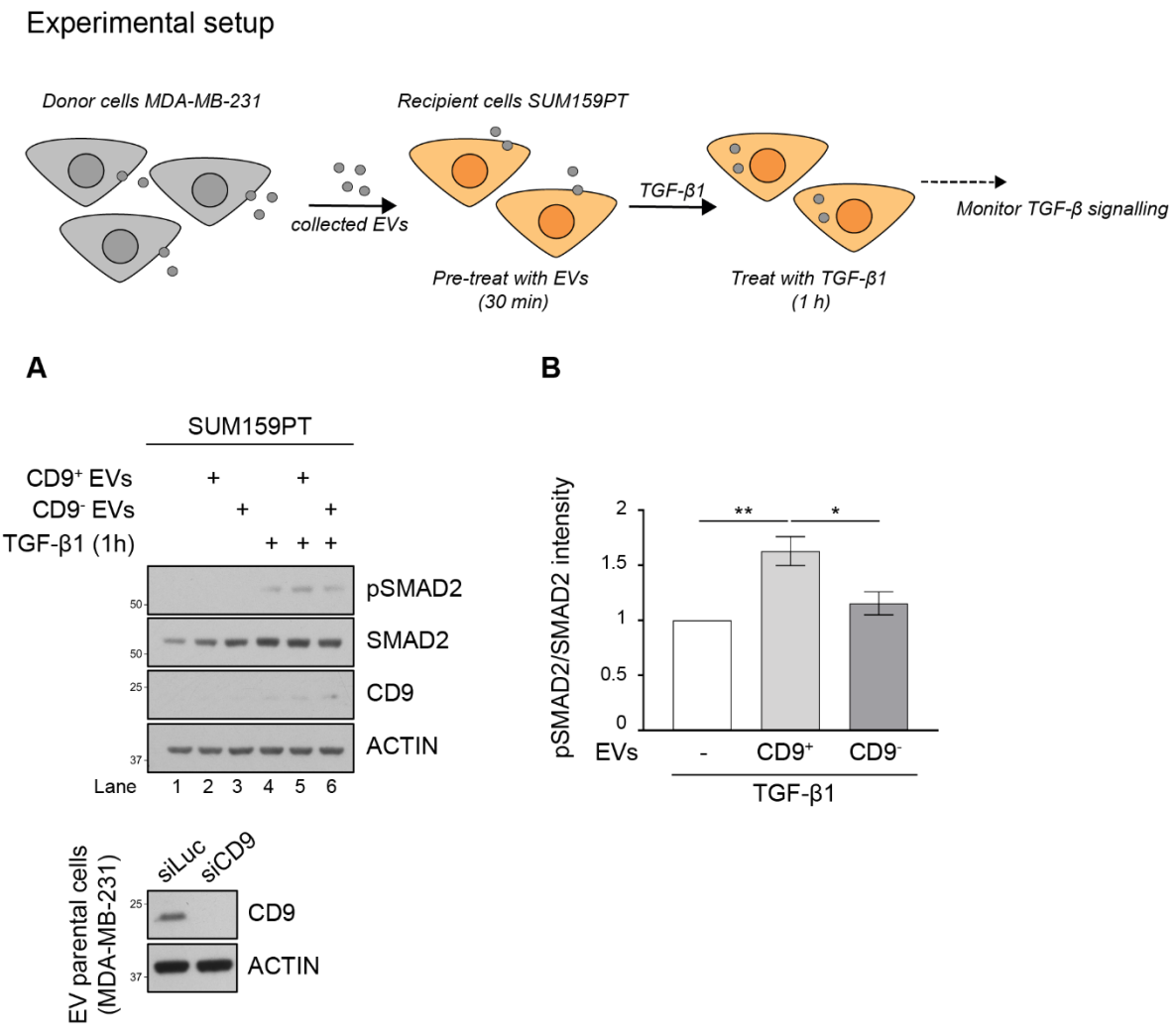


Figure 6.10 CD9 enriched EVs elicit TGF-β signalling in recipient cells. MDA-MB-231 were seeded (5 x 10^6 cells/plate) and transiently transfected with control siRNA (siLuc) or siRNA targeting CD9 mRNA and cultured in 0.1% FBS for 48 h after transfection. EVs were collected with a differential centrifugation protocol. An aliquot was resuspended in RIPA 1X for protein quantification and the remainder were resuspended in PBS. After normalisation, EVs or an equal volume of PBS were incubated for 30 min with SUM159PT cells, seeded 24 h before (5 x 10^5 cells/well in a 6-well plate), in duplicates. After 30 min of incubation, TGF-β1 was added to the medium for 1 h. Top, cartoon depicting the experimental setup. **A.** Cells were lysed and representative western blot analysis with the indicated antibodies is shown. Confirmation of the knockdown in the EV donor cell line (MDA-MB-231) is also reported. **B.** Quantification of WB band intensity of pSMAD2 normalised against total SMAD2 is plotted. Incubation of recipient SUM159PT cells with $CD9^+$ EVs results in significantly increased SMAD2 phosphorylation, compared to the untreated condition, upon TGF-β1 treatment. Data are represented as mean ± SEM of N=3. * $p \leq 0.05$ and ** $p \leq 0.01$ were calculated with Student's t-test.

To understand whether changes in the cascade would affect target gene transcription I performed the same experiment as in 6.10, in this case isolating mRNA from SUM159PT cells to assess transcription in different conditions.

Fig. 6.11 shows qPCR analysis of canonical TGF-β target genes in SUM159PT cells treated or not with EVs.

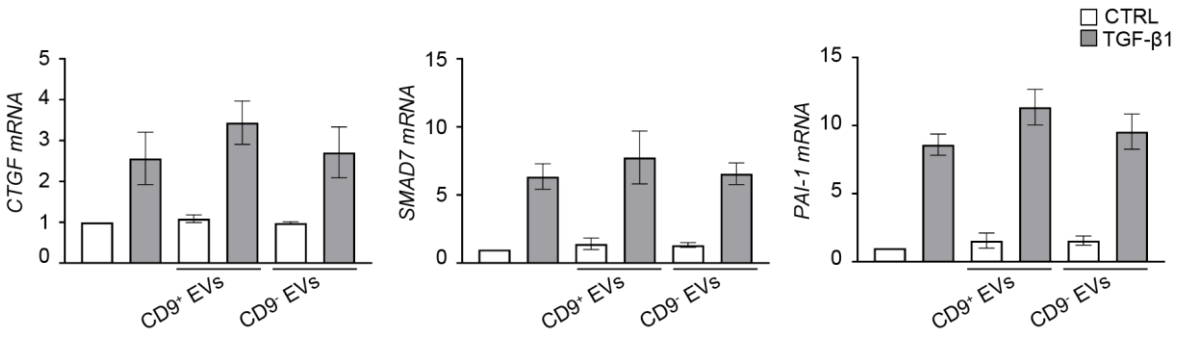


Figure 6.11 TGF-β transcriptional programme is not altered by CD9⁺ EVs. Experimental procedures were the same as in Fig. 6.10. 50,000 SUM159PT cells were lysed, cDNA prepared and qPCR was performed on a StepOnePlus™ Real-Time PCR machine. Expression of GAPDH was used as an internal control. Canonical TGF-β1 target genes expression was assessed after TGF-β1 treatment and no significant alteration in transcription was observed when cells were treated with $CD9^+$ or $CD9^-$ pools of EVs from MDA-MB-231. Data are represented as mean ± SEM of N=3.

Despite levels of pSMAD2 being elevated upon treatment with MDA-231 $CD9^+$ EVs (Fig. 6.10B) I could not establish a clear induction of transcription in the same conditions (Fig. 6.11).

The data so far indicate that CD9 enriched vesicles are able to elicit TGF-β signalling in recipient cells that lack CD9 expression. This observation establishes a great potential for CD9 EVs shed from cancer cells to propagate the TGF-β cascade in the tumour environment.

6.5.2 Treatment of recipient cells with CD9 positive EVs results in TGF-β mediated invasion

As initiation of an EMT programme and mediation of invasive phenotype is a fundamental feature of oncogenic TGF-β signalling (Massagué, 2008), I asked whether CD9 loaded onto EVs could elicit TGF-β mediated invasion in mammary

epithelial MCF10A cells. MCF10A were used because they are untransformed cells and thus closer to a normal epithelium, where I could monitor the effect of cancer $CD9^+$ EVs. To this end, I transfected MDA-231 cells with a control siRNA or siCD9 and 48 h after transfection I isolated EVs as described previously. EVs were normalised and incubated for 4 h with MCF10A cells. MCF10A were then trypsinised and seeded on Matrigel Boyden chambers (Corning) and subsequently treated with TGF-β1 (see experimental setup in Fig. 6.12). MCF10A invasive ability through Matrigel was assessed after 18 h.

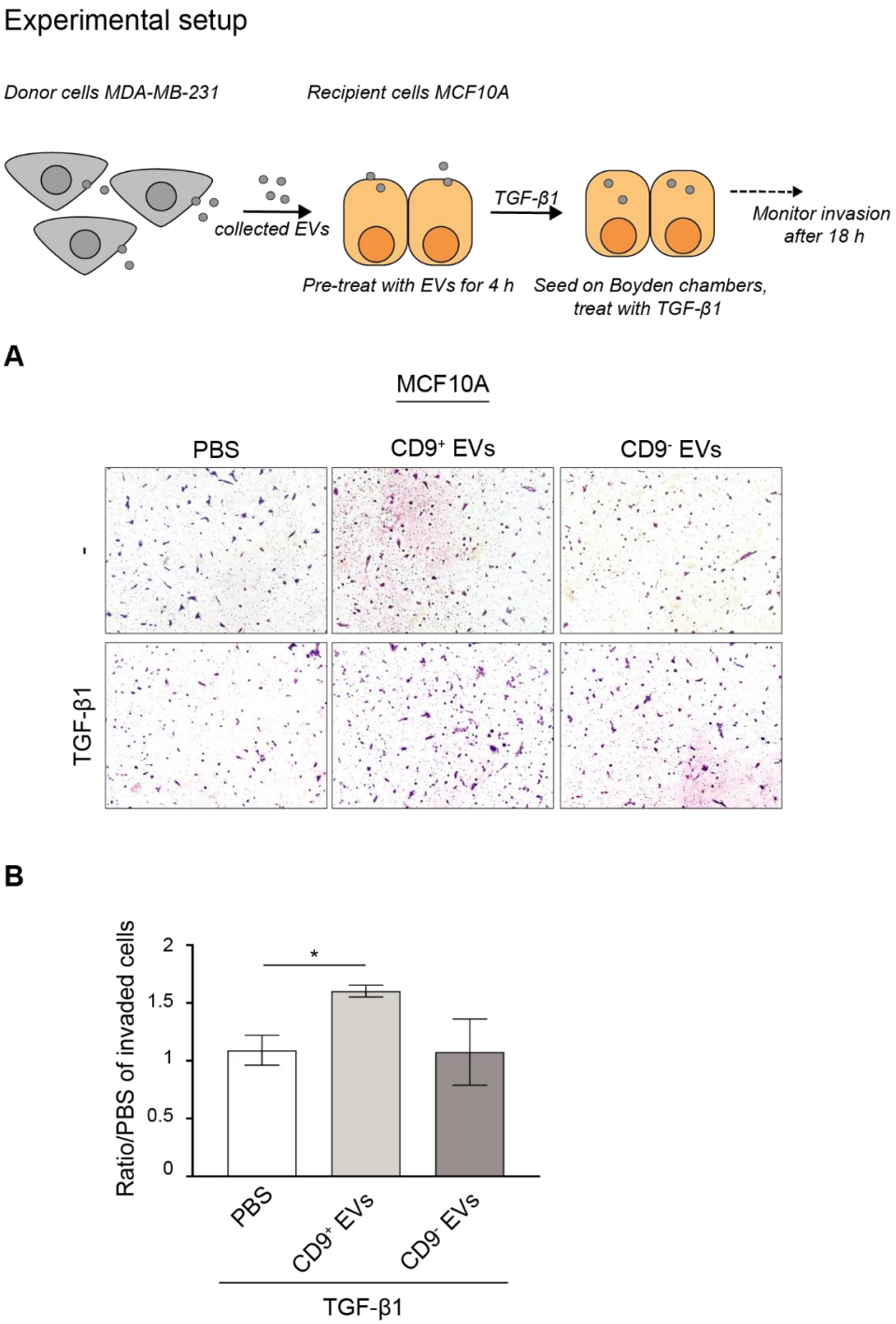


Figure 6.12 CD9 EVs stimulate TGF-β mediated invasion in MCF10A cells. MDA-MB-231 were seeded (5 x 10^6 cells/plate) and transiently transfected with control siRNA (siLuc) or siRNA targeting CD9 mRNA and cultured in 0.1% FBS for 48 h after transfection. EVs were collected after treatment with a differential centrifugation protocol. An aliquot was resuspended in RIPA 1X for protein quantification and the remainder were resuspended in PBS. After normalisation, EVs or an equal volume of PBS were incubated for 4 h with MCF10A cells, seeded 24 h before (5 x 10^4 cells/well in duplicates). After 4 h cells were trypsinised, counted and seeded onto Transwell Matrigel chambers (Corning). TGF-β1 was also added to the medium. After 18 h, invaded cells were fixed and stained and brightfield images were taken on a Nikon 90i light microscope. The number of cells that invaded the Matrigel was quantified with ImageJ software 1.51s. Top, cartoon depicting the experimental setup. **A.** Representative brightfield images per samples were taken. **B.** Bar graph shows quantification of the amount of invaded cells as a ratio over the PBS condition. Pre-incubation of recipient MCF10A cells with $CD9^+$ EVs results in significantly higher Matrigel invasion, compared to the PBS condition, when MCF10A are treated with TGF-β1. Data are represented as mean ± SEM of N=2 experiments. * $p \leq 0.05$ was calculated using one-tailed Student's t-test.

In Fig. 6.12 I observed that $CD9^+$ EVs induced a higher number of MCF10A cells to invade the Matrigel, compared to TGF-β alone. $CD9^-$ EVs instead did not stimulate the recipient cells to invade more than TGF-β alone (see Fig. 6.12B for quantification).

The presented data suggest that $CD9^+$ EVs mediate TGF-β driven invasion in untransformed recipient cells.

6.6 Discussion

In Chapter 6 I have investigated how CD9 modulates TGF-β signalling in a variety of breast cancer cell lines. First, I have established that CD9 loss decreases SMAD2 effector signal and delays pathway activation (Fig. 6.1-6.3). However, it has been previously demonstrated that in melanoma CD9 directly interacts with TGFβRII and mediates TGFβRI and RII coupling (H. Wang et al., 2015). It would be interesting to reproduce these results in MDA-231 cells, to clarify whether CD9 mediates early steps of receptor binding, via immunoprecipitation of the TGF-β receptors.

Moreover, it has been shown that TGFβRI couples to different endocytic structures within the cell and this leads to opposite receptor fates. If internalised in caveolae, marked by Caveolin-1, TGFβRI binds to the inhibitory SMAD, SMAD7, and to the E3 ligase SMURF1, and is processed for turnover. However, if it is engulfed in endocytic structures, marked by EEA1, TGFβRI binds to the SMAD2 anchor SARA and it thus promotes downstream signalling (Di Guglielmo et al., 2003; K. He et al., 2015). It would be interesting to understand whether CD9 shifts

TGFβRI regulation to one endocytic structure or the other and if CD9 loss may for instance promote early degradation of the receptor.

In this chapter, I have mainly looked at activation of the TGF-β effector SMAD2. Question remains whether the other TGF-β effector and SMAD2 homologue, SMAD3, shows a similar altered signalling in CD9 depleted cells. Preliminary evidence (shown in Appendix Fig. 8.7) suggested that both SMAD2 and SMAD3 were retained in the cytoplasm upon CD9 knockdown, whereas SMAD4 nuclear shuttling seemed unaffected. A nuclear/cytoplasmic fractionation experiment would clarify whether R-SMADs and co-SMAD localisation are impaired by CD9 depletion.

A recent study has also shown that the TGF-β cascade can propagate in a SMAD4 independent fashion in pancreatic ductal adenocarcinoma (PDAC) (David et al., 2016). Particular interest in this study was given to the transcription factor Sox4, shown to switch function from pro-tumourigenic in epithelial PDAC cells to pro-apoptotic if these cells undergo an EMT. Given that my preliminary results suggest independence of SMAD4 in CD9 mediated TGF-β signalling (Appendix Fig. 8.7), it would be also of interest to investigate Sox4 status in the presence or absence of CD9.

Interestingly, TGF-β induced transcription was delayed at early time-points (Fig. 6.7), but not altered at later time-points, in CD9 depleted cells (Fig. 6.6). This observation could be explained by the presence of alternative compensation routes that the pathway could take to trigger transcription. To this end, elucidating the role of SMAD3 and Sox4 and other transcription factors in this setup would help in understanding how TGF-β overcomes CD9 depletion.

The promiscuity in the regulation of target genes such as *CTGF*, regulated by both the TGF-β and the Hippo pathway, might also explain why I do not observe a strong response for this target gene in my experiments (Fig. 6.6, 6.7 and (Hiemer et al., 2014)).

Another possibility for not observing significant changes at the transcriptional level upon CD9 knockdown is that the concentration of TGF-β used to treat the cells (10 ng/mL) is over-compensating for the lack of CD9 and saturating the signal over time. To test this hypothesis, a growth factor titration experiment would prove whether high doses of TGF-β may conceal transcriptional impairment in CD9 depleted cells.

Of note, all the experiments proposed in this chapter were performed in a CD9 depleted background, using transient siRNA knockdown. Given the limitations of this technique, the generation of a stable CD9 knockout cell line may give more definitive answers in terms of altered TGF-β signalling at the transcriptional level. Moreover, CD9 exogenous expression experiments may help corroborate the hypothesis that CD9 mediates TGF-β signalling. I would speculate that increased CD9 levels promote and sustain signalling for longer time-points (i.e. pSMAD2 maintained up to 8 h). Promising preliminary results (see Appendix Fig. 8.8) suggest that CD9 over-expression indeed accelerates the onset of TGF-β downstream activation (expressed as establishment of pSMAD2, Fig. 8.8A) and maintains it for as long as 8 h (Fig. 8.8B).

In this chapter I have also described a further link between TGF-β signalling and extracellular vesicle release. When EV biogenesis is impaired due to chemical inhibition, SMAD2 shows a trend of maintained phosphorylation over time (Fig. 6.9). However, alternative EV inhibition methods should be employed to

strengthen this finding. Rab27a and Rab27b GTPases have been found important for MVE docking at the plasma membrane, thus playing a role in EV secretion (Bobrie et al., 2012; Ostrowski et al., 2010). siRNA mediated knockdown of Rab27a or Rab27b independently has suggested, in preliminary results, a possible involvement of Rab27b in fuelling TGF-β signalling (Appendix, Fig. 8.9). However, silencing of both Rab27 isoforms, as well as longer TGF-β time-points, need to be examined to address the involvement of Rab27 small GTPases in this context.

Finally, I have shown that CD9 enriched EVs have the ability to promote TGF-β signalling in recipient cells and drive TGF-β mediated invasion in untransformed cells. It would be interesting to analyse the transcriptional pattern of MCF10A untransformed cells, once treated with $CD9^+$ EVs, to verify whether a TGF-β EMT programme can be stimulated by the presence of CD9 from mesenchymal cells (MDA-231).

Collectively, the data showed in this chapter propose a novel role for the tetraspanin CD9 in mediating TGF-β signalling (summarised in Fig. 6.13). Loss of CD9 in breast cancer cells leads to a delay and reduced potency in TGF-β pathway activation. Moreover, the fraction of CD9 protein that is loaded onto EVs is able to trigger pathway activation in recipient cells and facilitate TGF-β mediated invasion.

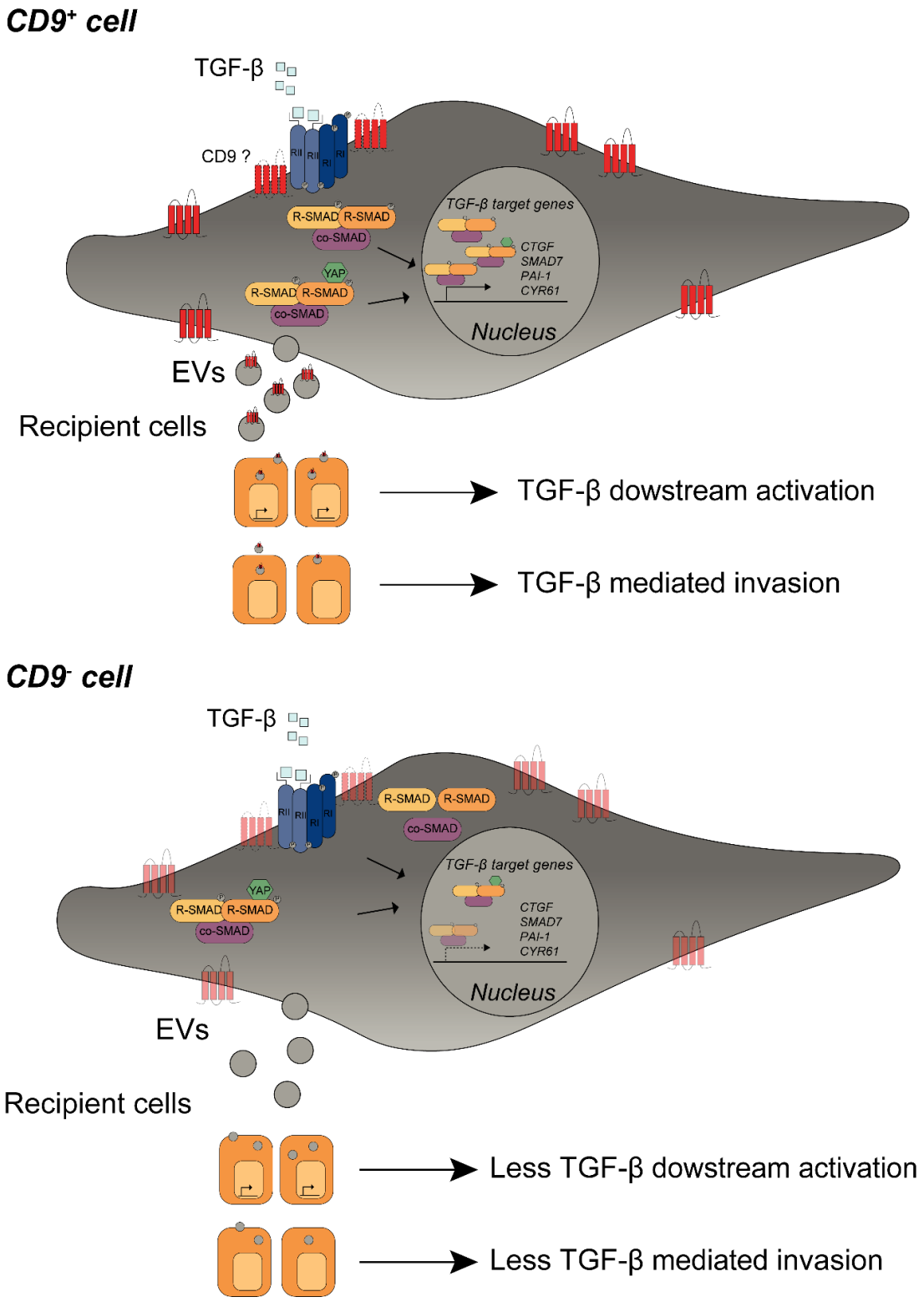


Figure 6.13 CD9 is a positive mediator of TGF-β signalling. The cartoon represents the key steps in TGF-β signalling where CD9 plays a role. When CD9 is present, SMAD2 is phosphorylated, it binds to SMAD4 and the complex translocates to the nucleus where a transcriptional response is started. When CD9 is absent, less SMAD2 is phosphorylated, less complexes are formed with SMAD4 and transcriptional activation is delayed. Moreover, $CD9^+$ EVs promote TGF-β signalling and TGF-β mediated invasion in recipient cells.

Chapter 7 Discussion

The primary cause of cancer morbidity and mortality is the dissemination of metastases or secondary tumours. Metastasis is a multi-step process which starts at the primary tumour site with acquisition, by specific cancer cells, of traits that enable them to dissociate from the primary site and travel to distant tissues. During this process, many cell types are involved, both in the primary tumour and during the metastatic colonisation: the cells that originate from the tumour and the variety of stromal and immune cells that interact with the cancer cells to either mediate or inhibit tumour progression. After having circumvented physical barriers, cancer cells intravasate in the blood circulation and here they interact with the endothelium as well as with immune cells. The collective effects of these interactions promote the transendothelial migration of cancer cells, which can be assisted by the same players that sustain tumour growth in the primary site. In the target organ, metastatic cells establish a microenvironment that facilitates angiogenesis and proliferation, resulting in macroscopic, malignant secondary tumours (Lambert et al., 2017). The tumour microenvironment is equally important in modulating tumour growth both in primary tumours and during the metastatic process.

In this thesis I have focussed on the functions of extracellular vesicles (EVs) in cancer progression. EVs are integral part of the complex network of the tumour microenvironment. Specifically, I investigated the pro-tumourigenic potential of vesicles released by cancer cells upon different stimuli (oncogene expression and growth factors). The role of EVs in cancer has been explored both at early stages

of the tumour development as well as at late, metastatic stages. During the early stages, EVs have been reported to mediate the crosstalk between different genetic clones of cancer cells present in the same tumour mass (Al-Nedawi et al., 2008); EVs have also been proposed to potentiate tumour growth and endothelial cell proliferation (Nazarenko et al., 2010; Skog et al., 2008). The conversion of stromal fibroblast to myofibroblasts has also been shown to take place after exposure to cancer EV-bound TGF-β (Webber et al., 2010). In a bilateral exchange, EVs from the stroma can also influence the tumour behaviour, rendering it more aggressive (Luga et al., 2012).

Cancer EVs may precede the disseminating tumour cells in modelling the pre-metastatic niche. Various seminal studies have reported the ability of vesicles to enter the blood stream and reach specific distant sites in a “seed and soil” fashion, redirecting the establishment of tumour cells, that normally lack the capacity to metastasise, to a specific organ (Costa-Silva et al., 2015; A. Hoshino et al., 2015; Peinado et al., 2012).

Similarly to events in the primary tumour, a bidirectional communication mediated by EVs is also present in the metastatic niche. For instance, the formation of brain metastases from breast and melanoma cancer cells can be modulated by miRNAs loaded onto astrocyte-derived EVs (L. Zhang et al., 2015).

The data presented in this thesis support the hypothesis that EVs released by cancer cells can transfer the oncogenic potential from more aggressive to less aggressive cancer cells or untransformed cells, thereby generating a new source of growth for the tumour.

Herein, I described a novel mechanism for the oncogene RASSF1C in mediating breast cancer progression, which is eliciting the release of vesicles that retain the

biophysical characteristics of small EVs (exosomes). The incubation of RASSF1C EVs with recipient less aggressive breast cancer cells induces these cells to migrate and invade *in vitro*. Moreover, I unravelled one of the mechanisms that RASSF1C exploits to promote EV release, which is the activation of the small GTPase RhoA. RASSF1C mediated activation of RhoA and its signalling cascade (RhoA/ROCK/pMLCII) does not only influence EV shedding, but also shifts the parental cell phenotype, to a more contractile, amoeboid-like type.

Furthermore, I have explored the role of TGF-β in exocytosis and described how the cytokine uses the secretion route to start a negative feedback loop and eliminate a positive mediator of the pathway, the tetraspanin CD9. Remarkably, I discovered a novel role for CD9 in TGF-β signalling cascade, in which CD9 mediates SMAD signalling and facilitates downstream activation. Finally, I reiterated the importance of EVs as carriers of information within the tumour environment, showing that CD9 positive EVs are able to elicit TGF-β signalling in recipient cells.

Epigenetic inactivation, via promoter methylation, of the tumour suppressor RASSF1A has been correlated to poor cancer prognosis and poor overall survival in breast, colorectal, lung and other cancers (Gao et al., 2012; Grawenda et al., 2015; Jiang et al., 2012; Meng et al., 2016; J. Wang et al., 2011). Therefore, clinical evidence supports the idea that loss of RASSF1A is correlated to more aggressive and metastatic cancers. Previous reports have highlighted the expression of an alternative isoform arising from an independent promoter within the *RASSF1* locus, RASSF1C. RASSF1C has been mostly described as an emerging oncogene, with a role in cell proliferation, migration, invasion and dedifferentiation (Amaar et al., 2006; Estrabaud et al., 2007; Reeves et al., 2010,

2014). Moreover, a recent study from our group has reported opposing functions in cancer progression for the two isoforms, RASSF1A and RASSF1C (Vlahov et al., 2015). In the study, in RASSF1A methylated cells, RASSF1C was found to mediate cancer invasion through activation of the kinase SRC and initiation of a transcriptional programme controlled by the β-catenin/YAP/TEAD complex. Conversely, in RASSF1A expressing cells, RASSF1A antagonised RASSF1C pro-tumourigenic functions by inhibiting SRC. In this thesis I further explored the oncogenic potential of RASSF1C, correlating expression of the protein with enhanced release of EVs and with amoeboid-like phenotype. Notably, RASSF1C exploits these functions via activation of the small GTPase RhoA. Both RASSF1A and RASSF1C share a RA (Ras association) domain and have been previously described to bind K-Ras (Rodriguez-Viciana et al., 2004; Vos et al., 2000). Interaction of the RASSF1A isoform with other small GTPases, such as Ran and Rho, has been reported (Dallol et al., 2009; M.-G. Lee et al., 2016). In the system used co-precipitation of RASSF1C and RhoA was observed. However, it is tempting to speculate that other indirect mechanisms may lead to RhoA activation. Our previous findings propose a crucial role for RASSF1C in activating the SRC family of kinases (SFK) (Vlahov et al., 2015). SRC is a non-receptor tyrosine kinase that is often upregulated or activated in tumours, where it controls a variety of processes, including cell adhesion complex assembly and turnover, cell motility, proliferation and survival. Given that links between SRC and RhoA have already been described in the literature, specifically in cytoskeleton remodelling (Arthur et al., 2000; B. Liu et al., 2015; Sreenivasappa et al., 2014), it would be interesting to investigate the hypothesis of a signalling axis, RASSF1C/SRC/RhoA in respect to amoeboid features and EV secretion.

SRC can also phosphorylate ROCK independently of RhoA in the regulation of focal adhesions (H. H. Lee et al., 2010). Another possibility to be tested could be that SRC, downstream of RASSF1C, activates ROCK signalling independent of RhoA.

The connector enhancer of KSR (CNK1) multidomain scaffold protein binds directly to both RASSF1A and RASSF1C (Rabizadeh et al., 2004) and to Rho in a GTP dependent manner (Jaffe et al., 2004). CNK1 binds to and activates RhoA in a study that described EphrinB1 and CNK1 as molecular scaffolds for the crosstalk between RhoA and JNK pathways (Cho et al., 2014). It would be thus interesting to explore the alternative axis RASSF1C/CNK1/RhoA.

An avenue that I left unexplored is the non-canonical activation of the Hippo effector YAP1 by RASSF1C (Vlahov et al., 2015). YAP, and its paralog TAZ, have been previously found to be nuclear relays of mechanical signals exerted by the ECM and cell shape. Importantly, this line of signal transduction requires RhoA activity, independently of the Hippo/LATS cascade (Dupont et al., 2011). Furthermore, RhoA controls YAP/TAZ signalling in the intestinal crypts (M. Liu et al., 2017), in the development of polycystic kidney disease (Cai et al., 2018) and in breast cancer cells (Z. Wang et al., 2014), both via Hippo dependent and independent mechanisms. These studies, along with our previous findings, would suggest YAP as a potential downstream effector of RhoA in the remodelling of cell morphology, also in our system.

The data presented in this thesis proposed an oncogenic mechanism triggered by RASSF1C in parental cells. However, an analysis on how EVs transfer the oncogenic phenotype from donor to recipient cells has not been provided.

One possibility would be the direct transfer of the oncogene, RASSF1C, from donor to recipient cells, carried on the vesicles. However, I failed to detect the RASSF1C protein on EVs. Nevertheless, it would be informative to isolate mRNA from EVs and verify the presence or absence of the RASSF1C transcript.

Previous data generated in the lab and confirmed in my experiments (Appendix Fig. 8.10) showed the presence of SRC protein in EV preparations. A second option would be thus to test whether RASSF1C EVs, depleted of SRC, could still trigger migration and invasion in recipient cells.

A third possibility would be to perform a comparative analysis of proteins enriched in control vs RASSF1C EVs, by mass spectrometry. Enrichment of pro-invasive markers (integrins for instance (A. Hoshino et al., 2015)) could justify the phenotype observed on the recipient cells.

The use of the previously published Cre-LoxP model (Zomer et al., 2015) throughout this thesis, revealed the versatility of this system. As already mentioned, the system allows us to follow the release (by donor Cre^+ cells) and the subsequent uptake (by $reporter^+$ cells) of EVs *in vitro* and *in vivo*. Additionally, it is possible to follow the fate of $reporter^+$ cells that have internalised EVs, due to the colour switch they undergo, from red to green. The application of this model to my experiments could be extended to functional assays where I study the migratory and invasive pattern of recombined (green) $reporter^+$ cells that have internalised RASSF1C EVs. Furthermore, replication of the performed *in vitro* experiments in an *in vivo* setup, using the Cre-LoxP model, would strengthen the hypothesis that RASSF1C plays a major role in the onset of metastasis, through the release of EVs. A collaboration with the lab of Jacco van Rheenen has been giving promising results in terms of the relevance of our findings *in vivo*.

Of note, limitations in the use of this model have already been identified (Zomer et al., 2016). One of them is that the system allows us to identify only the Cre^+ subpopulation of EVs released by the donor cells. Visualisation only of this subgroup of EVs may lead to underrepresented results, giving an incomplete picture of the potential of EV transfer.

Collectively, our previous findings together with the data presented in this thesis offer an appealing explanation for the aggressiveness of tumours lacking the tumour suppressor RASSF1A. In some cancers, methylation of the *RASSF1* promoter extends over the CpG island containing the 1α promoter (RASSF1A) and reaches the second downstream CpG island, containing the 2γ promoter, from which RASSF1C is transcribed. Therefore, in these malignancies, both isoforms would be silenced (Dreijerink et al., 2001; Vos et al., 2000). Given the importance of RASSF1A methylation as a prognostic marker for cancer risk (Grawenda et al., 2015), it would be significant to correlate the methylation data from CpG islands of both 1α and 2γ promoters and to evaluate whether addition of the second promoter confers better prognostic power to RASSF1A methylation. Findings from our group (Grawenda et al., unpublished) suggest that indeed patients carrying methylation on both RASSF1A and RASSF1C promoters have a better prognosis than ones who retain only the RASSF1A methylation.

It has been extensively studied how different stimuli within the tumour microenvironment can affect extracellular vesicle release. Growth factors and active molecules orchestrate a substantial number of events in the tumour microenvironment and they are also accountable for alterations in EV cargo and functions. A recent report described a role for histamine in triggering multivesicular body-plasma membrane fusion events that result in the secretion of exosomes

from different cell types (Verweij et al., 2018). Moreover, a number of publications have highlighted how extracellular vesicles are efficient carriers of growth factors or their coupled receptors (Chowdhury et al., 2015b; Kwon et al., 2014; Webber et al., 2015, 2010; H. Zhang et al., 2017).

Previous work from our group has highlighted a crosstalk between transforming growth factor β (TGF-β) and the Hippo pathway scaffold RASSF1A (Pefani et al., 2016). Given the novel role I have described for RASSF1C in EV secretion (Chapter 4) and given the opposite functions RASSF1A and RASSF1C have in breast cancer progression (Vlahov et al., 2015), my work in Chapter 5 has covered the potential interplay between RASSF1C and TGF-β in modulating EV release. The results suggest that TGF-β and RASSF1C modulate EVs with two independent mechanisms. However, a direct interplay between the growth factor and the oncogene within the cell has not been addressed. I would speculate that RASSF1C and TGF-β could act in concert to promote tumour progression, as the cytokine antagonises activity of the tumour suppressor and major isoform, RASSF1A (Pefani et al., 2016). Knockdown and exogenous expression experiments may clarify whether RASSF1C is involved in mediating the TGF-β invasive programme, in RASSF1A null cells.

The data in Chapter 5 propose a role for TGF-β in EV shedding, regardless of the presence of RASSF1C in the cells. My analysis of TGF-β driven EVs has uncovered their potential in mediating cell invasion. Interestingly, I found that a very low concentration of TGF-β ligand was carried on EVs, if compared to the conditioned medium. Various reports have highlighted the presence of endogenous TGF-β carried on the surface of prostate cancer cell exosomes and its role in promoting fibroblast to myofibroblast differentiation (Webber et al., 2015,

2010). It would be interesting to see if inhibition of the endogenous TGF-β already present on EVs, for example with a neutralising antibody, would hamper the invasive behaviour on recipient cells I reported.

As the above mentioned studies and others (Borges et al., 2013) have proposed a transactivation of the TGF-β cascade on target cells via exosomal TGF-β, a similar experiment would be relevant in my setup. The treatment of a cell line expressing a SMAD reporter with TGF-β driven vesicles could potentially address this point.

Multiple studies on TGF-β signalling in the past years have revealed a composite network made of several branches: canonical (SMADs) and non-canonical (ERK, JNK/p38, Rho, PI3K/AKT) (Y. E. Zhang, 2009); as well as the crosstalk with a plethora of other signalling pathways, such as the PI3K/AKT, MAPK, WNT, Rho and Hippo, among others (X. Guo et al., 2009; Mauviel et al., 2012).

In Chapter 5 I made an important observation in regard to the enrichment on EVs of the tetraspanin CD9, upon TGF-β treatment.

CD9 is a protein commonly associated to EVs, along with other tetraspanins, such as CD63 and CD81 (Van Niel et al., 2018). Despite having seen an enrichment of CD9 in EV preparations and a concomitant decrease of CD9 levels within the cells, at the analysed time-points, due to technical limitations, the intracellular levels of other tetraspanins have not been monitored. It has been previously demonstrated in melanoma that both CD9 and CD81 collaborate in mediating TGF-β receptors coupling (H. Wang et al., 2015). The association of CD9 and CD81 is not limited to cancer biology and is widely reported in mechanisms of cell fusion and adhesion (Charrin et al., 2013; Gordón-Alonso et al., 2006; Takeda et al., 2008, 2003). Hence, it would be informative to examine also the levels of other tetraspanins upon TGF-β treatment. I would speculate that CD81 associates to

CD9 in EVs released upon TGF-β stimulus and that both tetraspanins are involved in mediating TGF-β signalling in MDA-231 cells.

A previous report has highlighted the presence on the surface of prostate cancer exosomes of TGF-β ligand bound to the TGF-β receptor type III (betaglycan) (Webber et al., 2010). Given the importance of CD9 in mediating TGF-β signalling in MDA-231 cells, as illustrated in Chapter 6, it would be interesting to test for TGFβRIII presence in vesicle preparations.

Further to my initial observations in Chapter 5 on CD9 localisation at the plasma membrane soon after TGF-β stimulus (2 h) and its specific enrichment on EVs at a later time-point (8 h), the data presented in Chapter 6 suggest that CD9 plays a major role in TGF-β downstream activation, with loss of CD9 reducing SMAD2 phosphorylation, nuclear translocation and delaying the overall response.

Given the membranous origin of CD9, a key point that has not been addressed in this thesis is the direct association of CD9 with TGF-β receptors I and II at the plasma membrane. Several attempts have been made to visualise the tetraspanin and the receptors in a complex (data not shown), as previously described in melanoma (H. Wang et al., 2015). Failure in seeing this interaction in our system may be due to technical limitations or to the formation of a different complex. I would speculate that CD9 may associate to TGFβRIII instead and an immunoprecipitation assay would potentially address this point.

Notably, activation of TGF-β receptors upon ligand binding is not confined to the canonical route. Several reports have highlighted the existence of lateral signalling, mediated by the ALK5 subunit of TGF-β receptor I, to SMAD1/5, which are canonical downstream effectors of BMP signalling in breast cancer, normal epithelial cells, macrophages and chondrocytes (Daly et al., 2008; I. M. Liu et al.,

2009; Nurgazieva et al., 2015; Ramachandran et al., 2018; van Caam et al., 2017). Two of these studies also suggest that heterotypical interactions among the receptors are needed for SMAD1/5 activation. Namely, ALK2 and ALK3, classified as BMP type I receptors, appear to be required for SMAD1/5 phosphorylation upon TGF-β stimulation (Daly et al., 2008; Ramachandran et al., 2018). Moreover, ALK2 can form higher order receptor clusters at the plasma membrane with canonical TGFβRI/RII dimers or tetramers in order to modulate SMAD1/5 activation (Ramachandran et al., 2018).

Given that CD9 depletion does not seem to inhibit completely the signalling and target genes are still transcribed, even though the response is generally delayed, I may speculate that non canonical signalling may take place. It would be a compelling hypothesis to test whether TGF-β mediated SMAD1/5 activation is altered upon CD9 depletion and if SMAD1/5 target gene transcription is subsequently changed. Preliminary results indeed suggest a switch from SMAD2 activation to SMAD1/5 activation upon CD9 depletion (data not shown).

In regard to SMAD signalling, I focussed mostly on the dynamics of the most abundant R-SMAD activated by TGF-β, SMAD2. The SMAD2 paralog SMAD3, however, has been less characterised in this study (Appendix Fig. 8.7).

Given that the most abundant splice variant of SMAD2 is unable to bind DNA whereas SMAD3 is (Y. Shi et al., 1998), it has been proposed that the two paralogs work in concert as TGF-β downstream, but have also different affinity for transcription factors and can regulate different subsets of genes (Massagué et al., 2005).

In the absence of SMAD2 activation, SMAD3 may compensate in mediating the signalling. Preliminary results (Appendix Fig. 8.7B) suggest that SMAD3 is also

less localised in the nucleus, upon CD9 depletion. However, further investigation on the levels of SMAD3 phosphorylation and nuclear translocation in the absence of CD9 are needed.

SMAD4 is the common mediator in both TGF-β and BMP pathways and plays a major tumour suppressor role, being mutated in 50% of pancreatic cancers and to a lesser extent in other cancers (Hahn et al., 1996; Levy et al., 2006). In the preliminary data proposed in Appendix (Fig. 8.7A) SMAD4 nuclear translocation does not seem to be affected by CD9 depletion. Notably, SMAD4 is essential for many but not all TGF-β regulated transcriptional responses. Indeed, ablation of SMAD4 in various contexts does not affect the integrity of TGF-β pathway (Massagué, 2008). Moreover, alternative transcription factors have been identified in the absence of SMAD4, such as TRIM33 in haematopoiesis (W. He et al., 2006), IKKα in keratinocytes (Descargues et al., 2008), p68 in vascular smooth muscle cells (Davis et al., 2008), Sox4 in pancreatic cancer (David et al., 2016). Since CD9 modulation of TGF-β seems to be unrelated to SMAD4 cellular localisation, interaction of SMAD2/3 with alternative binding partners needs to be assessed.

A further advancement in the knowledge of CD9 modulation of the pathway could be achieved with a SMAD2/3 ChIP-Seq analysis. ChIP-Seq would help us confirm that the levels of genome-bound SMADs are decreased upon CD9 depletion and determine which target genes are affected.

The final part of Chapter 6 has been dedicated to the evaluation of the functionality of EVs carrying the CD9 marker. Given that previous results have demonstrated that CD9 mediates the TGF-β cascade and taken into account the

well-established role of EVs as signal carriers, I investigated the potential of CD9 positive EVs in mediating TGF-β signalling in CD9 null cells.

Indeed, TGF-β downstream is activated in CD9 null cells treated with CD9 EVs. However, in the target cells only canonical SMAD signalling was monitored. In light of the findings in parental cells, it would be interesting to assess the activation of other non-canonical routes also in recipient cells.

Furthermore, I analysed TGF-β mediated invasion in target cells treated with EVs (CD9 positive or negative). TGF-β is one of the major players in epithelial to mesenchymal transition (EMT), a process that leads to cellular invasion (Massagué, 2008). Untransformed cells have demonstrated higher invasion rate if treated with CD9 positive EVs. To obtain a full understanding of the ability of EVs to mediate EMT in untransformed cells, it would be important to assess the loss of epithelial and the gain of mesenchymal markers in these cells. A RNA-Seq on untransformed (i.e. MCF10A) cells treated with CD9 positive or negative EVs, in the presence of TGF-β, could provide further insight on how CD9 EVs facilitate the TGF-β invasive programme in recipient cells.

The accessibility of cancer related EVs in biofluids, such as plasma, lymph, cerebrospinal fluid, malignant ascites, urine or secretions brings forward some unprecedented diagnostic opportunities. Numerous studies have revealed the expression of specific molecular cargo (proteins, miRNAs, DNA) on cancer EVs that could be used as a tool for early diagnosis or prognosis. Reports on breast, lung, prostate, pancreatic, ovarian, colorectal cancers, glioblastoma and melanoma (reviewed in (Rak, 2013; Soung et al., 2017; R. Xu et al., 2018)) have presented EVs as a reliable source of molecules with potential as biomarkers.

For instance, the membranous protein Glypican-1 has been suggested as a biomarker for pancreatic cancer (Melo et al., 2015), survivin for prostate cancer (Khan et al., 2012), loss of EpCAM and presence of CD24 for breast cancer (Rupp et al., 2011), CD63 and Caveolin-1 in melanoma (Logozzi et al., 2009) and a phosphoprotein signature for breast cancer (Chen et al., 2017).

CD9 is considered an EV marker common to both tumour and normal vesicles. In this thesis, I have described how CD9 is selectively routed to EVs, in breast cancer cells stimulated with TGF-β. It would be interesting to isolate EVs from both normal and cancer cell lines, as a pilot study prior to further isolation from healthy donors and breast cancer patients, and compare the amount of CD9 present in the EV pools.

Interestingly, TCGA data from breast carcinoma patients analysed with the Oncomine™ Platform, support the hypothesis that CD9 expression is elevated in invasive breast carcinoma, if compared to normal breast tissue (see Appendix, Fig. 8.11). This evidence strengthens the possibility to use CD9 as a biomarker. An attractive perspective to refine CD9 as a biomarker on breast cancer EVs is to compare the post-translational modifications (PTMs) present on CD9. Proteins that are routed to endosomal compartments for further processing undergo ubiquitination, SUMOylation, phosphorylation (Moreno-Gonzalo et al., 2014). The presence of a specific PTM on CD9 in cancer or in normal EVs may reveal a pattern that could be used for diagnosis. Furthermore, CD9 EVs, according to the data presented in this thesis, may represent a mark for upregulated TGF-β signalling in cancer that could be further explored.

In summary, the work presented in this thesis (illustrated in the model in Fig. 7.1) provides a novel mechanism for two oncogenic stimuli in eliciting tumour

progression, which is the release of EVs. This work recapitulates how different stimuli in cancer cells may elicit similar routes to foster tumour growth and it emphasises the significance of EVs as a potent mean of communication among cancer cells.

In my proposed model (Fig. 7.1, left branch of the model), when the tumour suppressor RASSF1A is lost, due to promoter methylation, the oncogene RASSF1C affects the surroundings via extracellular vesicles, leading to cancer dissemination. RASSF1C acts both on the parental cells, where it activates the RhoA/ROCK cascade inducing a phenotypic switch to amoeboid-like phenotype, and on the recipient cells, via the release of pro-invasive EVs. Given my findings, I can predict that patients that display loss of RASSF1A, due to promoter methylation, may present a worse prognosis, by virtue of the presence of RASSF1C. These patients may thus benefit from treatment with drugs that restore RASSF1A expression, such as DNA methyltransferase (DNMT) inhibitors. Moreover, given RASSF1C activation of the RhoA/ROCK axis, ROCK inhibition could also be a potential therapeutic target.

Additionally, RASSF1A methylated cells also display aberrant TGF-β signalling (Pefani et al., 2016). The work presented in this thesis (highlighted in the right branch of the model, Fig. 7.1) proposes a novel role for TGF-β oncogenic signalling in RASSF1A methylated cells, which is the release of CD9 decorated extracellular vesicles. These vesicles have the potential to mediate TGF-β downstream signalling and invasion in target cells. In light of my findings, my model predicts that tumour derived CD9 EVs could be potentially correlated to high TGF-β signalling in cancer patients and could be used as circulating biomarkers. Moreover, if the correlation between aberrant TGF-β and circulating

CD9 is reliable, the use of TGF-β inhibitors in the clinic may be beneficial for patients displaying high levels of cancer derived CD9 extracellular vesicles.

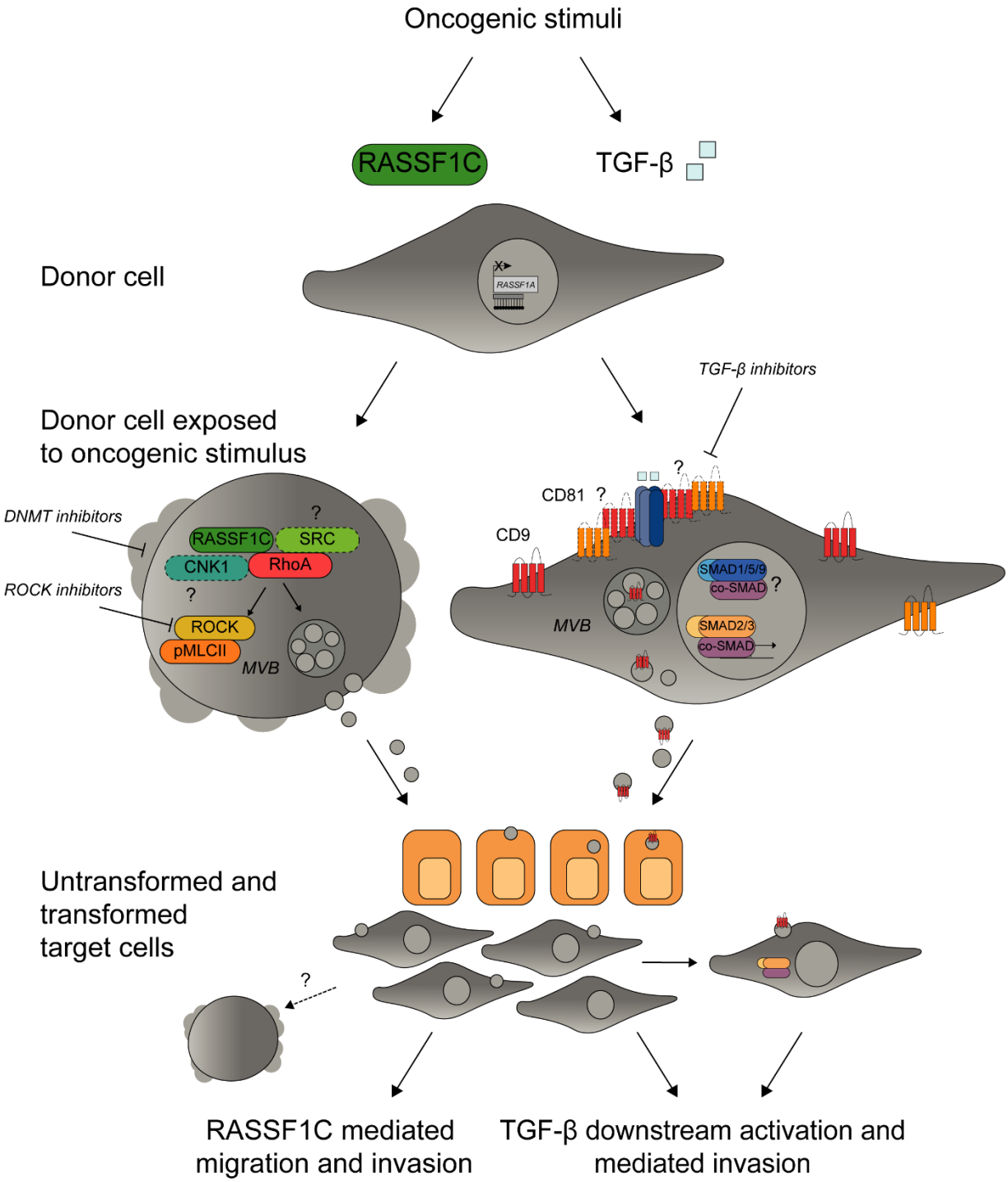


Figure 7.1 Graphical representation of the model generated from the data presented in this thesis. The two branches of oncogenic signalling (RASSF1C and TGF-β) explored in this project are represented here. RASSF1C, on the left, promotes changes in mesenchymal breast cancer cells that result in amoeboid transition and RhoA axis activation. Furthermore, RASSF1C drives the release of pro-invasive extracellular vesicles (EVs), likely in a RhoA dependent manner. A potentially more complex activation of RhoA by RASSF1C could involve SRC or CNK1 (dashed lines). A potential transition to amoeboid-like phenotype in the recipient cells that internalise RASSF1C EVs has not been explored in this study (dashed arrow). On the right, TGF-β also elicits the release of pro-invasive EVs. These EVs are decorated with the tetraspanin CD9. CD9 mediates canonical TGF-β signalling in both parental and recipient cells. However, the involvement of other tetraspanins, such as CD81, has not been investigated and a direct interaction between CD9 and the TGF-β receptors has not been confirmed (CD9 represented with dashed lines near TGFβRs). CD9 mediated activation or repression of other branches of the TGF-β pathway remain open questions.

Chapter 8 Appendix

8.1 RASSF1C and EV secretion in H1299 and MFC7 cells

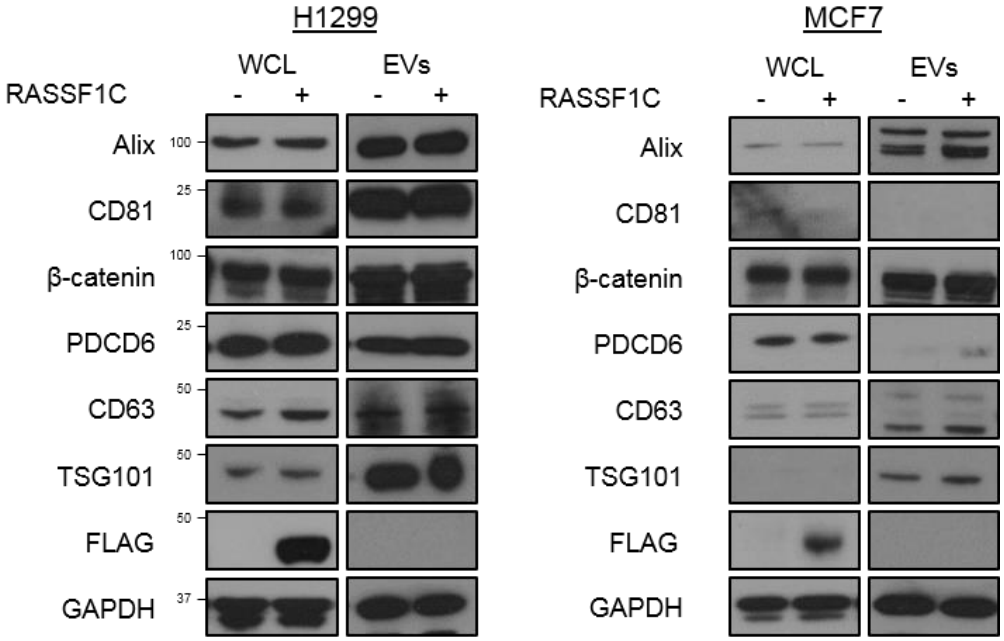


Figure 8.1 RASSF1C over-expression does not alter EV release in H1299 and MCF7 cells. H1299 and MCF7 cells were seeded (5 x 10^6 cells/plate) and transiently transfected with pcDNA3.1 or Flag-RASSF1C constructs. Cells were grown in 0.1% FBS medium for 72 h and EVs were isolated from conditioned media as stated before. WCL were lysed in Laemmli sample buffer and EVs were lysed in 1X RIPA buffer and kept for protein markers evaluation. EV protein content was normalised against the number of cells present in the plate at the end of the experiment, prior to SDS-PAGE and western blot analysis with the indicated antibodies. No difference between control and RASSF1C EV preparations are observed in the two analysed cell lines. Note that CD81 is undetectable in MCF7 EVs. These experiments were done by Nikola Vlahov.

8.2 RASSF1A levels in MDA-231 cells are negligible

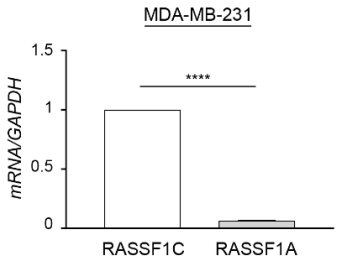


Figure 8.2 RASSF1A expression is lost in MDA-231 cells. MDA-MB-231 cells were seeded (1 x 10^5 cells/plate). After 48 h RNA was isolated from cell lysates and cDNA was prepared. qPCR (TaqMan assay) was performed on an Applied Biosystems 7500 Fast Real Time PCR system, to measure RASSF1C and RASSF1A mRNA levels. Expression of GAPDH was used as an internal control. RASSF1C mRNA levels are significantly higher than RASSF1A's. Data are representative of N=3 experiments and is represented as mean ± SEM. **** $p \leq 0.0001$ with Student's t-test.

8.3 RASSF1C exogenous expression leads to a 3-fold increase in RASSF1C mRNA levels

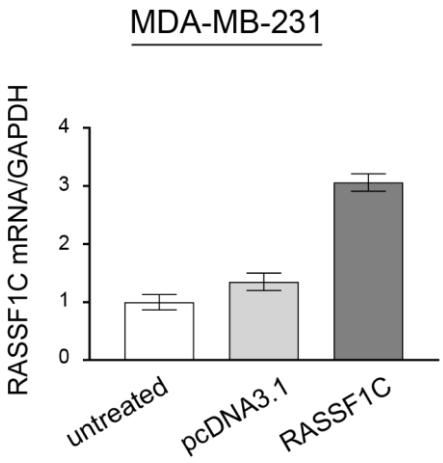


Figure 8.3 RASSF1C exogenous expression increases mRNA levels within a physiological range. MDA-MB-231 cells were seeded (1 x 10^5 cells/plate) and transiently transfected with pcDNA3.1 or Flag-RASSF1C constructs or left untreated. 48 h after transfection RNA was isolated from cell lysates and cDNA was prepared. qPCR (TaqMan assay) was performed on an Applied Biosystems 7500 Fast Real Time PCR system, to measure RASSF1C mRNA levels. Expression of GAPDH was used as an internal control. RASSF1C mRNA levels increase of 3-fold, compared to untreated cells. Data are representative of N=3 technical replicates and is represented as mean ± SEM.

8.4 RASSF1C mutants that fail to activate RhoA are unable to induce the amoeboid phenotype

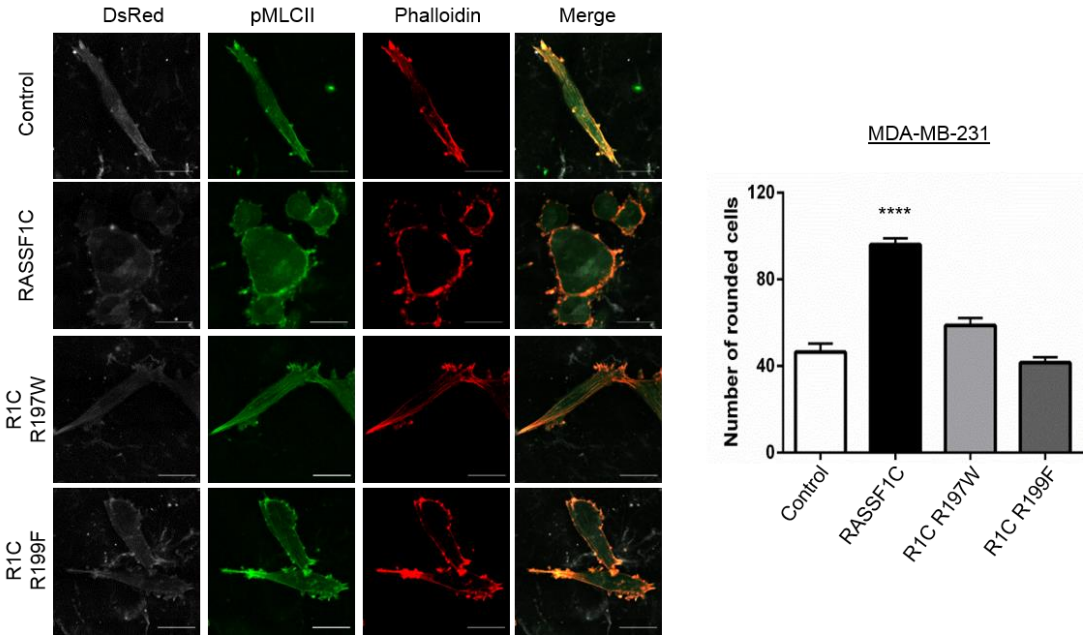


Figure 8.4 RASSF1C driven amoeboid phenotype is mediated by RhoA. Representative confocal images and quantification of the number of rounded cells per field of view of MDA-MB-231 cells transfected with DsRed, DsRASSF1C and two RASSF1C mutants, DsRASSF1C-R197W (R1C R197W) or DsRASSF1C-R199F (R1C R199F), grown in 3D-collagen and stained with Phalloidin-568 (red) and pMLCII/Alexa 633. DsRed is false-coloured white. The RASSF1C derivatives that fail to activate RhoA are not able to drive the amoeboid switch seen for RASSF1C. Scale bars represent 10 μm. Data are representative of N=3 experiments and it is represented as mean ± SEM. **** $p \leq 0.0001$ with Student's t-test. These experiments were done by Daniela Pankova. The DsRed-RASSF1C derivatives that are not able to activate RhoA were generated by Maria Laura Tognoli.

8.5 TGF-β may re-route CD9 to both degradative and exocytic pathways

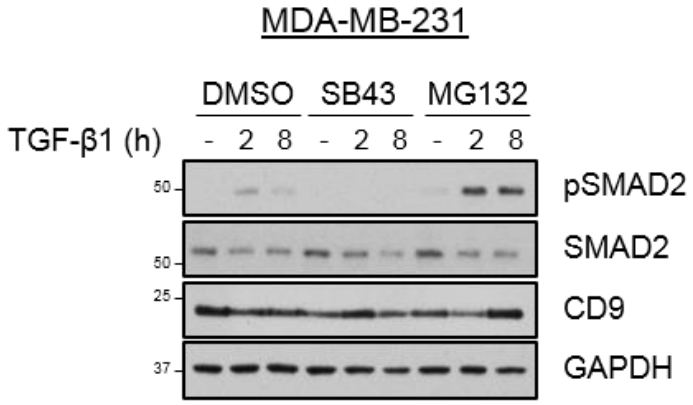


Figure 8.5 Proteasomal inhibition leads to intracellular accumulation of CD9. MDA-MB-231 cells were seeded (1 x 10^5 cells/plate). Cells were treated with 10 μM SB431542 (TGF-β receptor I subunit ALK5 selective inhibitor, Selleckchem), 10 μM MG132 (Sigma-Aldrich) or DMSO for 30 min in 0.1% FBS medium. Medium was then replaced and a new aliquot of inhibitor/DMSO and TGF-β1 (10 ng/mL) was added to the cells for the described time-points. After 2 or 8 h of treatment, cell lysates were collected for western blot analysis with the indicated antibodies. Pre-treatment with MG132 results in CD9 accumulation upon TGF-β treatment. Representative western blot is shown.

8.6 SUM159PT cells express undetectable levels of CD9 protein

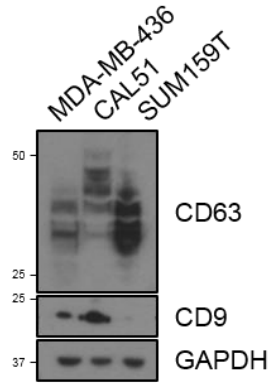
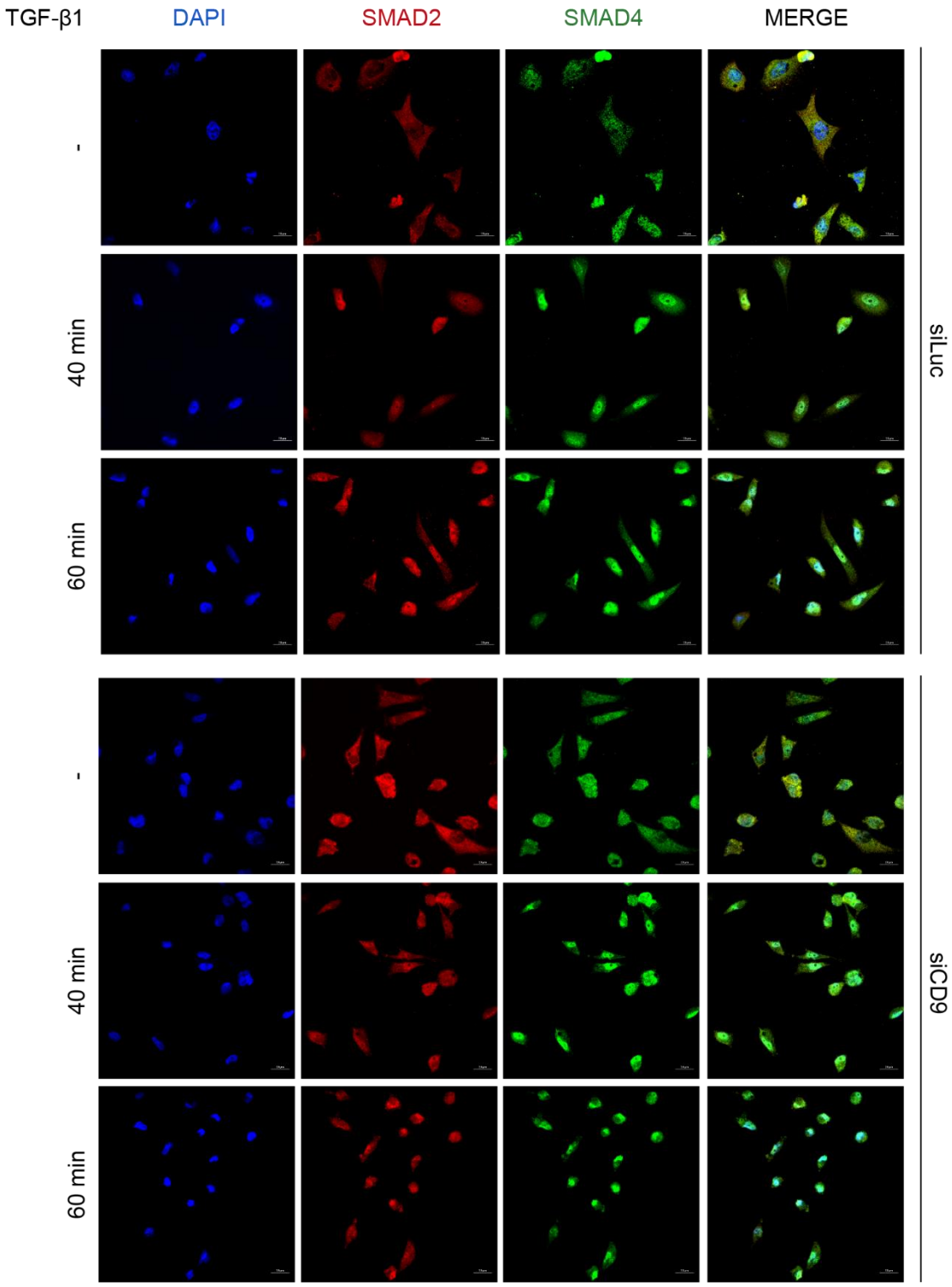


Figure 8.6 Comparison of protein levels of CD9 in different breast cancer cell lines. MDA-MB-436, CAL51 and SUM159PT cells were seeded (1 x 10^5 cells/plate) and 24 h after seeding cells were lysed for western blot analysis with the indicated antibodies. The amount of tetraspanin CD9 was evaluated among the 3 cell lines in order to choose the most suitable to perform the functional assays described in Fig. 6.10. SUM159PT cells were selected for their low/undetectable expression of CD9. CD63 was used as a reference for expression.

8.7 SMAD2/3 nuclear translocation is impaired upon CD9 depletion

A



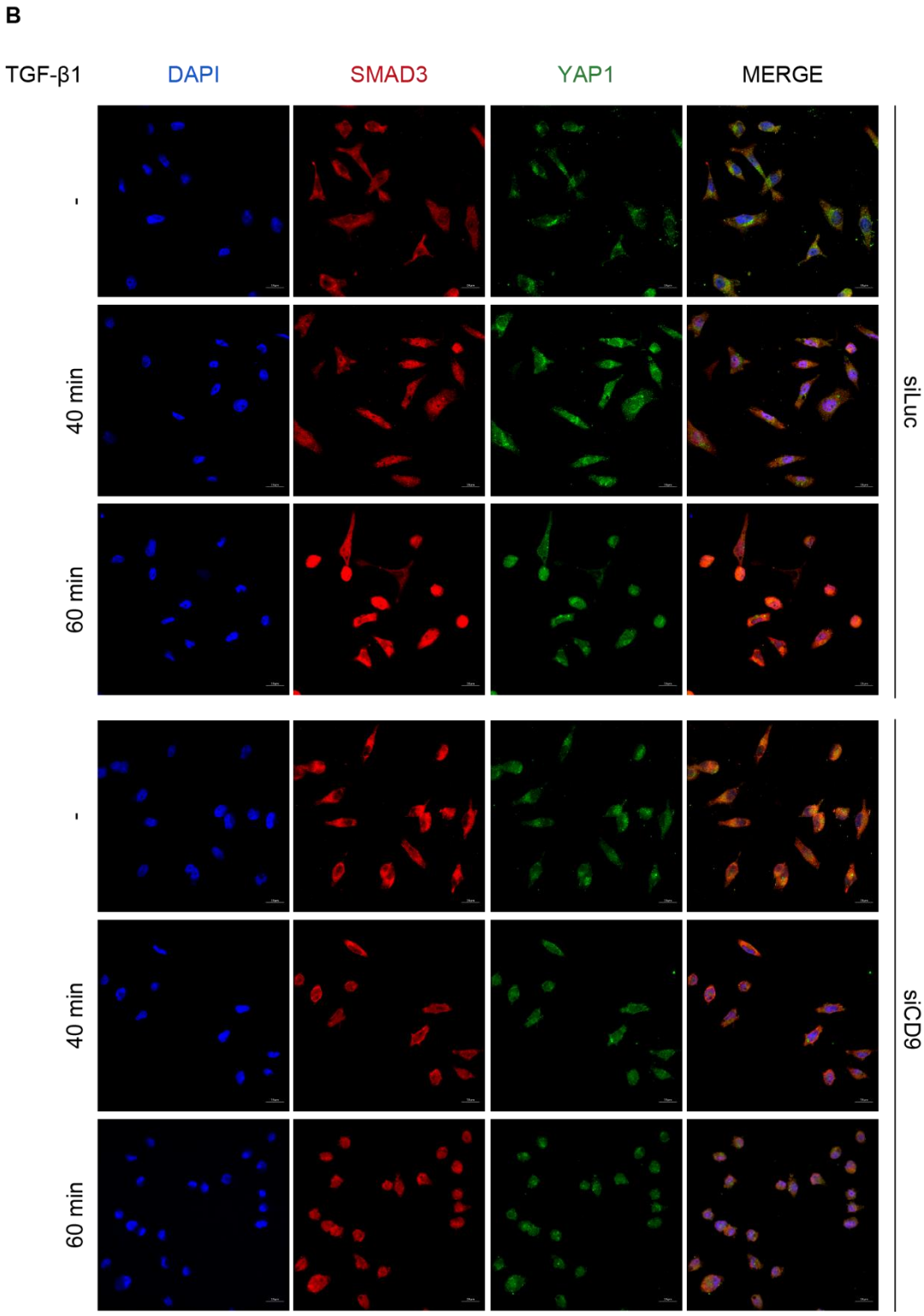


Figure 8.7 SMAD2 and SMAD3 nuclear translocation is reduced in CD9 depleted cells. MDA-MB-231 cells were seeded (1 x 10^5 cells/plate) and transiently transfected with control siRNA (siLuc) or siRNA targeting CD9 mRNA. 48 h after transfection cells were treated or not with TGF-β1 for 40 or 60 min. Cells were fixed in MeOH 100% and stained for the indicated antibodies. Coverslips were mounted onto slides using mounting media containing DAPI. **A.** Cells were stained for SMAD2 and SMAD4. SMAD2 nuclear translocation upon TGF-β1 stimulus is reduced in CD9 depleted cells. SMAD4 shuttling, however, does not appear to be affected. **B.** Cells were stained for SMAD3 and YAP1. Similarly to SMAD2, SMAD3 nuclear shuttling appears to be impaired, whereas localisation of the Hippo effector YAP1 is not altered upon CD9 knockdown. Scale bars represent 20 μm.

8.8 CD9 exogenous expression elicits TGF-β cascade

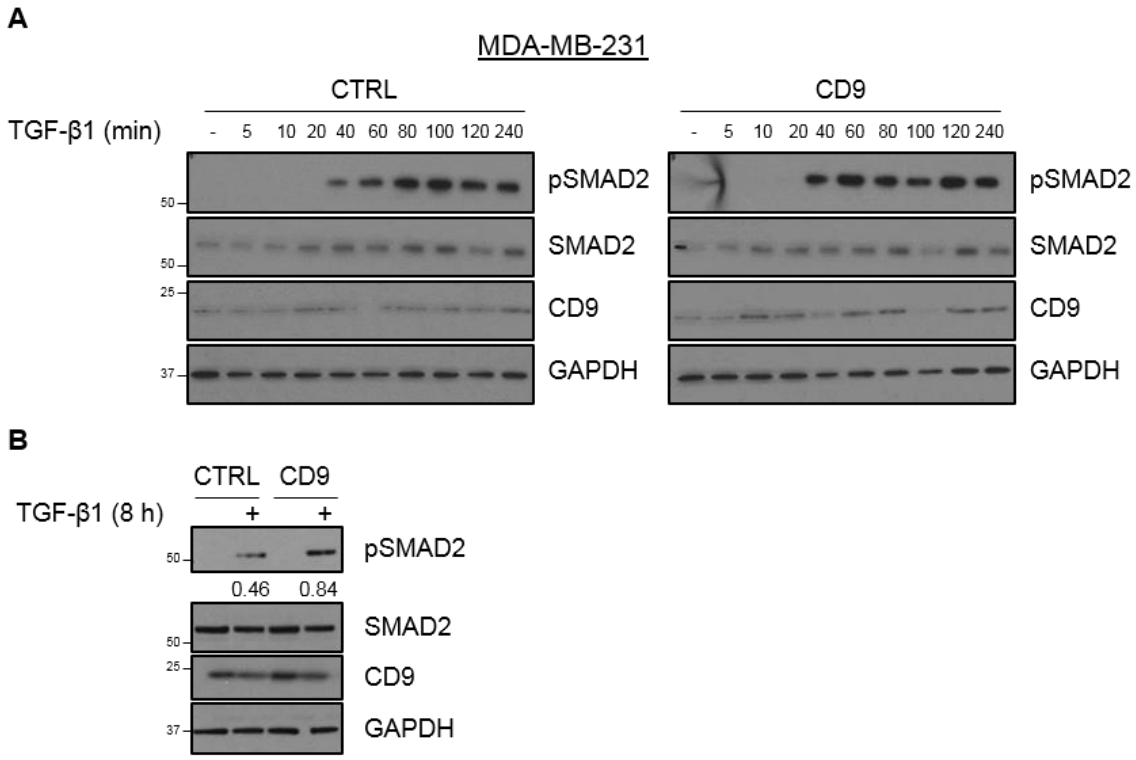


Figure 8.8 CD9 over-expression promotes TGF-β signalling. MDA-MB-231 cells were seeded (1 x 10^5 cells/plate) and transiently transfected with a control construct (mCherry-C1) or a CD9 construct (mCherry-CD9). 48 h after transfection cells were treated or not with TGF-β1 for the indicated time-points. Cell lysates were collected for western blot analysis with the indicated antibodies. **A.** CD9 expression results in earlier TGF-β downstream activation (expressed as SMAD2 phosphorylation). **B.** CD9 expression sustains TGF-β signalling for as long as 8 h after stimulus.

8.9 Rab27a/b knockdown in correlation to TGF-β signalling

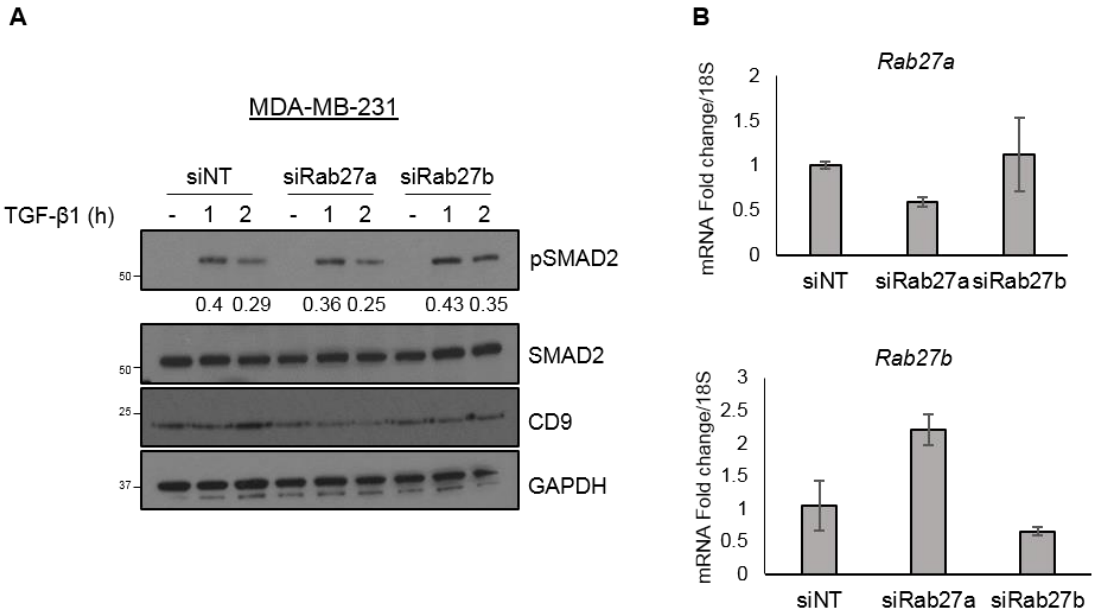


Figure 8.9 Rab27b depletion results in greater SMAD2 phosphorylation. MDA-MB-231 cells were seeded (1 x 10^5 cells/plate) and transiently transfected with control siRNA (siNT) or siRNA targeting Rab27a or Rab27b mRNA. 48 h after transfection cells were treated or not with TGF-β1 for 1 or 2 h. **A.** Cell lysates were collected for western blot analysis with the indicated antibodies. **B.** An aliquot of cells was kept to isolate RNA and prepare cDNA for qPCR, in order to validate Rab27a and Rab27b knockdown. Depletion of Rab27b appear to sustain SMAD2 phospho-signal. Data are representative of N=2 replicates.

8.10 SRC protein is enriched in RASSF1C driven EVs

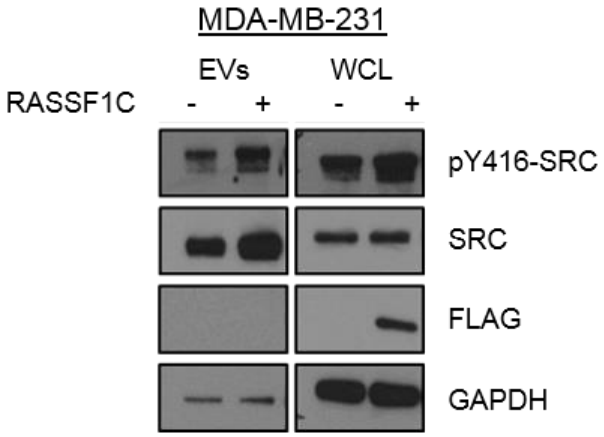


Figure 8.10 RASSF1C drives SRC accumulation on EVs. MDA-MB-231 cells were seeded (5 x 10^6 cells/plate) and transiently transfected with pcDNA3.1 or Flag-RASSF1C constructs. Cells were grown in 0.1% FBS medium for 72 h and EVs were isolated from conditioned media as stated before. WCL were lysed in Laemmli sample buffer and EVs were lysed in 1X RIPA buffer and kept for protein markers evaluation. EV protein content was normalised against the number of cells present in the plate at the end of the experiment, prior to SDS-PAGE and western blot analysis with the indicated antibodies. The active form of SRC (pY416) is also enriched in the vesicles. Data are representative of 3 independent experiments. This experiment was done by Nikola Vlahov.

8.11 CD9 mRNA levels are elevated in breast cancer patients

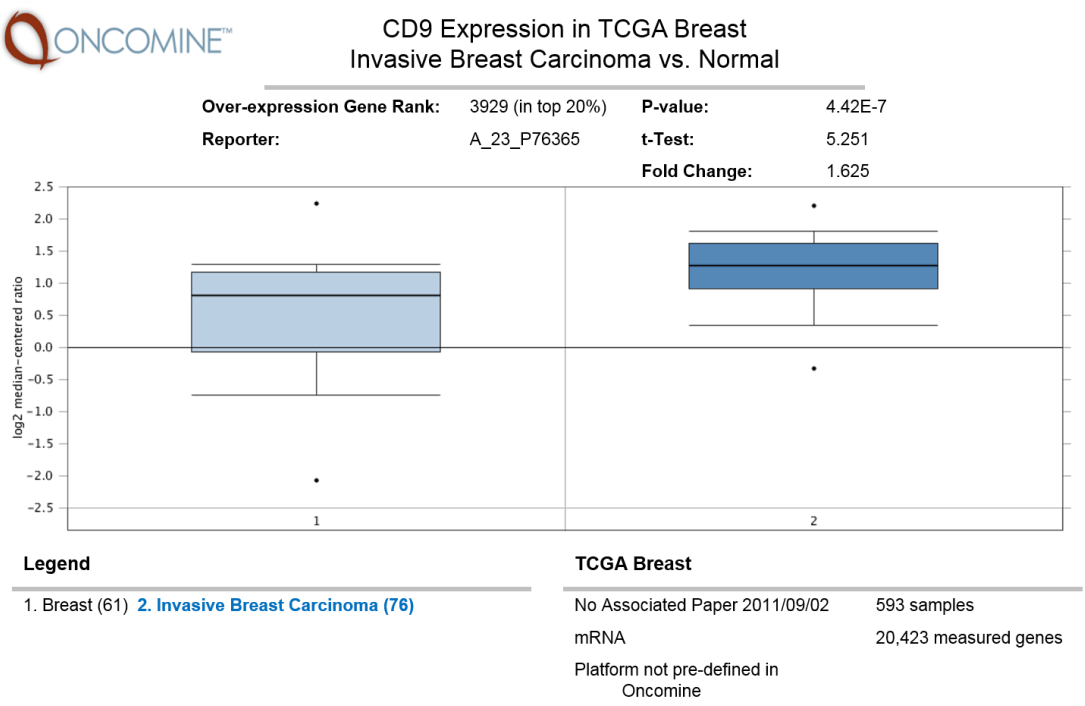


Figure 8.11 CD9 expression in TCGA reveals higher levels in invasive breast carcinoma patients. Analysis of healthy breast and invasive breast carcinoma tissue (from TCGA database) performed on the Oncomine database shows significantly higher CD9 mRNA expression in breast carcinomas. The Oncomine™ Platform (Thermo Fisher, Ann Arbor, MI) was used for analysis and visualisation.

8.12 Original copyright notices

Figure 1.8

SPRINGER NATURE LICENSE
TERMS AND CONDITIONS
Sep 15, 2018

This Agreement between University of Oxford -- Maria Laura Tognoli ("You") and Springer Nature ("Springer Nature") consists of your license details and the terms and conditions provided by Springer Nature and Copyright Clearance Center.

License Number	4401341343661
License date	Aug 03, 2018
Licensed Content Publisher	Springer Nature
Licensed Content Publication	Nature Reviews Cancer
Licensed Content Title	Tetraspanin proteins promote multiple cancer stages
Licensed Content Author	Martin E. Hemler
Licensed Content Date	Dec 23, 2013
Licensed Content Volume	14
Licensed Content Issue	1
Type of Use	Thesis/Dissertation
Requestor type	academic/university or research institute
Format	print and electronic
Portion	figures/tables/illustrations
Number of figures/tables/illustrations	1

High-res required	no
Will you be translating?	no
Circulation/distribution	>50,000
Author of this Springer Nature content	no
Title	DPhil Student
Instructor name	Eric O'Neill
Institution name	University of Oxford
Expected presentation date	Oct 2018
Portions	figure 1
Requestor Location	University of Oxford Old Road Campus Research Building Roosevelt Drive Oxford, OX3 7DQ United Kingdom Attn: Maria Laura Tognoli
Billing Type	Invoice
Billing Address	University of Oxford Old Road Campus Research Building Roosevelt Drive Oxford, United Kingdom OX3 7DQ Attn: Maria Laura Tognoli
Total	0.00 GBP

Terms and Conditions

Springer Nature Terms and Conditions for RightsLink Permissions

Springer Customer Service Centre GmbH (the Licensor) hereby grants you a non-exclusive, world-wide licence to reproduce the material and for the purpose and requirements specified in the attached copy of your order form, and for no other use, subject to the conditions below:

1. The Licensor warrants that it has, to the best of its knowledge, the rights to license reuse of this material. However, you should ensure that the material you are requesting is original to the Licensor and does not carry the copyright of another entity (as credited in the published version).

   If the credit line on any part of the material you have requested indicates that it was reprinted or adapted with permission from another source, then you should also seek permission from that source to reuse the material.

2. Where **print only** permission has been granted for a fee, separate permission must be obtained for any additional electronic re-use.

3. Permission granted **free of charge** for material in print is also usually granted for any electronic version of that work, provided that the material is incidental to your work as a whole and that the electronic version is essentially equivalent to, or substitutes for, the print version.

4. A licence for 'post on a website' is valid for 12 months from the licence date. This licence does not cover use of full text articles on websites.

5. Where **'reuse in a dissertation/thesis'** has been selected the following terms apply: Print rights for up to 100 copies, electronic rights for use only on a personal website or institutional repository as defined by the Sherpa guideline (www.sherpa.ac.uk/romeo/).

6. Permission granted for books and journals is granted for the lifetime of the first edition and does not apply to second and subsequent editions (except where the first edition permission was granted free of charge or for signatories to the STM Permissions Guidelines http://www.stm-assoc.org/copyright-legal-affairs/permissions/permissions-guidelines/), and does not apply for editions in other languages unless additional translation rights have been granted separately in the licence.

7. Rights for additional components such as custom editions and derivatives require additional permission and may be subject to an additional fee. Please apply to Journalpermissions@springernature.com/bookpermissions@springernature.com for these rights.

8. The Licensor's permission must be acknowledged next to the licensed material in print. In electronic form, this acknowledgement must be visible at the same time as the figures/tables/illustrations or abstract, and must be hyperlinked to the journal/book's homepage. my required acknowledgement format is in the Appendix below.

9. Use of the material for incidental promotional use, minor editing privileges (this does not include cropping, adapting, omitting material or any other changes that affect the meaning, intention or moral rights of the author) and copies for the disabled are permitted under this licence.

10. Minor adaptations of single figures (changes of format, colour and style) do not require the Licensor's approval. However, the adaptation should be credited as shown in Appendix below.

Appendix — Acknowledgements:

For Journal Content:
Reprinted by permission from [**the Licensor**]: [**Journal Publisher** (e.g. Nature/Springer/Palgrave)] [**JOURNAL NAME**] [**REFERENCE CITATION** (Article name, Author(s) Name), [**COPYRIGHT**] (year of publication)
For **Advance Online Publication papers:**
Reprinted by permission from [**the Licensor**]: [**Journal Publisher** (e.g. Nature/Springer/Palgrave)] [**JOURNAL NAME**] [**REFERENCE CITATION** (Article name, Author(s) Name), [**COPYRIGHT**] (year of publication), advance online publication, day month year (doi:

10.1038/sj.[JOURNAL ACRONYM].)

For Adaptations/Translations:

Adapted/Translated by permission from [**the Licensor**]: [**Journal Publisher** (e.g. Nature/Springer/Palgrave)] [**JOURNAL NAME**] [**REFERENCE CITATION** (Article name, Author(s) Name), [**COPYRIGHT**] (year of publication)

Note: For any republication from the British Journal of Cancer, the following credit line style applies:

Reprinted/adapted/translated by permission from [**the Licensor**]: on behalf of Cancer Research UK: : [**Journal Publisher** (e.g. Nature/Springer/Palgrave)] [**JOURNAL NAME**] [**REFERENCE CITATION** (Article name, Author(s) Name), [**COPYRIGHT]** (year of publication)

For **Advance Online Publication** papers:

Reprinted by permission from The [**the Licensor**]: on behalf of Cancer Research UK: [**Journal Publisher** (e.g. Nature/Springer/Palgrave)] [**JOURNAL NAME**] [**REFERENCE CITATION** (Article name, Author(s) Name), [**COPYRIGHT**] (year of publication), advance online publication, day month year (doi: 10.1038/sj.[JOURNAL ACRONYM])

For Book content:

Reprinted/adapted by permission from [**the Licensor**]: [**Book Publisher** (e.g. Palgrave Macmillan, Springer etc) [**Book Title**] by [**Book author**(s)] [**COPYRIGHT**] (year of publication)

Chapter 9 References

Aaronson, S. A. (1991). Growth factors and cancer. *Science (New York, N.Y.)*, *254*(5035), 1146–1153. https://doi.org/10.1126/SCIENCE.1659742

Al-Nedawi, K., Meehan, B., Micallef, J., Lhotak, V., May, L., Guha, A., & Rak, J. (2008). Intercellular transfer of the oncogenic receptor EGFRvIII by microvesicles derived from tumour cells. *Nature Cell Biology*, *10*(5), 619–624. https://doi.org/10.1038/ncb1725

Alarcón, C., Zaromytidou, A.-I., Xi, Q., Gao, S., Yu, J., Fujisawa, S., … Massagué, J. (2009). Nuclear CDKs Drive Smad Transcriptional Activation and Turnover in BMP and TGF-β Pathways. *Cell*, *139*(4), 757–769. https://doi.org/10.1016/J.CELL.2009.09.035

Amaar, Y. G., Minera, M. G., Hatran, L. K., Strong, D. D., Mohan, S., & Reeves, M. E. (2006). Ras association domain family 1C protein stimulates human lung cancer cell proliferation. *American Journal of Physiology-Lung Cellular and Molecular Physiology*, *291*(6), L1185–L1190. https://doi.org/10.1152/ajplung.00072.2006

Andreu, Z., & Yáñez-Mó, M. (2014). Tetraspanins in extracellular vesicle formation and function. *Frontiers in Immunology*, *5*(SEP), 1–12. https://doi.org/10.3389/fimmu.2014.00442

Annes, J. P., Munger, J. S., & Rifkin, D. B. (2003). Making sense of latent TGFbeta activation. *Journal of Cell Science*, *116*(Pt 2), 217–224. Retrieved from http://www.ncbi.nlm.nih.gov/pubmed/12482908

Aragon, E., Goerner, N., Zaromytidou, A.-I., Xi, Q., Escobedo, A., Massague, J., & Macias, M. J. (2011). A Smad action turnover switch operated by WW domain readers of a phosphoserine code. *Genes & Development*, *25*(12), 1275–1288. https://doi.org/10.1101/gad.2060811

Aragona, M., Panciera, T., Manfrin, A., Giulitti, S., Michielin, F., Elvassore, N., … Piccolo, S. (2013). A Mechanical Checkpoint Controls Multicellular Growth through YAP/TAZ Regulation by Actin-Processing Factors. *Cell*, *154*(5), 1047–1059. https://doi.org/10.1016/j.cell.2013.07.042

Arthur, W. T., Petch, L. A., & Burridge, K. (2000). Integrin engagement suppresses RhoA activity via a c-Src-dependent mechanism. *Current Biology*, *10*(12), 719–722. https://doi.org/10.1016/S0960-9822(00)00537-6

Ashman, L. K., & Zöller, M. (2013). Tetraspanins in Cancer. In *Tetraspanins* (pp. 257–298). Dordrecht: Springer Netherlands. https://doi.org/10.1007/978-94-007-6070-7_11

Attisano, L., & Wrana, J. L. (2013). Signal integration in TGF-β, WNT, and Hippo pathways. *F1000prime Reports*, *5*, 17. https://doi.org/10.12703/P5-17

Baietti, M. F., Zhang, Z., Mortier, E., Melchior, A., Degeest, G., Geeraerts, A., … David, G. (2012). Syndecan–syntenin–ALIX regulates the biogenesis of exosomes. *Nature Cell Biology*, *14*(7), 677–685. https://doi.org/10.1038/ncb2502

Balaj, L., Lessard, R., Dai, L., Cho, Y.-J., Pomeroy, S. L., Breakefield, X. O., & Skog, J. (2011). Tumour microvesicles contain retrotransposon elements and amplified oncogene sequences. *Nature Communications*, *2*(1), 180. https://doi.org/10.1038/ncomms1180

Balkwill, F. R., Capasso, M., & Hagemann, T. (2012). The tumor microenvironment at a glance. *Journal of Cell Science*, *125*(Pt 23), 5591–5596. https://doi.org/10.1242/jcs.116392

Barreiro, O., Yáñez-Mó, M., Sala-Valdés, M., Gutiérrez-López, M. D., Ovalle, S., Higginbottom, A., … Sánchez-Madrid, F. (2005). Endothelial tetraspanin microdomains regulate leukocyte firm adhesion during extravasation. *Blood*, *105*(7), 2852–2861. https://doi.org/10.1182/blood-2004-09-3606

Becker, A., Thakur, B. K., Weiss, J. M., Kim, H. S., Peinado, H., & Lyden, D. (2016). Extracellular Vesicles in Cancer: Cell-to-Cell Mediators of Metastasis. *Cancer Cell*, *30*(6), 836–848. https://doi.org/10.1016/j.ccell.2016.10.009

Berditchevski, F., & Odintsova, E. (1999). Characterization of integrin-tetraspanin adhesion complexes: role of tetraspanins in integrin signaling. *The Journal of Cell Biology*, *146*(2), 477–492. Retrieved from http://www.ncbi.nlm.nih.gov/pubmed/10427099

Beyer, T. A., Weiss, A., Khomchuk, Y., Huang, K., Ogunjimi, A. A., Varelas, X., & Wrana, J. L. (2013). Switch Enhancers Interpret TGF-β and Hippo Signaling to Control Cell Fate in Human Embryonic Stem Cells. *Cell Reports*, *5*(6), 1611–1624. https://doi.org/10.1016/J.CELREP.2013.11.021

Bhowmick, N. A., Ghiassi, M., Bakin, A., Aakre, M., Lundquist, C. A., Engel, M. E., … Moses, H. L. (2001). Transforming Growth Factor-β1 Mediates Epithelial to Mesenchymal Transdifferentiation through a RhoA-dependent Mechanism. *Molecular Biology of the Cell*, *12*(1), 27–36. https://doi.org/10.1091/mbc.12.1.27

Bhowmick, N. A., Neilson, E. G., & Moses, H. L. (2004). Stromal fibroblasts in cancer initiation and progression. *Nature*, *432*(7015), 332–337. https://doi.org/10.1038/nature03096

Bobrie, A., Krumeich, S., Reyal, F., Recchi, C., Moita, L. F., Seabra, M. C., … Thery, C. (2012). Rab27a Supports Exosome-Dependent and -Independent Mechanisms That Modify the Tumor Microenvironment and Can Promote Tumor Progression. *Cancer Research*, *72*(19), 4920–4930. https://doi.org/10.1158/0008-5472.CAN-12-0925

Booth, A. M., Fang, Y., Fallon, J. K., Yang, J.-M., Hildreth, J. E. K., & Gould, S. J. (2006). Exosomes and HIV Gag bud from endosome-like domains of the T cell plasma membrane. *The Journal of Cell Biology*, *172*(6), 923–935. https://doi.org/10.1083/jcb.200508014

Borges, F. T., Melo, S. A., Ozdemir, B. C., Kato, N., Revuelta, I., Miller, C. A., … Kalluri, R. (2013). TGF- 1-Containing Exosomes from Injured Epithelial Cells Activate Fibroblasts to Initiate Tissue Regenerative Responses and Fibrosis. *Journal of the American Society of Nephrology*, *24*(3), 385–392. https://doi.org/10.1681/ASN.2012101031

Boucheix, C., & Benoit, P. (1988). CD9 antigen: will platelet physiology help to explain the function of a surface molecule during hemopoietic differentiation? *Nouvelle Revue Francaise d'hematologie*, *30*(4), 201–202. Retrieved from http://www.ncbi.nlm.nih.gov/pubmed/2848215

Bradley, L., Koennig, D., Tognoli, M. L., van der Vaart, J., & O'Neill, E. (2018). RASSF Family. In S. Choi (Ed.), *Encyclopedia of Signaling Molecules* (pp. 4501–4523). Cham: Springer International Publishing. https://doi.org/10.1007/978-3-319-67199-4_101852

Bryan, B. A., Li, D., Wu, X., & Liu, M. (2005). The Rho family of small GTPases: crucial regulators of skeletal myogenesis. *CMLS, Cell. Mol. Life Sci*, *6205*, 1547–1555. https://doi.org/10.1007/s00018-005-5029-z

Burbee, D. G., Forgacs, E., Zöchbauer-Müller, S., Shivakumar, L., Fong, K., Gao, B., … Minna, J. D. (2001). Epigenetic inactivation of RASSF1A in lung and breast cancers and malignant phenotype suppression. *Journal of the National Cancer Institute*, *93*(9), 691–699. https://doi.org/10.1093/JNCI/93.9.691

Buschow, S. I., Nolte-'t Hoen, E. N. M., van Niel, G., Pols, M. S., ten Broeke, T., Lauwen, M., … Stoorvogel, W. (2009). MHC II in Dendritic Cells is Targeted to Lysosomes or T Cell-Induced Exosomes Via Distinct Multivesicular Body Pathways. *Traffic*, *10*(10), 1528–1542. https://doi.org/10.1111/j.1600-0854.2009.00963.x

Cai, J., Song, X., Wang, W., Watnick, T., Pei, Y., Qian, F., & Pan, D. (2018). A RhoA-YAP-c-Myc signaling axis promotes the development of polycystic kidney disease. *Genes & Development*, *32*(11–12), 781–793. https://doi.org/10.1101/gad.315127.118

Cantelli, G., Orgaz, J. L., Rodriguez-Hernandez, I., Karagiannis, P., Maiques, O., Matias-Guiu, X., … Sanz-Moreno, V. (2015). TGF-β-Induced Transcription Sustains Amoeboid Melanoma Migration and Dissemination. *Current Biology : CB*, *25*(22), 2899–2914.

Chairoungdua, A., Smith, D. L., Pochard, P., Hull, M., & Caplan, M. J. (2010). Exosome release of β-catenin: A novel mechanism that antagonizes Wnt signaling. *Journal of Cell Biology*, *190*(6), 1079–1091. https://doi.org/10.1083/jcb.201002049

Chalmin, F., Ladoire, S., Mignot, G., Vincent, J., Bruchard, M., Remy-Martin, J.-P., … Ghiringhelli, F. (2010). Membrane-associated Hsp72 from tumor-derived exosomes mediates STAT3-dependent immunosuppressive function of mouse and human myeloid-derived suppressor cells. *Journal of Clinical Investigation*. https://doi.org/10.1172/JCI40483

Charrin, S., Latil, M., Soave, S., Polesskaya, A., Chrétien, F., Boucheix, C., & Rubinstein, E. (2013). Normal muscle regeneration requires tight control of muscle cell fusion by tetraspanins CD9 and CD81. *Nature Communications*, *4*(1), 1674. https://doi.org/10.1038/ncomms2675

Chen, I.-H., Xue, L., Hsu, C.-C., Paez, J. S. P., Pan, L., Andaluz, H., … Tao, W. A. (2017). Phosphoproteins in extracellular vesicles as candidate markers for breast cancer. *Proceedings of the National Academy of Sciences*, *114*(12), 3175–3180. https://doi.org/10.1073/pnas.1618088114

Cho, H. J., Hwang, Y.-S., Mood, K., Ji, Y. J., Lim, J., Morrison, D. K., & Daar, I. O. (2014). EphrinB1 Interacts with CNK1 and Promotes Cell Migration through c-Jun N-terminal Kinase (JNK) Activation. *Journal of Biological Chemistry*, *289*(26), 18556–18568. https://doi.org/10.1074/jbc.M114.558809

Chowdhury, R., Webber, J. P., Gurney, M., Mason, M. D., Tabi, Z., & Clayton, A. (2015a). Cancer

exosomes trigger mesenchymal stem cell differentiation into pro-angiogenic and pro-invasive myofibroblasts. *Oncotarget*, *6*(2), 715–731. https://doi.org/10.18632/oncotarget.2711

Chowdhury, R., Webber, J. P., Gurney, M., Mason, M. D., Tabi, Z., & Clayton, A. (2015b). Cancer exosomes trigger mesenchymal stem cell differentiation into pro-angiogenic and pro-invasive myofibroblasts. *Oncotarget*, *6*(2), 715–731. https://doi.org/10.18632/oncotarget.2711

Christianson, H. C., Svensson, K. J., van Kuppevelt, T. H., Li, J.-P., & Belting, M. (2013). Cancer cell exosomes depend on cell-surface heparan sulfate proteoglycans for their internalization and functional activity. *Proceedings of the National Academy of Sciences*, *110*(43), 17380–17385. https://doi.org/10.1073/pnas.1304266110

Chrzanowska-Wodnicka, M., & Burridge, K. (1996). Rho-stimulated contractility drives the formation of stress fibers and focal adhesions. *The Journal of Cell Biology*, *133*(6), 1403–1415. https://doi.org/10.1083/JCB.133.6.1403

Clancy, J. W., Sedgwick, A., Rosse, C., Muralidharan-Chari, V., Raposo, G., Method, M., … D'Souza-Schorey, C. (2015). Regulated delivery of molecular cargo to invasive tumour-derived microvesicles. *Nature Communications*, *6*(1), 6919. https://doi.org/10.1038/ncomms7919

Cohen, S. (1960). PURIFICATION OF A NERVE-GROWTH PROMOTING PROTEIN FROM THE MOUSE SALIVARY GLAND AND ITS NEURO-CYTOTOXIC ANTISERUM. *Proceedings of the National Academy of Sciences of the United States of America*, *46*(3), 302–311. https://doi.org/10.1073/PNAS.46.3.302

Cohen, S. (1962). Isolation of a Mouse Submaxillary Gland Protein Accelerating Incisor Eruption and Eyelid Opening in the New-born Animal. *The Journal of Biological Chemistry.*, *237*, 1555–1562. Retrieved from http://www.jbc.org/content/237/5/1555.citation

Cohen, S., Levi-Montalcini, R., & Hamburger, V. (1954). A NERVE GROWTH-STIMULATING FACTOR ISOLATED FROM SARCOM AS 37 AND 180. *Proceedings of the National Academy of Sciences of the United States of America*, *40*(10), 1014–1018. Retrieved from http://www.ncbi.nlm.nih.gov/pubmed/16589582

Colombo, M., Moita, C., van Niel, G., Kowal, J., Vigneron, J., Benaroch, P., … Raposo, G. (2013). Analysis of ESCRT functions in exosome biogenesis, composition and secretion highlights the heterogeneity of extracellular vesicles. *Journal of Cell Science*, *126*(Pt 24). https://doi.org/10.1242/jcs.128868

Colombo, M., Raposo, G., & Théry, C. (2014). Biogenesis, Secretion, and Intercellular Interactions of Exosomes and Other Extracellular Vesicles. *Annual Review of Cell and Developmental Biology*, *30*(1), 255–289. https://doi.org/10.1146/annurev-cellbio-101512-122326

Cook, G. A., Longhurst, C. M., Grgurevich, S., Cholera, S., Crossno, J. T., & Jennings, L. K. (2002). Identification of CD9 extracellular domains important in regulation of CHO cell adhesion to fibronectin and fibronectin pericellular matrix assembly. *Blood*, *100*(13), 4502–4511. https://doi.org/10.1182/blood.V100.13.4502

Cook, G. A., Wilkinson, D. A., Crossno, J. T., Raghow, R., & Jennings, L. K. (1999). The Tetraspanin CD9 Influences the Adhesion, Spreading, and Pericellular Fibronectin Matrix Assembly of Chinese Hamster Ovary Cells on Human Plasma Fibronectin. *Experimental Cell Research*, *251*(2), 356–371. https://doi.org/10.1006/excr.1999.4596

Copeland, B. T., Bowman, M. J., Boucheix, C., & Ashman, L. K. (2013). Knockout of the tetraspanin Cd9 in the TRAMP model of de novo prostate cancer increases spontaneous metastases in an organ-specific manner. *International Journal of Cancer*, *133*(8), 1803–1812. https://doi.org/10.1002/ijc.28204

Corrigan, L., Redhai, S., Leiblich, A., Fan, S.-J., Perera, S. M. W., Patel, R., … Wilson, C. (2014). BMP-regulated exosomes from Drosophila male reproductive glands reprogram female behavior. *The Journal of Cell Biology*, *206*(5), 671–688. https://doi.org/10.1083/jcb.201401072

Costa-Silva, B., Aiello, N. M., Ocean, A. J., Singh, S., Zhang, H., Thakur, B. K., … Lyden, D. (2015). Pancreatic cancer exosomes initiate pre-metastatic niche formation in the liver. *Nature Cell Biology*, *17*(6), 816–826. https://doi.org/10.1038/ncb3169

Costa Verdera, H., Gitz-Francois, J. J., Schiffelers, R. M., & Vader, P. (2017). Cellular uptake of extracellular vesicles is mediated by clathrin-independent endocytosis and macropinocytosis. *Journal of Controlled Release*, *266*, 100–108. https://doi.org/10.1016/j.jconrel.2017.09.019

da Costa Prando, E., Cavalli, L. R., & Rainho, C. A. (2011). Evidence of epigenetic regulation of the tumor suppressor gene cluster flanking RASSF1 in breast cancer cell lines. *Epigenetics*, *6*(12), 1413–1424. https://doi.org/10.4161/epi.6.12.18271

Dai, X., Cheng, H., Bai, Z., & Li, J. (2017). Breast Cancer Cell Line Classification and Its

Relevance with Breast Tumor Subtyping. *Journal of Cancer*, *8*(16), 3131–3141. https://doi.org/10.7150/jca.18457

Dallol, A., Agathanggelou, A., Fenton, S. L., Ahmed-Choudhury, J., Hesson, L., Vos, M. D., … Latif, F. (2004). RASSF1A interacts with microtubule-associated proteins and modulates microtubule dynamics. *Cancer Research*, *64*(12), 4112–4116. https://doi.org/10.1158/0008-5472.CAN-04-0267

Dallol, A., Agathanggelou, A., Tommasi, S., Pfeifer, G. P., Maher, E. R., & Latif, F. (2005). Involvement of the RASSF1A tumor suppressor gene in controlling cell migration. *Cancer Research*, *65*(17), 7653–7659. https://doi.org/10.1158/0008-5472.CAN-05-0247

Dallol, A., Hesson, L. B., Matallanas, D., Cooper, W. N., O'Neill, E., Maher, E. R., … Latif, F. (2009). RAN GTPase Is a RASSF1A Effector Involved in Controlling Microtubule Organization. *Current Biology*, *19*(14), 1227–1232. https://doi.org/10.1016/j.cub.2009.05.064

Daly, A. C., Randall, R. A., & Hill, C. S. (2008). Transforming Growth Factor -Induced Smad1/5 Phosphorylation in Epithelial Cells Is Mediated by Novel Receptor Complexes and Is Essential for Anchorage-Independent Growth. *Molecular and Cellular Biology*, *28*(22), 6889–6902. https://doi.org/10.1128/MCB.01192-08

Dammann, R., Li, C., Yoon, J. H., Chin, P. L., Bates, S., & Pfeifer, G. P. (2000). Epigenetic inactivation of a RAS association domain family protein from the lung tumour suppressor locus 3p21.3. *Nature Genetics*, *25*(3), 315–319. https://doi.org/10.1038/77083

Dammann, R., Schagdarsurengin, U., Strunnikova, M., Rastetter, M., Seidel, C., Liu, L., … Pfeifer, G. P. (2003). Epigenetic inactivation of the Ras-association domain family 1 (RASSF1A) gene and its function in human carcinogenesis. *Histology and Histopathology*, *18*(2), 665–677. Retrieved from http://www.ncbi.nlm.nih.gov/pubmed/12647816

David, C. J., Huang, Y. H., Chen, M., Su, J., Zou, Y., Bardeesy, N., … Massagué, J. (2016). TGF-β Tumor Suppression through a Lethal EMT. *Cell*, *164*(5), 1015–1030. https://doi.org/10.1016/j.cell.2016.01.009

Davis, B. N., Hilyard, A. C., Lagna, G., & Hata, A. (2008). SMAD proteins control DROSHA-mediated microRNA maturation. *Nature*, *454*(7200), 56–61. https://doi.org/10.1038/nature07086

de Winde, C. M., Zuidscherwoude, M., Vasaturo, A., van der Schaaf, A., Figdor, C. G., & van Spriel, A. B. (2015). Multispectral imaging reveals the tissue distribution of tetraspanins in human lymphoid organs. *Histochemistry and Cell Biology*, *144*(2), 133–146. https://doi.org/10.1007/s00418-015-1326-2

del Conde, I., Shrimpton, C. N., Thiagarajan, P., & López, J. A. (2005). Tissue-factor-bearing microvesicles arise from lipid rafts and fuse with activated platelets to initiate coagulation. *Blood*, *106*(5), 1604–1611. https://doi.org/10.1182/blood-2004-03-1095

Descargues, P., Sil, A. K., Sano, Y., Korchynskyi, O., Han, G., Owens, P., … Karin, M. (2008). IKKalpha is a critical coregulator of a Smad4-independent TGFbeta-Smad2/3 signaling pathway that controls keratinocyte differentiation. *Proceedings of the National Academy of Sciences of the United States of America*, *105*(7), 2487–2492. https://doi.org/10.1073/pnas.0712044105

Detchokul, S., Williams, E. D., Parker, M. W., & Frauman, A. G. (2014). Tetraspanins as regulators of the tumour microenvironment: implications for metastasis and therapeutic strategies. *British Journal of Pharmacology*, *171*(24), 5462–5490. https://doi.org/10.1111/bph.12260

Di Guglielmo, G. M., Le Roy, C., Goodfellow, A. F., & Wrana, J. L. (2003). Distinct endocytic pathways regulate TGF-β receptor signalling and turnover. *Nature Cell Biology*, *5*(5), 410–421. https://doi.org/10.1038/ncb975

Donninger, H., Allen, N., Henson, A., Pogue, J., Williams, A., Gordon, L., … Clark, G. J. (2011). Salvador protein is a tumor suppressor effector of RASSF1A with hippo pathway-independent functions. *The Journal of Biological Chemistry*, *286*(21), 18483–18491. https://doi.org/10.1074/jbc.M110.214874

Donninger, H., Clark, J. A., Monaghan, M. K., Schmidt, M. L., Vos, M., & Clark, G. J. (2014). Cell Cycle Restriction Is More Important Than Apoptosis Induction for RASSF1A Protein Tumor Suppression *. *The Journal of Biological Chemistry*, *289*(45), 31287–3129. https://doi.org/10.1074/jbc.M114.609537

Dreijerink, K., Braga, E., Kuzmin, I., Geil, L., Duh, F. M., Angeloni, D., … Zabarovsky, E. R. (2001). The candidate tumor suppressor gene, RASSF1A, from human chromosome 3p21.3 is involved in kidney tumorigenesis. *Proceedings of the National Academy of Sciences of the United States of America*, *98*(13), 7504–7509. https://doi.org/10.1073/pnas.131216298

Dubois, F., Keller, M., Calvayrac, O., Soncin, F., Hoa, L., Hergovich, A., … Zalcman, G. (2016).

RASSF1A Suppresses the Invasion and Metastatic Potential of Human Non-Small Cell Lung Cancer Cells by Inhibiting YAP Activation through the GEF-H1/RhoB Pathway. *Cancer Research*, *76*(6), 1627–1640. https://doi.org/10.1158/0008-5472.CAN-15-1008

Dupont, S., Morsut, L., Aragona, M., Enzo, E., Giulitti, S., Cordenonsi, M., … Piccolo, S. (2011). Role of YAP/TAZ in mechanotransduction. *Nature*, *474*(7350), 179–183. https://doi.org/10.1038/nature10137

Edlund, S., Landström, M., Heldin, C.-H., & Aspenström, P. (2002). Transforming Growth Factor-β–induced Mobilization of Actin Cytoskeleton Requires Signaling by Small GTPases Cdc42 and RhoA. *Molecular Biology of the Cell*, *13*(3), 902–914. https://doi.org/10.1091/mbc.01-08-0398

Estrabaud, E., Lassot, I., Blot, G., Le Rouzic, E., Tanchou, V., Quemeneur, E., … Benarous, R. (2007). RASSF1C, an Isoform of the Tumor Suppressor RASSF1A, Promotes the Accumulation of -Catenin by Interacting with TrCP. *Cancer Research*, *67*(3), 1054–1061. https://doi.org/10.1158/0008-5472.CAN-06-2530

Etienne-Manneville, S., & Hall, A. (2002). Rho GTPases in Cell Biology. *Nature*, *420*(December), 629–635. https://doi.org/10.1038/nature01148\rnature01148 [pii]

Fan, J., Zhu, G.-Z., & Niles, R. M. (2009). Expression and function of CD9 in melanoma cells. *Molecular Carcinogenesis*, *49*(1), n/a-n/a. https://doi.org/10.1002/mc.20580

Fleming, Y. M., Ferguson, G. J., Spender, L. C., Larsson, J., Karlsson, S., Ozanne, B. W., … Inman, G. J. (2009). TGF-β-mediated activation of RhoA signalling is required for efficient V12HaRas and V600EBRAF transformation. *Oncogene*, *28*(7), 983–993. https://doi.org/10.1038/onc.2008.449

Friedl, P., Locker, J., Sahai, E., & Segall, J. E. (2012). Classifying collective cancer cell invasion. *Nature Cell Biology*, (14), 777–783. https://doi.org/10.1038/ncb2548

Friedl, P., & Wolf, K. (2010). Plasticity of cell migration: a multiscale tuning model. *The Journal of Cell Biology*, *188*(1), 11–19. https://doi.org/10.1083/jcb.200909003

Friese, M. A., Wischhusen, J., Wick, W., Weiler, M., Eisele, G., Steinle, A., & Weller, M. (2004). RNA Interference Targeting Transforming Growth Factor-β Enhances NKG2D-Mediated Antiglioma Immune Response, Inhibits Glioma Cell Migration and Invasiveness, and Abrogates Tumorigenicity ***In vivo*** . *Cancer Research*, *64*(20), 7596–7603. https://doi.org/10.1158/0008-5472.CAN-04-1627

Fujii, M., Toyoda, T., Nakanishi, H., Yatabe, Y., Sato, A., Matsudaira, Y., … Sekido, Y. (2012). TGF-β synergizes with defects in the Hippo pathway to stimulate human malignant mesothelioma growth. *The Journal of Experimental Medicine*, *209*(3), 479–494. https://doi.org/10.1084/jem.20111653

Furuya, M., Kato, H., Nishimura, N., Ishiwata, I., Ikeda, H., Ito, R., … Ishikura, H. (2005). Down-regulation of CD9 in human ovarian carcinoma cell might contribute to peritoneal dissemination: morphologic alteration and reduced expression of beta1 integrin subsets. *Cancer Research*, *65*(7), 2617–2625. https://doi.org/10.1158/0008-5472.CAN-04-3123

Gao, T., Wang, S., He, B., Pan, Y., Song, G., Gu, L., … Li, R. (2012). The Association of RAS Association Domain Family Protein1A (RASSF1A) Methylation States and Bladder Cancer Risk: A Systematic Review and Meta-Analysis. *PLoS ONE*, *7*(11), e48300. https://doi.org/10.1371/journal.pone.0048300

Garnier, D., Magnus, N., Lee, T. H., Bentley, V., Meehan, B., Milsom, C., … Rak, J. (2012). Cancer cells induced to express mesenchymal phenotype release exosome-like extracellular vesicles carrying tissue factor. *The Journal of Biological Chemistry*, *287*(52), 43565–43572. https://doi.org/10.1074/jbc.M112.401760

Gellibert, F. *, Woolven, J. ‡, Fouchet, -MH †, Mathews, N. §, Goodland, H. ‖, Lovegrove, V. ‖, … ‖ H. D. (2004). Identification of 1,5-Naphthyridine Derivatives as a Novel Series of Potent and Selective TGF-β Type I Receptor Inhibitors. https://doi.org/10.1021/JM0400247

Giampieri, S., Manning, C., Hooper, S., Jones, L., Hill, C. S., & Sahai, E. (2009). Localized and reversible TGFβ signalling switches breast cancer cells from cohesive to single cell motility. *Nature Cell Biology*, *11*(11), 1287–1296. https://doi.org/10.1038/ncb1973

Gordón-Alonso, M., Yañez-Mó, M., Barreiro, O., Alvarez, S., Muñoz-Fernández, M. A., Valenzuela-Fernández, A., & Sánchez-Madrid, F. (2006). Tetraspanins CD9 and CD81 modulate HIV-1-induced membrane fusion. *Journal of Immunology (Baltimore, Md.: 1950)*, *177*(8), 5129–5137. Retrieved from http://www.ncbi.nlm.nih.gov/pubmed/17015697

Grawenda, A. M., & O'Neill, E. (2015). Clinical utility of RASSF1A methylation in human malignancies. *British Journal of Cancer*, *113*(3), 372–381. https://doi.org/10.1038/bjc.2015.221

Guo, W., Cui, L., Wang, C., Guo, Y., Shen, S., Kuang, G., & Dong, Z. (2014). Decreased expression of RASSF1A and up-regulation of RASSF1C is associated with esophageal squamous cell carcinoma. *Clinical & Experimental Metastasis*, *31*(5), 521–533. https://doi.org/10.1007/s10585-014-9646-5

Guo, X., & Wang, X.-F. (2009). Signaling cross-talk between TGF-β/BMP and other pathways. *Cell Research*, *19*(1), 71–88. https://doi.org/10.1038/cr.2008.302

Hachim, I. Y., Villatoro, M., Canaff, L., Hachim, M. Y., Boudreault, J., Haiub, H., … Lebrun, J.-J. (2017). Transforming Growth Factor-beta Regulation of Ephrin Type-A Receptor 4 Signaling in Breast Cancer Cellular Migration. *Scientific Reports*, *7*(1), 14976. https://doi.org/10.1038/s41598-017-14549-9

Hahn, S. A., Schutte, M., Hoque, A. T., Moskaluk, C. A., da Costa, L. T., Rozenblum, E., … Kern, S. E. (1996). DPC4, a candidate tumor suppressor gene at human chromosome 18q21.1. *Science (New York, N.Y.)*, *271*(5247), 350–353. https://doi.org/10.1126/SCIENCE.271.5247.350

Hamilton, G., Yee, K. S., Scrace, S., & O'Neill, E. (2009). ATM regulates a RASSF1A-dependent DNA damage response. *Curr Biol*, *19*(23), 2020–2025. https://doi.org/10.1016/j.cub.2009.10.040

Hanahan, D., & Weinberg, R. a. (2000). The hallmarks of cancer. *Cell*, *100*, 57–70. https://doi.org/10.1016/S0092-8674(00)81683-9

Hanahan, D., & Weinberg, R. a. (2011). Hallmarks of cancer: The next generation. *Cell*, *144*(5), 646–674. https://doi.org/10.1016/j.cell.2011.02.013

Hanson, P. I., & Cashikar, A. (2012). Multivesicular Body Morphogenesis. *Annual Review of Cell and Developmental Biology*, *28*(1), 337–362. https://doi.org/10.1146/annurev-cellbio-092910-154152

Harada, K., Toyooka, S., Maitra, A., Maruyama, R., Toyooka, K. O., Timmons, C. F., … Gazdar, A. F. (2002). Aberrant promoter methylation and silencing of the RASSF1A gene in pediatric tumors and cell lines. *Oncogene*, *21*(27), 4345–4349. https://doi.org/10.1038/sj.onc.1205446

Harding, C., Heuser, J., & Stahl, P. (1983). Receptor-mediated endocytosis of transferrin and recycling of the transferrin receptor in rat reticulocytes. *The Journal of Cell Biology*, *97*(2), 329–339. Retrieved from http://www.ncbi.nlm.nih.gov/pubmed/6309857

Harding, C., Heuser, J., & Stahl, P. (1984). Endocytosis and intracellular processing of transferrin and colloidal gold-transferrin in rat reticulocytes: demonstration of a pathway for receptor shedding. *European Journal of Cell Biology*, *35*(2), 256–263. Retrieved from http://www.ncbi.nlm.nih.gov/pubmed/6151502

Harris, D. a., Patel, S. H., Gucek, M., Hendrix, A., Westbroek, W., & Taraska, J. W. (2015). Exosomes Released from Breast Cancer Carcinomas Stimulate Cell Movement. *Plos One*, *10*(3), e0117495. https://doi.org/10.1371/journal.pone.0117495

Hayashi, H., & Sakai, T. (2012). Biological Significance of Local TGF-β Activation in Liver Diseases. *Frontiers in Physiology*, *3*, 12. https://doi.org/10.3389/fphys.2012.00012

He, K., Yan, X., Li, N., Dang, S., Xu, L., Zhao, B., … Chen, Y.-G. (2015). Internalization of the TGF-β type I receptor into caveolin-1 and EEA1 double-positive early endosomes. *Cell Research*, *25*(6), 738–752. https://doi.org/10.1038/cr.2015.60

He, W., Dorn, D. C., Erdjument-Bromage, H., Tempst, P., Moore, M. A. S., & Massagué, J. (2006). Hematopoiesis Controlled by Distinct TIF1γ and Smad4 Branches of the TGFβ Pathway. *Cell*, *125*(5), 929–941. https://doi.org/10.1016/J.CELL.2006.03.045

Heikkinen, P. T., Nummela, M., Leivonen, S.-K., Westermarck, J., Hill, C. S., Kähäri, V.-M., & Jaakkola, P. M. (2010). Hypoxia-activated Smad3-specific dephosphorylation by PP2A. *The Journal of Biological Chemistry*, *285*(6), 3740–3749. https://doi.org/10.1074/jbc.M109.042978

Hemler, M. E. (2005). Tetraspanin functions and associated microdomains. *Nature Reviews Molecular Cell Biology*, *6*(10), 801–811. https://doi.org/10.1038/nrm1736

Hemler, M. E. (2014). Tetraspanin proteins promote multiple cancer stages. *Nature Reviews Cancer*, *14*(1), 49–60. https://doi.org/10.1038/nrc3640

Hesson, L. B., Cooper, W. N., & Latif, F. (2007). Evaluation of the 3p21.3 tumour-suppressor gene cluster. *Oncogene*, *26*(52), 7283–7301. https://doi.org/10.1038/sj.onc.1210547

Heusermann, W., Hean, J., Trojer, D., Steib, E., von Bueren, S., Graff-Meyer, A., … Meisner-Kober, N. C. (2016). Exosomes surf on filopodia to enter cells at endocytic hot spots, traffic within endosomes, and are targeted to the ER. *Journal of Cell Biology*. https://doi.org/10.1083/jcb.201506084

Hiemer, S. E., Szymaniak, A. D., & Varelas, X. (2014). The transcriptional regulators TAZ and YAP direct transforming growth factor beta-induced tumorigenic phenotypes in breast cancer cells.

Journal of Biological Chemistry, *289*(19), 13461–13474. https://doi.org/10.1074/jbc.M113.529115

Hodge, K., Have, S. Ten, Hutton, L., & Lamond, A. I. (2013). Cleaning up the masses: exclusion lists to reduce contamination with HPLC-MS/MS. *Journal of Proteomics*, *88*, 92–103. https://doi.org/10.1016/j.jprot.2013.02.023

Hori, H., Yano, S., Koufuji, K., Takeda, J., & Shirouzu, K. (2004). CD9 expression in gastric cancer and its significance. *Journal of Surgical Research*, *117*(2), 208–215. https://doi.org/10.1016/J.JSS.2004.01.014

Hoshino, A., Costa-Silva, B., Shen, T. L., Rodrigues, G., Hashimoto, A., Tesic Mark, M., … Lyden, D. (2015). Tumour exosome integrins determine organotropic metastasis. *Nature*, *527*(7578), 329–335. https://doi.org/10.1038/nature15756

Hoshino, D., Kirkbride, K. C., Costello, K., Clark, E. S., Sinha, S., Grega-Larson, N., … Weaver, A. M. (2013). Exosome Secretion Is Enhanced by Invadopodia and Drives Invasive Behavior. *Cell Reports*, *5*(5), 1159–1168. https://doi.org/10.1016/j.celrep.2013.10.050

Hsu, C., Morohashi, Y., Yoshimura, S. I., Manrique-Hoyos, N., Jung, S., Lauterbach, M. a., … Simons, M. (2010). Regulation of exosome secretion by Rab35 and its GTPase-activating proteins TBC1D10A-C. *Journal of Cell Biology*, *189*(2), 223–232. https://doi.org/10.1083/jcb.200911018

Huang, J. J., & Blobe, G. C. (2016). Dichotomous roles of TGF-β in human cancer. *Biochemical Society Transactions*, *44*(5), 1441–1454. https://doi.org/10.1042/BST20160065

Huveneers, S., & Danen, E. H. J. (2009). Adhesion signaling - crosstalk between integrins, Src and Rho. *Journal of Cell Science*, *122*(Pt 8), 1059–1069. https://doi.org/10.1242/jcs.039446

Inman, G. J., Nicolás, F. J., & Hill, C. S. (2002). Nucleocytoplasmic Shuttling of Smads 2, 3, and 4 Permits Sensing of TGF-β Receptor Activity. *Molecular Cell*, *10*(2), 283–294. https://doi.org/10.1016/S1097-2765(02)00585-3

Inoue, Y., & Imamura, T. (2008). Regulation of TGF-β family signaling by E3 ubiquitin ligases. *Cancer Science*, *99*(11), 2107–2112. https://doi.org/10.1111/j.1349-7006.2008.00925.x

Jaffe, A. B., Aspenström, P., & Hall, A. (2004). Human CNK1 acts as a scaffold protein, linking Rho and Ras signal transduction pathways. *Molecular and Cellular Biology*, *24*(4), 1736–1746. Retrieved from http://www.ncbi.nlm.nih.gov/pubmed/14749388

Jahn, R., & Scheller, R. H. (2006). SNAREs — engines for membrane fusion. *Nature Reviews Molecular Cell Biology*, *7*(9), 631–643. https://doi.org/10.1038/nrm2002

Jiang, Y., Cui, L., Chen, W., Shen, S., & Ding, L. (2012). The prognostic role of RASSF1A promoter methylation in breast cancer: a meta-analysis of published data. *PloS One*, *7*(5), e36780. https://doi.org/10.1371/journal.pone.0036780

Johnstone, R. M., Adam, M., Hammonds, J. R., & Turbide, C. (1987). Vesicle Formation during Reticulocyte Maturation, *262*(1), 9412–9420.

Jones, P. H., Bishop, L. A., & Watt, F. M. (1996). Functional significance of CD9 association with beta 1 integrins in human epidermal keratinocytes. *Cell Adhesion and Communication*, *4*(4–5), 297–305. Retrieved from http://www.ncbi.nlm.nih.gov/pubmed/9117348

Kahlert, C., Melo, S. A., Protopopov, A., Tang, J., Seth, S., Koch, M., … Kalluri, R. (2014). Identification of double-stranded genomic DNA spanning all chromosomes with mutated KRAS and p53 DNA in the serum exosomes of patients with pancreatic cancer. *The Journal of Biological Chemistry*, *289*(7), 3869–3875. https://doi.org/10.1074/jbc.C113.532267

Kaji, K., Oda, S., Shikano, T., Ohnuki, T., Uematsu, Y., Sakagami, J., … Kudo, A. (2000). The gamete fusion process is defective in eggs of Cd9-deficient mice. *Nature Genetics*, *24*(3), 279–282. https://doi.org/10.1038/73502

Kalluri, R. (2016). The biology and function of exosomes in cancer. *The Journal of Clinical Investigation*, *126*(4), 1208–1215. https://doi.org/10.1172/JCI81135

Kalra, H., Adda, C. G., Liem, M., Ang, C.-S., Mechler, A., Simpson, R. J., … Mathivanan, S. (2013). Comparative proteomics evaluation of plasma exosome isolation techniques and assessment of the stability of exosomes in normal human blood plasma. *PROTEOMICS*, *13*(22), 3354–3364. https://doi.org/10.1002/pmic.201300282

Kanada, M., Bachmann, M. H., & Contag, C. H. (2016). Signaling by Extracellular Vesicles Advances Cancer Hallmarks. *Trends in Cancer*, *2*(2), 84–94. https://doi.org/10.1016/j.trecan.2015.12.005

Khan, S., Jutzy, J. M. S., Valenzuela, M. M. A., Turay, D., Aspe, J. R., Ashok, A., … Wall, N. R. (2012). Plasma-Derived Exosomal Survivin, a Plausible Biomarker for Early Detection of Prostate Cancer. *PLoS ONE*, *7*(10), e46737. https://doi.org/10.1371/journal.pone.0046737

Kitagawa, D., Kajiho, H., Negishi, T., Ura, S., Watanabe, T., Wada, T., … Nishina, H. (2006).

Release of RASSF1C from the nucleus by Daxx degradation links DNA damage and SAPK/JNK activation. *The EMBO Journal*, *25*(14), 3286–3297. https://doi.org/10.1038/sj.emboj.7601212

Klumperman, J., & Raposo, G. (2014). The Complex Ultrastructure of the Endolysosomal System. *Cold Spring Harbor Perspectives in Biology*, *6*(10), a016857–a016857. https://doi.org/10.1101/cshperspect.a016857

Kowal, J., Arras, G., Colombo, M., Jouve, M., Morath, J. P., Primdal-Bengtson, B., … Théry, C. (2016). Proteomic comparison defines novel markers to characterize heterogeneous populations of extracellular vesicle subtypes. *Proceedings of the National Academy of Sciences of the United States of America*, *113*(8), E968-77. https://doi.org/10.1073/pnas.1521230113

Kozma, R., Ahmed, S., Best, A., & Lim, L. (1995). The Ras-related protein Cdc42Hs and bradykinin promote formation of peripheral actin microspikes and filopodia in Swiss 3T3 fibroblasts. *Molecular and Cellular Biology*, *15*(4), 1942–1952. Retrieved from http://www.ncbi.nlm.nih.gov/pubmed/7891688

Kraynov, V. S., Chamberlain, C., Bokoch, G. M., Schwartz, M. A., Slabaugh, S., & Hahn, K. M. (2000). Localized Rac activation dynamics visualized in living cells. *Science (New York, N.Y.)*, *290*(5490), 333–337. Retrieved from http://www.ncbi.nlm.nih.gov/pubmed/11030651

Kwon, S.-H., Liu, K. D., & Mostov, K. E. (2014). Intercellular transfer of GPRC5B via exosomes drives HGF-mediated outward growth. *Current Biology : CB*, *24*(2), 199–204. https://doi.org/10.1016/j.cub.2013.12.010

Lamaze, C., Chuang, T.-H., Terlecky, L. J., Bokoch, G. M., & Schmid, S. L. (1996). Regulation of receptor-mediated endocytosis by Rho and Rac. *Nature*, *382*(6587), 177–179. https://doi.org/10.1038/382177a0

Lambert, A. W., Pattabiraman, D. R., & Weinberg, R. A. (2017). Emerging Biological Principles of Metastasis. *Cell*, *168*(4), 670–691. https://doi.org/10.1016/j.cell.2016.11.037

Lämmermann, T., & Sixt, M. (2009). Mechanical modes of 'amoeboid' cell migration. *Current Opinion in Cell Biology*, *21*(5), 636–644. https://doi.org/10.1016/J.CEB.2009.05.003

Lamouille, S., & Derynck, R. (2011). Emergence of the Phosphoinositide 3-Kinase-Akt- Mammalian Target of Rapamycin Axis in Transforming Growth Factor-β-Induced Epithelial-Mesenchymal Transition. *Cells Tissues Organs*, *193*(1–2), 8–22. https://doi.org/10.1159/000320172

Laulagnier, K., Motta, C., Hamdi, S., Roy, S., Fauvelle, F., Pageaux, J.-F., … Record, M. (2004). Mast cell- and dendritic cell-derived exosomes display a specific lipid composition and an unusual membrane organization. *The Biochemical Journal*, *380*(Pt 1), 161–171. https://doi.org/10.1042/BJ20031594

Laverty, H. G., Wakefield, L. M., Occleston, N. L., O'Kane, S., & Ferguson, M. W. J. (2009). TGF-β3 and cancer: A review. *Cytokine & Growth Factor Reviews*, *20*(4), 305–317. https://doi.org/10.1016/J.CYTOGFR.2009.07.002

Le Naour, F., Rubinstein, E., Jasmin, C., Prenant, M., & Boucheix, C. (2000). Severely reduced female fertility in CD9-deficient mice. *Science (New York, N.Y.)*, *287*(5451), 319–321. Retrieved from http://www.ncbi.nlm.nih.gov/pubmed/10634790

Lee, H. H., Tien, S.-C., Jou, T.-S., Chang, Y.-C., Jhong, J.-G., & Chang, Z.-F. (2010). Src-dependent phosphorylation of ROCK participates in regulation of focal adhesion dynamics. *Journal of Cell Science*, *123*(19), 3368–3377. https://doi.org/10.1242/jcs.071555

Lee, M.-G., Jeong, S.-I., Ko, K.-P., Park, S.-K., Ryu, B.-K., Kim, I.-Y., … Chi, S.-G. (2016). RASSF1A Directly Antagonizes RhoA Activity through the Assembly of a Smurf1-Mediated Destruction Complex to Suppress Tumorigenesis. *Cancer Research*, *76*(7), 1847–1859. https://doi.org/10.1158/0008-5472.CAN-15-1752

Levy, L., & Hill, C. (2006). Alterations in components of the TGF-β superfamily signaling pathways in human cancer. *Cytokine & Growth Factor Reviews*, *17*(1–2), 41–58. https://doi.org/10.1016/j.cytogfr.2005.09.009

Li, B., Antonyak, M. A., Zhang, J., & Cerione, R. A. (2012). RhoA triggers a specific signaling pathway that generates transforming microvesicles in cancer cells. *Oncogene*, *31*(45), 4740–4749. https://doi.org/10.1038/onc.2011.636

Lin, X., Duan, X., Liang, Y.-Y., Su, Y., Wrighton, K. H., Long, J., … Feng, X.-H. (2006). PPM1A Functions as a Smad Phosphatase to Terminate TGFβ Signaling. *Cell*, *125*(5), 915–928. https://doi.org/10.1016/J.CELL.2006.03.044

Liu, B., Lu, S., Hu, Y., Liao, X., Ouyang, M., & Wang, Y. (2015). RhoA and Membrane Fluidity Mediates the Spatially Polarized Src/FAK Activation in Response to Shear Stress. *Scientific Reports*, *4*(1), 7008. https://doi.org/10.1038/srep07008

Liu, F., Lagares, D., Choi, K. M., Stopfer, L., Marinković, A., Vrbanac, V., … Tschumperlin, D. J. (2015). Mechanosignaling through YAP and TAZ drives fibroblast activation and fibrosis. *American Journal of Physiology-Lung Cellular and Molecular Physiology*, *308*(4), L344–L357. https://doi.org/10.1152/ajplung.00300.2014

Liu, I. M., Schilling, S. H., Knouse, K. A., Choy, L., Derynck, R., & Wang, X.-F. (2009). TGFbeta-stimulated Smad1/5 phosphorylation requires the ALK5 L45 loop and mediates the pro-migratory TGFbeta switch. *The EMBO Journal*, *28*(2), 88–98. https://doi.org/10.1038/emboj.2008.266

Liu, L., Vo, A., & Mckeehan, W. L. (2005). *Specificity of the Methylation-Suppressed A Isoform of Candidate Tumor Suppressor RASSF1 for Microtubule Hyperstabilization Is Determined by Cell Death Inducer C19ORF5*. Retrieved from www.aacrjournals.org

Liu, M., Zhang, Z., Sampson, L., Zhou, X., Nalapareddy, K., Feng, Y., … Zheng, Y. (2017). RHOA GTPase Controls YAP-Mediated EREG Signaling in Small Intestinal Stem Cell Maintenance. *Stem Cell Reports*, *9*(6), 1961–1975. https://doi.org/10.1016/j.stemcr.2017.10.004

Liu, Y., He, K., Hu, Y., Guo, X., Wang, D., Shi, W., … Song, J. (2017). YAP modulates TGF-β1-induced simultaneous apoptosis and EMT through upregulation of the EGF receptor. *Scientific Reports*, *7*(1), 45523. https://doi.org/10.1038/srep45523

Liu, Z., Shi, H., Szymczak, L. C., Aydin, T., Yun, S., Constas, K., … Liu, J. (2015). Promotion of Bone Morphogenetic Protein Signaling by Tetraspanins and Glycosphingolipids. *PLOS Genetics*, *11*(5), e1005221. https://doi.org/10.1371/journal.pgen.1005221

Llorente, A., Skotland, T., Sylvänne, T., Kauhanen, D., Róg, T., Orłowski, A., … Sandvig, K. (2013). Molecular lipidomics of exosomes released by PC-3 prostate cancer cells. *Biochimica et Biophysica Acta*, *1831*(7), 1302–1309. Retrieved from http://www.ncbi.nlm.nih.gov/pubmed/24046871

Logozzi, M., De Milito, A., Lugini, L., Borghi, M., Calabrò, L., Spada, M., … Fais, S. (2009). High Levels of Exosomes Expressing CD63 and Caveolin-1 in Plasma of Melanoma Patients. *PLoS ONE*, *4*(4), e5219. https://doi.org/10.1371/journal.pone.0005219

López-Casillas, F., Wrana, J. L., & Massagué, J. (1993). Betaglycan presents ligand to the TGF beta signaling receptor. *Cell*, *73*(7), 1435–1444. Retrieved from http://www.ncbi.nlm.nih.gov/pubmed/8391934

Lorenzato, A., Martino, C., Dani, N., Oligschläger, Y., Ferrero, A. M., Biglia, N., … Di Renzo, M. F. (2012). The cellular apoptosis susceptibility CAS/CSE1L gene protects ovarian cancer cells from death by suppressing RASSF1C. *FASEB Journal : Official Publication of the Federation of American Societies for Experimental Biology*, *26*(6), 2446–2456. https://doi.org/10.1096/fj.11-195982

Lötvall, J., Hill, A. F., Hochberg, F., Buzï¿½s, E. I., Vizio, D. Di, Gardiner, C., … Thï¿½ry, C. (2014). Minimal experimental requirements for definition of extracellular vesicles and their functions: A position statement from the International Society for Extracellular Vesicles. *Journal of Extracellular Vesicles*, *3*(1). https://doi.org/10.3402/jev.v3.26913

Luga, V., Zhang, L., Viloria-Petit, A. M., Ogunjimi, A. a., Inanlou, M. R., Chiu, E., … Wrana, J. L. (2012). Exosomes mediate stromal mobilization of autocrine Wnt-PCP signaling in breast cancer cell migration. *Cell*, *151*(7), 1542–1556. https://doi.org/10.1016/j.cell.2012.11.024

Malpeli, G., Amato, E., Dandrea, M., Fumagalli, C., Debattisti, V., Boninsegna, L., … Scarpa, A. (2011). Methylation-associated down-regulation of RASSF1A and up-regulation of RASSF1Cin pancreatic endocrine tumors. *BMC Cancer*, *11*(1), 351. https://doi.org/10.1186/1471-2407-11-351

Masellis-Smith, A., & Shaw, A. R. (1994). CD9-regulated adhesion. Anti-CD9 monoclonal antibody induce pre-B cell adhesion to bone marrow fibroblasts through de novo recognition of fibronectin. *Journal of Immunology (Baltimore, Md. : 1950)*, *152*(6), 2768–2777. Retrieved from http://www.ncbi.nlm.nih.gov/pubmed/7511626

Massagué, J. (2000). How cells read TGF-β signals. *Nature Reviews Molecular Cell Biology*, *1*(3), 169–178. https://doi.org/10.1038/35043051

Massagué, J. (2008). TGFβ in Cancer. *Cell*, *134*(2), 215–230. https://doi.org/10.1016/j.cell.2008.07.001

Massagué, J., Cheifetz, S., Boyd, F. . T., & Andres, J. L. (1990). TGF-beta receptors and TGF-beta binding proteoglycans: recent progress in identifying their functional properties. *Annals of the New York Academy of Sciences*, *593*, 59–72. Retrieved from http://www.ncbi.nlm.nih.gov/pubmed/2165378

Massagué, J., & Gomis, R. R. (2006). The logic of TGFβ signaling. *FEBS Letters*, *580*(12), 2811–2820. https://doi.org/10.1016/J.FEBSLET.2006.04.033

Massagué, J., Seoane, J., & Wotton, D. (2005). Smad transcription factors, 2783–2810. https://doi.org/10.1101/gad.1350705

Matallanas, D., Romano, D., Al-Mulla, F., O'Neill, E., Al-Ali, W., Crespo, P., … Kolch, W. (2011). Mutant K-Ras Activation of the Proapoptotic MST2 Pathway Is Antagonized by Wild-Type K-Ras. *Molecular Cell*, *44*(6), 893–906. https://doi.org/10.1016/j.molcel.2011.10.016

Matallanas, D., Romano, D., Yee, K., Meissl, K., Kucerova, L., Piazzolla, D., … O'Neill, E. (2007). RASSF1A Elicits Apoptosis through an MST2 Pathway Directing Proapoptotic Transcription by the p73 Tumor Suppressor Protein. *Molecular Cell*, *27*(6), 962–975. https://doi.org/10.1016/j.molcel.2007.08.008

Mauviel, A., Nallet-Staub, F., & Varelas, X. (2012). Integrating developmental signals: A Hippo in the (path)way. *Oncogene*, *31*(14), 1743–1756. https://doi.org/10.1038/onc.2011.363

Mehal, W. Z., Sheikh, S. Z., Gorelik, L., & Flavell, R. A. (2005). TGF-β signaling regulates CD8+ T cell responses to high- and low-affinity TCR interactions. *International Immunology*, *17*(5), 531–538. https://doi.org/10.1093/intimm/dxh233

Melo, S. a., Luecke, L. B., Kahlert, C., Fernandez, A. F., Gammon, S. T., Kaye, J., … Kalluri, R. (2015). Glypican-1 identifies cancer exosomes and detects early pancreatic cancer. *Nature*, *523*(7559), 177–182. https://doi.org/10.1038/nature14581

Melo, S. a., Sugimoto, H., O'Connell, J. T., Kato, N., Villanueva, A., Vidal, A., … Kalluri, R. (2014). Cancer Exosomes Perform Cell-Independent MicroRNA Biogenesis and Promote Tumorigenesis. *Cancer Cell*, *26*(5), 707–721. https://doi.org/10.1016/j.ccell.2014.09.005

Meng, R.-W., Li, Y.-C., Chen, X., Huang, Y.-X., Shi, H., Du, D.-D., … Lu, M.-X. (2016). Aberrant Methylation of RASSF1A Closely Associated with HNSCC, a Meta-Analysis. *Scientific Reports*, *6*(1), 20756. https://doi.org/10.1038/srep20756

Mineo, M., Garfield, S. H., Taverna, S., Flugy, A., De Leo, G., Alessandro, R., & Kohn, E. C. (2012). Exosomes released by K562 chronic myeloid leukemia cells promote angiogenesis in a src-dependent fashion. *Angiogenesis*, *15*(1), 33–45. https://doi.org/10.1007/s10456-011-9241-1

Mitsuzuka, K., Handa, K., Satoh, M., Arai, Y., & Hakomori, S. (2005). A Specific Microdomain ("Glycosynapse 3") Controls Phenotypic Conversion and Reversion of Bladder Cancer Cells through GM3-mediated Interaction of α3β1 Integrin with CD9. *Journal of Biological Chemistry*, *280*(42), 35545–35553. https://doi.org/10.1074/jbc.M505630200

Miyado, K., Yamada, G., Yamada, S., Hasuwa, H., Nakamura, Y., Ryu, F., … Mekada, E. (2000). Requirement of CD9 on the egg plasma membrane for fertilization. *Science (New York, N.Y.)*, *287*(5451), 321–324. Retrieved from http://www.ncbi.nlm.nih.gov/pubmed/10634791

Miyake, M., Nakano, K., Ieki, Y., Adachi, M., Huang, C. L., Itoi, S., … Taki, T. (1995). Motility related protein 1 (MRP-1/CD9) expression: inverse correlation with metastases in breast cancer. *Cancer Research*, *55*(18), 4127–4131. https://doi.org/10.1158/0008-5472.can-04-3123

Morelli, A. E., Larregina, A. T., Shufesky, W. J., Sullivan, M. L. G., Stolz, D. B., Papworth, G. D., … Thomson, A. W. (2004). Endocytosis, intracellular sorting, and processing of exosomes by dendritic cells. *Blood*, *104*(10), 3257–3266. https://doi.org/10.1182/blood-2004-03-0824

Moreno-Gonzalo, O., Villarroya-Beltri, C., & Sánchez-Madrid, F. (2014). Post-translational modifications of exosomal proteins. *Frontiers in Immunology*, *5*(AUG), 1–7. https://doi.org/10.3389/fimmu.2014.00383

Moroishi, T., Hayashi, T., Pan, W. W., Fujita, Y., Holt, M. V., Qin, J., … Guan, K. L. (2016). The Hippo Pathway Kinases LATS1/2 Suppress Cancer Immunity. *Cell*, *167*(6), 1525–1539.e17. https://doi.org/10.1016/j.cell.2016.11.005

Mu, Y., Gudey, S. K., & Landström, M. (2012). Non-Smad signaling pathways. *Cell and Tissue Research*, *347*(1), 11–20. https://doi.org/10.1007/s00441-011-1201-y

Mulcahy, L. A., Pink, R. C., & Carter, D. R. F. (2014). Routes and mechanisms of extracellular vesicle uptake. *Journal of Extracellular Vesicles*, *3*(1), 1–14. https://doi.org/10.3402/jev.v3.24641

Muralidharan-Chari, V., Clancy, J., Plou, C., Romao, M., Chavrier, P., Raposo, G., & D'Souza-Schorey, C. (2009). ARF6-Regulated Shedding of Tumor Cell-Derived Plasma Membrane Microvesicles. *Current Biology*, *19*(22), 1875–1885. https://doi.org/10.1016/j.cub.2009.09.059

Murayama, Y., Miyagawa, J., Oritani, K., Yoshida, H., Yamamoto, K., Kishida, O., … Shinomura, Y. (2004). CD9-mediated activation of the p46 Shc isoform leads to apoptosis in cancer cells. *Journal of Cell Science*, *117*(15), 3379–3388. https://doi.org/10.1242/jcs.01201

Nazarenko, I., Rana, S., Baumann, A., McAlear, J., Hellwig, A., Trendelenburg, M., … Zoller, M. (2010). Cell Surface Tetraspanin Tspan8 Contributes to Molecular Pathways of Exosome-

Induced Endothelial Cell Activation. *Cancer Research*, *70*(4), 1668–1678. https://doi.org/10.1158/0008-5472.CAN-09-2470

Nobes, C. D., & Hall, A. (1995). Rho, rac, and cdc42 GTPases regulate the assembly of multimolecular focal complexes associated with actin stress fibers, lamellipodia, and filopodia. *Cell*, *81*(1), 53–62. Retrieved from http://www.ncbi.nlm.nih.gov/pubmed/7536630

Nurgazieva, D., Mickley, A., Moganti, K., Ming, W., Ovsyi, I., Popova, A., … Gratchev. (2015). TGF-β1, but not bone morphogenetic proteins, activates Smad1/5 pathway in primary human macrophages and induces expression of proatherogenic genes. *Journal of Immunology (Baltimore, Md. : 1950)*, *194*(2), 709–718. https://doi.org/10.4049/jimmunol.1300272

Ostrowski, M., Carmo, N. B., Krumeich, S., Fanget, I., Raposo, G., Savina, A., … Thery, C. (2010). Rab27a and Rab27b control different steps of the exosome secretion pathway. *Nature Cell Biology*, *12*(1), 19-30; sup pp 1-13. https://doi.org/10.1038/ncb2000

Ozdamar, B., Bose, R., Barrios-Rodiles, M., Wang, H.-R., Zhang, Y., & Wrana, J. L. (2005). Regulation of the Polarity Protein Par6 by TGF Receptors Controls Epithelial Cell Plasticity. *Science*, *307*(5715), 1603–1609. https://doi.org/10.1126/science.1105718

Padua, D., Zhang, X. H. F., Wang, Q., Nadal, C., Gerald, W. L., Gomis, R. R., & Massagué, J. (2008). TGFβ Primes Breast Tumors for Lung Metastasis Seeding through Angiopoietin-like 4. *Cell*, *133*(1), 66–77. https://doi.org/10.1016/j.cell.2008.01.046

Paduch, M., Jeleñ, F., & Otlewski, J. (2001). Structure of small G proteins and their regulators. *Acta Biochimica Polonica*, *48*(4), 829–850. Retrieved from http://www.actabp.pl/pdf/4_2001/829.pdf

Pan, B. T., & Johnstone, R. M. (1983). Fate of the transferrin receptor during maturation of sheep reticulocytes in vitro: selective externalization of the receptor. *Cell*, *33*(3), 967–978. Retrieved from http://www.ncbi.nlm.nih.gov/pubmed/6307529

Pan, B. T., Teng, K., Wu, C., Adam, M., & Johnstone, R. M. (1985). Electron microscopic evidence for externalization of the transferrin receptor in vesicular form in sheep reticulocytes. *The Journal of Cell Biology*, *101*(3). Retrieved from http://jcb.rupress.org/content/101/3/942?ijkey=c4770c33a5d4e90c9eaecf33e0673fef982f0205&keytype2=tf_ipsecsha

Panciera, T., Azzolin, L., Cordenonsi, M., & Piccolo, S. (2017). Mechanobiology of YAP and TAZ in physiology and disease. *Nature Reviews. Molecular Cell Biology*, *18*(12), 758–770. https://doi.org/10.1038/nrm.2017.87

Pandya, P., Orgaz, J. L., & Sanz-Moreno, V. (2017). Modes of invasion during tumour dissemination. *Molecular Oncology*, *11*(1), 5–27. https://doi.org/10.1002/1878-0261.12019

Pardali, K., & Moustakas, A. (2007). Actions of TGF-β as tumor suppressor and pro-metastatic factor in human cancer. *Biochimica et Biophysica Acta (BBA) - Reviews on Cancer*, *1775*(1), 21–62. https://doi.org/10.1016/J.BBCAN.2006.06.004

Pefani, D.-E., Pankova, D., Abraham, A. G., Grawenda, A. M., Vlahov, N., Scrace, S., & O' Neill, E. (2016). TGF-β Targets the Hippo Pathway Scaffold RASSF1A to Facilitate YAP/SMAD2 Nuclear Translocation. *Molecular Cell*, *63*(1), 156–166. https://doi.org/10.1016/J.MOLCEL.2016.05.012

Pefani, D. E., Latusek, R., Pires, I., Grawenda, A. M., Yee, K. S., Hamilton, G., … O'Neill, E. (2014). RASSF1A-LATS1 signalling stabilizes replication forks by restricting CDK2-mediated phosphorylation of BRCA2. *Nature Cell Biology*, *16*(August), 962–971, 1–8. https://doi.org/10.1038/ncb3035

Pefani, D. E., Tognoli, M. L., Pirincci Ercan, D., Gorgoulis, V., & O'Neill, E. (2018). MST2 kinase suppresses rDNA transcription in response to DNA damage by phosphorylating nucleolar histone H2B. *The EMBO Journal*, *37*(15), e98760. https://doi.org/10.15252/embj.201798760

Peinado, H., Alečković, M., Lavotshkin, S., Matei, I., Costa-Silva, B., Moreno-Bueno, G., … Lyden, D. (2012). Melanoma exosomes educate bone marrow progenitor cells toward a pro-metastatic phenotype through MET. *Nature Medicine*, *18*(6), 883–891. https://doi.org/10.1038/nm.2753

Peinado, H., Lavotshkin, S., & Lyden, D. (2011). The secreted factors responsible for pre-metastatic niche formation: Old sayings and new thoughts. *Seminars in Cancer Biology*, *21*(2), 139–146. https://doi.org/10.1016/J.SEMCANCER.2011.01.002

Pelosi, G., Fumagalli, C., Trubia, M., Sonzogni, A., Rekhtman, N., Maisonneuve, P., … Viale, G. (2010). Dual role of RASSF1 as a tumor suppressor and an oncogene in neuroendocrine tumors of the lung. *Anticancer Research*, *30*(10), 4269–4281. Retrieved from http://www.ncbi.nlm.nih.gov/pubmed/21036752

Piccin, A., Murphy, W. G., & Smith, O. P. (2007). Circulating microparticles: pathophysiology and

clinical implications. *Blood Reviews*, *21*(3), 157–171. https://doi.org/10.1016/J.BLRE.2006.09.001

Pinxteren, J. A., O'Sullivan, A. J., Larbi, K. Y., Tatham, P. E. ., & Gomperts, B. D. (2000). Thirty years of stimulus-secretion coupling: From Ca2+ toGTP in the regulation of exocytosis. *Biochimie*, *82*(4), 385–393. https://doi.org/10.1016/S0300-9084(00)00197-8

Plebanek, M. P., Angeloni, N. L., Vinokour, E., Li, J., Henkin, A., Martinez-Marin, D., … Volpert, O. V. (2017). Pre-metastatic cancer exosomes induce immune surveillance by patrolling monocytes at the metastatic niche. *Nature Communications*, *8*(1), 1319. https://doi.org/10.1038/s41467-017-01433-3

Pugholm, L. H., Bæk, R., Søndergaard, E. K. L., Revenfeld, A. L. S., Jørgensen, M. M., & Varming, K. (2016). Phenotyping of Leukocytes and Leukocyte-Derived Extracellular Vesicles. *Journal of Immunology Research*, *2016*, 1–12. https://doi.org/10.1155/2016/6391264

Purushothaman, A., Bandari, S. K., Liu, J., Mobley, J. A., Brown, E. E., & Sanderson, R. D. (2016). Fibronectin on the Surface of Myeloma Cell-derived Exosomes Mediates Exosome-Cell Interactions. *Journal of Biological Chemistry*, *291*(4), 1652–1663. https://doi.org/10.1074/jbc.M115.686295

Rabizadeh, S., Xavier, R. J., Ishiguro, K., Bernabeortiz, J., Lopez-Ilasaca, M., Khokhlatchev, A., … Seed, B. (2004). The scaffold protein CNK1 interacts with the tumor suppressor RASSF1A and augments RASSF1A-induced cell death. *The Journal of Biological Chemistry*, *279*(28), 29247–29254. https://doi.org/10.1074/jbc.M401699200

Rak, J. (2013). Extracellular Vesicles – Biomarkers and Effectors of the Cellular Interactome in Cancer. *Frontiers in Pharmacology*, *4*, 21. https://doi.org/10.3389/fphar.2013.00021

Ramachandran, A., Vizán, P., Das, D., Chakravarty, P., Vogt, J., Rogers, K. W., … Hill, C. S. (2018). TGF-β uses a novel mode of receptor activation to phosphorylate SMAD1/5 and induce epithelial-to-mesenchymal transition. *ELife*, *7*. https://doi.org/10.7554/eLife.31756

Rana, S., Claas, C., Kretz, C. C., Nazarenko, I., & Zoeller, M. (2011). Activation-induced internalization differs for the tetraspanins CD9 and Tspan8: Impact on tumor cell motility. *The International Journal of Biochemistry & Cell Biology*, *43*(1), 106–119. https://doi.org/10.1016/j.biocel.2010.10.002

Raposo, G., Nijman, H. W., Stoorvogel, W., Liejendekker, R., Harding, C. V, Melief, C. J., & Geuze, H. J. (1996). B lymphocytes secrete antigen-presenting vesicles. *Journal of Experimental Medicine*, *183*(3). Retrieved from http://jem.rupress.org/content/183/3/1161?ijkey=369eb5255b11affbc11ba73421c24f5cd53c2953&keytype2=tf_ipsecsha

Raposo, G., & Stoorvogel, W. (2013). Extracellular vesicles: exosomes, microvesicles, and friends. *The Journal of Cell Biology*, *200*(4), 373–383. https://doi.org/10.1083/jcb.201211138

Rappa, G., Green, T. M., Karbanová, J., Corbeil, D., & Lorico, A. (2015). Tetraspanin CD9 determines invasiveness and tumorigenicity of human breast cancer cells. *Oncotarget*, *6*(10), 7970–7991. https://doi.org/10.18632/oncotarget.3419

Ratajczak, J., Miekus, K., Kucia, M., Zhang, J., Reca, R., Dvorak, P., & Ratajczak, M. Z. (2006). Embryonic stem cell-derived microvesicles reprogram hematopoietic progenitors: evidence for horizontal transfer of mRNA and protein delivery. *Leukemia*, *20*(5), 847–856. https://doi.org/10.1038/sj.leu.2404132

Reeves, M. E., Baldwin, S. W., Baldwin, M. L., Chen, S.-T., Moretz, J. M., Aragon, R. J., … Amaar, Y. G. (2010). Ras-association domain family 1C protein promotes breast cancer cell migration and attenuates apoptosis. *BMC Cancer*, *10*, 562. https://doi.org/10.1186/1471-2407-10-562

Reeves, M. E., Firek, M., Chen, S.-T., & Amaar, Y. (2013). The RASSF1 Gene and the Opposing Effects of the RASSF1A and RASSF1C Isoforms on Cell Proliferation and Apoptosis. *Molecular Biology International*, *2013*, 145096. https://doi.org/10.1155/2013/145096

Reeves, M. E., Firek, M., Chen, S.-T., Amaar, Y. G., Dammann, R., Takahashi, T., … O'Neill, E. (2014). Evidence that RASSF1C Stimulation of Lung Cancer Cell Proliferation Depends on IGFBP-5 and PIWIL1 Expression Levels. *PLoS ONE*, *9*(7), e101679. https://doi.org/10.1371/journal.pone.0101679

Reyes, R., Monjas, A., Yánez-Mó, M., Cardeñes, B., Morlino, G., Gilsanz, A., … Cabañas, C. (2015). Different states of integrin LFA-1 aggregation are controlled through its association with tetraspanin CD9. *Biochimica et Biophysica Acta (BBA) - Molecular Cell Research*, *1853*(10), 2464–2480. https://doi.org/10.1016/j.bbamcr.2015.05.018

Richards, K. E., Zeleniak, A. E., Fishel, M. L., Wu, J., Littlepage, L. E., & Hill, R. (2017). Cancer-associated fibroblast exosomes regulate survival and proliferation of pancreatic cancer cells. *Oncogene*, *36*(13), 1770–1778. https://doi.org/10.1038/onc.2016.353

Ridley, A. J. (2001). Rho proteins: Linking signaling with membrane trafficking. *Traffic*, *2*(5), 303–310. https://doi.org/10.1034/j.1600-0854.2001.002005303.x

Ridley, A. J. (2006). Rho GTPases and actin dynamics in membrane protrusions and vesicle trafficking. *Trends in Cell Biology*, *16*(10), 522–529. https://doi.org/10.1016/J.TCB.2006.08.006

Ridley, A. J., & Hall, A. (1992). The small GTP-binding protein rho regulates the assembly of focal adhesions and actin stress fibers in response to growth factors. *Cell*, *70*(3), 389–399. Retrieved from http://www.ncbi.nlm.nih.gov/pubmed/1643657

Ridley, A. J., Paterson, H. F., Johnston, C. L., Diekmann, D., & Hall, A. (1992). The small GTP-binding protein rac regulates growth factor-induced membrane ruffling. *Cell*, *70*(3), 401–410. Retrieved from http://www.ncbi.nlm.nih.gov/pubmed/1643658

Ridley, A. J., Schwartz, M. A., Burridge, K., Firtel, R. A., Ginsberg, M. H., Borisy, G., … Horwitz, A. R. (2003). Cell Migration: Integrating Signals from Front to Back. *Science*, *302*(5651), 1704–1709. https://doi.org/10.1126/science.1092053

Roberts, A. B., Anzano, M. A., Lamb, L. C., Smith, J. M., Frolik, C. A., Marquardt, H., … Sporn, M. B. (1982). Isolation from murine sarcoma cells of novel transforming growth factors potentiated by EGF. *Nature*, *295*(5848), 417–419. https://doi.org/10.1038/295417a0

Robertson, I. B., Horiguchi, M., Zilberberg, L., Dabovic, B., Hadjiolova, K., & Rifkin, D. B. (2015). Latent TGF-β-binding proteins. *Matrix Biology*, *47*, 44–53. https://doi.org/10.1016/J.MATBIO.2015.05.005

Rodriguez-Viciana, P., Sabatier, C., & McCormick, F. (2004). Signaling specificity by Ras family GTPases is determined by the full spectrum of effectors they regulate. *Molecular and Cellular Biology*, *24*(11), 4943–4954. https://doi.org/10.1128/MCB.24.11.4943-4954.2004

Rong, R., Jin, W., Zhang, J., Saeed Sheikh, M., & Huang, Y. (2004). Tumor suppressor RASSF1A is a microtubule-binding protein that stabilizes microtubules and induces G2/M arrest. *Oncogene*, *23*(50), 8216–8230. https://doi.org/10.1038/sj.onc.1207901

Rupp, A.-K., Rupp, C., Keller, S., Brase, J. C., Ehehalt, R., Fogel, M., … Altevogt, P. (2011). Loss of EpCAM expression in breast cancer derived serum exosomes: Role of proteolytic cleavage. *Gynecologic Oncology*, *122*(2), 437–446. https://doi.org/10.1016/j.ygyno.2011.04.035

Sadej, R., Romanska, H., Kavanagh, D., Baldwin, G., Takahashi, T., Kalia, N., & Berditchevski, F. (2010). Tetraspanin CD151 regulates transforming growth factor β signaling: Implication in tumor metastasis. *Cancer Research*, *70*(14), 6059–6070. https://doi.org/10.1158/0008-5472.CAN-09-3497

Sahai, E. (2005). Mechanisms of cancer cell invasion. *Current Opinion in Genetics & Development*, *15*(1), 87–96. https://doi.org/10.1016/J.GDE.2004.12.002

Sahai, E., & Marshall, C. J. (2003). Differing modes for tumour cell invasion have distinct requirements for Rho/ROCK signalling and extracellular proteolysis. *Nature Cell Biology*, *5*(8), 711–719. https://doi.org/10.1038/ncb1019

Sanz-Moreno, V., Gadea, G., Ahn, J., Paterson, H., Marra, P., Pinner, S., … Marshall, C. J. (2008). Rac Activation and Inactivation Control Plasticity of Tumor Cell Movement. *Cell*, *135*(3), 510–523. https://doi.org/10.1016/j.cell.2008.09.043

Savina, A., Vidal, M., & Colombo, M. I. (2002). The exosome pathway in K562 cells is regulated by Rab11. *Journal of Cell Science*, *115*(12).

Schillaci, O., Fontana, S., Monteleone, F., Taverna, S., Bella, M. A. Di, Vizio, D. Di, & Alessandro, R. (2017). Exosomes from metastatic cancer cells transfer amoeboid phenotype to non-metastatic cells and increase endothelial permeability: Their emerging role in tumor heterogeneity. *Scientific Reports*, *7*(1). https://doi.org/10.1038/s41598-017-05002-y

Schmidt, O., & Teis, D. (2012). The ESCRT machinery. *Current Biology : CB*, *22*(4), R116-20. https://doi.org/10.1016/j.cub.2012.01.028

Sedgwick, A. E., Clancy, J. W., Olivia Balmert, M., & D'Souza-Schorey, C. (2015). Extracellular microvesicles and invadopodia mediate non-overlapping modes of tumor cell invasion. *Scientific Reports*, *5*(1), 14748. https://doi.org/10.1038/srep14748

Sheldon, H., Heikamp, E., Turley, H., Dragovic, R., Thomas, P., Oon, C. E., … Harris, A. L. (2010). New mechanism for Notch signaling to endothelium at a distance by Delta-like 4 incorporation into exosomes. *Blood*, *116*(13), 2385–2394. https://doi.org/10.1182/blood-2009-08-239228

Shi, W., Fan, H., Shum, L., & Derynck, R. (2000). The tetraspanin CD9 associates with transmembrane TGF-alpha and regulates TGF-alpha-induced EGF receptor activation and cell proliferation. *The Journal of Cell Biology*, *148*(3), 591–602. Retrieved from http://www.ncbi.nlm.nih.gov/pubmed/10662783

Shi, Y., & Massagué, J. (2003). Mechanisms of TGF-beta signaling from cell membrane to the nucleus. *Cell*, *113*(6), 685–700. https://doi.org/10.1016/S0092-8674(03)00432-X

Shi, Y., Wang, Y.-F., Jayaraman, L., Yang, H., Massagué, J., & Pavletich, N. P. (1998). Crystal Structure of a Smad MH1 Domain Bound to DNA: Insights on DNA Binding in TGF-β Signaling. *Cell*, *94*(5), 585–594. https://doi.org/10.1016/S0092-8674(00)81600-1

Shivakumar, L., Minna, J., Sakamaki, T., Pestell, R., & White, M. A. (2002). The RASSF1A tumor suppressor blocks cell cycle progression and inhibits cyclin D1 accumulation. *Molecular and Cellular Biology*, *22*(12), 4309–4318. https://doi.org/10.1128/MCB.22.12.4309-4318.2002

Skog, J., Würdinger, T., Van Rijn, S., Meijer, D. H., Gainche, L., Sena-Esteves, M., … Breakefield, X. O. (2008). Glioblastoma microvesicles transport rNA and proteins that promote tumour growth and provide diagnostic biomarkers. *Nature Cell Biology*, *10*(12), 1470–1476. https://doi.org/10.1038/ncb1800

Skotland, T., Sandvig, K., & Llorente, A. (2017). Lipids in exosomes: Current knowledge and the way forward. *Progress in Lipid Research*, *66*, 30–41. https://doi.org/10.1016/j.plipres.2017.03.001

Song, M. S., Song, S. J., Ayad, N. G., Chang, J. S., Lee, J. H., Hong, H. K., … Lim, D.-S. (2004). The tumour suppressor RASSF1A regulates mitosis by inhibiting the APC–Cdc20 complex. *Nature Cell Biology*, *6*(2), 129–137. https://doi.org/10.1038/ncb1091

Soung, Y. H., Ford, S., Zhang, V., & Chung, J. (2017). Exosomes in Cancer Diagnostics. *Cancers*, *9*(1). https://doi.org/10.3390/cancers9010008

Soyuer, S., Soyuer, I., Unal, D., Ucar, K., Yildiz, O. G., & Orhan, O. (2010). Prognostic significance of CD9 expression in locally advanced gastric cancer treated with surgery and adjuvant chemoradiotherapy. *Pathology - Research and Practice*, *206*(9), 607–610. https://doi.org/10.1016/j.prp.2010.04.004

Sreenivasappa, H., Chaki, S. P., Lim, S.-M., Trzeciakowski, J. P., Davidson, M. W., Rivera, G. M., & Trache, A. (2014). Selective regulation of cytoskeletal tension and cell-matrix adhesion by RhoA and Src. *Integrative Biology : Quantitative Biosciences from Nano to Macro*, *6*(8), 743–754. https://doi.org/10.1039/c4ib00019f

Stefani, F., Zhang, L., Taylor, S., Donovan, J., Rollinson, S., Doyotte, A., … Woodman, P. (2011). UBAP1 Is a Component of an Endosome-Specific ESCRT-I Complex that Is Essential for MVB Sorting. *Current Biology*, *21*(14), 1245–1250. https://doi.org/10.1016/j.cub.2011.06.028

Stoorvogel, W., Strous, G. J., Geuze, H. J., Oorschot, V., & Schwartzt, A. L. (1991). Late endosomes derive from early endosomes by maturation. *Cell*, *65*(3), 417–427. https://doi.org/10.1016/0092-8674(91)90459-C

Stuffers, S., Sem Wegner, C., Stenmark, H., & Brech, A. (2009). Multivesicular Endosome Biogenesis in the Absence of ESCRTs. *Traffic*, *10*(7), 925–937. https://doi.org/10.1111/j.1600-0854.2009.00920.x

Subauste, M. C., Von Herrath, M., Benard, V., Chamberlain, C. E., Chuang, T. H., Chu, K., … Hahn, K. M. (2000). Rho family proteins modulate rapid apoptosis induced by cytotoxic T lymphocytes and Fas. *The Journal of Biological Chemistry*, *275*(13), 9725–9733. https://doi.org/10.1074/JBC.275.13.9725

Sung, B. H., Ketova, T., Hoshino, D., Zijlstra, A., & Weaver, A. M. (2015). Directional cell movement through tissues is controlled by exosome secretion. *Nature Communications*, *6*(May), 7164. Retrieved from http://www.nature.com/doifinder/10.1038/ncomms8164

Svensson, K. J., Christianson, H. C., Wittrup, a., Bourseau-Guilmain, E., Lindqvist, E., Svensson, L. M., … Belting, M. (2013). Exosome Uptake Depends on ERK1/2-Heat Shock Protein 27 Signaling and Lipid Raft-mediated Endocytosis Negatively Regulated by Caveolin-1. *Journal of Biological Chemistry*, *288*(24), 17713–17724. https://doi.org/10.1074/jbc.M112.445403

Tachibana, I., & Hemler, M. E. (1999). Role of transmembrane 4 superfamily (TM4SF) proteins CD9 and CD81 in muscle cell fusion and myotube maintenance. *The Journal of Cell Biology*, *146*(4), 893–904. Retrieved from http://www.ncbi.nlm.nih.gov/pubmed/10459022

Takeda, Y., He, P., Tachibana, I., Zhou, B., Miyado, K., Kaneko, H., … Kawase, I. (2008). Double deficiency of tetraspanins CD9 and CD81 alters cell motility and protease production of macrophages and causes chronic obstructive pulmonary disease-like phenotype in mice. *The Journal of Biological Chemistry*, *283*(38), 26089–26097. https://doi.org/10.1074/jbc.M801902200

Takeda, Y., Tachibana, I., Miyado, K., Kobayashi, M., Miyazaki, T., Funakoshi, T., … Mekada, E. (2003). Tetraspanins CD9 and CD81 function to prevent the fusion of mononuclear phagocytes. *The Journal of Cell Biology*, *161*(5), 945–956. https://doi.org/10.1083/jcb.200212031

Taylor, D. D., & Shah, S. (2015). Methods of isolating extracellular vesicles impact down-stream analyses of their cargoes. *Methods*, 1–8. https://doi.org/10.1016/j.ymeth.2015.02.019

Termini, C. M., & Gillette, J. M. (2017). Tetraspanins Function as Regulators of Cellular Signaling. *Frontiers in Cell and Developmental Biology*, *5*, 34. https://doi.org/10.3389/fcell.2017.00034

Thakur, B. K., Zhang, H., Becker, A., Matei, I., Huang, Y., Costa-Silva, B., … Lyden, D. (2014). Double-stranded DNA in exosomes: a novel biomarker in cancer detection. *Cell Research*, *24*(6), 766–769. https://doi.org/10.1038/cr.2014.44

Thaler, S., Hähnel, P. S., Schad, A., Dammann, R., & Schuler, M. (2009). RASSF1A Mediates p21Cip1/Waf1-Dependent Cell Cycle Arrest and Senescence through Modulation of the Raf-MEK-ERK Pathway and Inhibition of Akt. *Cancer Research*, *69*(5).

Théry, C., Amigorena, S., Raposo, G., & Clayton, A. (2006). Isolation and characterization of exosomes from cell culture supernatants and biological fluids. *Current Protocols in Cell Biology / Editorial Board, Juan S. Bonifacino ... [et Al.]*, *Chapter 3*, Unit 3.22. https://doi.org/10.1002/0471143030.cb0322s30

Théry, C., Boussac, M., Véron, P., Ricciardi-Castagnoli, P., Raposo, G., Garin, J., & Amigorena, S. (2001). Proteomic analysis of dendritic cell-derived exosomes: a secreted subcellular compartment distinct from apoptotic vesicles. *Journal of Immunology (Baltimore, Md. : 1950)*, *166*(12), 7309–7318. Retrieved from http://www.ncbi.nlm.nih.gov/pubmed/11390481

Théry, C., Ostrowski, M., & Segura, E. (2009). Membrane vesicles as conveyors of immune responses. *Nature Reviews. Immunology*, *9*(8), 581–593. https://doi.org/10.1038/nri2567

Thiery, J. P., Acloque, H., Huang, R. Y. J., & Nieto, M. A. (2009). Epithelial-Mesenchymal Transitions in Development and Disease. *Cell*, *139*(5), 871–890. https://doi.org/10.1016/j.cell.2009.11.007

Thomas, D. A., & Massagué, J. (2005). TGF-β directly targets cytotoxic T cell functions during tumor evasion of immune surveillance. *Cancer Cell*, *8*(5), 369–380. https://doi.org/10.1016/j.ccr.2005.10.012

Tian, T., Zhu, Y.-L., Zhou, Y.-Y., Liang, G.-F., Wang, Y.-Y., Hu, F.-H., & Xiao, Z.-D. (2014). Exosome Uptake through Clathrin-mediated Endocytosis and Macropinocytosis and Mediating miR-21 Delivery. *Journal of Biological Chemistry*, *289*(32), 22258–22267. https://doi.org/10.1074/jbc.M114.588046

Tkach, M., & Théry, C. (2016). Communication by Extracellular Vesicles: Where we Are and Where we Need to Go. *Cell*, *164*(6), 1226–1232. https://doi.org/10.1016/j.cell.2016.01.043

Trajkovic, K., Hsu, C., Chiantia, S., Rajendran, L., Wenzel, D., Wieland, F., … Simons, M. (2008). Ceramide triggers budding of exosome vesicles into multivesicular endosomes. *Science (New York, N.Y.)*, *319*(5867), 1244–1247. https://doi.org/10.1126/science.1153124

Valadi, H., Ekström, K., Bossios, A., Sjöstrand, M., Lee, J. J., & Lötvall, J. O. (2007). Exosome-mediated transfer of mRNAs and microRNAs is a novel mechanism of genetic exchange between cells. *Nature Cell Biology*, *9*(6), 654–659. https://doi.org/10.1038/ncb1596

van Niel, G., Bergam, P., Di Cicco, A., Hurbain, I., Lo Cicero, A., Dingli, F., … Raposo, G. (2015). Apolipoprotein E Regulates Amyloid Formation within Endosomes of Pigment Cells. *Cell Reports*, *13*(1), 43–51. https://doi.org/10.1016/j.celrep.2015.08.057

van Caam, A., Madej, W., Garcia de Vinuesa, A., Goumans, M.-J., Ten Dijke, P., Blaney Davidson, E., & van der Kraan, P. (2017). TGFβ1-induced SMAD2/3 and SMAD1/5 phosphorylation are both ALK5-kinase-dependent in primary chondrocytes and mediated by TAK1 kinase activity. *Arthritis Research & Therapy*, *19*(1), 112. https://doi.org/10.1186/s13075-017-1302-4

van der Weyden, L., & Adams, D. J. (2007). The Ras-association domain family (RASSF) members and their role in human tumourigenesis. *Biochimica et Biophysica Acta - Reviews on Cancer*, *1776*(1), 58–85. https://doi.org/10.1016/j.bbcan.2007.06.003

van der Weyden, L., Tachibana, K. K., Gonzalez, M. . A., Adams, D. J., Ng, B. L., Petty, R., … Bradley, A. (2005). The RASSF1A isoform of RASSF1 promotes microtubule stability and suppresses tumorigenesis. *Molecular and Cellular Biology*, *25*(18), 8356–8367. https://doi.org/10.1128/MCB.25.18.8356-8367.2005

van Niel, G., Charrin, S., Simoes, S., Romao, M., Rochin, L., Saftig, P., … Raposo, G. (2011). The Tetraspanin CD63 Regulates ESCRT-Independent and -Dependent Endosomal Sorting during Melanogenesis. *Developmental Cell*, *21*(4), 708–721. https://doi.org/10.1016/j.devcel.2011.08.019

Van Niel, G., D'Angelo, G., & Raposo, G. (2018). Shedding light on the cell biology of extracellular vesicles. *Nature Reviews Molecular Cell Biology*, *19*(4), 213–228. https://doi.org/10.1038/nrm.2017.125

Varelas, X., Sakuma, R., Samavarchi-Tehrani, P., Peerani, R., Rao, B. M., Dembowy, J., …

Wrana, J. L. (2008). TAZ controls Smad nucleocytoplasmic shuttling and regulates human embryonic stem-cell self-renewal. *Nat Cell Biol*, *10*(7), 837–848. https://doi.org/10.1038/ncb1748

Varelas, X., Samavarchi-Tehrani, P., Narimatsu, M., Weiss, A., Cockburn, K., Larsen, B. G., … Wrana, J. L. (2010). The Crumbs Complex Couples Cell Density Sensing to Hippo-Dependent Control of the TGF-β-SMAD Pathway. *Developmental Cell*, *19*(6), 831–844. https://doi.org/10.1016/j.devcel.2010.11.012

Verweij, F. J., Bebelman, M. P., Jimenez, C. R., Garcia-Vallejo, J. J., Janssen, H., Neefjes, J., … Pegtel, D. M. (2018). Quantifying exosome secretion from single cells reveals a modulatory role for GPCR signaling. *The Journal of Cell Biology*, *217*(3), 1129–1142. https://doi.org/10.1083/jcb.201703206

Vlahov, N., Scrace, S., Soto, M. S., Grawenda, A. M., Bradley, L., Pankova, D., … O'Neill, E. (2015). Alternate RASSF1 Transcripts Control SRC Activity, E-Cadherin Contacts, and YAP-Mediated Invasion. *Current Biology*, *25*(23), 3019–3034. https://doi.org/10.1016/j.cub.2015.09.072

Volodko, N., Gordon, M., Salla, M., & Ghazaleh, H. A. (2014). RASSF tumor suppressor gene family: Biological functions and regulation. *FEBS Letters*, *588*(16), 2671–2684. https://doi.org/10.1016/j.febslet.2014.02.041

Volodko, N., Salla, M., Zare, A., Abulghasem, E.-A., Vincent, K., Benesch, M., … Baksh, S. (2016). RASSF1A Site-Specific Methylation Hotspots in Cancer and Correlation with RASSF1C and MOAP-1. *Cancers*, *8*(6), 55. https://doi.org/10.3390/cancers8060055

Vos, M. D., Dallol, A., Eckfeld, K., Allen, N. P. C., Donninger, H., Hesson, L. B., … Clark, G. J. (2006). The RASSF1A Tumor Suppressor Activates Bax via MOAP-1. *Journal of Biological Chemistry*, *281*(8), 4557–4563. https://doi.org/10.1074/jbc.M512128200

Vos, M. D., Ellis, C. A., Bell, A., Birrer, M. J., & Clark, G. J. (2000). Ras uses the novel tumor suppressor RASSF1 as an effector to mediate apoptosis. *The Journal of Biological Chemistry*, *275*(46), 35669–35672. https://doi.org/10.1074/jbc.C000463200

Vos, M. D., Martinez, A., Elam, C., Dallol, A., Taylor, B. J., Latif, F., & Clark, G. J. (2004). A Role for the RASSF1A Tumor Suppressor in the Regulation of Tubulin Polymerization and Genomic Stability. *Cancer Research*, *64*(12).

Wandinger-Ness, A., & Zerial, M. (2014). Rab proteins and the compartmentalization of the endosomal system. *Cold Spring Harbor Perspectives in Biology*, *6*(11), a022616. https://doi.org/10.1101/cshperspect.a022616

Wang, H., Sharma, C., Knoblich, K., Granter, S. R., & Hemler, M. E. (2015). EWI-2 negatively regulates TGF-β signaling leading to altered melanoma growth and metastasis. *Cell Research*, *25*(3), 370–385. https://doi.org/10.1038/cr.2015.17

Wang, J., Wang, B., Chen, X., & Bi, J. (2011). The prognostic value of RASSF1A promoter hypermethylation in non-small cell lung carcinoma: a systematic review and meta-analysis. *Carcinogenesis*, *32*(3), 411–416. https://doi.org/10.1093/carcin/bgq266

Wang, L., Liu, Z., Shi, H., & Liu, J. (2017). Two Paralogous Tetraspanins TSP-12 and TSP-14 Function with the ADAM10 Metalloprotease SUP-17 to Promote BMP Signaling in Caenorhabditis elegans. *PLOS Genetics*, *13*(1), e1006568. https://doi.org/10.1371/journal.pgen.1006568

Wang, Z., Wu, Y., Wang, H., Zhang, Y., Mei, L., Fang, X., … Huang, L. (2014). Interplay of mevalonate and Hippo pathways regulates RHAMM transcription via YAP to modulate breast cancer cell motility. *Proceedings of the National Academy of Sciences of the United States of America*, *111*(1), E89-98. https://doi.org/10.1073/pnas.1319190110

Webber, J., Spary, L. K., Sanders, A. J., Chowdhury, R., Jiang, W. G., Steadman, R., … Clayton, A. (2015). Differentiation of tumour-promoting stromal myofibroblasts by cancer exosomes. *Oncogene*, *34*(3), 290–302. https://doi.org/10.1038/onc.2013.560

Webber, J., Steadman, R., Mason, M. D., Tabi, Z., & Clayton, A. (2010). Cancer Exosomes Trigger Fibroblast to Myofibroblast Differentiation. *Cancer Research*, *70*(23), 9621–9630. https://doi.org/10.1158/0008-5472.CAN-10-1722

Weiss, A., & Attisano, L. (2013). The TGFbeta Superfamily Signaling Pathway. *WIREs Dev Biol*, *2*, 47–63. https://doi.org/10.1002/wdev.86

Whang, Y. M., Kim, Y. H., Kim, J. S., & Yoo, Y. Do. (2005). RASSF1A suppresses the c-Jun-NH2-kinase pathway and inhibits cell cycle progression. *Cancer Research*, *65*(9), 3682–3690. https://doi.org/10.1158/0008-5472.CAN-04-2792

Wiercinska, E., Naber, H. P. H., Pardali, E., van der Pluijm, G., van Dam, H., & ten Dijke, P. (2011). The TGF-β/Smad pathway induces breast cancer cell invasion through the up-

regulation of matrix metalloproteinase 2 and 9 in a spheroid invasion model system. *Breast Cancer Research and Treatment*, *128*(3), 657–666. https://doi.org/10.1007/s10549-010-1147-x

Willms, E., Johansson, H. J., Mäger, I., Lee, Y., Blomberg, K. E. M., Sadik, M., … Vader, P. (2016). Cells release subpopulations of exosomes with distinct molecular and biological properties. *Scientific Reports*, *6*(1), 22519. https://doi.org/10.1038/srep22519

Witsch, E., Sela, M., & Yarden, Y. (2010). Roles for Growth Factors in Cancer Progression. *Physiology*, *25*(2), 85–101. https://doi.org/10.1152/physiol.00045.2009

Witwer, K. W., Soekmadji, C., Hill, A. F., Wauben, M. H., Buzás, E. I., Di Vizio, D., … Théry, C. (2017). Updating the MISEV minimal requirements for extracellular vesicle studies: building bridges to reproducibility. *Journal of Extracellular Vesicles*, *6*(1). https://doi.org/10.1080/20013078.2017.1396823

Worthylake, R. A., Lemoine, S., Watson, J. M., & Burridge, K. (2001). RhoA is required for monocyte tail retraction during transendothelial migration. *The Journal of Cell Biology*, *154*(1), 147–160. Retrieved from http://www.ncbi.nlm.nih.gov/pubmed/11448997

Wrana, J. L., Attisano, L., Cárcamo, J., Zentella, A., Doody, J., Laiho, M., … Massague, J. (1992). TGFβ signals through a heteromeric protein kinase receptor complex. *Cell*, *71*(6), 1003–1014. https://doi.org/10.1016/0092-8674(92)90395-S

Wrighton, K. H., & Feng, X.-H. (2008). To (TGF)β or not to (TGF)β: Fine-tuning of Smad signaling via post-translational modifications. *Cellular Signalling*, *20*(9), 1579–1591. https://doi.org/10.1016/j.cellsig.2008.02.003

Wubbolts, R., Leckie, R. S., Veenhuizen, P. T. M., Schwarzmann, G., Möbius, W., Hoernschemeyer, J., … Stoorvogel, W. (2003). Proteomic and Biochemical Analyses of Human B Cell-derived Exosomes. *Journal of Biological Chemistry*, *278*(13), 10963–10972. https://doi.org/10.1074/jbc.M207550200

Xu, L. (2006). Regulation of Smad activities. *Biochimica et Biophysica Acta*, *1759*(11–12), 503–513. https://doi.org/10.1016/j.bbaexp.2006.11.001

Xu, R., Rai, A., Chen, M., Suwakulsiri, W., Greening, D. W., & Simpson, R. J. (2018). Extracellular vesicles in cancer — implications for future improvements in cancer care. *Nature Reviews Clinical Oncology*, 1. https://doi.org/10.1038/s41571-018-0036-9

Yáñez-Mó, M., Barreiro, O., Gordon-Alonso, M., Sala-Valdés, M., & Sánchez-Madrid, F. (2009). Tetraspanin-enriched microdomains: a functional unit in cell plasma membranes. *Trends in Cell Biology*, *19*(9), 434–446. https://doi.org/10.1016/j.tcb.2009.06.004

Yang, X. H., Kovalenko, O. V., Kolesnikova, T. V., Andzelm, M. M., Rubinstein, E., Strominger, J. L., & Hemler, M. E. (2006). Contrasting effects of EWI proteins, integrins, and protein palmitoylation on cell surface CD9 organization. *Journal of Biological Chemistry*, *281*(18), 12976–12985. https://doi.org/10.1074/jbc.M510617200

Yoshioka, Y., Konishi, Y., Kosaka, N., Katsuda, T., Kato, T., & Ochiya, T. (2013). Comparative marker analysis of extracellular vesicles in different human cancer types. *Journal of Extracellular Vesicles*, *2*(1), 1–9. https://doi.org/10.3402/jev.v2i0.20424

Yu, F.-X., Zhao, B., & Guan, K.-L. (2015). Hippo Pathway in Organ Size Control, Tissue Homeostasis, and Cancer. *Cell*, *163*(4), 811–828. https://doi.org/10.1016/j.cell.2015.10.044

Yu, J., Pan, L., Qin, X., Chen, H., Xu, Y., Chen, Y., & Tang, H. (2010). MTMR4 attenuates transforming growth factor beta (TGFbeta) signaling by dephosphorylating R-Smads in endosomes. *The Journal of Biological Chemistry*, *285*(11), 8454–8462. https://doi.org/10.1074/jbc.M109.075036

Zhang, H., Deng, T., Liu, R., Bai, M., Zhou, L., Wang, X., … Ba, Y. (2017). Exosome-delivered EGFR regulates liver microenvironment to promote gastric cancer liver metastasis. *Nature Communications*, *8*, 15016. https://doi.org/10.1038/ncomms15016

Zhang, L., Zhang, S., Yao, J., Lowery, F. J., Zhang, Q., Huang, W. C., … Yu, D. (2015). Microenvironment-induced PTEN loss by exosomal microRNA primes brain metastasis outgrowth. *Nature*, *527*(7576), 100–104. https://doi.org/10.1038/nature15376

Zhang, Y. E. (2009). Non-Smad pathways in TGF-β signaling. *Cell Research*, *19*(1), 128–139. https://doi.org/10.1038/cr.2008.328

Zhao, B., Li, L., Tumaneng, K., Wang, C.-Y., & Guan, K.-L. (2010). A coordinated phosphorylation by Lats and CK1 regulates YAP stability through SCF -TRCP. *Genes & Development*, *24*(1), 72–85. https://doi.org/10.1101/gad.1843810

Zhao, B., Wei, X., Li, W., Udan, R. S., Yang, Q., Kim, J., … Guan, K.-L. (2007). Inactivation of YAP oncoprotein by the Hippo pathway is involved in cell contact inhibition and tissue growth control. *Genes & Development*, *21*(21), 2747–2761. https://doi.org/10.1101/gad.1602907

Zhou, X., Li, T.-T., Feng, X., Hsiang, E., Xiong, Y., Guan, K.-L., & Lei, Q.-Y. (2012). Targeted polyubiquitylation of RASSF1C by the Mule and SCFβ-TrCP ligases in response to DNA damage. *The Biochemical Journal*, *441*(1), 227–236. https://doi.org/10.1042/BJ20111500

Zitvogel, L., Regnault, A., Lozier, A., Wolfers, J., Flament, C., Tenza, D., … Amigorena, S. (1998). Eradication of established murine tumors using a novel cell-free vaccine: dendritic cell-derived exosomes. *Nature Medicine*, *4*(5), 594–600. Retrieved from http://www.ncbi.nlm.nih.gov/pubmed/9585234

Zöller, M. (2009). Tetraspanins: push and pull in suppressing and promoting metastasis. *Nature Reviews Cancer*, *9*(1), 40–55. https://doi.org/10.1038/nrc2543

Zomer, A., Maynard, C., Verweij, F. J., Kamermans, A., Schäfer, R., Beerling, E., … van Rheenen, J. (2015). In Vivo Imaging Reveals Extracellular Vesicle-Mediated Phenocopying of Metastatic Behavior. *Cell*, *161*(5), 1046–1057. https://doi.org/10.1016/j.cell.2015.04.042

Zomer, A., Steenbeek, S. C., Maynard, C., & Van Rheenen, J. (2016). Studying extracellular vesicle transfer by a Cre-loxP method. *Nature Protocols*, *11*(1). https://doi.org/10.1038/nprot.2015.138